AD-A146 546 STUDIES OF THE OCEAN SURFACE AND THE COUPLING BETWEEN THE SEA AND THE ATMOSPHERE(U) NEVADA UNIV RENO DESERT RESEARCH INST J W TELFORD 01 OCT 84 N00014-75-C-0598 1/3

UNCLASSIFIED F/G 4/2 NL

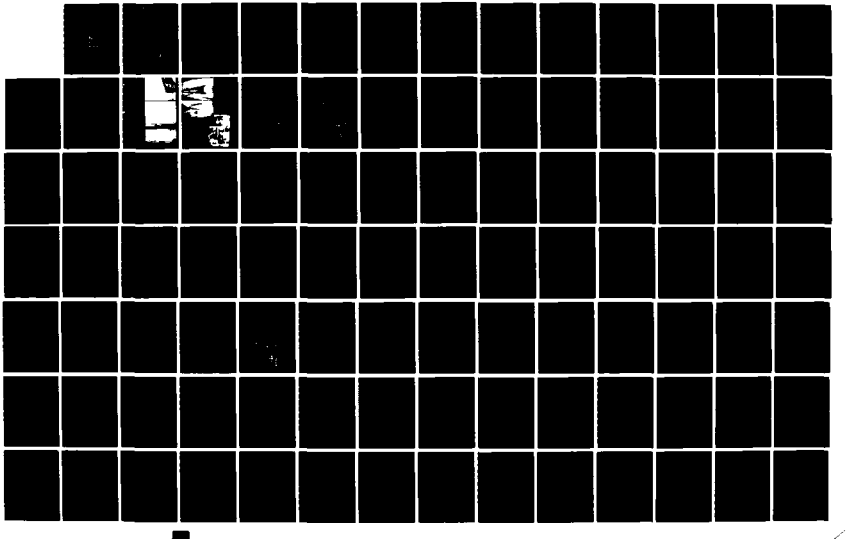

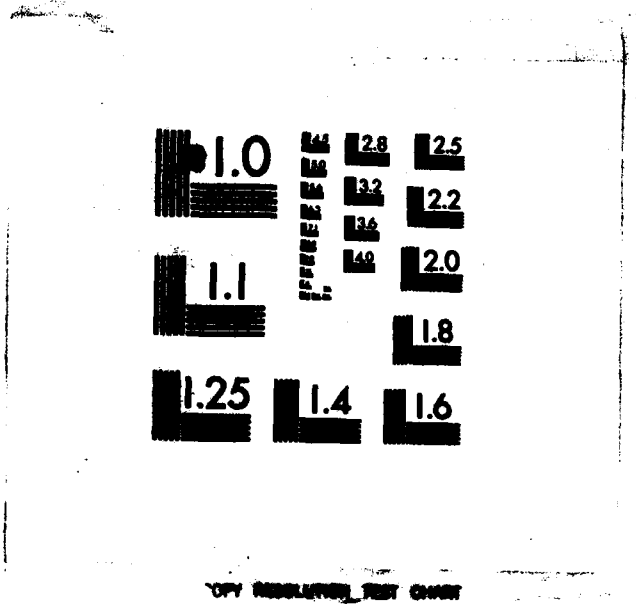
1.0
1.1
1.25
1.4
1.6
1.8
2.0
2.2
2.5
2.8
3.2
3.6
4.0

Final Report, Contract No. N00014-75-C-0598

# STUDIES OF THE OCEAN SURFACE AND THE COUPLING BETWEEN THE SEA AND THE ATMOSPHERE

Dr. James W. Telford
Desert Research Institute-ASC
University of Nevada System
P.O. Box 60220
Reno, NV 89506

1 October 1984

Final Report for Period 1 September 1974 - 31 March 1984



Prepared for

DEPARTMENT OF THE NAVY
Office of Naval Research
800 N. Quincy
Arlington, VA 22217

ONRRR, Mr. Robin Simpson
Stanford University
165 Durand Aeronautics Bldg.
Stanford, CA 94305

F-200.1473 *DD Form 1473:* Report Documentation Page

SECURITY CLASSIFICATION OF THIS PAGE (When Data Entered)

| REPORT DOCUMENTATION PAGE | READ INSTRUCTIONS BEFORE COMPLETING FORM |
|---|---|
| 1. REPORT NUMBER: Final Report | 2. GOVT ACCESSION NO: AD-A146 546 / 3. RECIPIENT'S CATALOG NUMBER |
| 4. TITLE (and Subtitle): STUDIES OF THE OCEAN SURFACE AND THE COUPLING BETWEEN THE SEA AND THE ATMOSPHERE | 5. TYPE OF REPORT & PERIOD COVERED: Final Report 1 Sept 1974 - 31 March 1984 |
| | 6. PERFORMING ORG. REPORT NUMBER |
| 7. AUTHOR(s): Dr. James W. Telford | 8. CONTRACT OR GRANT NUMBER(s): N00014-75-C-0598 |
| 9. PERFORMING ORGANIZATION NAME AND ADDRESS: Desert Research Institute-ASC, Univ. of Nevada System, P.O. Box 60220, Reno, NV 89506 | 10. PROGRAM ELEMENT, PROJECT, TASK AREA & WORK UNIT NUMBERS |
| 11. CONTROLLING OFFICE NAME AND ADDRESS: Department of the Navy, Office of Naval Research, 800 N. Quincy, Arlington, VA 22217 | 12. REPORT DATE: 1 October 1984<br>13. NUMBER OF PAGES: 280 |
| 14. MONITORING AGENCY NAME & ADDRESS (if different from Controlling Office): ONRRR, Mr. Robin A. Simpson, Stanford University, 165 Durand Aeronautics Bldg., Stanford, CA 94305 | 15. SECURITY CLASS. (of this report): Unclassified<br>15a. DECLASSIFICATION/DOWNGRADING SCHEDULE |

16. DISTRIBUTION STATEMENT (of this Report)

Scientific Officer — NRL
ONR Branch Office — ONR
ACO — DTIC

Approved for public release; distribution is unlimited.

17. DISTRIBUTION STATEMENT (of the abstract entered in Block 20, if different from Report)

18. SUPPLEMENTARY NOTES

19. KEY WORDS (Continue on reverse side if necessary and identify by block number)

Electric Field Mill
Electric Field Measurements
von Karman's Constant
Convection Over Cooler Water
Boundary Layer Roughness
Formation of Fog
Formation of Stratus Cloud

20. ABSTRACT (Continue on reverse side if necessary and identify by block number)

Studies of the electric field above fog and the construction of a unique electric field mill are described. Work on the formation of fog includes the studies of the surface roughness, von Karman's constant, stratus formation in the convecting marine boundary layer and studies of how convection is initiated and continues in the marine boundary layer when the water is initially colder than the air. These results show why fog is more prevalent over colder water and why fog frequently forms in

DD FORM 1 JAN 73 1473 EDITION OF 1 NOV 65 IS OBSOLETE

SECURITY CLASSIFICATION OF THIS PAGE (When Data Entered)

F-200.1473 *DD Form 1473: Report Documentation Page*

SECURITY CLASSIFICATION OF THIS PAGE(When Data Entered)

20. ABSTRACT (Continued)

ocean areas adjacent to deserts.

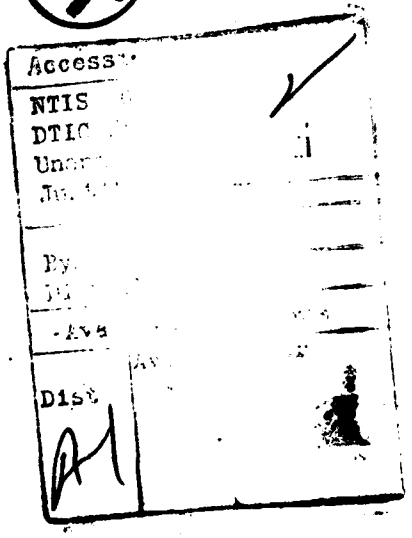


SECURITY CLASSIFICATION OF THIS PAGE(When Data Entered)

TABLE OF CONTENTS

# STUDIES OF THE OCEAN SURFACE AND THE COUPLING BETWEEN THE SEA AND THE ATMOSPHERE

## INTRODUCTION

This contract was in support of an evolving study of marine fog from 1 September 1974 until 31 March 1984. The program began with a small field program to examine electric fields at the top of marine fog and stratus, and in later years evolved into theoretical studies of the structure of fog and the boundary layer surface roughness.

The development and dissipation of marine fog was the scientific topic under investigation. It was clear from the start that entrainment of dry air at fog tops would play a major role in fog dissipation and consequently the electric charge layer at fog tops should show variations related to the entrainment of the charges in the clear air and on the drops residing at the top of the fog, deeper down into the fog. Thus a measurement plan was formulated and carried out with this goal in view. An earlier ONR contract had first supported this work and a new electric field mill design was developed and built for use in this work. A number of new ideas were involved and five patents were assigned to the Navy in the following years (patents dated 11/4/75, 2/10/76, 12/7/76, 3/22/77, 12/27/77, attached). This instrument was particularly suitable to the measurement of electric fields near fogs because, due to its unique design, it worked well in cloud, fog and rain. These conditions are usually a source of severe problems when it is desirable to measure small electric fields, such as needed here.

Aircraft support for the measurement program was obtained from the Research Aviation Facility at the National Center for Atmospheric Research at no cost to the project. In 1976 fourteen flights were made beginning on 9/17/76 and ending 10/8/76 off the California coast near Cape Mendicino. In 1977 sixteen flights were made in the same area beginning 8/22/77 and ending on 9/6/77. In 1978 we proposed to address our principal effort

towards data processing and theoretical analysis.

In the more recent years the effort has been directed towards the theory of the boundary layer and thunderstorm electrification, both being areas of work which were greatly stimulated by the initial efforts on the study of fogs and their electrification.

## DISCUSSION OF ACCOMPLISHMENTS BY YEAR

The developments of the project are documented in a series of reports and scientific papers which are attached in the Appendix.

At the Third Annual Conference on the Physics of Marine Fogs in San Diego, CA, January 7-8, 1975, our presentation was entitled "Natural Marine Fog Charging" by P.B. Wagner and J.W. Telford.

The field mill incorporated a number of new design features which were new and raised a number of questions. These were summarized in a letter (Appendix, Letter 7/21/75) which explained the operating principles in detail and why the enclosing glass cylinder around the electrodes was such an advantage in keeping the device clean and dry without introducing any significant compromises to performance.

A paper was presented at the Fourth Annual Marine Fog Investigation Program Review on January 6, 1976, in Reno. It was entitled "Model of Convection Fog" by S.K. Chai and J.W. Telford.

The work through 1976 was summarized in a document prepared on 12/17/76 to justify further support (see Appendix). Here the background of the cloud physics of fog is discussed. The possibility of electric charges promoting fog droplet coalescence is discussed. However, the stabilizing effect of equal signed charges on droplets is also considered together with the possibilities of introducing opposite charges from a ship to promote coalescence.

The work summary for 1977 is found in the Appendix. We here refer to the theoretical model developed to represent the fields at the edge of a fog when the top surface of the fog carries a charge. The Appendix next contains the flight summary for 1976

and 1977.

A paper was presented at the Fifth Marine Fog Progress Review, Buffalo, NY, April 5-7, 1977, entitled "The Electric and Velocity Fields Near and Within the Tops of Fog Layers of the West Coast" by P.B. Wagner and J.W. Telford.

In 1978 the effort was directed more towards the theoretical work on fog formation and a paper was prepared describing the field mill and the measurements of the charge near the edge of a fog bank. The simple model calculations are plotted against the data (see Appendix, "The Measurement of Atmospheric Electric Fields from Aircraft" by P.B. Wagner and J.W. Telford). Two papers were presented at the Conference on Cloud Physics and Atmospheric Electricity," July 31-August 4, 1978, in Isaquah, WA. The first paper "Dissipation of Marine Stratus" by P.B. Wagner and J.W. Telford (in Appendix) described aircraft observations of the fragmented edge of a stratus layer and analyzed the dynamics associated with the density differences associated with the cloud to clear air transition.

The second paper "On the Formation of Convective Marine Fog" by S.K. Chai and J.W. Telford (in Appendix), described the convective plume model applied to marine stratus and its relationship to our observational restraints.

The work related to sea stratus and fog is summarized in "The Airborne Atmospheric Electricity and Fog Dissipation Program" by P.B. Wagner and J.W. Telford (see Appendix).

In 1979 the work undertaken became largely theoretical with studies of charge transfer during convective activity in cloud and studies of how the boundary layer coupled with the surface.

The paper "Electric Charge Separation in Severe Storms" by J.W. Telford and P.B. Wagner was published in Pure and Applied Geophysics, 117, 891-903 in 1979. This paper analyzed the charges in thermal elements in thunderstorms. It argued that the cooler descending thermal elements formed by entrainment and evaporation at cloud top would preferentially evaporate the smaller ice particles. If the smaller particles were preferentially positively charged and the larger particles negatively

charged, the descending thermals would tend to lose the positive ions left by evaporation of the smaller original ice particles, and hence carry negative charges downwards. This would give negative charges lower down and positive higher up. It would also tend to accumulate the negative charge at about the -10°C level, where the descending thermals would tend to become more buoyant by virtue of the rising liquid water cloud below and around them. Before freezing the liquid water cloud is slightly colder and denser than after freezing, when the latent heat of freezing is released.

This paper was followed by a much more extensive study "Cloud Dynamics and an Electric Charge Separation Mechanism in Convective Clouds" by P.B. Wagner and J.W. Telford. Here the ideas of the previous paper were extended to study the effects of cosmic ray ionization in the descending thermal entity. Since the descending parcel will have fewer particles because they are rapidly evaporating then fewer of the cosmic ray charged ions will be captured in the entity as compared to the rising air around it, and hence the entity will have a higher conductivity than the rest of the cloud. The fair weather field will thus transfer positive charges from the descending entity into the air flowing back around it, at its front edge. The descending entities will thus transport negative charge downwards regardless of any charging propensities of the ice particles of different sizes. The negative charge will again accumulate at about the -10°C level and the positive charge will be carried higher up. The field from the separated charges will augment the earlier field so the charging rate will increase and the charge separated will grow exponentially. A mathematical model in the paper showed that the rate of growth, and charges separated, are in reasonable agreement with observations of thunderstorms.

The studies of how the convective theory could take account of the sea surface in matching the fluxes to the atmospheric conditions, lead to a detailed study of surface roughness. As a preliminary to studying the surface roughness of waves and ripples, a study was undertaken of an ideal roughness surface of

identical thin cylinders of equal height standing on end and close enough that the mounting surface was not involved in the drag. A physical description of the process using entraining slabs of turbulent air allowed the roughness length to be derived in terms of the area of the cylinders per unit area perpendicular to the wind direction per unit length downwind, and the drag coefficients of the cylinders. The result is close to measurements made in wind tunnels (see Appendix, "The Surface Roughness and Planetary Boundary Layer" by J.W. Telford, Pure and Applied Physics, 119, 278-293, 1981).

This study was followed by more detailed analysis of the turbulent slabs (or layers parallel to the surface) of air against the interface. The horizontal momentum passes down from slab to slab until it is absorbed by the drag of the surface roughness elements. These slabs are constrained in thickness to meet similarity considerations relative to the surface boundary in neutral conditions. The slabs are an average concept, and to derive the surface roughness length it was necessary to allow the slabs to be centered at any height, but with a probability density which gives the logarithmic profile when the nth slab retains the same velocity as it varies up and down in height. The range of variation in height is enough to bridge the gap to the next slab, so that the probable height of the slabs varies continuously from height to height, and its thickness varies at the same time to maintain a thickness as a constant ratio of the height. Note that for each slab the average turbulence, average horizontal velocity and average dissipation rate are still used. The velocity at any given level matches the logarithm profile velocity because each level experiences some time in each of two adjacent slabs with different velocities and the probability of the slab being at each level then gives the average velocity at that level.

The von Karman constant can be derived by the additional assumption that the dissipation rate of the turbulence in each instantaneous realization of each slab is determined by the corresponding thickness of the slab at that moment. By averaging

the dissipation rate at a given height, for all possible height variations of the slabs covering a fixed point, in the same way the velocity profile was derived from a similar averaging, this average dissipation rate can be estimated. It is then compared to the dissipation rate found by treating the whole depth of the layer below the level concerned as half of a parallel channel, where the same principles give another estimate of the dissipation rate. This comparison leads directly to a value for von Karman's constant of, $k = 0.37$. Channel flow gives $k = 0.40$ while atmospheric boundary layer measurements have given $k = 0.35$. The new value of k also improves the fit of the calculated boundary layer roughness length to the experimental values. This analysis is published in the paper "A Theoretical Value of von Karman's Constant" by J.W. Telford, Pure and Applied Geophysics, 120, 648-661, 1982 (see Appendix for papers).

In 1982 the work turned more towards seeking an explanation of how the convection over the sea was determined. The first effort related to convection over warm water and was then extended to convection over cooler water. The earlier model for dry air convection was modified to allow the formation of stratus clouds at the top of the convecting layer. Once it is recognized that turbulent entrainment at cloud tops is negligible, compared to density driven negatively buoyant entrainment produced by the evaporation of cloud drops in parcels of dry air mixed in cloud top, then the whole structure of the stratus and fog formation and dissipation cycle becomes accessible.

A preliminary paper was presented at the Conference on Cloud Physics, November 15-18, 1982 in Chicago. The paper was entitled "Fog, Stratus and Cumulus Formation in Warm Air Over Cooler Water" by J.W. Telford and S.K. Chai.

Continued work resulted in a paper "Convective Model for Stratus Cloud Over a Warm Water Surface" by S.K. Chai and J.W. Telford which was published in Boundary Layer Meteorology, 26, 25-49, 1983. This paper established many of the principles involved and set down the equations. It gave quantitative estimates for the case of lowering of cloud base to form fog, and

the dissipation rate at a given height, for all possible height variations of the slabs covering a fixed point, in the same way the velocity profile was derived from a similar averaging, this average dissipation rate can be estimated. It is then compared to the dissipation rate found by treating the whole depth of the layer below the level concerned as half of a parallel channel, where the same principles give another estimate of the dissipation rate. This comparison leads directly to a value for von Karman's constant of, $k = 0.37$. Channel flow gives $k = 0.40$ while atmospheric boundary layer measurements have given $k = 0.35$. The new value of k also improves the fit of the calculated boundary layer roughness length to the experimental values. This analysis is published in the paper "A Theoretical Value of von Karman's Constant" by J.W. Telford, Pure and Applied Geophysics, 120, 648-661, 1982 (see Appendix for papers).

In 1982 the work turned more towards seeking an explanation of how the convection over the sea was determined. The first effort related to convection over warm water and was then extended to convection over cooler water. The earlier model for dry air convection was modified to allow the formation of stratus clouds at the top of the convecting layer. Once it is recognized that turbulent entrainment at cloud tops is negligible, compared to density driven negatively buoyant entrainment produced by the evaporation of cloud drops in parcels of dry air mixed in cloud top, then the whole structure of the stratus and fog formation and dissipation cycle becomes accessible.

A preliminary paper was presented at the Conference on Cloud Physics, November 15-18, 1982 in Chicago. The paper was entitled "Fog, Stratus and Cumulus Formation in Warm Air Over Cooler Water" by J.W. Telford and S.K. Chai.

Continued work resulted in a paper "Convective Model for Stratus Cloud Over a Warm Water Surface" by S.K. Chai and J.W. Telford which was published in Boundary Layer Meteorology, 26, 25-49, 1983. This paper established many of the principles involved and set down the equations. It gave quantitative estimates for the case of lowering of cloud base to form fog, and

showed that radiative cooling at cloud top would be relatively unimportant.

The efforts in 1983 were concerned with producing a paper which clearly stated the determining factors for stratus and fog formation over cooler water. In order to proceed with calculations of how convection could be driven by the density of the water vapor leaving the sea surface, the thermodynamics of the mixing of cloudy air with either cloudy air or clear air had to be completely recast to achieve the necessary accuracy of 0.0001°C, between alternative thermodynamic paths. This is because the virtual temperature differences between updraft and downdraft were only a few times 0.01°C. This analysis showed that fog can form when the air is ten degrees centigrade or more warmer than the water surface, and that these are the conditions which favor fog formation. Air heated over the desert and blowing back out to sea near San Diego is ideal for fog or stratus formation, as we all know. The reason is that the warmer air limits surface convection to a relative low level which can be saturated more readily by the sea surface moisture flux.

The paper explaining this phenomenon "Inversions, and Fog, Stratus and Cumulus Formation in Warm Air Over Cooler Water" by J.W. Telford and S.K. Chai has just been published in Boundary Layer Meteorology.

## SUMMARY

This grant began with studies of the electric field above stratus and fog layers and verified that such measurement could be obtained on a routine basis. This work emphasized the need for a better understanding of fog and cloud top entrainment and the need for simultaneous measurements of drop sizes and conductivity in the cloud.

The theoretical work has generated a model which has explained the major features of fog formation and entrainment. The understanding of the surface boundary has been advanced by this work to the point where the basic theory for computing the surface roughness length and surface drag are in sight.

Future work needs to be in two categories. First, direct observation of fog and stratus top entrainment is needed, with some form of tracing material to directly verify the stop-start nature of entrainment, both observed and explained theoretically.

Secondly, the sea surface wave and ripple structure needs to be observed in the open ocean from aircraft where other parameters are directly observed at the same time. In addition, the theoretical advances in understanding surface roughness, developed under this contract, need to be pursued vigorously, so that the relationships between the generation of ripples by the wind and the way the ripples produce an equivalent roughness height to control the air flow, can be established with a physical theory.

# APPENDIX

Electric field mill which was flown in past years on a nose boom: This tail mounting proved satisfactory despite some vibration. Lower supports mounted in rubber provided added stiffness and dampening.


Close-up of rotating cylindrical electric field mill: Note glass enclosed capacitive plates and compensation probe beneath cylinder to offset effects of the aircraft tail. The writing pen provides a size reference.

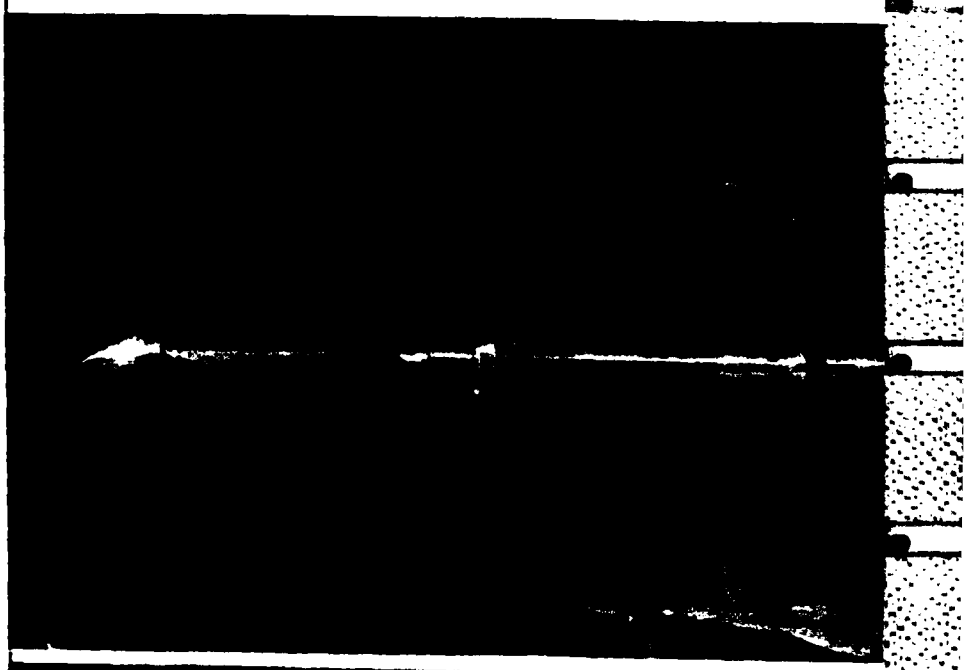

Electricalconductive cell: This Gerdian-type cell is capable of measuring both ionic components of electrical conductivity as well as total small ion population. Air turbine at the rear of the tube measures flow rates. An electrometer amplifier and other electronics are the housing above the tube.

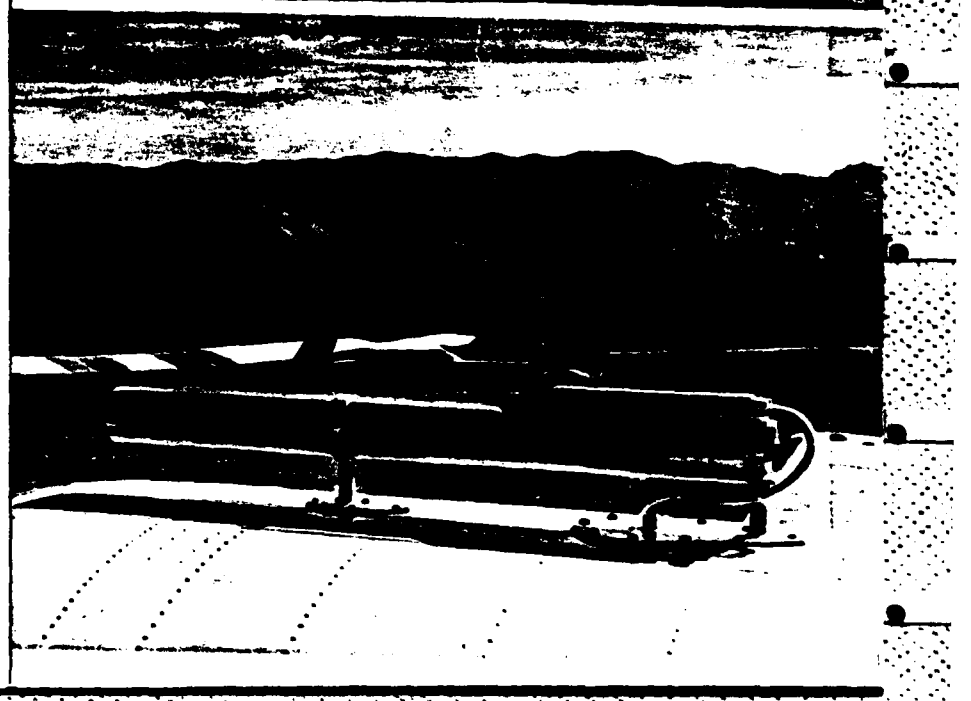

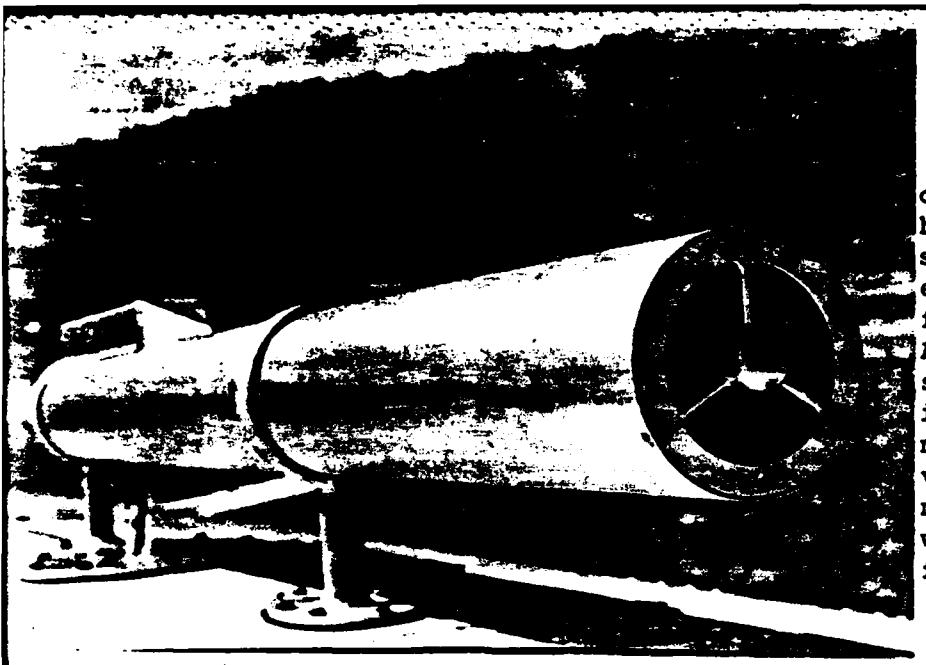

Front view of conductivity cell: The large difference between inner and outer shell sizes is utilized to minimize effects of fringing electric fields in the electrode area. An electrical problem which surfaced in 1975 during fligh in rain has been solved. A mechanical problem caused by vibration of the new roof mount was noted this year and will be corrected before further use.

New vertical electric field mill: Functionally similar to the rear mounted mill, this mill measures the horizontal field components. Note the taped ground plane and glass enclosed capacitive plates.

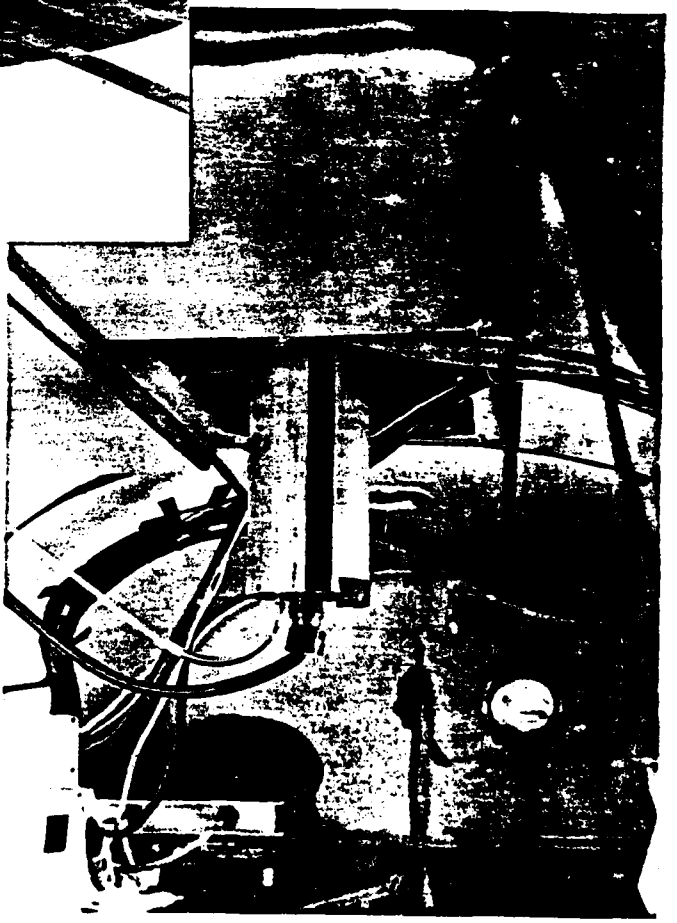

Interior projection of new mill: During the 1976 experiment this mill performed credibly in overcast conditions and in fog, however it proved to be sensitive to sun angle in bright sunlight This effect was unexpected and is perhaps an effect of the sun on the aircraft paint and skin charging beyond the ground plane. No further explanation is known, and more investigation will be necessary. Note the clear tube for dry air. Circulation of dry air has proven to be an excellent way to maintain electrical integrity of all the above instruments in wet conditions.

rec'd 2/12/76


# United States Patent [19]

**Wagner et al.**

[11] **3,917,996**

[45] **Nov. 4, 1975**


## [54] ELECTRIC FIELD MEASURING DEVICE


[75] Inventors: Peter B. Wagner; James W. Telford; Richard W. Hanaway, all of Reno, Nev.

[73] Assignee: The United States of America as represented by the Secretary of the Navy, Washington, D.C.



[22] Filed: July 5, 1974

[21] Appl. No.: 486,035

[52] U.S. Cl. ..... 324/72; 324/139; 324/144

[51] Int. Cl.[2] ..... G01R 31/02

[58] Field of Search ..... 324/72, 139, 144; 250/236



[56] References Cited

UNITED STATES PATENTS

3,691,392 9/1972 Tringali ..... 250/236



*Primary Examiner*—Alfred E. Smith
*Assistant Examiner*—Michael J. Tokar
*Attorney, Agent, or Firm*—R. S. Sciascia; Charles D. B. Curry



[57] ABSTRACT

An electric field measuring device that is particularly suited for being mounted on the nose boom of an aircraft for periodically measuring the atmospheric electric field intensity and orientation. The device includes a rotating assembly that includes a pair of capacitor plates, analog signal processing equipment, digital processing equipment, a slip ring assembly, orientation light transmitter and receiver assemblies and an information light transmitter. All of these elements are mounted on a rotatable shaft that is driven by an electric motor. The light from the rotating information light transmitter is received by a stationary information light receiver, the output of which is applied to the input of a stationary digital receiver and storage device. Floating D. C. power is transmitted by a brush assembly through the slip ring assembly to the rotating electrical equipment.


3 Claims, 3 Drawing Figures

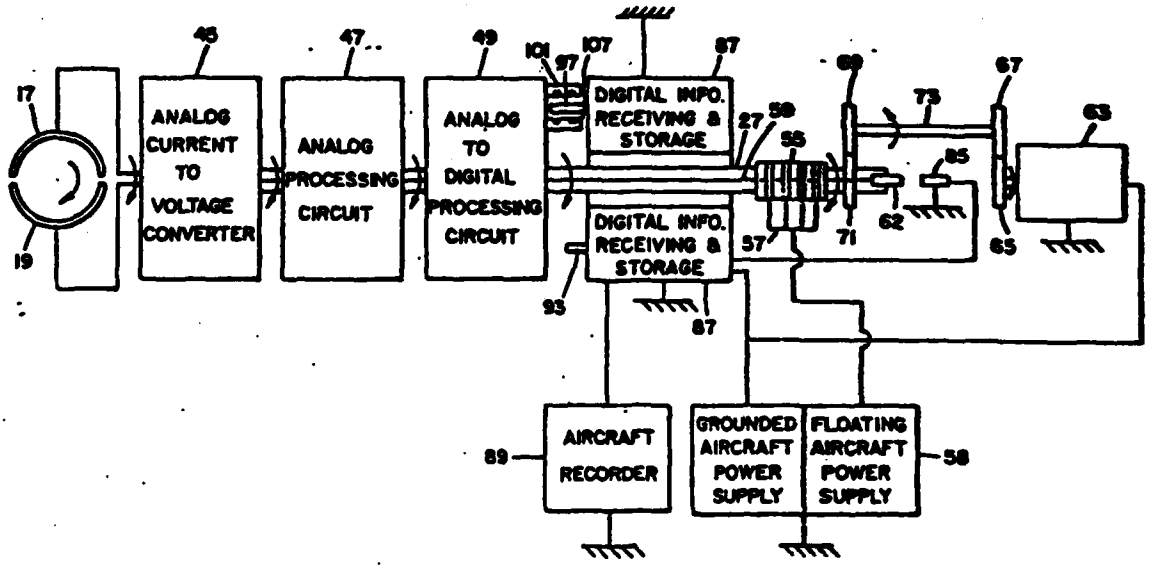

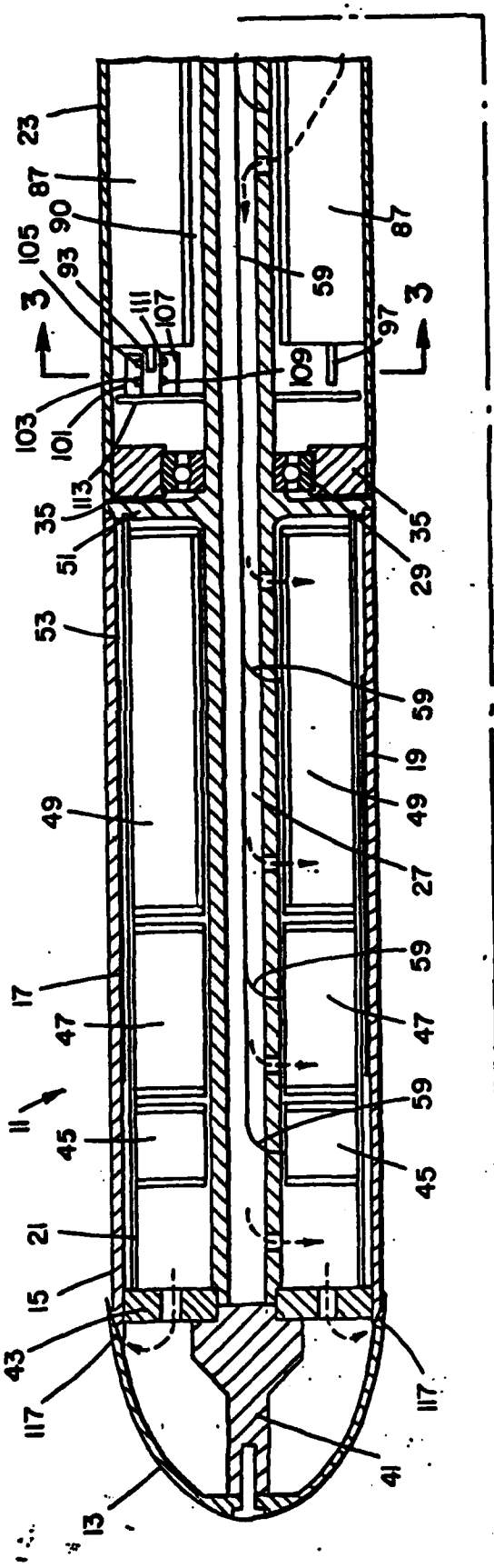
23
87
105
90
93
3
111
107
59
87
97
3
109
103
101
113
35
51
29
35
53
59
19
49
49
27
59
17
47
47
59
11
45
45
21
15
43
117
117
41
13

FIG_3

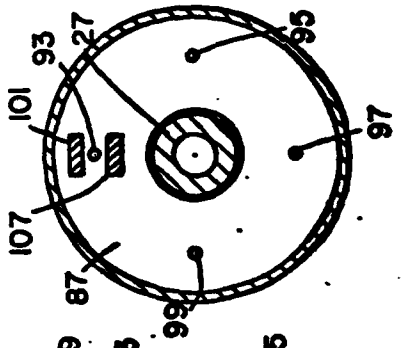
93
27
95
101
97
107
87
99

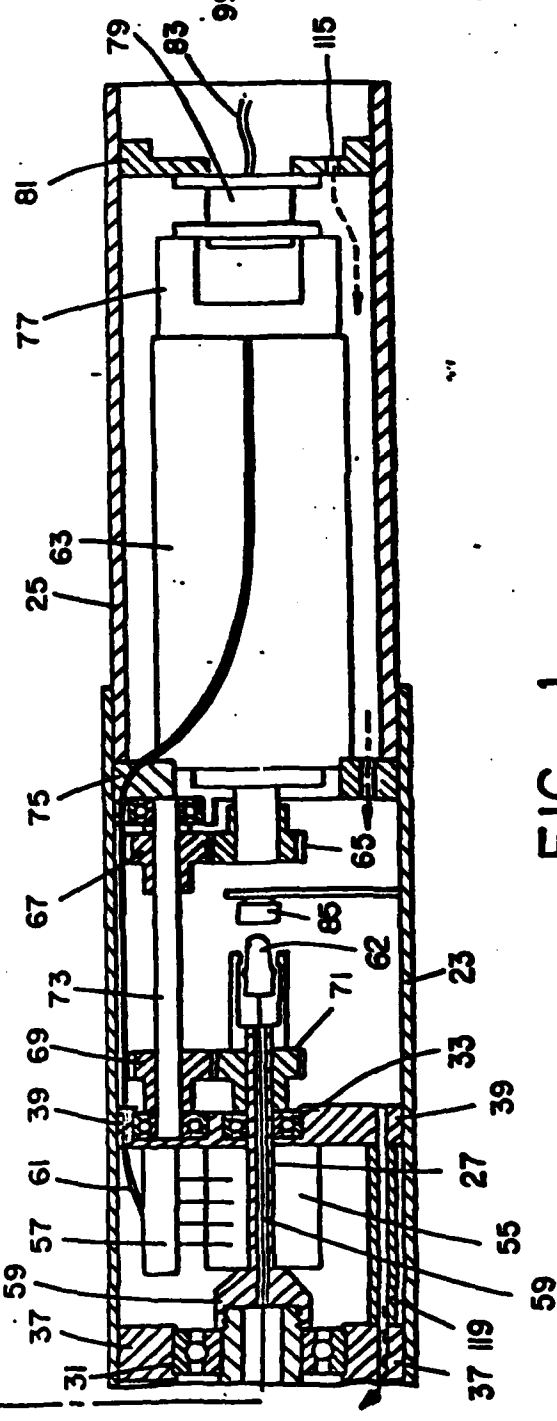
79
83
115
81
77
63
25
75
65
67
85
62
23
73
71
69
33
39
39
61
27
57
55
59
59
37
37 119
31

FIG_1

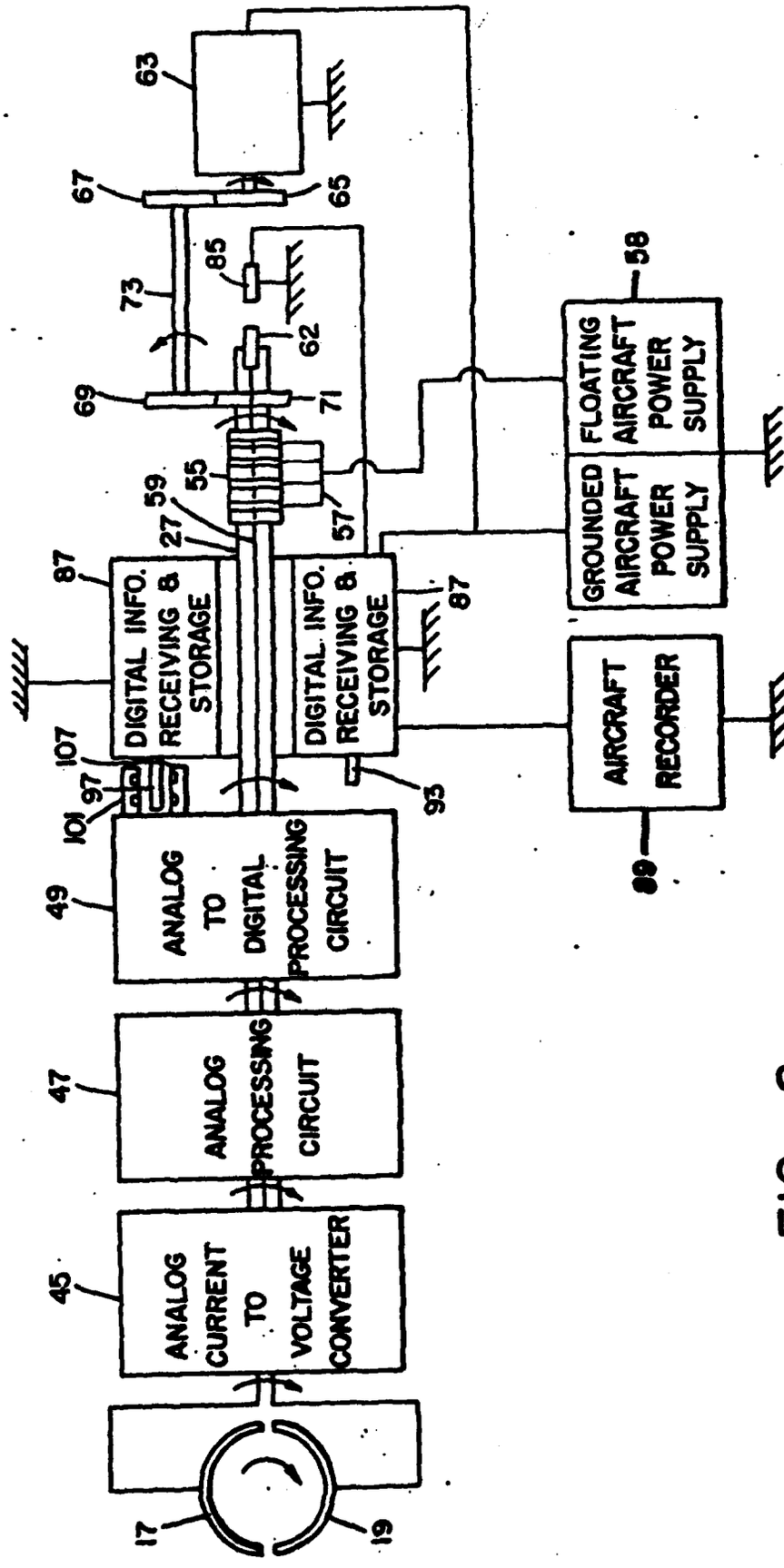
63
67
65
73
85
62
69
71
59
55
27
57
87
87
87
107
97
101
93
49
47
45
17
19
ANALOG CURRENT TO VOLTAGE CONVERTER
ANALOG PROCESSING CIRCUIT
ANALOG TO DIGITAL PROCESSING CIRCUIT
DIGITAL INFO. RECEIVING & STORAGE
DIGITAL INFO. RECEIVING & STORAGE
AIRCRAFT RECORDER
89
GROUNDED AIRCRAFT POWER SUPPLY
FLOATING AIRCRAFT POWER SUPPLY
58

FIG_2

# ELECTRIC FIELD MEASURING DEVICE

## BACKGROUND OF THE INVENTION

1. Field of the Invention

The present invention relates to an electric field measuring device and more particularly to a very sensitive electric field measuring device for measuring atmospheric electric fields.

2. Description of the Prior Art

Prior rotating electric field measuring devices have been too bulky and heavy, particularly for mounting on small aircraft booms. In addition, they exhibit measuring sensitivities limited excessively by noise in brush contacts to rotating shields and/or the noise effects of brushes or other electrical coupling upon analog signal transmission between rotating and stationary members. The present invention overcomes these difficulties by employing uniquely cooperating rotating and stationary assemblies that are compact, light weight and efficient. Moreover, the present invention employs a unique optical information technique that eliminates brush noise in the transmitted information signal.

## SUMMARY OF THE INVENTION

Briefly, the present invention comprises an electric field measuring device that is particularly suited for being mounted on the nose boom of an aircraft for periodically measuring the atmospheric electric field intensity and orientation. The device includes a rotating assembly that includes a pair of capacitor plates, analog signal processing equipment, digital processing equipment, a slip ring assembly, orientation light transmitter and receiver assemblies and an information light transmitter. All of these elements are mounted on a rotatable shaft that is driven by an electric motor. The light from the rotating information light transmitter is received by a stationary information light receiver, the output of which is applied to the input of a stationary digital receiver and storage device. Floating D.C. power is transmitted by a brush assembly through the slip ring assembly to the rotating electrical equipment.

## STATEMENT OF THE OBJECTS OF THE INVENTION

An object of the present invention is to provide an electric field measuring device that is compact and light weight;

Another object of the present invention is to provide an electric field measuring device that is accurate and very sensitive;

Still another object of the present invention is to provide an electric field measuring device that minimizes noise in the information signal;

Still another object of the present invention is to provide an electric field measuring device that may be mounted on an aircraft to measure atmospheric field intensity;

A still further object of the present invention is to provide an electric field measuring device that may be mounted on the nose of an aircraft to measure the atmospheric field orientation; and

A still further object of the present invention is to provide orientation of the rotating member with respect to the stationary member by interrupting light from optical devices;

A still further object of the present invention is to provide an electric field measuring device that optically transmits the information signal from a rotating member to a stationary member.



Other objects, advantages and novel features of the present invention will become apparent from the following detailed description of the invention when considered in conjunction with the accompanying drawings wherein:

## BRIEF DESCRIPTION OF THE DRAWINGS

FIG. 1 is a side elevation of the electric field measuring device of the present invention which illustrates the overall system and the arrangement of components;

FIG. 2 is a block diagram of the electrical system of the electric field measuring device of the present invention; and

FIG. 3 is a section view taken at section 3—3 of FIG. 1 and illustrates the optical orientation technique employed in the electric field measuring device of the present invention.

## DESCRIPTION OF THE PREFERRED EMBODIMENT

The purpose of the electric field measuring device of the present invention is to measure the electric field in atmosphere. This is achieved by positioning the electric field measuring device at different locations within the atmospheric electric field. In accordance with the present invention this is preferably achieved by mounting the electric field measuring device on the nose of an aircraft and periodically measuring the electric field intensity and orientation as the aircraft flies through the atmosphere. The electric field is measured in two of its three vector components, namely the horizontal and vertical components. To achieve this objective the electric field measuring device is mounted to be cylindrically symmetric with the nose boom of the aircraft wherein the nose boom preferably extends several feet in front of the aircraft center. In this manner the charge on the aircraft will have a minimum effect on the field measurement made by the electric field measuring device. It is to be understood that the third or axial component of the electric field may be measured, along with either the horizontal or vertical components, by orienting a second electric field measuring device in a direction that is normal to axis of the first electric field measuring device. It is also to be understood that the noise rejection system of the electric field measuring device of the present invention may be used on any device where it is necessary to transmit power from a stationary member to a rotating member and to transmit information from a rotating member to a stationary member.

In FIG. 1 is a side elevation of the electric field measuring device 11 of the present invention which illustrates the overall system and the arrangement of components. FIG. 2 is a block diagram illustrating the electrical system of the electric field measuring device 11 of the present invention. Referring to FIG. 1, electric field measuring device 11 includes a nose cone 13, an outer cylindrical glass insulating sleeve 15, a pair of capacitive plates 17 and 19 (see also FIG. 2), an interior cylindrical shield 21, a centrally positioned outer stationary cylindrical sleeve 23 and a rearwardly positioned outer stationary cylindrical sleeve 25. Capacitive plates 17 and 19 are preferably metal foil that are mechanically and electrically separated and are attached to the interior surface of glass insulating sleeve 15.

An elongated hollow shaft 27 is rotatably supported by bearings 29, 31 and 33 which are respectively supported by metal support members 35, 37 and 39 which are supported by outer stationary cylindrical sleeve 23. The nose cone 13 is connected to the forward end of rotatable hollow shaft 27 by support members 41 and 43.

Referring to FIGS. 1 and 2 concentrically mounted on the forward section of shaft 27 are analog current to voltage converter 45, analog processing circuit 47 and analog to digital processing circuit 49. Circuits 45, 47 and 49 are packaged in a cylindrical configuration with an opening in the center. These circuits are packaged to slide over shaft 27 and within cylindrical shield 21 to provide a force fit and a rigid interconnection. Electrical plugs, not shown, are provided to electrically and mechanically interconnect these circuits. Referring to FIG. 1, a collar 51 extends from shaft 27 to support one end of sleeve 15, the other end of which is supported by support member 43. An air gap 53 is provided between sleeve 15 and shield 21 to prevent shorting of capacitive plates 15 and 17.

Cylindrically mounted on the rearward part of shaft 27, having a small diameter, is slip ring assembly 55 which is used to transmit D.C. power to circuits 45, 47 and 49. This is achieved by transmitting power to a plurality of slip rings of slip ring assembly 55 from the brushes of brush assembly 57 which are connected to a floating aircraft power supply 58. Although not shown, for reasons of clarity, each slip ring is connected to a wire which passes through the hollow section of shaft 27 to the various electrical packages 45, 47 and 49 as generally indicated by electrical cable 59. D.C. power is transmitted through cable 61 to brush assembly 57 from the floating aircraft power supply 58 of FIG. 2.

Connected to the rearward end of rotatable hollow shaft 27 is light transmitter 62 which is preferably capable of transmitting infra-red light. Light transmitter 62 is connected to the output of analog to digital processing circuit 49, as generally indicated by cable 59. Preferably circuit 49 controls light transmitter 62 to convey information by means of a pulse width modulated signal.

Shaft 27 is rotated by means of electric motor 63 through gears 65, 67, 69 and 71. Gears 67 and 69, which are connected by shaft 73, are made of a dielectric material, preferably nylon, to prevent electrical coupling between the motor armature and the rotating assembly. Electrical coupling to the rotating assembly is undesirable because the motor armature normally has brush noise.

The forward end of the electric motor 63 is supported by support member 75 which is attached to support 39. Connected to the rear end of motor 63 is electrical connector assembly 77. A connector plug 79 (having a plurality of pins, not shown) is connected to the assembly 77 and is supported by support member 81 which is connected to sleeve 25. An electrical cable 83 is connected from the connector plug 79 to the equipment on board the aircraft.

The pulse modulated light from rotating light transmitter 62 is transmitted to stationary light receiver 85. As illustrated in FIG. 2, the output of stationary light receiver 85 is applied to the input of stationary digital information receiver and storage circuit 87, the output of which is connected to an aircraft recorder 89. The package containing digital information receiver and storage circuit 87 has a cylindrical configuration, has a concentric opening 90, and is rigidly connected to stationary cylindrical sleeve 23. The concentric opening 90 is sufficiently large to allow free rotation of shaft 27.

Referring to FIGS. 1, 2 and 3, the forward end of the package containing circuit 87 has extending therefrom stationary pins 93, 95, 97 and 99. Pins 93, 95 and 99 are short and pin 97 is long. Mounted on rotating shaft is orientation light transmitting assembly 101 having light transmitters 103 and 105, and orientation light receiver 107 having light receivers 109 and 111. The light transmitter assembly 101 and the light receiver assembly 107 are mounted on support member 113 in spaced apart relationship and with light transmitter 103 in alignment with light receiver 109 and light transmitter 105 in alignment with light receiver 111. The length of short pins 93, 95 and 99 are selected to interrupt the light transmitted from light transmitter 105 and the length of pin 97 is selected to interrupt the light from light transmitters 103 as well as 105. From this it can be seen that 90°, 180°, 270° and 360° reference positions of shaft 27, and the rotating assembly, are electrically determined. Also a positive 360° reference is available because pin 97 interrupts the light from light transmitter 103 once each revolution or at 360°. This provides the required orientation of the rotating assembly with respect to the stationary assembly.

The electric field measuring device 11 of the present invention is prevented from collecting condensate, due to cooling, by passing dry air through both the stationary and rotating assemblies. This is indicated by the dotted line arrows in FIG. 1. Dry air, which is supplied by an aircraft source, enters through opening 115 in support member 81 and exits through a plurality of opening 117 formed around the periphery of the rear section of the nose cone 13. It should be noted however, that the section containing the slip ring assembly 55 and brush assembly 57 is sealed and dry air is bypassed through conduit 119.

The dielectric cylinder 15 is preferably made of glass. Although glass has lesser dielectric characteristics then teflon, teflon is not employed because it can maintain an unwanted charge on the surface due to handling and the like. Also capacitor plates 17 and 19 are preferably mounted on the interior of the sleeve to maintain them in a dry condition rather than on the exterior.

What is claimed is:

1. An electric field measuring device comprising:
   a. a rotatable assembly;
   b. a stationary assembly;
   c. said rotatable assembly including means for providing an electrical signal that contains information defining a condition;
   d. said electrical signal being operably connected to an optical transmitter;
   e. said optical transmitter being operably connected to said rotatable assembly;
   f. an optical receiver being operably connected to said stationary assembly and positioned to provide an optical coupling with the optical signal from said optical transmitter;
   g. said rotatable assembly including a sleeve made of dielectric material;
   h. said means includes first and second capacitor plates and signal processing means;
   i. said first and second capacitor plates being spaced apart and operably connected to said sleeve;
   j. said first and second capacitor plates being operably connected to the input of said signal processing

means; and

k. the output of said signal processing means being operably connected to the input of said optical transmitter.

2. The device of claim 1 including:

a. an orientation optical transmitter assembly and an orientation optical receiver assembly being operably connected to said rotatable assembly and being spaced apart and spaced from the rotational axis of said rotatable assembly; and

b. an orientation means operably connected to said stationary assembly for interrupting the transmission of energy from said orientation optical transmitter assembly to said orientation optical receiver assembly.

3. The device of claim 2 wherein:

a. said orientation means including a plurality of spaced apart pins wherein one of said pins has a greater length than the other pins to provide a rotational orientation with respect to the other pins.

* * * * *

N.C. 57,922


# United States Patent [19]

Wagner et al.

[11] 3,938,029

[45] Feb. 10, 1976


[54] LOW NOISE DC POWER SUPPLY SYSTEM FOR ELECTRONICS ON A ROTATING ASSEMBLY


[75] Inventors: Peter B. Wagner; James W. Telford, both of Reno, Nev.

[73] Assignee: The United States of America as represented by the Secretary of the Navy, Washington, D.C.



[22] Filed: July 5, 1974

[21] Appl. No.: 486,036

[52] U.S. Cl. ..... 323/2; 307/154

[51] Int. Cl.[2] ..... H02J 1/00

[58] Field of Search ..... 307/149, 150, 151, 154; 310/72; 317/262 R; 321/2, 10; 323/1, 2, 93, 100



[56] References Cited

UNITED STATES PATENTS

| | | | |
|---|---|---|---|
| 2,008,377 | 7/1935 | Whitaker | 310/72 X |
| 2,015,667 | 10/1935 | Fleming et al. | 310/72 |
| 3,665,291 | 5/1972 | Weischedel et al. | 321/2 X |
| 3,736,491 | 5/1973 | Kuster | 321/2 X |



*Primary Examiner*—A. D. Pellinen

*Attorney, Agent, or Firm*—R. S. Sciascia; Charles D. B. Curry



[57] ABSTRACT

A low noise D. C. power supply system that is particularly suited for supplying D. C. power from a stationary source to electronics equipment mounted on a rotating assembly. Brush and slip ring assemblies are used to transfer the D. C. power to the rotating assembly and brush noise is minimized by having non-inductive impedences on both sides of the brush and slip ring assemblies. Floating circuits are employed to transfer the D. C. power from the stationary assembly to the rotating assembly with the return reference ground being through the brush and slip ring assemblies to the stationary assembly. Higher than usual voltages are supplied to a capacitor mounted on the rotating assembly to charge the capacitor providing reserve energy storage, providing a voltage margin for further regulation and thus minimizing the effect of brush noise.


6 Claims, 2 Drawing Figures

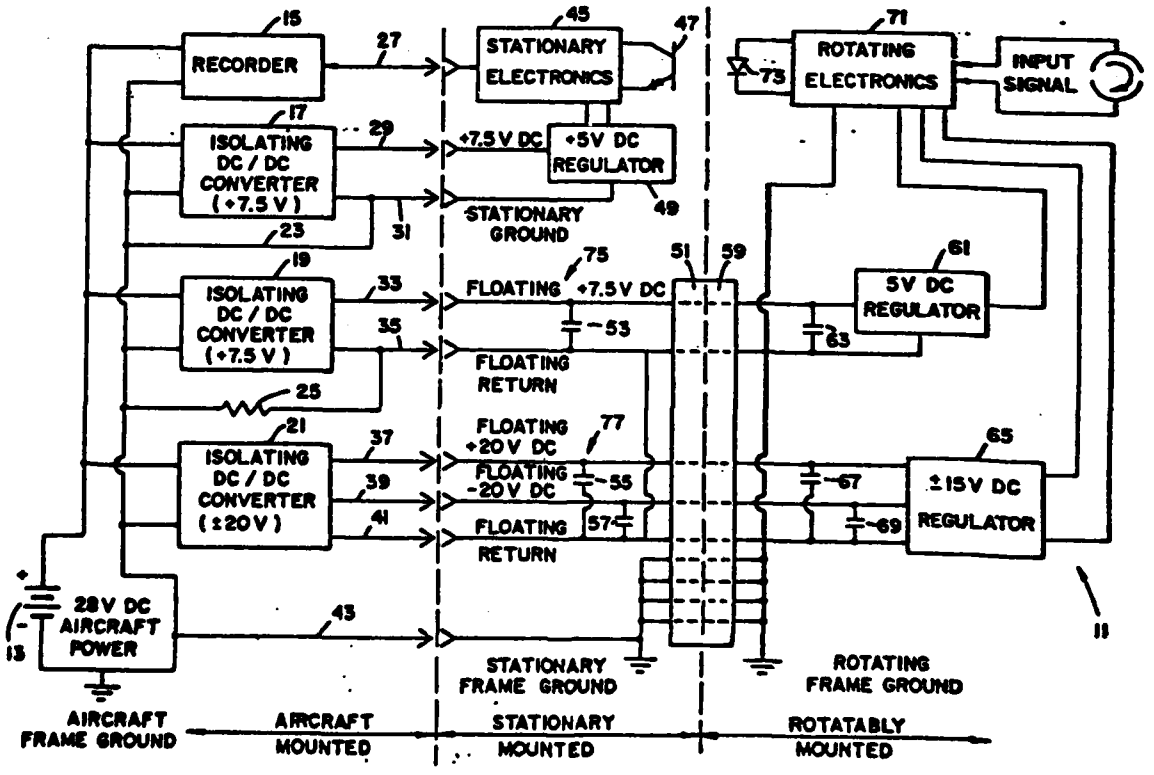

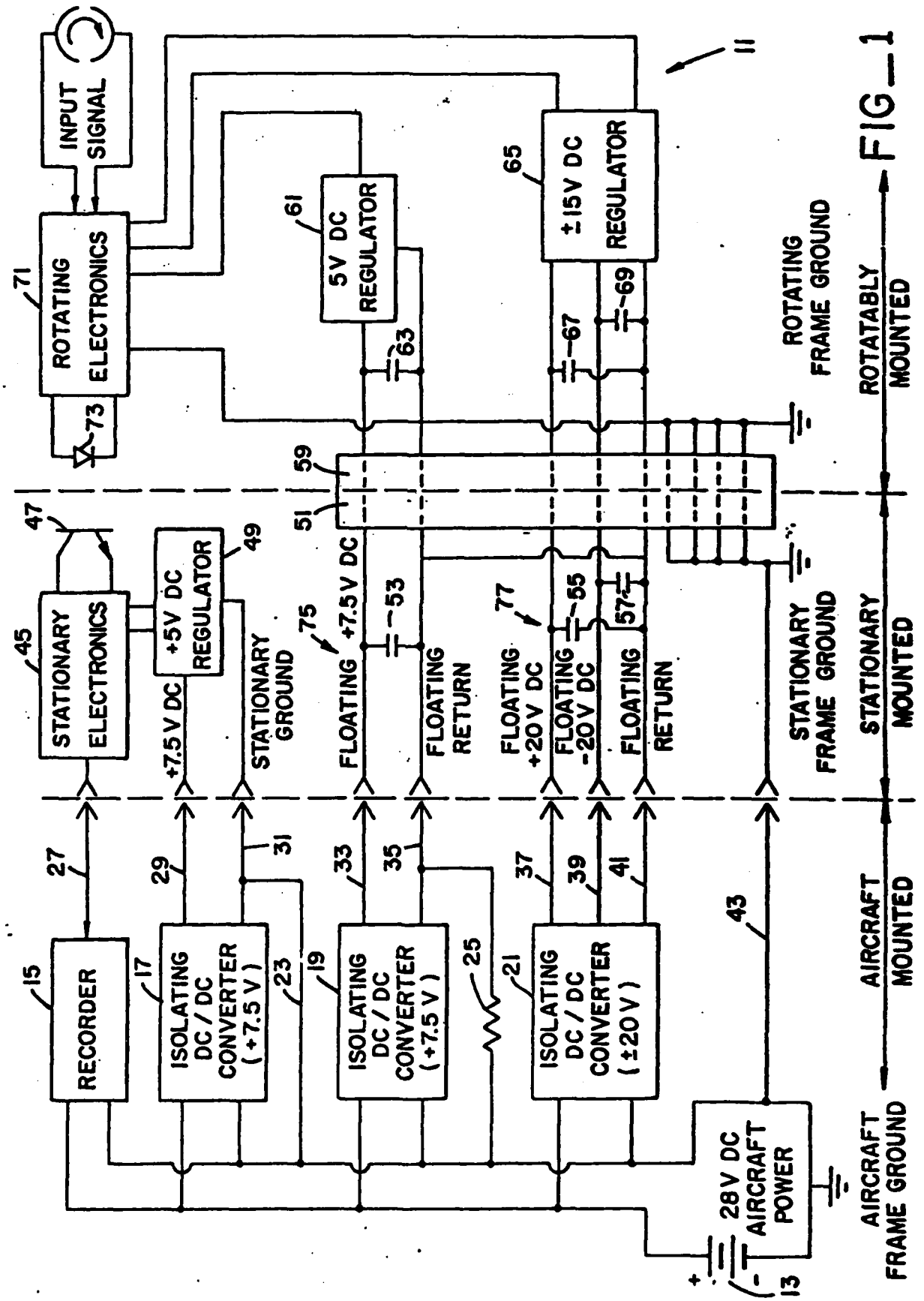
INPUT SIGNAL
ROTATING ELECTRONICS
71
73
5V DC REGULATOR
61
63
±15V DC REGULATOR
65
67
69
11
ROTATING FRAME GROUND
ROTATABLY MOUNTED
59
51
47
STATIONARY ELECTRONICS
45
+5V DC REGULATOR
49
+7.5 V DC
STATIONARY GROUND
75
+7.5 V DC
FLOATING
53
FLOATING RETURN
77
FLOATING +20 V DC
55
FLOATING -20 V DC
57
FLOATING RETURN
STATIONARY FRAME GROUND
STATIONARY MOUNTED
27
29
31
33
35
37
39
41
43
RECORDER
15
ISOLATING DC/DC CONVERTER (+7.5 V)
17
23
ISOLATING DC/DC CONVERTER (+7.5 V)
19
25
ISOLATING DC/DC CONVERTER (±20 V)
21
AIRCRAFT MOUNTED
28 V DC AIRCRAFT POWER
13
AIRCRAFT FRAME GROUND

FIG_1

FIG_2

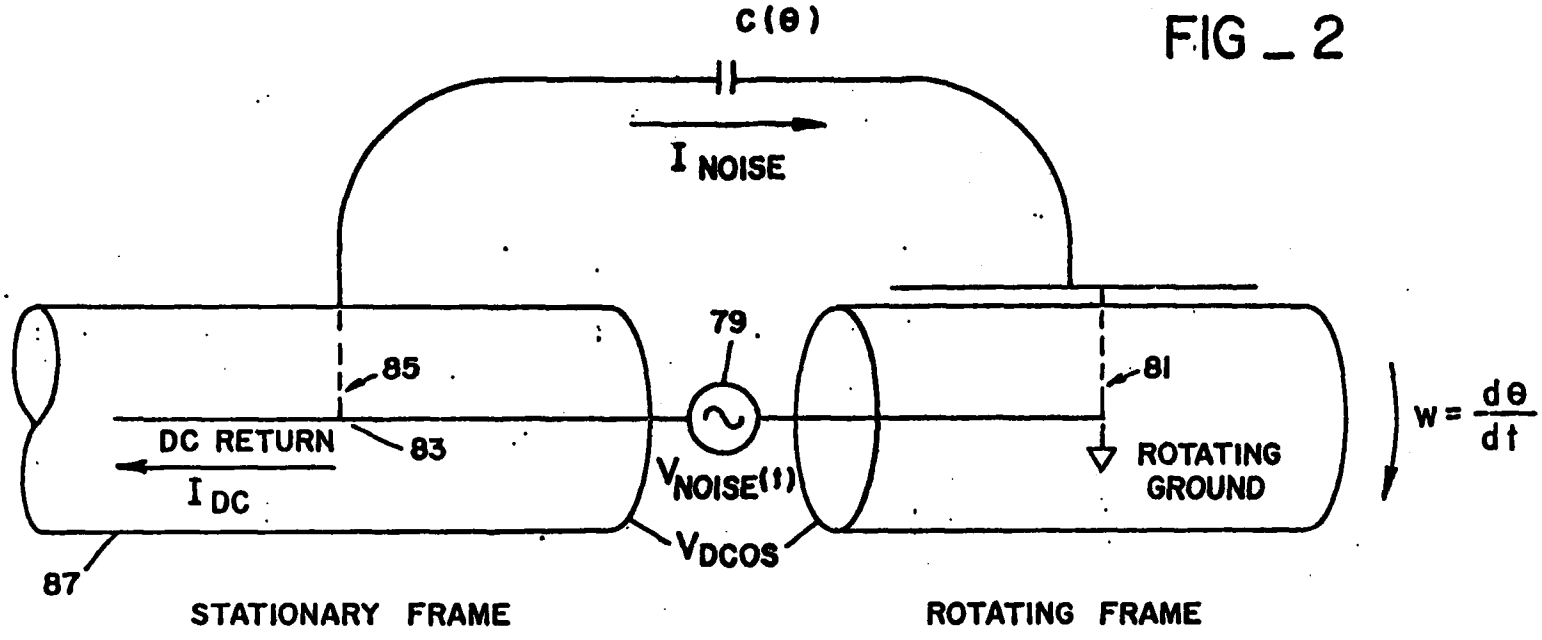


$$I_{NOISE} = \frac{d}{dt}\left[\frac{V_{DCOS}-V_{NOISE}}{C(\theta)}\right]$$

$$\simeq \frac{1}{C(\theta)}\frac{d}{dt}V_{NOISE} + V_{DCOS}\frac{d}{dt}\frac{1}{C(\theta)}$$

$$\simeq \frac{V'_{NOISE}}{C(\theta)} + V_{DCOS}\frac{C'(\theta)}{C^2(\theta)}$$

# LOW NOISE DC POWER SUPPLY SYSTEM FOR ELECTRONICS ON A ROTATING ASSEMBLY

## BACKGROUND OF THE INVENTION

1. Field of the Invention

The present invention relates to a power supply system and more particularly to a low noise floating D. C. power supply system.

2. Description of the Prior ARt

Low-noise D. C. power is normally required for satisfactory operation of sensitive electronic equipment. When the electronic equipment is mounted on a rotating shaft the supply of the D. C. power is normally through brushes to slip rings mounted on the shaft or by mounting a D. C. battery on the rotating shaft itself. Brushes in contact with slip rings are invariably a source of noise due to varying resistance during rotation. Batteries are normally heavy, bulky and must be periodically replaced or recharged. The floating D. C. power supply system of the present invention overcomes these difficulties by providing a D. C. power supply system for electronics mounted on a rotating assembly that has low noise characteristics and is of small size and weight.

## SUMMARY OF THE INVENTION

Briefly, the present invention comprises a low noise D. D. power supply system that is particularly suited for supplying D. C. power from a stationary source to electronics equipment mounted on a rotating assembly. Brush and slip ring assemblies are used to transfer the D. C. power to the rotating assembly and brush noise is minimized by having non-inductive impedences on both sides of the brush and slip ring assemblies. Floating circuits are employed to transfer the D. C. power from the stationary assembly to the rotating assembly with the return reference ground being through the brush and slip ring assemblies to the stationary assembly. Higher than usual voltages are supplied to a capacitor mounted on the rotating assembly to charge the capacitor providing reserve energy storage, providing a voltage margin for further regulation and thus minimizing the effect of brush noise.

## STATEMENT OF THE OBJECTS OF THE INVENTION

An object of the present invention is to provide low noise D. C. power from a stationary member to a rotating member;

Another object of the present invention is to provide a floating ground D. C. power supply system;

Still another object of the present invention is to provide a D. C. power system that employs capacitive storage;

A further object of the present invention is to provide a D. C. power system that minimizes the noise introduced by brushes and slip rings; and

A still further object of the present invention is to provide a floating D. C. power supply system that employs a low current flow path that provides a reference to ground.

Other objects, advantages and novel features of the present invention will become apparent from the following detailed description of the invention when considered in conjunction with the accompanying drawings wherein:



## BRIEF DESCRIPTION OF THE DRAWINGS

FIG. 1 is a schematic diagram of the low noise D. C. power supply system of the present invention; and

FIG. 2 is a diagram illustrating an equivalent circuit to explain the operation of the floating circuits of the low noise D.C. power supply system of the present invention.

## DESCRIPTION OF THE PREFERRED EMBODIMENT

In FIG. 1 is illustrated the low noise D. C. power supply system 11 of the present invention for supplying power to electronics equipment mounted on a rotating assembly. FIG. 1 is divided into three parts: (1) the components mounted on an aircraft, for example; (2) the stationary mounted components on an electric field measuring device, for example; (3) the rotatably mounted components on an electric field measuring device, for example. This power supply of the present invention has been found to be particularly useful for supplying high quality low noise D. C. power to an electric field measuring device that is mounted on the nose boom of a flying aircraft. Since atmospheric electric fields can be as low as several volts per meter it is necessary to supply exceedingly low noise D. C. power to the rotating electronics of the electric field measuring device which senses and processes the low level signals received from these atmospheric fields.

Mounted on the aircraft are battery 13, having a 28 VDC output, for example, recorder 15, isolating D. C. to D. C. converter 17 having a +7.5 VDC output, for example, isolating D. C. to D. C. converter 19 having a +7.5 VDC output, for example, and isolating D. C. to D. C. converter 21 having a ± 20 VDC output, for example. The aircraft mounted battery 13 has one side, the positive side, for example, connected to the respective inputs of recorder 15 and D. C. to D. C. converters 17, 19 and 21. The other side of battery 13, the negative side, for example, is connected to ground (the aircraft frame, for example) and to the respective other inputs of recorder 15, and to D. C. to D. C. converters 17, 19 and 21. The ground output of D. C. to D. C. converter 17 is directly connected to aircraft ground by cable 23 and the ground output of D. C. to D. C. converter 19 is connected through resistor 25 to aircraft ground. Resistor 25 is selected to have a high value, for example 10 K ohms, for reasons to be hereinafter explained.

As illustrated in FIG. 1, the input of recorder 15, the outputs of isolating D. C. to D. C. converters 17, 19 and 21, and aircraft ground are respectively connected through a plurality of lead wires 27 through 43 and cable connectors to the stationary components of an electric field measuring device, for example. The input of recorder 15 is connected by lead wire 27 to the output of stationary electronics 45. The input to stationary electronics 45 is connected to the output of a stationary optical receiver 47 that may be an infrared phototransistor, for example. The outputs of isolating D. C. to D. C. converter 17 are connected to the inputs of +5VDC regulator 49, for example, that supplies regulated D. C. power to stationary electronics 45. The outputs of isolating D. C. to D. C. converters 19 and 21, through lead wires 33, 35, 37, 39 and 41 are connected to the respective brushes, schematically illustrated by dotted lines, of brush assembly 51. The aircraft ground, through lead wire 43, is connected to the stationary

frame ground and to a plurality of brushes, schematically illustrated by dotted lines, of brush assembly 51.

Connected across lead wires 33 and 35 of the +7.5VDC floating power output of isolating D. C. to D. C. converter 19 is capacitor 53. Connected across lead wires 37 and 41 of the +20VDC floating power output of isolating D. C. to D. C. converter 21 is capacitor 55. Connected across lead lines 39 and 41 of the −20VDC floating power output of isolating D. C. to D. C. converter 21 is capacitor 57.

The slip rings, schematically illustrated by dotted lines, of slip ring assembly 59 connect the output of isolating D. C. to D. C. converter 19 to the inputs of 5VDC, for example, rotating regulator 61. A capacitor 63 is connected across the input and ground of regulator 61. The slip rings, schematically illustrated by dotted lines, of slip ring assembly 59 connect the outputs of isolating D. C. to D. C. converter 21 to the inputs of ± 15VDC, for example, rotating regulator 65. Capacitor 67 is connected across the +20VDC input and ground of regulator 65 and capacitor 69 is connected across the −20VDC input and ground of regulator 65. The outputs of rotating regulators 61 and 65 are connected to the power inputs of rotating electronics 71. The output of rotating electronics 71 is connected to the input of rotating optical transmitter 73 which may be an infrared light emitting diode, for example. In response to an input signal, indicating an electric field, for example, the light from rotating optical transmitter 73 is transmitted across an air gap to the input of stationary optical receiver 47 where it is processed by stationary electronics 45 and then applied to the input of aircraft mounted recorder 15.

It should be particularly noted that the grounds of rotating electronics 71 and rotating regulators 61 and 65 are interconnected and are connected to the rotating frame ground and to a plurality of slip rings, schematically illustrated by dotted lines of slip ring assembly 59. These slip rings are operably connected to the respective brushes of brush assembly 51 that are connected to the stationary frame ground and to the aircraft ground.

The operation of the power supply of FIG. 1 is as follows. At the outset it should be noted that a slip ring and associated brush have a variable resistance contact and current flowing through the contact will therefore generate a variable voltage drop which may be viewed as undesirable noise. To reduce the noise across the brush and associated slip ring it is desirable that the impedence in both directions be non-inductive. For this reason, and to provide energy storage, large capacitors are employed on each side and physically located near to the brush and associated slip ring. In FIG. 1 this is illustrated with reference to isolating D. C. to D. C. converter 19 by the use of capacitors 53 and 63. This is also illustrated with reference to isolating D. C. to D. C. converter 21 by the use of capacitor pair 55 and 67 and capacitor pair 57 and 69. Resistor 25 is provided to provide a high impedence current discharge path to prevent converters 19 and 21 from applying a leakage potential to floating circuits 75 and 77 when the rotatable electronics are not in operation or are removed.

It should be particularly noted that capacitors 63, 67 and 69 are selected to have large values of capacitance, such as 10 or more microfarads, depending on the current requirement. Not only does this provide a capacitive impedence but it also provides a current source which will supply current to the rotating regulators 61 and 65 when the resistance of the brush and associated slip ring increases and thereby minimizes the effect of brush noise.

It should be particularly noted that circuits 75 and 77 are floating. That is, without the rotating member these circuits would be floating in that there is no connection, except through resistor 25, which has a high value, to any other circuit or D. C. reference such as aircraft ground. It should be particularly noted however, that these floating circuits 75 and 77 have an aircraft ground reference, through slip ring assembly 59 and brush assembly 51 and lead line 43, when the rotatably mounted circuits are connected in place as shown in FIG. 1.

In FIG. 2 is illustrated an equivalent circuit illustrating the reason for coupling the ground of circuits 75 and 77 through the brush and slip assemblies rather than directly connecting to aircraft ground.

In FIG. 2 the noise signal generated by current through brush contacts in the D. C. returns is illustrated by generator 79. Capacitive coupling between one capacitive plate on the rotating member and the stationary frame is equal to $C(\theta)$, a function of the angular position of the rotating member. The capacitive plate is held at ground by associated electronics in the rotating frame. This is represented by the dotted lines connection 81. Should there also be a connection represented by the dotted lines 85 between the D. C. return 33 and the stationary frame 85 the completed circuit made by this connection would induce a noise current $V'_{ac}/C(\theta)$ in the capacitive plates. This would, at best, reduce the signal-to-noise ratio at the input to the rotating electronics and, at worst (in the case of high gain configuration), saturate the electronics and eliminate their further function. For this reason the entire supply circuit of FIG. 1 must have no low-impedence connection to the stationary frame.

Note also that since the capacitance in FIG. 2 is a function of angular position, $\theta$, any D. C. voltage offset $V_{DCOS}$ will also appear as a signal on the capacitive plate on the rotating frame. It is important to minimize this effect first by carefully connecting the rotating and stationary frames electrically through multiple parallel brush and associated slip ring contacts as shown in FIG. 1; second, by eliminating sources of current flowing through these contacts; third, by constructing the capacitive plate and stationary frame exerior of the same material to eliminate a contact potential difference between the capacitive plate and stationary body and last, by reducing the angular dependence of $C(\theta)$ to a minimum.

What is claimed is:

1. A low noise D. C. power supply comprising:
   a. a stationary assembly and a rotatable assembly;
   b. a brush assembly operably connected to said stationary assembly and a slip ring assembly operably connected to said rotatable assembly;
   c. said brush assembly including at least first, second and third brushes and said slip ring assembly including at least first, second and third slip rings, said first, second and third brushes being respectively operably connected to said first, said and third slip rings;
   d. a stationary D. C. power source having one side connected to a stationary ground, to said third brush and to one input of a stationary D. C. to D. C. converter and the other side connected to the other input of said D. C. to D. C. counter;

e. a first ouput of said stationary D. C. to D. C. converter being connected to said first brush and a second output being connected to said second brush;

f. said first and second slip rings being connected to a D. C. regulator mounted on said rotatable assembly;

g. the output of said D. C. regulator being connected to one input of an electronic assembly mounted on said rotatable assembly; and

h. the ground of said electronics assembly and said second slip ring being connected to said third slip ring.

2. The device of claim 1 including:

a. a first capacitor connected between said first and second brushes.

3. The device of claim 2 including:



a. a second capacitor connected between said first and second slip rings.

4. The device of claim 3 wherein:

a. said second capacitor is greater than about 10 microfarads.

5. The device of claim 4 including:

a. a resistor operably connected between said second output of said stationary D. C. to D. C. converter and said one side of said stationary D. C. power source.

6. The device of claim 5 wherein:

a. the D. C. voltage supplied to said second capacitor is substantially greater than required to provide the required power supplied by said rotatable D. C. regulator.

* * * * *

# United States Patent [19]

**Wagner**

[11] **3,996,519**

[45] **Dec. 7, 1976**


## [54] DIGITAL SIGNAL PROCESSOR


[75] Inventor: Peter B. Wagner, Reno, Nev.

[73] Assignee: The United States of America as represented by the Secretary of the Navy, Washington, D.C.



[22] Filed: July 2, 1975

[21] Appl. No.: 592,851

[52] U.S. Cl. ..... 325/142; 340/353

[51] Int. Cl.² ..... G01R 7/00

[58] Field of Search ..... 325/142, 321; 340/353, 340/206; 178/82 A, 112, 66, 67, 68; 332/1, 11



[56] References Cited

UNITED STATES PATENTS

3,510,780 5/1970 Buehrle ..... 178/68

OTHER PUBLICATIONS

Rosen, "IBM Technical Disclosure Bulletin" vol. 16, No. 8, Jan. 1974, pp. 2744–2745.

Shcingold, "Analog-Digital Conversion Handbook" 1972, pp. I-31 to I-37.



*Primary Examiner*—Charles D. Miller

*Attorney, Agent, or Firm*—R. S. Sciascia; Charles D. B. Curry



[57] ABSTRACT

A digital signal processor that is particularly suitable for converting an analog input signal into a stored digital signal for serial transmission in short and long time duration signals which will be indicative of the analog input signal. The system employs a digital gain control to maintain nearly uniform transmission signal levels, two parity generators to assure proper signal transmission, and a set-reset flip-flop shift register and logic system for controlling the output of the serially connected shift register containing the information to be serially transmitted.


**7 Claims, 5 Drawing Figures**

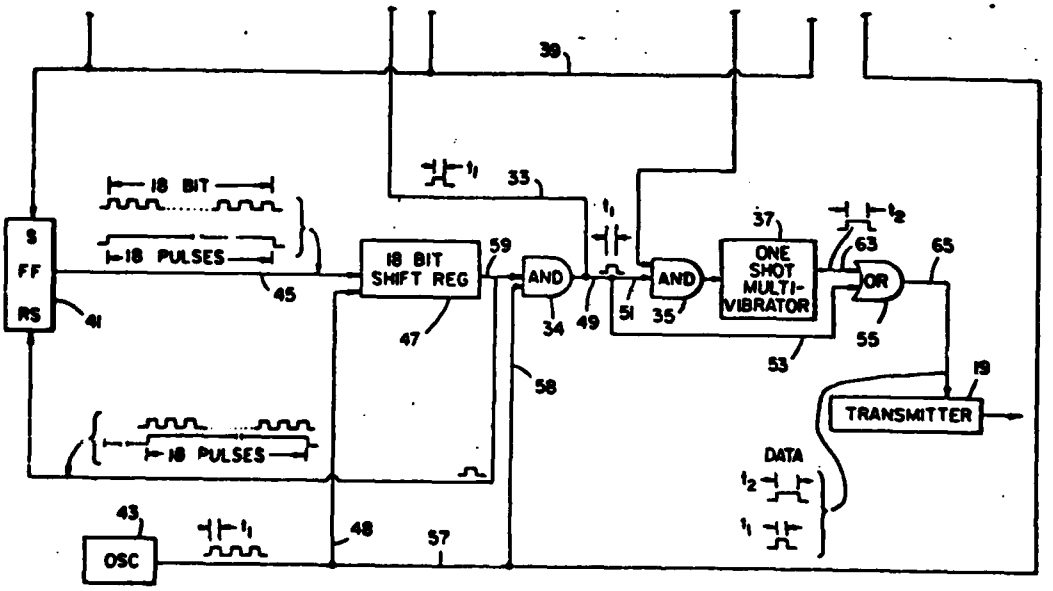

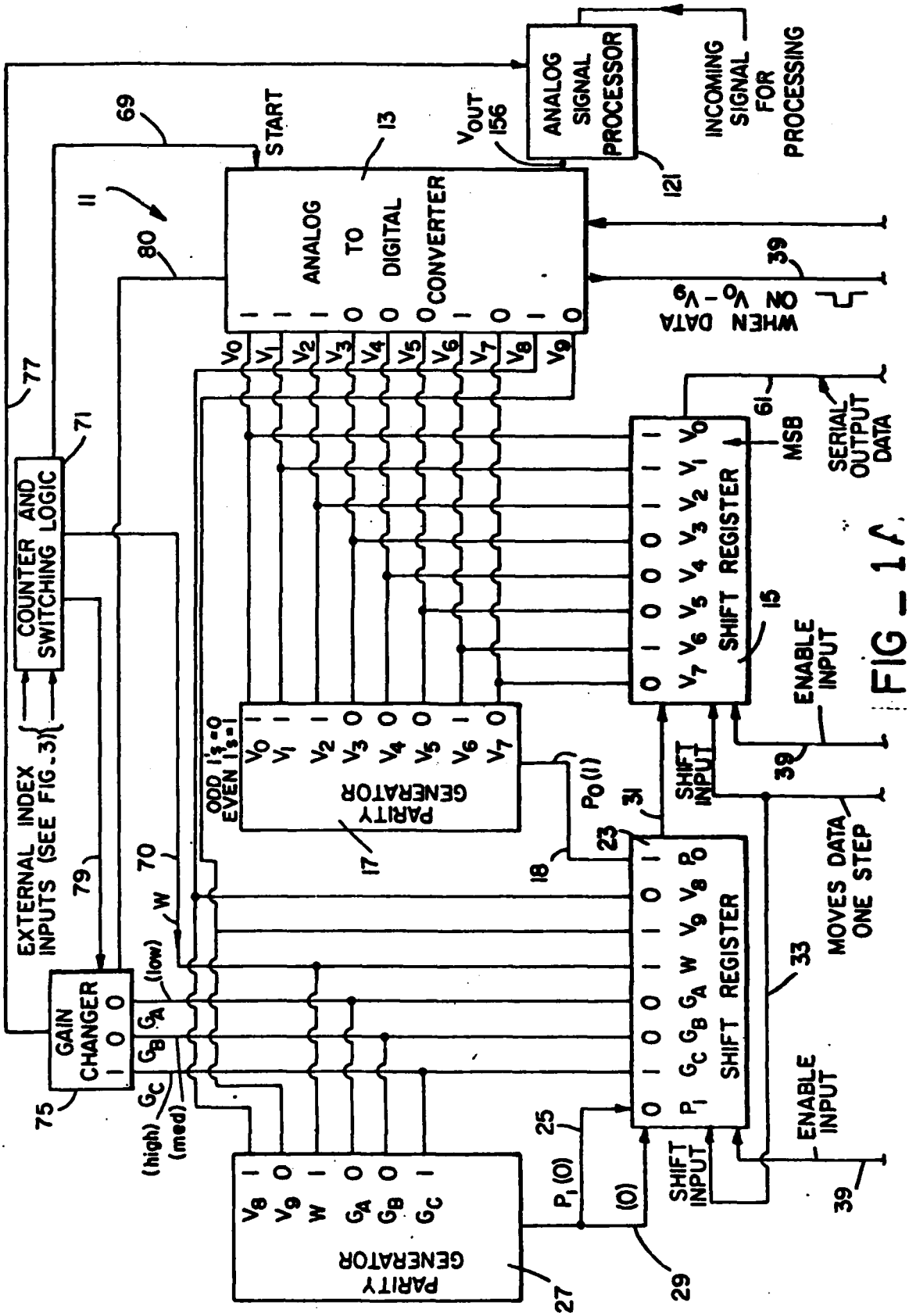
ANALOG SIGNAL PROCESSOR
INCOMING SIGNAL FOR PROCESSING
121
START
13
$V_{OUT}$ 156
ANALOG TO DIGITAL CONVERTER
69
11
80
39
WHEN DATA ON $V_0$-$V_9$
77
71
COUNTER AND SWITCHING LOGIC
$V_0$ $V_1$ $V_2$ $V_3$ $V_4$ $V_5$ $V_6$ $V_7$ $V_8$ $V_9$
61
MSB
SERIAL OUTPUT DATA
SHIFT REGISTER
15
ENABLE INPUT
39
EXTERNAL INDEX INPUTS (SEE FIG. 3)
79
70
W (low)
ODD $I_3$=0
EVEN $I_3$=1
PARITY GENERATOR
17
$P_0$(1)
31
SHIFT INPUT
18
23
GAIN CHANGER
75
$G_A$
$G_B$
$G_C$
(high)
(med)
SHIFT REGISTER
33
MOVES DATA ONE STEP
ENABLE INPUT
39
25
$P_1$(0)
(0)
SHIFT INPUT
PARITY GENERATOR
27
29

FIG_1A

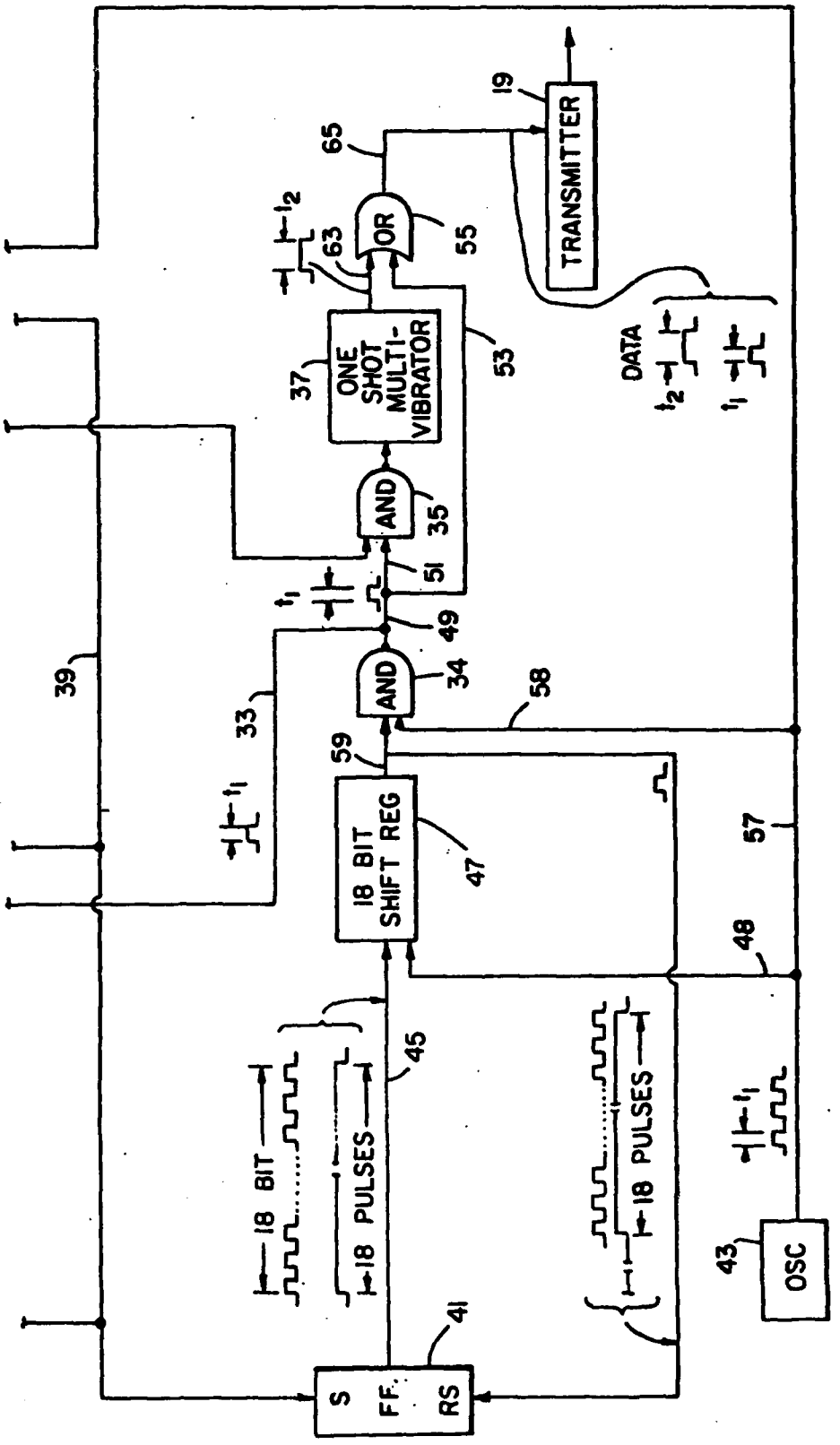
19
TRANSMITTER
65
OR
55
63
$t_2$
37
ONE SHOT MULTI-VIBRATOR
53
DATA
$t_2$
$t_1$
AND
35
51
$t_1$
49
AND
34
58
39
33
$t_1$
59
18 BIT SHIFT REG
47
57
48
18 BIT
18 PULSES
45
18 PULSES
$t_1$
43
OSC
41
S
FF
RS

FIG._1B

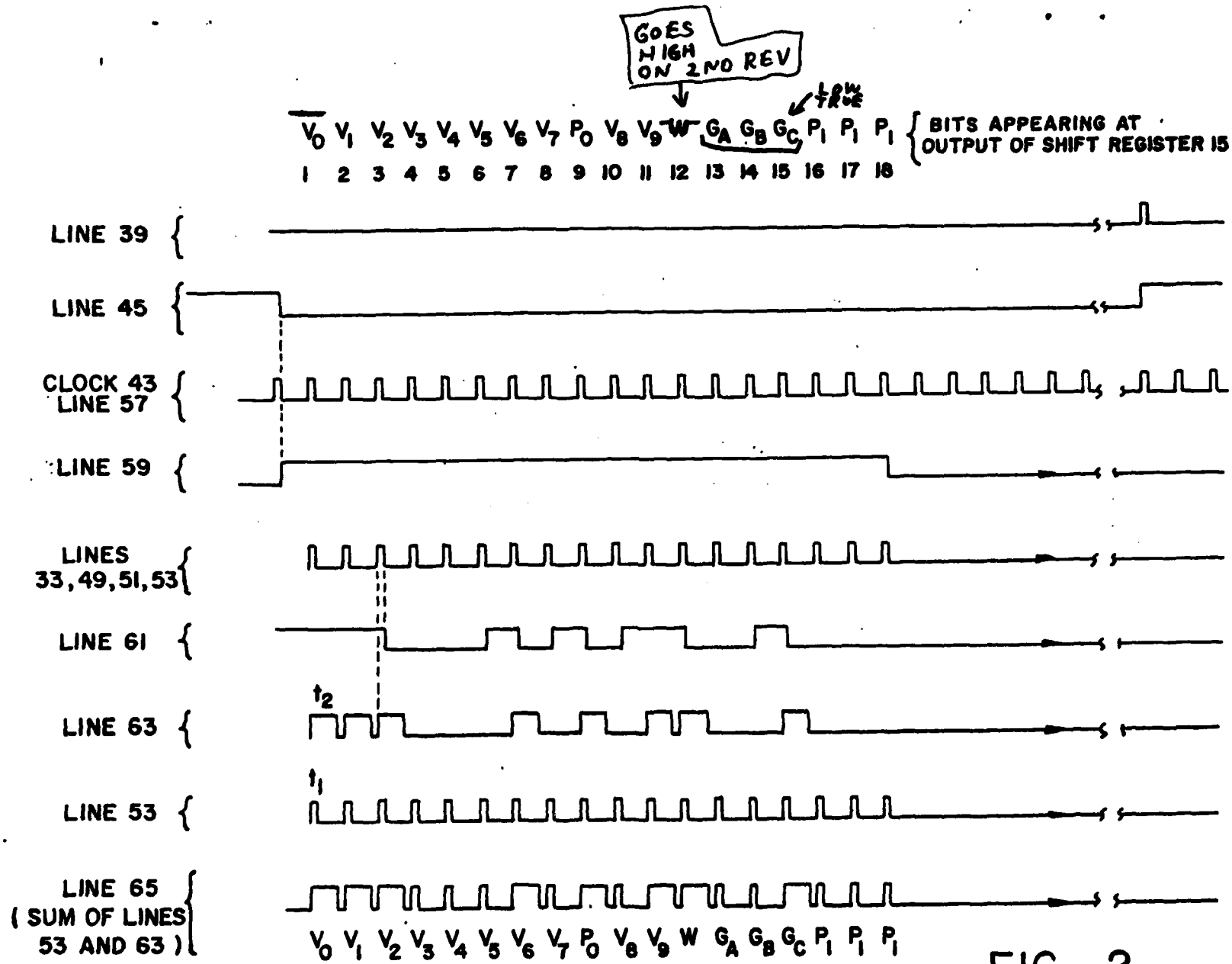
GOES HIGH ON 2ND REV
LOW TRUE
$\overline{V_0}$ $V_1$ $V_2$ $V_3$ $V_4$ $V_5$ $V_6$ $V_7$ $P_0$ $V_8$ $V_9$ $\overline{W}$ $G_A$ $G_B$ $G_C$ $P_1$ $P_1$ $P_1$
BITS APPEARING AT OUTPUT OF SHIFT REGISTER 15
1 2 3 4 5 6 7 8 9 10 11 12 13 14 15 16 17 18
LINE 39
LINE 45
CLOCK 43 LINE 57
LINE 59
LINES 33,49,51,53
LINE 61
$t_2$
LINE 63
$t_1$
LINE 53
LINE 65 ( SUM OF LINES 53 AND 63 )
$V_0$ $V_1$ $V_2$ $V_3$ $V_4$ $V_5$ $V_6$ $V_7$ $P_0$ $V_8$ $V_9$ W $G_A$ $G_B$ $G_C$ $P_1$ $P_1$ $P_1$

FIG_2

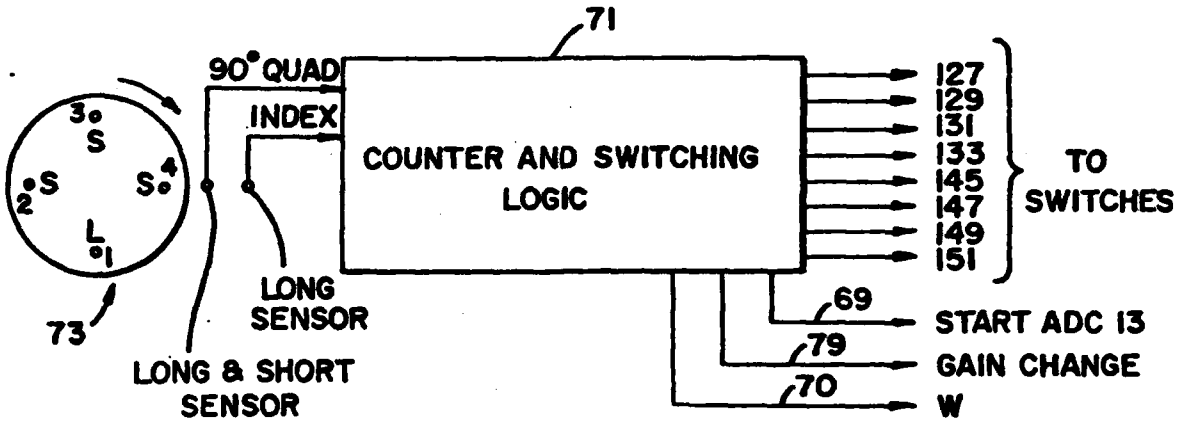
71
90° QUAD
INDEX
COUNTER AND SWITCHING LOGIC
127
129
131
133
145
147
149
151
TO SWITCHES
69
START ADC 13
79
GAIN CHANGE
70
W
3
S
2
S
S
4
L
1
73
LONG SENSOR
LONG & SHORT SENSOR

FIG_3

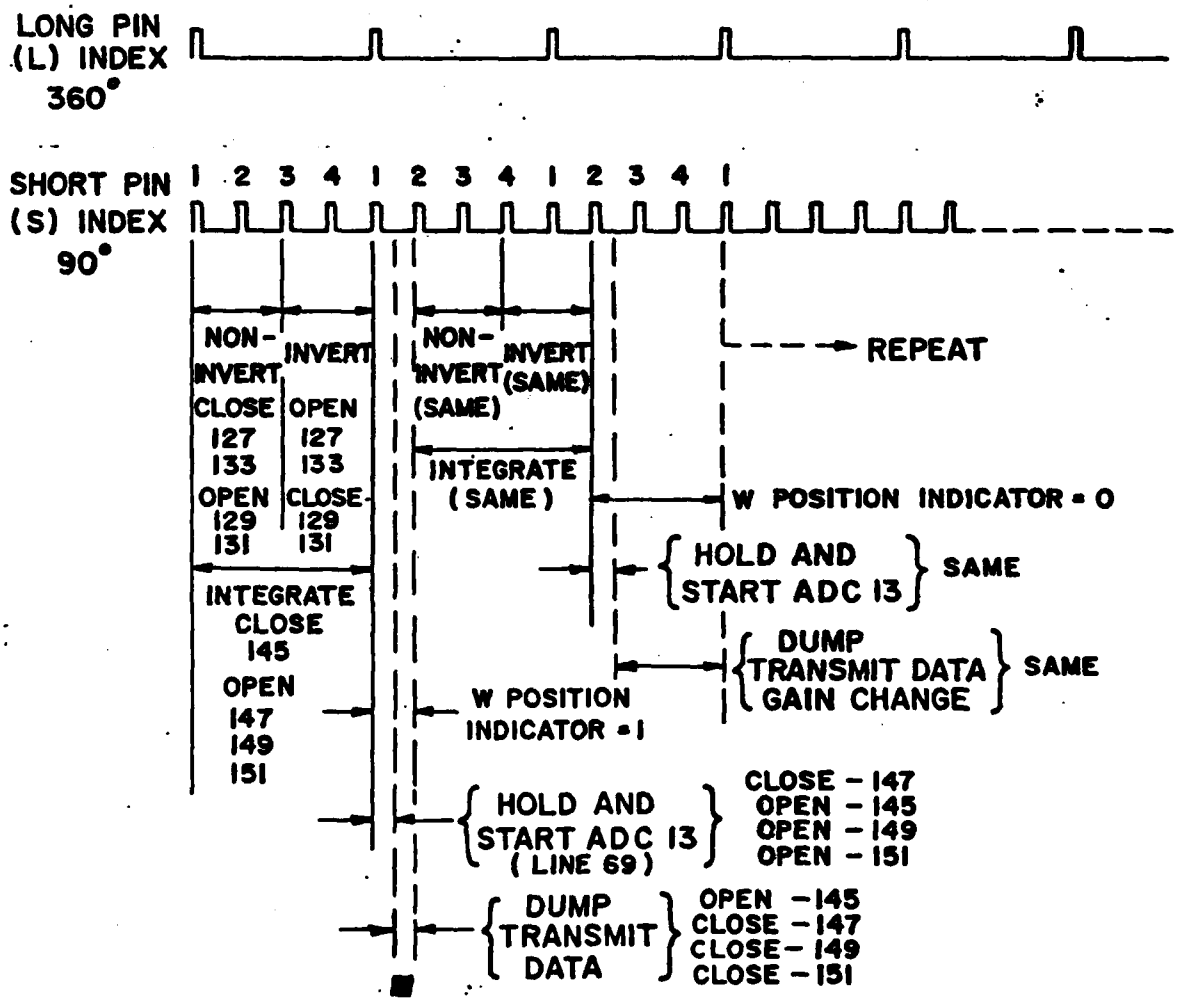
LONG PIN (L) INDEX 360°
SHORT PIN (S) INDEX 90°
1 2 3 4 1 2 3 4 1 2 3 4 1
NON-INVERT
INVERT
CLOSE 127 133
OPEN 127 133
OPEN 129 131
CLOSE 129 131
NON-INVERT (SAME)
INVERT (SAME)
REPEAT
INTEGRATE (SAME)
W POSITION INDICATOR = 0
HOLD AND START ADC 13
SAME
INTEGRATE CLOSE 145
OPEN 147 149 151
DUMP TRANSMIT DATA GAIN CHANGE
SAME
W POSITION INDICATOR = 1
HOLD AND START ADC 13 (LINE 69)
CLOSE - 147
OPEN - 145
OPEN - 149
OPEN - 151
DUMP TRANSMIT DATA
OPEN - 145
CLOSE - 147
CLOSE - 149
CLOSE - 151

FIG_4

# DIGITAL SIGNAL PROCESSOR

## BACKGROUND OF THE INVENTION

1. Field of the Invention

The present invention relates to a digital signal processor and more particularly to a digital signal processor that converts analog information into digital information and stores the digital information for subsequent pulse modulation serial data transmission.

2. Description of the Prior Art

One of the difficulties in prior art digital signal processors is that they have been rather complex and of relatively large size. This has been especially disadvantages in situations where the processor must be airborne and be built into a relatively small package. This present invention has overcome these difficulties by providing a digital signal processor that performs both storage and control functions and is reliable, compact and is light in weight.

## SUMMARY OF THE INVENTION

Briefly, the present invention comprises a digital signal processor that is particularly suitable for converting an analog input signal into a stored digital signal for serial transmission in short and long time duration signals which will be indicative of the analog input signal. The system employs a digital gain control to maintain nearly uniform transmission signal levels, two parity generators to assure proper signal transmissions, and a set-reset flip-flop shift register and logic system for controlling the output of the serially connected shift register containing the information to be serially transmitted.

In addition, this digital control system of the present invention is particularly suited for being mounted on a rotating shaft and the digital rotating electronics may serve several primary functions, although the circuitry is designed fo economy of size and part count such that the function may be interdependent. The conversion to digital, from an analog signal input, and storage of the digital signal in a shift register for subsequent serial data transmission is one of the chief functions of the system. Another function that the system is capable of performing is the digital sequence control of an analog circuit for acquisition of the analog input signal. Still another function that the system is capable of performing is the conversion of the digital data and other digital information, including parity bits, in serial format to a pulse width modulated light beam such as shown and described in U.S. patent application Ser. No. 486,035 now U.S. Pat. No. 3,917,996 by Peter B. Wagner filed on July 5, 1974. Still another function that the system is capable of performing is the digital control of gain circuitry (See co-pending patent application, Navy Case No. 58,393.) based upon the magnitude of the digital output from the analog to digital convertor. The purpose of the gain control is to automatically keep the analog signal input to the digital convertor is a high accuracy operating region of the convertor.

## STATEMENT OF THE OBJECTS OF THE INVENTION

An object of the present invention is to provide a light weight, compact and reliable digital signal processor;

Another object of the present invention is to provide a digital signal processor that will receive an analog signal, convert the analog signal into a digital format and store the digital information for subsequent serial transmission;

Still another object of the present invention is to provide a digital signal processor that will receive an analog signal, convert the analog signal into a digital serial format for conversion into a pulse width modulated signal;

A still further object of the present invention is to provide a digital signal processor that employs parity bits to assure accurate transmission;

A still further object of the present invention is to provide a digital signal processor that employs gain control that may regulate the magnitude of the incoming analog signal.

Other objects, advantages and novel features of the invention will become apparent from the following detailed description of the invention when considered in conjunction with the accompanying drawings *wherein:*

## BRIEF DESCRIPTION OF THE DRAWINGS

FIGS. 1A and 1B together comprise is a schematic diagram of the digital signal processor of the present invention;

FIG. 2 is a diagram illustrating the operation of the digital signal processor of FIGS. 1A and 1B;

FIG. 3 is a schematic diagram of the counter and switching logic of the circuit shown in FIGS. 1A and 1B; and

FIG. 4 is a timing diagram illustrating the operation of the counter and switching circuit of FIG. 3 and how it relates to the overall invention.

## DESCRIPTION OF THE PREFERRED EMBODIMENT

In FIGS. 1A and 1B is shown a schematic diagram of the digital signal processor 11 of the present invention. It should be noted that the incoming signal is an analog signal $V_{out}$ from analog signal processor 121 that is applied to one of the inputs of analog to digital convertor 13. (Analog signal processor 121 may be of the type shown and described in co-pending patent application, Navy Case No. 58,393.) Normally the analog signal $V_{out}$ will be in the range of $\pm$ 10 volts, for example, and therefore to provide sufficient resolution, the digitized binary word reperesenting $V_{out}$ is selected to have 10 bits, for example. Therefore, the least significant bit will represent about 20 milivolts which is sufficient resolution for most purposes.

Analog to digital convertor 13 is of standard design and will therefore not be described in detail. However, the 10 bit output is represented by the symbols $V_0$, $V_1$, $V_2$, $V_3$, $V_4$, $V_5$, $V_6$, $V_7$, $V_8$, and $V_9$ and where $V_9$ is the most significant bit (MSB) and $V_0$ is the least significant bit (LSB). In order to illustrate operation of digital signal processor 11 numerical values have been selected for the bit symbols $V_0$ through $V_9$ as shown in FIG. 1 of the drawings.

The $V_0$ through $V_7$ outputs of analogs to digital convertor 13 are applied in parallel to serial shift register 15 and the parity generator 17. The function of serial shift register 15 is to store and serially transfer, bit by bit, the coded bit information contained therein, as well as the coded bit information transferred thereto from register 23, on command and as hereinafter described in detail.

The function of parity generator 17 is to provide assurance that the information shifted from shift register 15 and ultimately transmitted by transmitter 19 is the correct and accurate information that was digitized by analog to digital converter 13. Parity generator 17 is selected to provide a 1 output signal when the 1 bits sensed thereby are odd and a 0 or no signal when the 1 bits sensed thereby are even. That is, odd 1's = 0 bit and even 1's = 1 bit. Therefore, using the example of FIG. 1 it can be seen that the bits $V_8$, $V_1$, $V_2$ and $V_4$ are 1's and comprise 4 bits and therefore the parity output signal $P_0$ on line 18 is a 1. That is, $P_0 = 1$.

This $P_0 = 1$ bit is stored in the $P_0$ position of serial shift register 23. Serial shift register 23 is an eight bit register and the bit positions from right to left are designated $P_0$, $V_8$, $V_9$, W, $G_A$, $G_B$, $G_C$, and $P_1$ the functions of which will be hereinafter explained.

The input to serial shift register 23 for the positons $P_0$, $V_8$, $V_9$, W, $G_A$, $G_B$, $G_C$, and $P_1$ are respectively 1, 0, 1, 1, 0, 0, 1, 0, for example. The $V_8$ and $V_9$ bits have been previously described as being part of the digitized $V_{out}$ signal where $V_8$ is the least significant bit (LSB). $P_0$ is the parity bit from parity generator 17 and is a 1 for reasons previously explained. W is a control bit which will be hereafter explained and the gain control information $G_A$, $G_B$, and $G_C$ bits are bits which will also be hereinafter explained. Parity bit $P_1$ on line 25 is derived from parity generator 27. From FIG. 1 it can be seen that the inputs to parity generator 27 are $V_8$, $V_9$, W, $G_A$, $G_B$, and $G_C$ and are shown respectively as 1,0, 1, 0, 0, 1. The function of parity generator 27 is similar to that of parity generator 17 in that it provides assurance that the information shifted from serial shift register 23 and ultimately transmitted by transmitter 19 is the correct and accurate information that was digitized and stored in serial shift register 23 which was obtained in part from analog to digital convertor 13 ($V_8$ and $V_9$), in part from counter and switching logic 71 (W) and in part from gain changer 75 ($G_A$, $G_B$ and $G_C$). Parity generator 27 is selected to provide a 1 output when the 1 bits sensed thereby are even and a 0 when the 1 bits sensed thereby are odd. That is, odd 1's = 0 bit and even 1's = 1 bit. Therefore, using the example of FIG. 1 it can be seen that the bits $V_8$, W and $G_C$ are 1's and therefore comprise 3 bits and, therefore, the parity generator output signal $P_1$ on line 25 is a 0. That is, $P_1 = 0$.

In addition, the parity bit generated by parity generator 27 is also applied to the serial input 29 of shift register 23. When shift pulses are applied to shift registers 23 and 15 on line 33, the serial parity bit on line 29 is shifted into shift register 23 and on through shift register 15 as hereinafter explained. The purpose is to make available an 18 bit word from the two 8 bit shift registers, 15 and 23, and place parity bit $P_1$ in position 16 and 17 as well as in positions 15 ($P_1$). Entry of parity in an odd number of positions in the second half of the 18 bit overall word does not alter the resultant parity of that second half of that word. These three P1 parity bits are also shown in FIG. 2 as $P_1$, $P_1$, and $P_1$.

It should be noted that shift registers 15 and 23 are serially connected by line 31 and the digital information will be serially shifted, from left to right, through these two registers, bit by bit, upon command from each sequential signal pulse that appears on line 33 which will be obtained from AND gate 34 as hereinafter explained. It should be noted that the time duration of the pulse from AND gate 34 is $t_1$. The output from line 61 of shift register 15 will be applied to one input of AND gate 35 the output of AND gate 35 which will be applied to the input of one shot multivibrator 37 which is selected to have a signal time duration of $t_2$. It should be noted that $t_2 > t_1$.

Referring to FIGS. 1A, 1B and 2, analog to digital convertor 13 provides an output signal on line 39 when data appears on all of the outputs $V_0$ through $V_9$. When this condition occurs the latch inputs to shift register 15, shift register 23 and the set input to flip-flop 41 are activated. When this occurs then a continuous 1 or up signal will appear at the output of flip-flop 41 on line 45 and therefore a series of 1's will be clocked into 18 bit shift reigster 47 from line 48 which is connected to the output of clock 43. After 18 bits have been shifted into shift register 47 then clock 43 will shift out the first entered bit (which will be a 1) which will be simultaneously applied to the input of AND gate 34 and to the reset (RS) input of flip-flop 41. When the 1 signal is applied to the reset input of flip-flop 41 then the output therefrom will be a 0 which will appear on line 45. This will remain at 0 until a new data complete pulse appears on line 39 from analog to digital convertor 13. Therefore a 0 will remain at the input of shift register 47 until a set signal is received on line 39. After the input to register 47 goes to 0 then 18 one bits will be shifted out and applied to the input of AND gate 34. Since clock pulses are also being applied to AND gate 34 on line 58 then 18 pulses will appear in sequence at the output of AND gate 34 and on lines 33, 49, 51 and 53.

When the series of the 18 pulses are occuring then the shift registers 15 and 23 are shifting and line 51 of AND gate 35 is receiving these sequented pulses and line 53 of OR gate 55 is also receiving these sequented pulses each $t_1$ in length. When a 1 is present on the output 61 of shift register 15, one shot multivibrator 37 is triggered and pulse $t_2$ in length appears on line 63. The $t_2$ pulse on line 63 extends beyond the $t_1$ pulse on line 53. The result is that a pulse $t_2$ to $t_1$ in length appears at the output 65 of OR gate 55 depending on whether shift register 15 output on line 61 is a 1 or a 0, respectively. When the output of AND gate 34 is 0 then no shift signals are applied to the input of shift registers 15 and 23, no signal is applied to line 51 of AND gate 35 and no signal is applied to the line 53 of the input of OR gate 55. In FIG. 2 is illustrated the opertion of the above described digitized signal processor when the previously defined conditions prevail.

The overall system is initiated and generally controlled by counter and switch logic 71 of FIGS. 1A, 1B and 3. In FIG. 3 is also shown a stationary orientation assembly 73 including a long pin L (indexed as 1) and a pluraltiy of short pins (indexed as 2, 3 and 4) and long and short pin sensors which cooperate with the long and short pins. The details of operation of this assembly will not be described herein since they are shown and described in patent application Ser. No. 486,035. The outputs of the long sensor (index) is connected to the input of counter and switching logic 71 and the output of the long and short sensor is connected to another input of counter and switching logic 71.

The operation and sequences of switching of the various switches 127, 129, 131, 133, 145, 147, 149 and 151, and the start signal on line 69 for the start of ADC 13 the word (W) on line 70 and the gain charge signal on line 79 are shown in FIG. 3 and in the timing diagram of FIG. 4 along with the positions of the short and long pin signals. It would be obvious to one skilled in

the art to design the various switching elements and logic of counter and switching logic 71 to obtain the appropriate signals on the various output lines as defined in FIGS 2, 3 and 4 and the details thereof will not be described.

It should be particularly noted that the circuit of FIGS. 1A and 1B, as explained in conjunction with the timing diagram of FIG. 2 is sufficient to stand by itself as a separate and independent invention to perform the function of converting a given DC signal on line 156 into a digital pulse modulated signal on line 65 that may be then transmitted by transmitter 19. Many different various gain control schemes for $G_A$, $G_B$ and $G_C$ and word index schemes for W could be also employed.

The purpose of showing the specific counter and switching logic schemes of FIGS 3 and 4 is to more completely illustrate how the digital signal processor 11 of the present invention may be used in an electric field measuring device such as shown in patent application, Ser. No. 486,035 and with an analog signal processor such as shown and described in Navy Case No. 58,393.

Gain changer 75 may be responsive to either the analog signal $V_{out}$ or its digital equivalent (such as the first 4 or 5 most significant digits) as shown by line 80. Many different types of gain changer devices 75 could be employed; however, its basic function is to assure that the analog signal processor 12 provides a signal $V_{out}$ that is within an acceptable voltage range. If not then the gain changer must modify the amplification level of the analog signal processor 12 by a signal over line 77 to increase or decrease the gain level. In this particular example three gain levels are shown bits $G_A$, $G_B$ and $G_C$, which represent low, medium and high gains. In the example given a high gain is used ($G_A = G_B = 0$, $G_C = 1$). Therefore, analog signal processor 12 is operating at a high gain and it is important that this information be transmitted over transmitter 19 so that an accurate measure of the $V_{out}$ signal is known. This is done by identifying the $G_A$, $G_B$ or $G_C$ signal that is being used and inserting this information into shift register 23 for subsequent transmission.

What is claimed is:

1. A digital signal processor comprising
   a. an analog to digital convertor for converting analog information into digital information comprising bits of 1's and 0's;
   b. at least one shift register;
   c. at least one parity generator;
   d. said digital information from said analog to digital convertor being transmitted to and stored in said at least one shift register and transmitted to said at least one parity generator;
   e. said at least one parity generator providing output information defining whether the number of 1 bits transmitted thereto was an odd number or an even number;
   f. said output information from said at least one parity generator being applied and stored in said at least one shift register;
   g. first means for serially shifting out the information bits stored in said at least one shift register to second means for converting the 0's from said at least one shift register into pulses of a first time duration $t_1$ and 1's from said at least one shift register into pulses of a second time duration $t_2$;
   h. said analog to digital convertor provides a first output signal when the conversion of the analog information into digital information is complete;
   i. said first output signal being applied to the enable input of said at least one shift register and to the set input of a first flip-flop circuit;
   j. the output of said first flip-flop circuit being applied to the input of a control shift register;
   k. an oscillator having its output connected to another input of said control shift register; and
   l. the output of said control shift register connected to second means for controlling the shift sequence of said at least one shift register.

2. The digital signal processor of claim 1 wherein:
   a. said second means includes a first AND gate and a feedback from said output of said control shift register to the reset input of said flip-flop;
   b. the output of said control shift register connected to one input of said first AND gate and the output of said oscillator connected to the other input of said first AND gate; and
   c. the output of said first AND gate being connected to the shift input of said at least one shift register.

3. The digital signal processor of claim 2 wherein:
   a. the input of said control shift register receives an input signal for a first predetermined number of clock pulses and the output of said control shift register provide no output signal for said first predetermined number of clock pulses and at the end of said predetermined number of clock pulses said output of said control shift register provides an output signal that is applied to the reset input of said flip-flop; whereby
   b. no signals are applied to the input of said control shift register for a second predetermined period of time; whereby
   c. said second predetermined period of time is the same as said first predetermined period of time.

4. The digital signal processor of claim 2 wherein:
   a. the output of said first AND gate being connected to one input of a second AND gate and to the input of a first OR gate;
   b. the output of said at least one shift register being connected to the other input of said second AND gate; and
   c. the output of said first AND gate being connected to the other input of said OR gate.

5. A digital signal processor comprising:
   a. an analog to digital convertor for converting analog information into digital information comprising bits of 1's and 0's;
   b. at least one shift register;
   c. at least one parity generator;
   d. said digital information from said analog to digital convertor being transmitted to and stored in said at least one shift register and transmitted to said at least one parity generator;
   e. said at least one parity generator providing output information defining whether the number of 1 bits transmitted thereto was an odd number or an even number;
   f. said output information from said at least one parity generator being applied and stored in said at least one shift register;
   g. first means for serially shifting out the information bits stored in said at least one shift register to second means for converting the 0's from said at least one shift register into pulses of a first time duration $t_1$ and said 1's from said at least one shift register into pulses of a second time duration $t_2$;
   h. said at least one shift register are first and second shift registers;

i. said at least one partity generator are first and second parity generators;
j. a first predetermined group of bits from said analog to digital processor are applied and stored in respective inputs of said first shift register;
k. said first predetermined group of bits being applied to the input of said first parity generator;
l. the output of said first parity generator being applied to and stored in one input of said first shift register;
m. a second predetermined group of bits from said analog to digital processor are applied to and stored in respective inputs of said second shift register;
n. a gain changer having a predetermined number of output signals indicating gain; and
o. said predetermined number of output signals being applied and stored in respective inputs of said second shift register and applied to the respective inputs of said second parity generator.

6. The digital processor of claim 5 wherein:
a. the output of said parity generator being applied to and stored in one input of said second shift register; and
b. said output of said parity indicator also being applied to the last digit signal reception input of said second shift register.

7. The digital processor of claim 6 including:
a. a counter and switching logic circuit providing a first position signal W;
b. said first position signal W being connected to and stored in another input of said second shift register and applied to another input of said second parity generator; and
c. a second output of said counter and switching logic being connected to the start input of said analog to digital convertor, and a third output of said counter and switching logic circuit being connected to the input of said gain changer.

* * * * *

N.C. 58,393


# United States Patent [19]

**Wagner**

[11] **4,013,955**

[45] **Mar. 22, 1977**


[54] **ANALOG SIGNAL PROCESSOR**


[75] Inventor: Peter B. Wagner, Reno, Nev.

[73] Assignee: The United States of America as represented by the Secretary of the Navy, Washington, D.C.



[22] Filed: July 2, 1975

[21] Appl. No.: 592,852

[52] U.S. Cl. ..... 324/72; 324/115; 328/260; 307/260; 321/9 R; 321/8 R; 321/18; 321/27

[51] Int. Cl.² ..... H02M 7/00; H03K 5/00

[58] Field of Search ..... 328/26; 307/260; 321/9 R, 8 R, 18, 27; 324/115, 72



[56] **References Cited**

UNITED STATES PATENTS

| | | | |
|---|---|---|---|
| 3,238,383 | 3/1966 | Falk | 307/88.5 |
| 3,305,769 | 2/1967 | Julie | 323/74 |
| 3,480,794 | 11/1969 | Richman | 307/229 |
| 3,491,252 | 1/1970 | Petrohkos | 307/229 |
| 3,539,936 | 11/1970 | McGhee | 330/29 |
| 3,564,387 | 2/1971 | Gadberry | 321/8 |
| 3,586,973 | 6/1971 | Lawton | 324/72 |
| 3,825,816 | 7/1974 | Togneri et al. | 321/18 |



*Primary Examiner*—R. V. Rolinec
*Assistant Examiner*—Vincent J. Sunderdick
*Attorney, Agent, or Firm*—R. S. Sciascia; Charles D. B. Curry



[57] **ABSTRACT**

An analog signal processor that is particularly suitable for measuring, integrating and holding a single or a pair of analog signals. The input signal to the analog signal processor may be sinusoidal of relatively low frequency and of low signal strength and slowly varying phase such as may be obtained from a pair of capacitive plates used in electric field measuring devices. The analog signal processor includes an analog current to voltage convertor, a synchronous rectifier and an integrate and hold circuit. In practice the analog signal processor may be mounted on a rotating shaft and converts the very low differentially alternating current input to a proportional d.c. voltage output. The analog signal processor includes timing and switching circuits to provide the desired information about vertical, horizontal and inclined electric fields.


**6 Claims, 14 Drawing Figures**

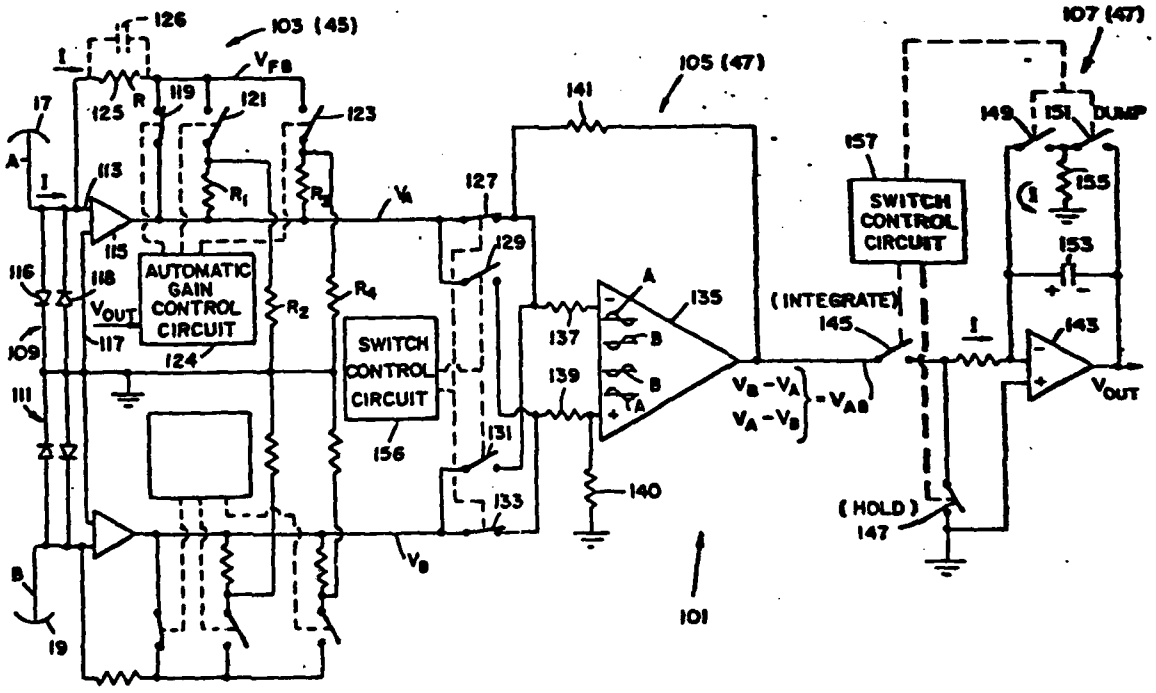


Encl (4)

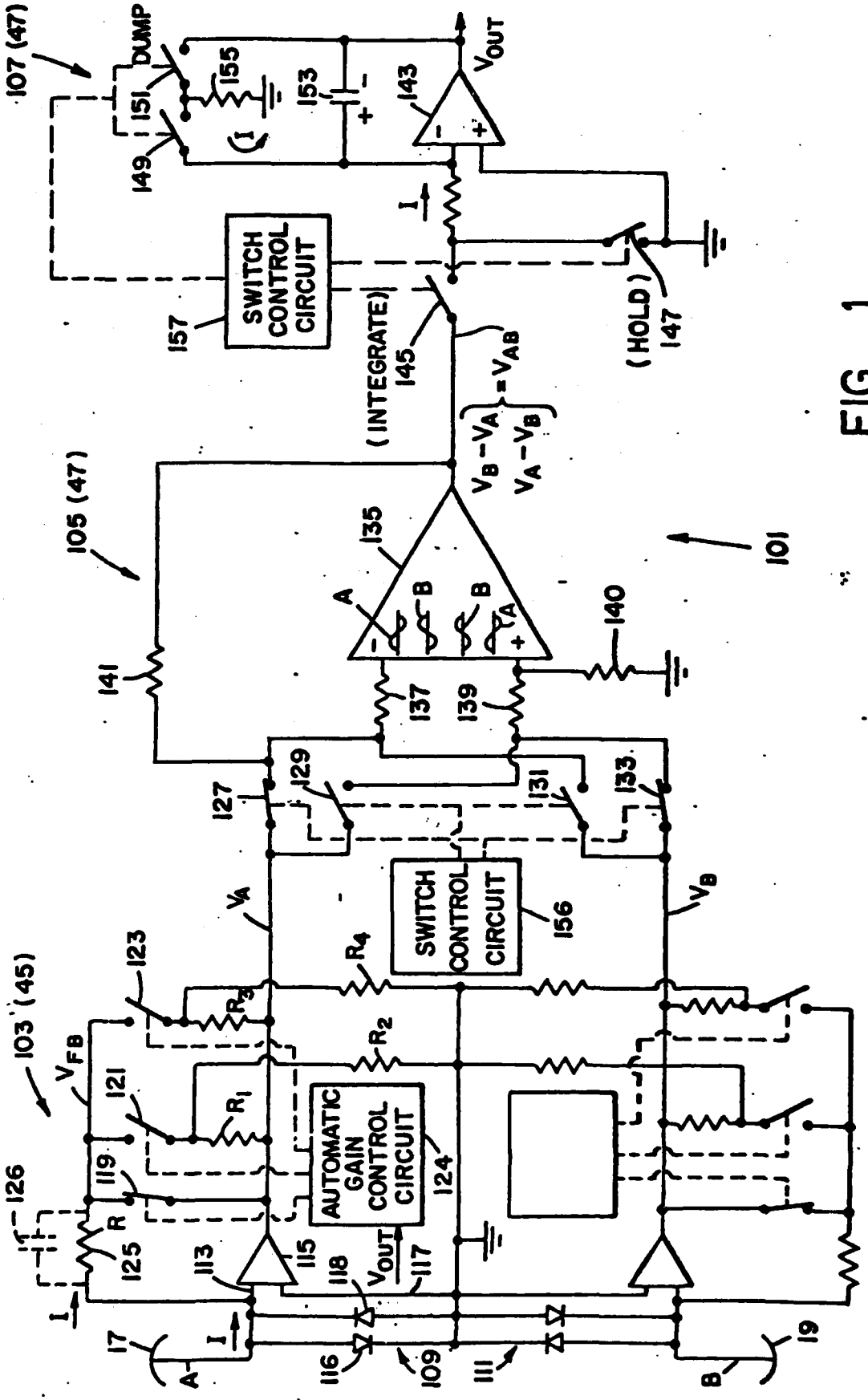
107 (47)
DUMP
151
149
155
153
143
$V_{OUT}$
SWITCH CONTROL CIRCUIT
157
(INTEGRATE)
145
(HOLD)
147
$V_B - V_A = V_{AB}$
$V_A - V_B$
105 (47)
135
A
B
B
A
140
101
141
137
139
129
127
131
133
SWITCH CONTROL CIRCUIT
156
$V_A$
$V_B$
123
$R_4$
$R_3$
$R_2$
$R_1$
103 (45)
$V_{FB}$
121
AUTOMATIC GAIN CONTROL CIRCUIT
124
119
126
R
125
113
115
118
$V_{OUT}$
117
I
17
A
116
109
111
B
19

FIG - 1

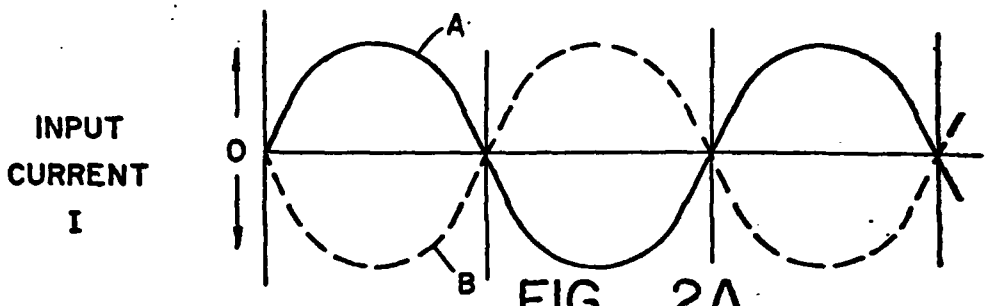


FIG _ 2A

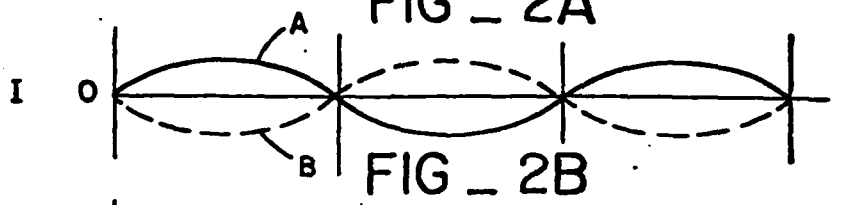


FIG _ 2B

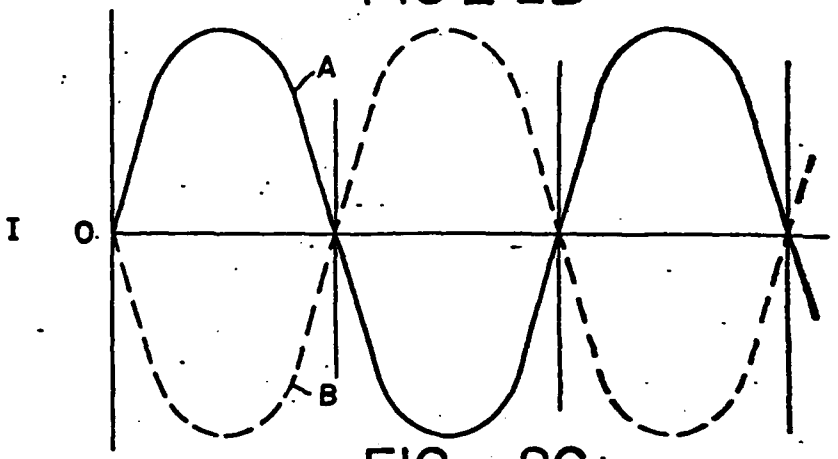


FIG _ 2C

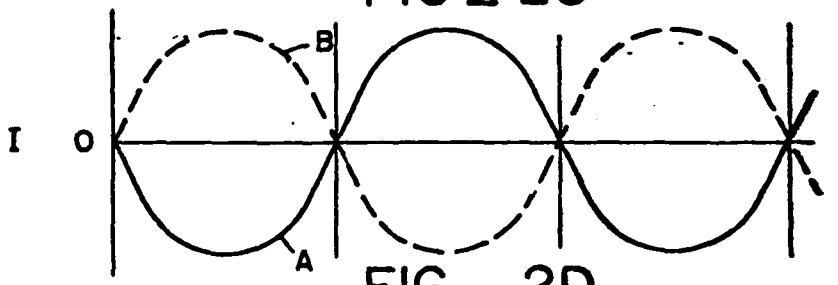


FIG _ 2D

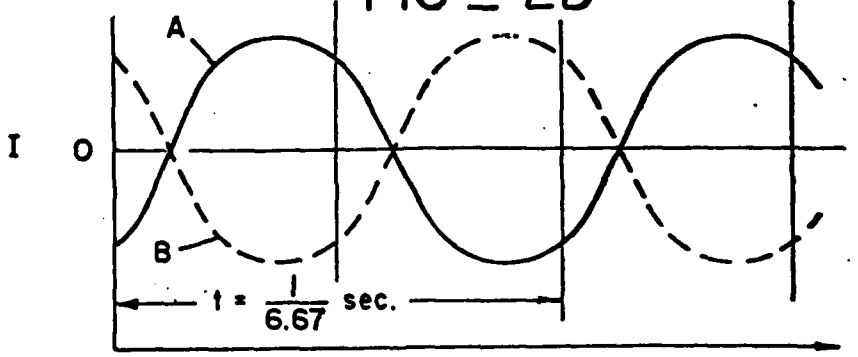


FIG _ 2E

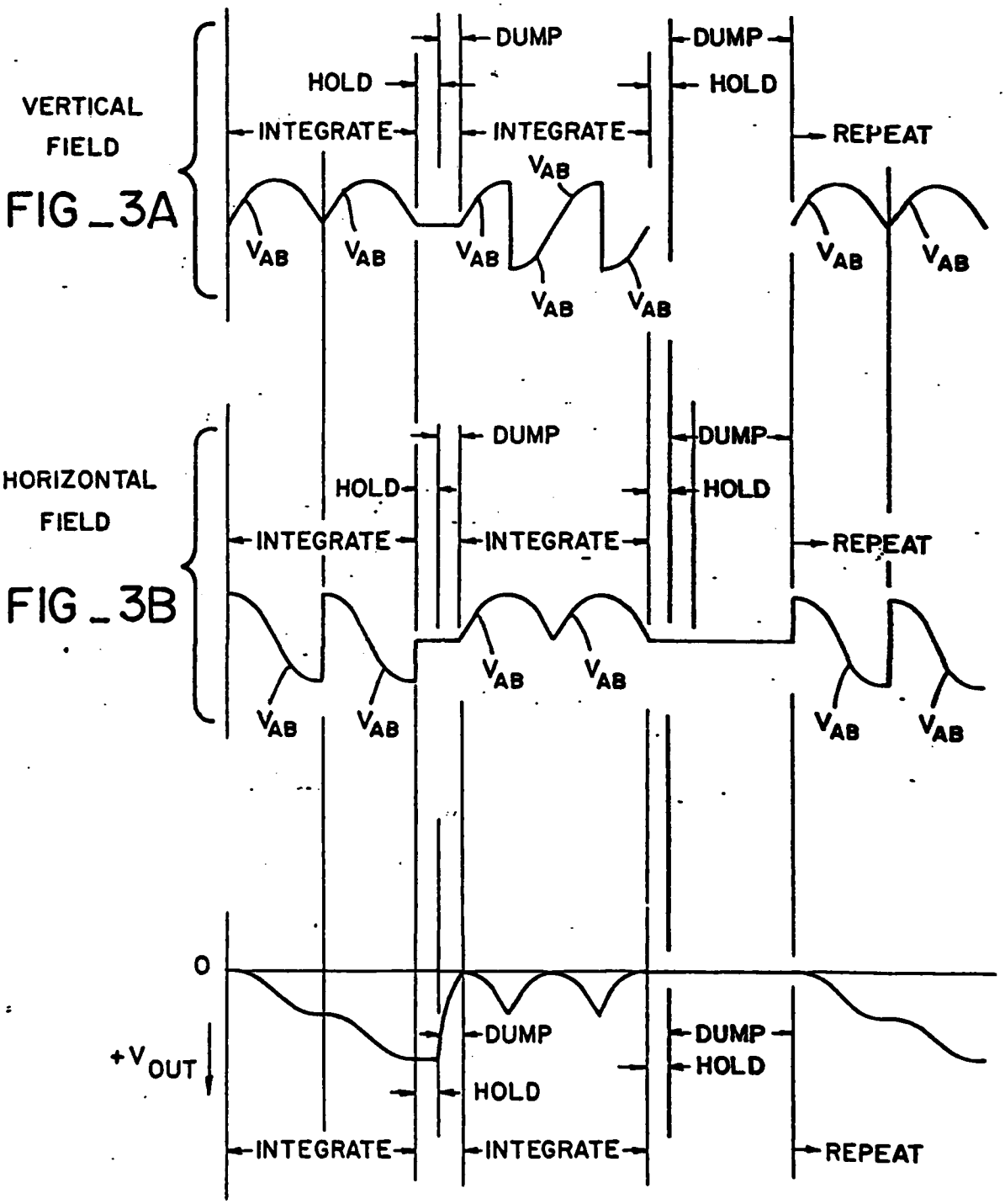


FIG_3A

FIG_3B

FIG_4

(FOR VERTICAL FIELD OF FIG_3A)

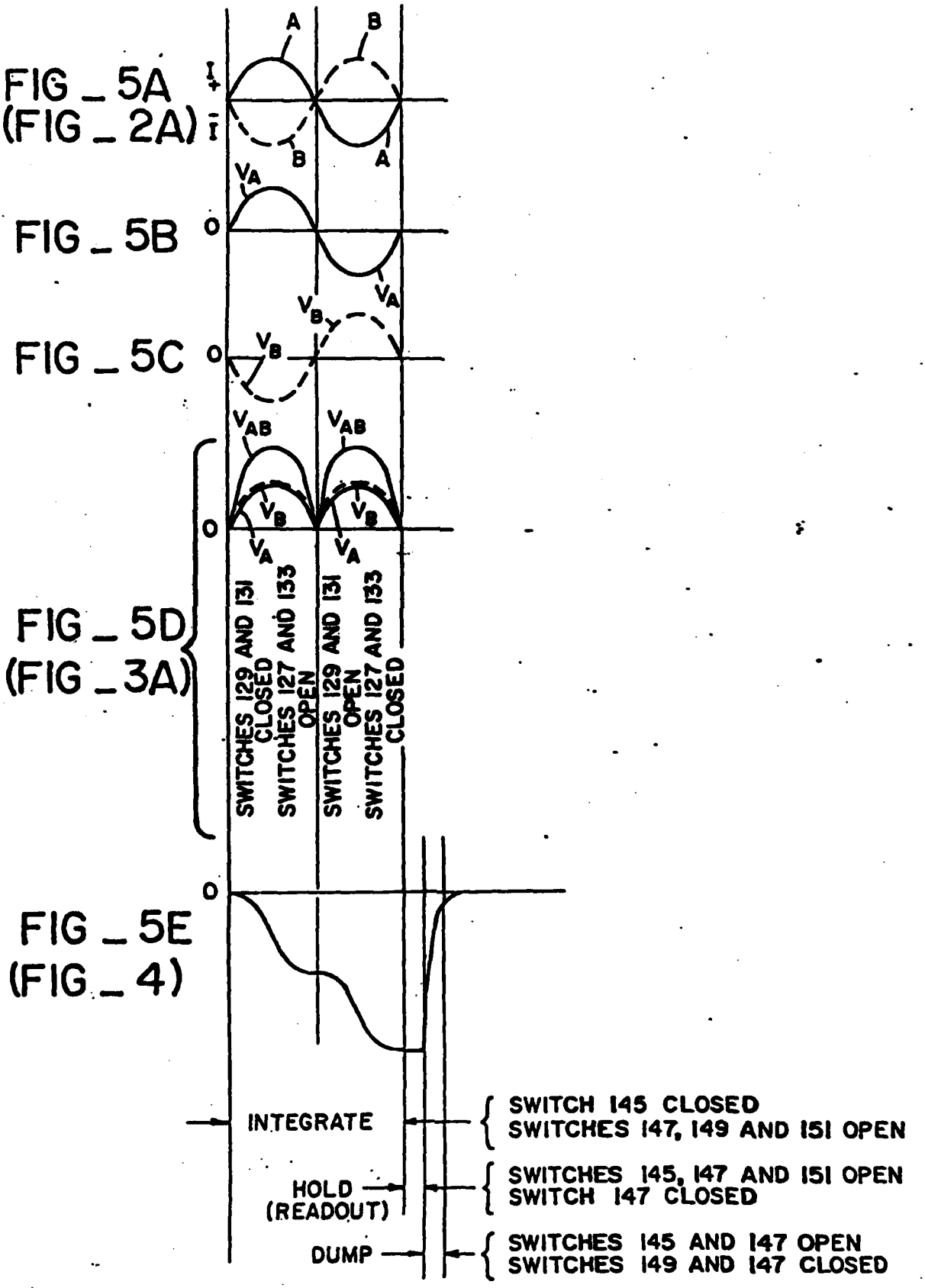
FIG_5A
(FIG_2A)
FIG_5B
FIG_5C
FIG_5D
(FIG_3A)
FIG_5E
(FIG_4)
A
B
$V_A$
$V_B$
$V_{AB}$
SWITCHES 129 AND 131 CLOSED
SWITCHES 127 AND 133 OPEN
SWITCHES 129 AND 131 OPEN
SWITCHES 127 AND 133 CLOSED
INTEGRATE
SWITCH 145 CLOSED
SWITCHES 147, 149 AND 151 OPEN
HOLD (READOUT)
SWITCHES 145, 147 AND 151 OPEN
SWITCH 147 CLOSED
DUMP
SWITCHES 145 AND 147 OPEN
SWITCHES 149 AND 147 CLOSED

# ANALOG SIGNAL PROCESSOR

## BACKGROUND OF THE INVENTION

1. Field of the Invention

The present invention relates to an analog processing circuit and more particularly to an analog processing circuit that is capable of processing very low differentially alternating current to a proportional d.c. voltage output.

2. Description of the Prior Art

Prior analog processing circuits have been unable to properly automatically detect and process successively different selected phase components from a very low differential alternating current input signal to a proportional d.c. voltage output suitable for digital processing where the input signal is widely variable in magnitude and phase and contains comparable or higher levels of harmonic signals and other undesirable noise. The present invention overcomes these difficulties by providing a phase discriminating analog signal processor that is capable of processing such signals having a very low frequency and strength into proportional d.c. voltage output signals suitable for digital processing.

## SUMMARY OF THE INVENTION

Briefly, the present invention comprises an analog signal processor that is particularly suitable for measuring, integrating and holding a single or a pair of analog signals. The input signal to the analog signal processor may be sinusoidal, of relatively low frequency and of low signal strength and slowly varying phase such as may be obtained from a pair of capacitive plates used in electric field measuring devices. The analog signal processor includes an analog current to voltage convertor, a synchronous rectifier and an integrate and hold circuit. In practice the analog signal processor may be mounted on a rotating shaft and converts the very low differentially alternating current input to a proportional d.c. voltage output. The analog signal processor includes timing and switching circuits to provide the desired information about vertical, horizontal and inclined electric fields.

## STATEMENT OF THE OBJECTS OF THE INVENTION

An object of the invention is to provide an analog signal processor that is compact and reliable.

Another object of the present invention is to provide an analog signal processor that is capable of processing successively different choices of phase of very low differential alternating currents to proportional d.c. voltage outputs in the presence of input noise including comparable harmonic signals.

Still another object of the present invention is to provide an analog signal processor that can measure, integrate and hold a single or a pair of analog signals.

Still another object of the present invention is to provide an analog signal processor that may be mounted on a rotating shaft.

A still further object of the present invention is to provide an analog signal processor that may be used in conjunction with an electric field measuring device.

Other objects, advantages and novel features of the invention will become apparent from the following detailed description of the invention when considered in conjunction with the accompanying drawings wherein:



## BRIEF DESCRIPTION OF THE DRAWINGS

FIG. 1 is a schematic diagram of the analog signal processor of the present invention;

FIG. 2 is a diagram illustrating the various input signals that may be processed by the analog signal processor of the present invention wherein possible noise, offset levels, signal harmonics are omitted for reasons of clarity;

FIGS. 3A and 3B are wave form and timing diagrams illustrating the operation and output of the synchronous rectifier and the operation of the integrate and hold circuit of FIG. 1 for typical vertical and horizontal field measurements, respectively;

FIG. 4 is a diagram illustrating the integrate, hold and dump operation of the integrate and hold circuit and the output thereof which is part of the analog signal processor FIG. 1; and

FIGS. 5A through 5E illustrate the operation of the synchronous rectifier and integrate and hold circuits during one cycle of the vertical field measurement operation.

## DESCRIPTION OF THE PREFERRED EMBODIMENT

In U.S. Pat. No. 3,917,996 issued Nov. 4, 1975, by Peter B. Wagner is described an electric field measuring device. More particularly, in this patent application is described an electric field measuring device that is particularly suited for being mounted on the nose boom of an aircraft for periodically measuring the atmospheric electric field intensity and orientation. The device includes a rotating assembly that includes a pair of capacitor plates, analog signal processing equipment, digital processing equipment, a slip ring assembly, orientation light transmitter and receiver assemblies and an information light transmitter. All of these elements are mounted on a rotatable shaft that is driven by an electric motor. The light from the rotating information light transmitter is received by a stationary information light receiver, the output of which is applied to the input of a stationary digital receiver and storage device. Floating d.c. power is transmitted by a brush assembly through the slip ring assembly to the rotating electrical equipment.

In this patent application is a description of the method for generating signals proportional to the atmospheric electric field that is being investigated. This is achieved by positioning the electric field measuring device at different locations within the atmospheric electric field. This is preferably achieved by mounting the electric field measuring device on the nose of an aircraft and periodically measuring the electric field intensity and orientation as the aircarft flies through the atmosphere. The electric field is measured in two of its three vector components, namely the horizontal and vertical components.

The electric field measuring device includes a pair of capacitive plates 17 and 19 that are preferably of metal foil that are mechanically and electrically separated and are rotated at a predetermined rate. By referring to U.S. Pat. No. 3,917,996 and to FIG. 1 of the present invention it can be seen that an analog signal processor 101 includes an analog current to voltage covertor 103 (45) and the synchronous rectifier 105 (47) and an integrate and hold circuit 107 (47) which are the subjects of the present invention. It should be noted that the capacitive plates 17 and 19, the analog current to

voltage convertor 103 and the synchronous rectifier 105 and the integrate and hold circuit 107 may be all mounted for rotation.

Typical signals that may be obtained from capacitive plates 17 and 19 are shown in FIGS. 2A through 2E. These signals are of general sinusoidal configuration and will vary in amplitude and phase depending upon the particular field that is being measured. The frequency is selected to be about 400 rpm (6.67 rps) which is determined primarily by the rate of rotation of the rotatable assembly shown in U.S. Pat. No. 3,917,996. The solid line curves of FIGS. 2A through 2E represent the A signal from capacitive plate 17 of FIG. 1 and the dotted line curves of FIGS. 2A through 2E represent the B signal from capacitive plate 19 of FIG. 1. The lower limit of the rate of rotation is determined by the sensitivity of the analog electronics, certain current leakage considerations about the capacitive plates, and by the desired spacial revolution when flown on an aircraft or the like. The maximum limit of the rate of rotation is determined by the wear rate or life expectancy of the mechanical rotating parts as well as by the available band width of the instrumentation.

The typical amplitude of the field induced current from plates 17 and 19 will vary from zero to about $10^{-7}$ amperes. Currents that are $10^{-7}$ amperes are those that may be typically encountered in a thunder storm, for example. If larger currents were introduced it would be required to make circuit modifications that would be obvious to one skilled in the art. It should be noted that capacitive plates 17 and 19 are preferably maintained at zero voltage level. It is to be understood that the analog signal processor 101 of the present invention may be used in virtually all situations where it is desirable to measure, integrate and hold either a single or a pair of analog signals.

In FIG. 1 is illustrated the analog signal processor 101 of the present invention. The analog signal processor 101 includes an analog current to voltage convertor 103 (referred to as 45 in U.S. Pat. No. 3,917,996), a synchronous rectifier 105 (referred to as 47 in U.S. Pat. No. 3,917,996), and an integrate and hold circuit 107 (referred to as 47 in U.S. Pat. No. 3,917,996).

The analog current to voltage convertor 103 includes two identical sections 109 and 111 and therefore only section 109 will be described below in detail. The field signal A of FIGS. 1 and 2 is derived from plate 17 and is applied to the inverting input 113 of operational amplifier 115. The non-inverting input 117 of operational amplifier 115 is connected to ground. Operational amplifier 115 amplifies the difference between the signal applied to the inverting input 113 and the signal applied to the non-inverting input 117. The operational amplifier 115 has an extremely high gain, a factor of about $10^6$, to provide sufficient amplification for low level incoming signals. The output of operational amplifier 115 is applied to a plurality of electronic switches 119, 121, and 123 and through a feedback network including resistor 125. This functions as a negative feedback to the inverting input 113 and therefore reduces the voltage level between plate 17 (A signal) and the ground potential. This is necessary to provide for the high gain of operational amplifier 115. Side by side diodes 116 and 118, having high resistance, are employed to protect operational amplifier 115 by shunting abnormally high currents to ground.

Switches 119, 121 and 123 function to control the overall gain of the circuit and are controlled by an automatic gain control circuit 124 when the magnitude of the analog output signal $V_{out}$ becomes too high or too low. Many different automatic gain control circuits could be used and therefore the details of circuit 124 will not be described herein. The operation of switches 119, 121 and 123 will be described in detail as follows. When switch 119 is closed, and switches 121 and 123 are open, then the output voltage $V_A = IR = V_{FB}$ where R is the resistance of resistor 125 and I is the current from plate 17. However, when switch 121 is closed, and switches 119 and 123 are open, then $V_A = (R_1 + R_2/R_2)IR$ and therefore $V_A > V_{FB}$. By selecting different resistances for $R_3$ and $R_4$ then $V_A >> V_{FB}$ by closing switch 123 and opening switches 119 and 121. From the foregoing it can be seen that the output voltage $V_{out}$ may be maintained at an acceptable level even though the value of the charge A on plate 17 varies over a wide range. In situations where it is necessary to employ a smaller bandwidth it will be desirable to shunt resistor 125 with a capacitor 126 shown in dotted lines.

In FIG. 1 is shown synchronous rectifier 105 which includes four electronic switches 127, 129, 131 and 133. Swtich 127 connects the $V_A$ signal to the negative input of differential voltage amplifier 135 through resistor 137 and switch 131 connects the $V_B$ signal to the negative input of differential voltage amplifier 135 through resistor 137. Switch 133 connects the $V_B$ signal to the positive input of differential voltage amplifier 135 through resistor 139 and switch 129 connects the $V_A$ signal to the positive input of differential voltage amplifier 135 through resistor 139. These switches operate in pairs and have alternative action. That is, when switches 127 and 133 are closed then switches 129 and 131 are open and conversely when switches 127 and 133 are open then switches 129 and 131 are closed. Resistor 140 is placed between the positive input and ground. Differential voltage amplifier 135 is made to have unity gain by selecting the proper values for resistors 137, 139, 140 and 141, which is in the feedback loop. Referring to FIG. 2A, for example, it can be seen that differential voltage amplifier will invert and add the $V_A$ and $V_B$ signals so that the resulting signal will be the sum of $V_B - V_A$ when the switches are in the position shown. When the four switches are reversed then the output from amplifier 135 will be $V_A = V_B$. It should be noted that the switching times and sequences may be varied in accordance with the particular fields being measured and the particular information desired. One particular switching sequence, for vertical fields, is shown in FIG. 5. Other switching sequences will be obvious to one skilled in the art from the following discussion of FIGS. 3, 4 and 5. Many different types of switch control circuits 156 could be used and therefore the details of circuit 156 will not be described herein. However, it should be noted that the switching by switch control circuit 156 must be in accordance with the above description of operation and in accordance with the various timing diagrams.

In FIG. 1 is shown the integrate and hold circuit 107 which includes an amplifier 143, an integrate switch 145, a hold switch 147, and a pair of dump switches 149 and 151 which are operated as a pair. The dump switches 149 and 151 function to short integrating capacitor 153 through resistor 155 to ground when it is desired to discharge the capacitor 153 as hereinafter explained.

During that period of time that it is desired to integrate the incoming signal, then switch 145 is closed,

switches 149 and 151 are open and switch 147 is open. Therefore capacitor 153 will become charged to d.c. level that corresponds to the integration of the signal $V_{AB}$ shown in FIG. 3A which represents the measurement of a vertical field, for example. In FIG. 4 is illustrated the signal $V_{out}$ that will appear at the output of amplifier 143 during the first two cycles of FIG. 3A. From FIG. 4 it can be seen that after the integration time, then switch 145 is opened, switch 147 is closed and switches 149 and 151 are open. This is referred to as the hold period. Switch 147 is employed to assure that any extraneous charges will be shunted to ground and will not be applied to integrating capacitor 153 which would provide erroneous readings. Effectively the amplifier continues to integrate with time the grounded (zero) input and therefore no change in $V_{out}$ results. During this hold period the signal $V_{out}$ will be read and recorded by external circuitry, not shown. After a suitable hold period switches 149 and 151 are closed thereby discharging or dumping integrating capacitor 153 through resistor 155 to ground. This is referred to as the dump period. After the dump period, the cycle is then repeated.

It should be noted that FIGS. 3A (for the first integrate, hold and dump cycle), FIG. 4 (for the first integrate, hold and dump cycle) and FIG. 5 are to taken together and show the complete switching sequence, timing and operation of synchronous rectifier 105 and integrate and hold circuit 107. This sequence is considered sufficient to clearly demonstrate the operation of the system. To completely describe all possible switching modes and combinations would unduly complicate the description and would be obvious to one skilled in the art. Resistor 155 is used to somewhat limit the discharge rate of the capacitor through switches 149 and 151.

Switches 145, 147, 149 and 151 are controlled by switch control circuit 157. Many different types of switch control circuits 157 could be used and therefore the details of circuit 157 will not be described herein. However, it should be noted that the switching by switch control circuit 157 must be in accordance with the above description of operation and in accordance with the various timing diagrams. With the low frequencies involved solenoid mechanical switches could be employed, however, it is preferable to employ electronic switching.

What is claimed is:

1. A analog signal processor comprising:
a. an analog current to voltage convertor;
b. a synchronous rectifier;
c. an integrate and hold circuit;
d. said analog current to voltage convertor includes first and second operational amplifiers;
e. first current means for producing a first alternating current signal and second current means for producing a second alternating current signal that is 180° out of phase with respect to said first alternating current signal;
f. said first current means being connected to the input of said first operational amplifier;
g. said second current means being connected to the input of said second operational amplifier;
h. the output of said first operational amplifier and the output of said second operational amplifier being connected to the input of said synchronous rectifier;
i. means for controlling said synchronous rectifier whereby the negative portion of the output siganl from said second operation amplifier is inverted and added to the positive portion of the output signal from said first operational amplifier and the negative portion of the output signal from said first operational amplifier is inverted and added to the positive portion of the output signal from said second operational amplifier;
j. the output of said synchronous rectifier being connected to the input of said integrate and hold circuit; whereby
k. the output of said integrate and hold circuit indicates a d.c. voltage output that is proportional to the output of said synchronous rectifier.

2. The analog signal processor of claim 1 including:
a. said integrate and hold circuit including an amplifier; and
b. an integrate switch connected between the output of said synchronous rectifier and the input of said amplifier.

3. The analog signal processor of claim 2 including:
a. a hold switch connected between said input of said amplifier and ground.

4. The analog signal processor of claim 3 including:
a. an integrating capacitor connected between the input and the output of said amplifier.

5. The analog signal processor of claim 4 including:
a. first and second dump switches connected in series with each other and in parallel with said integrating capacitor; and
b. a resistor connected between said first and second dump switches and ground.

6. The analog signal processor of claim 5 including:
a. switch control means for closing said integrate switch and opening said hold and first and second dump switches during the 360° time period of said first and second alternating current signals, then closing said hold switch and opening said integrate and first and second dump switch and then opening said integrate and hold switch and closing said first and second dump switches.

* * * * *

# United States Patent [19]

**Wagner**

[11] **4,065,765**

[45] **Dec. 27, 1977**


[54] **PULSE-WIDTH DEMODULATOR AND INFORMATION STORAGE DEVICE**


[75] Inventor: Peter B. Wagner, Reno, Nev.

[73] Assignee: The United States of America as represented by the Secretary of the Navy, Washington, D.C.



[21] Appl. No.: 603,777

[22] Filed: Aug. 11, 1975

[51] Int. Cl.² ..... G06F 3/00

[52] U.S. Cl. ..... 340/347 DD

[58] Field of Search ..... 340/167 A, 347 DD; 178/26 A, 66, 67, 68; 179/15 AW, 15.55 T, 15 AQ; 328/112, 111; 360/44; 235/92 SH



[56] References Cited

U.S. PATENT DOCUMENTS

| | | | |
|---|---|---|---|
| 2,870,429 | 1/1959 | Hales | 340/167 A |
| 3,263,030 | 7/1966 | Stiefel | 179/15 AQ |
| 3,789,137 | 1/1974 | Newell | 179/15.55 T |
| 3,823,397 | 7/1974 | Howard | 178/26 A |



*Primary Examiner*—Charles D. Miller

*Attorney, Agent, or Firm*—R. S. Sciascia; Charles D. B. Curry



[57] ABSTRACT

A pulse-width demodulator and information storage device including a data processing clocking system and an independent data readout and recorder control clocking system. The data input may comprise a pair of words for each data collection cycle. By means of an index signal, which is synchronized with the data input, the device distinguished between each word of the data pair being processed. The device converts each pulse-width modulated word into a digital format and stores each pair of words alternately in one of a pair of shift registers. The readout is alternately from the other of the pair of shift registers to the recorder on command from the recorder.


**10 Claims, 5 Drawing Figures**

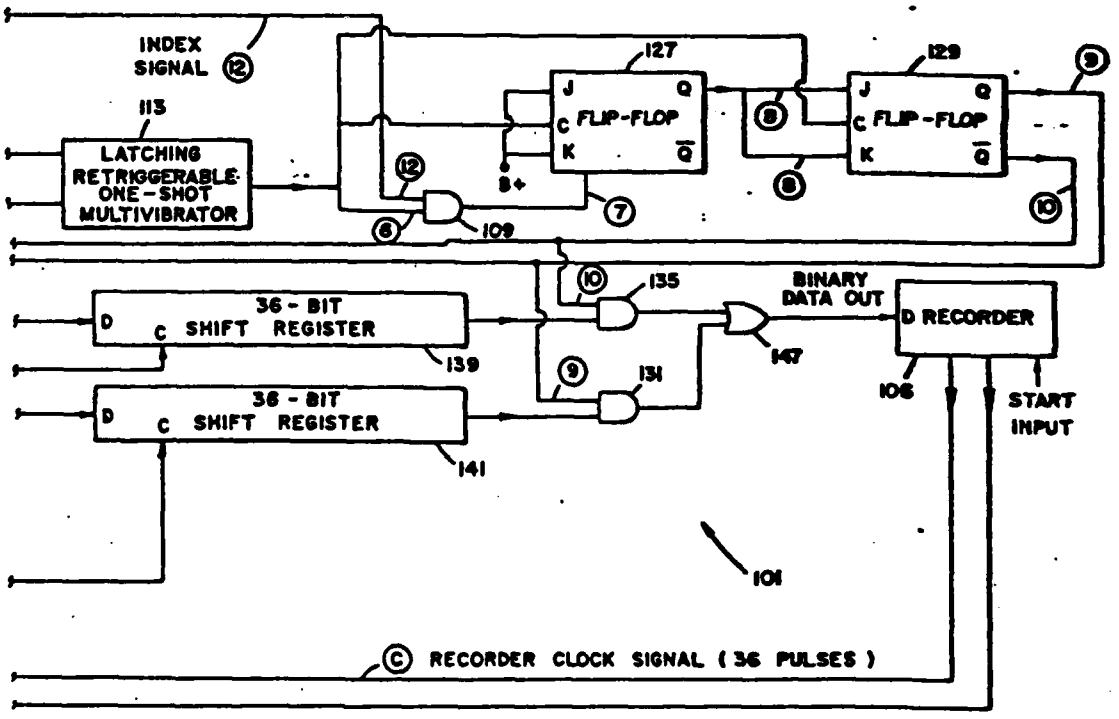

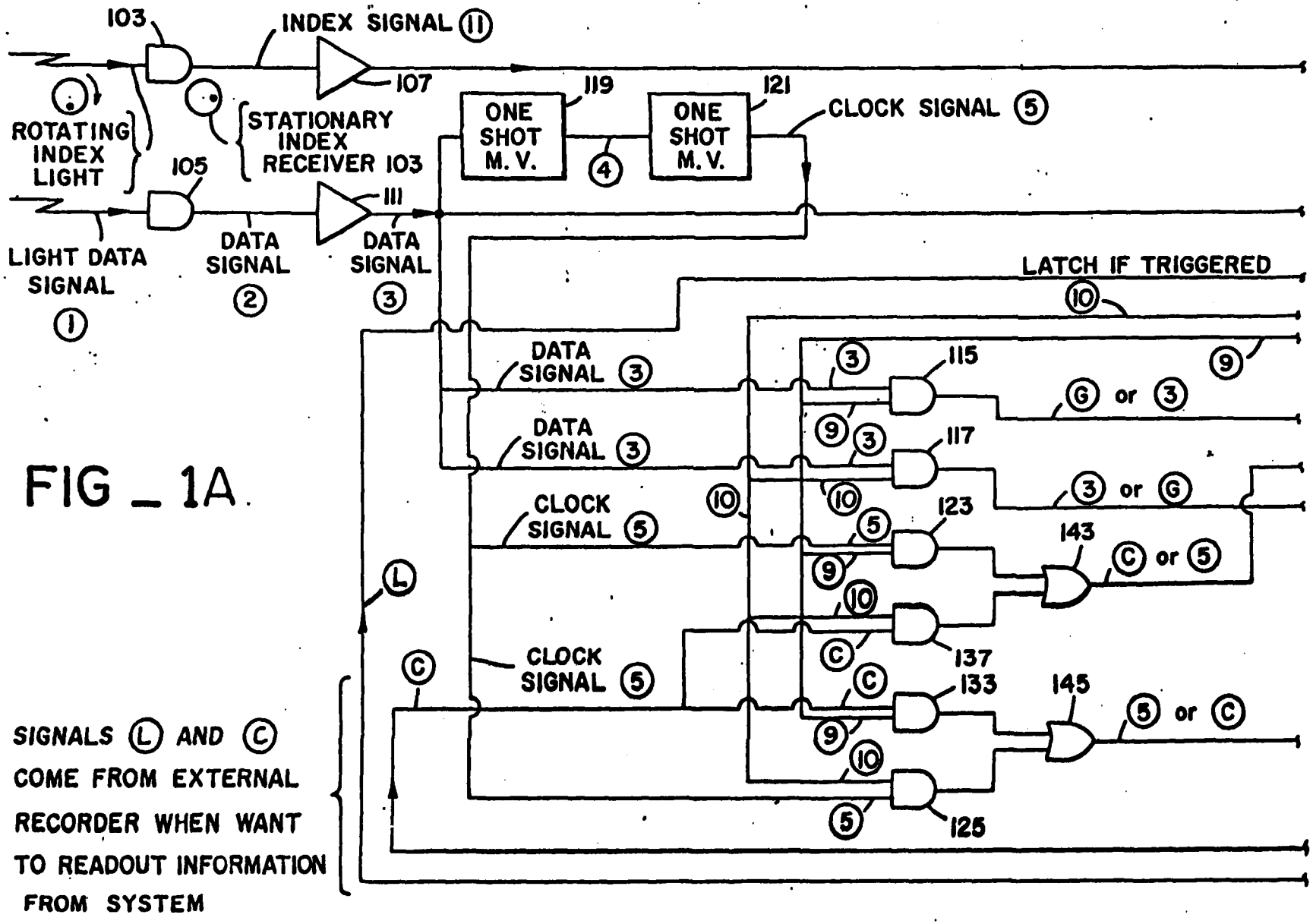
103
INDEX SIGNAL (11)
107
ROTATING INDEX LIGHT
STATIONARY INDEX RECEIVER 103
105
111
LIGHT DATA SIGNAL (1)
DATA SIGNAL (2)
DATA SIGNAL (3)
ONE SHOT M.V.
119
ONE SHOT M.V.
121
CLOCK SIGNAL (5)
(4)
LATCH IF TRIGGERED
(10)
DATA SIGNAL (3)
DATA SIGNAL (3)
CLOCK SIGNAL (5)
(L)
(C)
CLOCK SIGNAL (5)
115
117
123
143
137
133
145
125
(3) or (G)
(3) or (G)
(C) or (5)
(5) or (C)
SIGNALS (L) AND (C) COME FROM EXTERNAL RECORDER WHEN WANT TO READOUT INFORMATION FROM SYSTEM

FIG _ 1A

FIG_1B

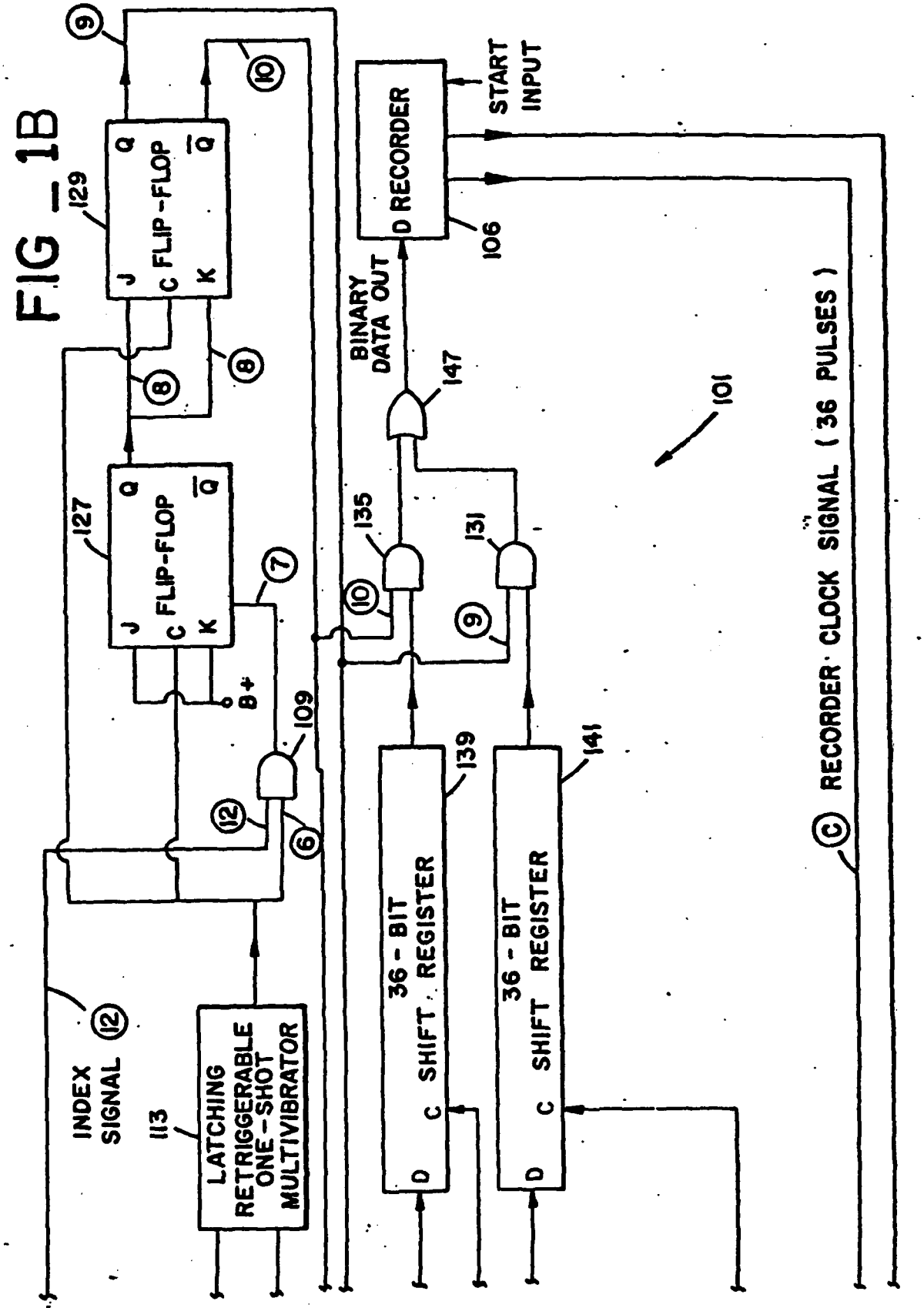
9
10
129
Q
$\bar{Q}$
J
C FLIP-FLOP
K
8
8
127
Q
$\bar{Q}$
J
C FLIP-FLOP
K
7
B+
109
12
6
INDEX SIGNAL
12
113
LATCHING RETRIGGERABLE ONE-SHOT MULTIVIBRATOR
D RECORDER
START INPUT
106
BINARY DATA OUT
147
135
131
10
9
101
36 - BIT SHIFT REGISTER
D C
139
36 - BIT SHIFT REGISTER
D C
141
C RECORDER CLOCK SIGNAL ( 36 PULSES )

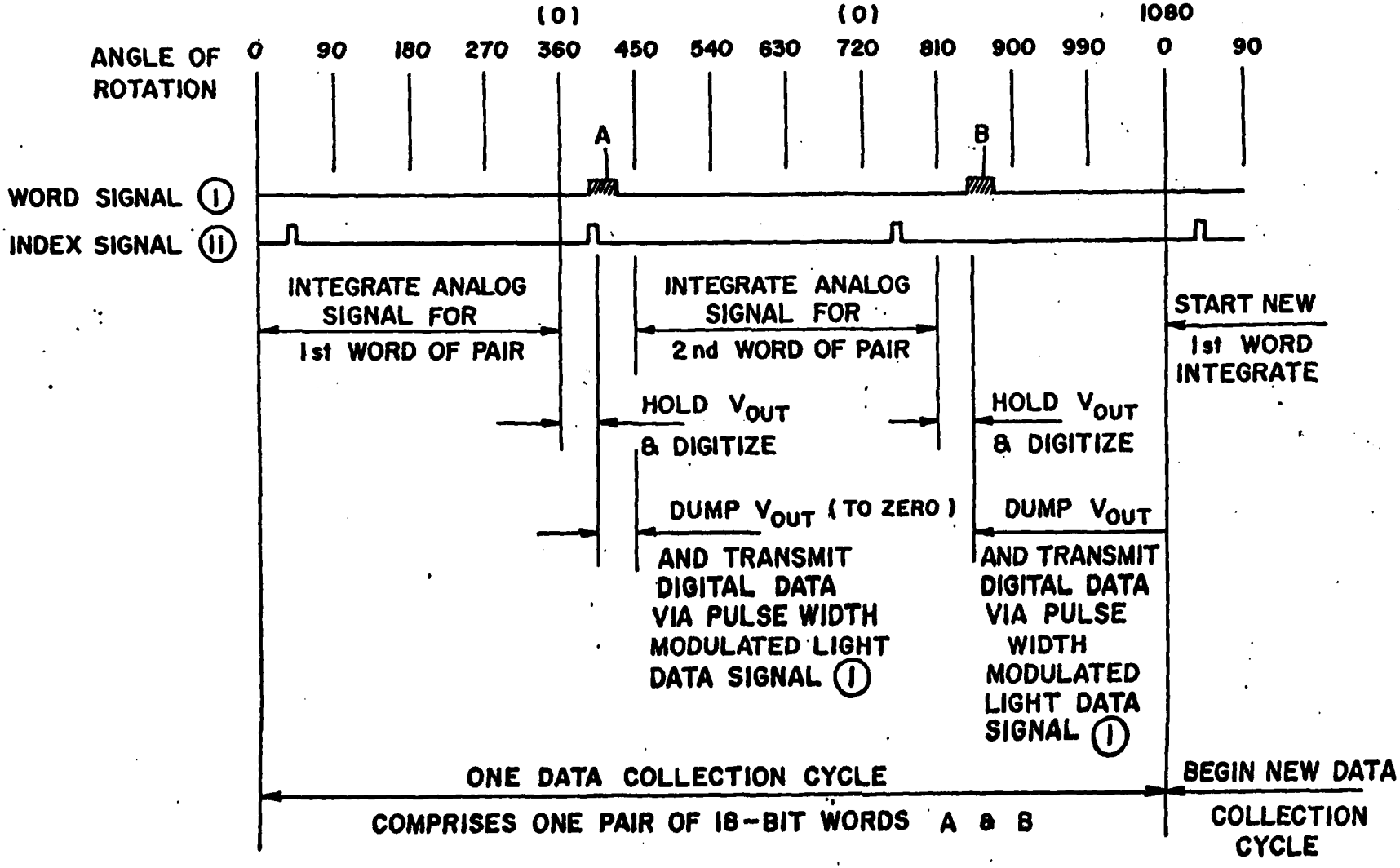
ANGLE OF ROTATION
0
90
180
270
(0) 360
450
540
630
(0) 720
810
900
990
1080 0
90
A
B
WORD SIGNAL (I)
INDEX SIGNAL (II)
INTEGRATE ANALOG SIGNAL FOR 1st WORD OF PAIR
INTEGRATE ANALOG SIGNAL FOR 2nd WORD OF PAIR
START NEW 1st WORD INTEGRATE
HOLD $V_{OUT}$ & DIGITIZE
HOLD $V_{OUT}$ & DIGITIZE
DUMP $V_{OUT}$ (TO ZERO) AND TRANSMIT DIGITAL DATA VIA PULSE WIDTH MODULATED LIGHT DATA SIGNAL (I)
DUMP $V_{OUT}$ AND TRANSMIT DIGITAL DATA VIA PULSE WIDTH MODULATED LIGHT DATA SIGNAL (I)
ONE DATA COLLECTION CYCLE
COMPRISES ONE PAIR OF 18-BIT WORDS A & B
BEGIN NEW DATA COLLECTION CYCLE

FIG_2

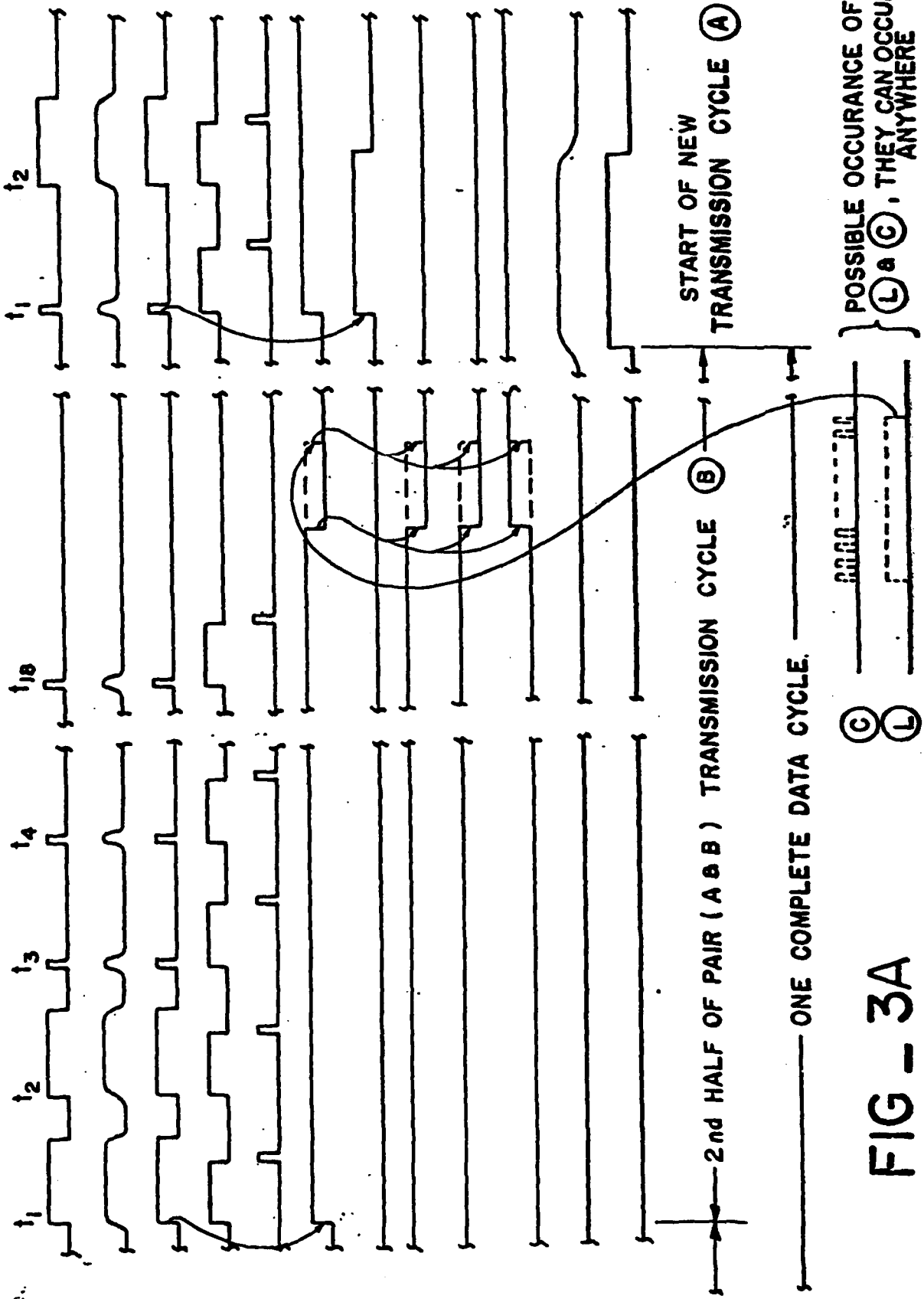
t1
t2
t3
t4
t18
START OF NEW TRANSMISSION CYCLE (A)
POSSIBLE OCCURANCE OF (L) & (C), THEY CAN OCCUR ANYWHERE
2nd HALF OF PAIR (A & B) TRANSMISSION CYCLE (B)
ONE COMPLETE DATA CYCLE
(C)
(L)

FIG - 3A

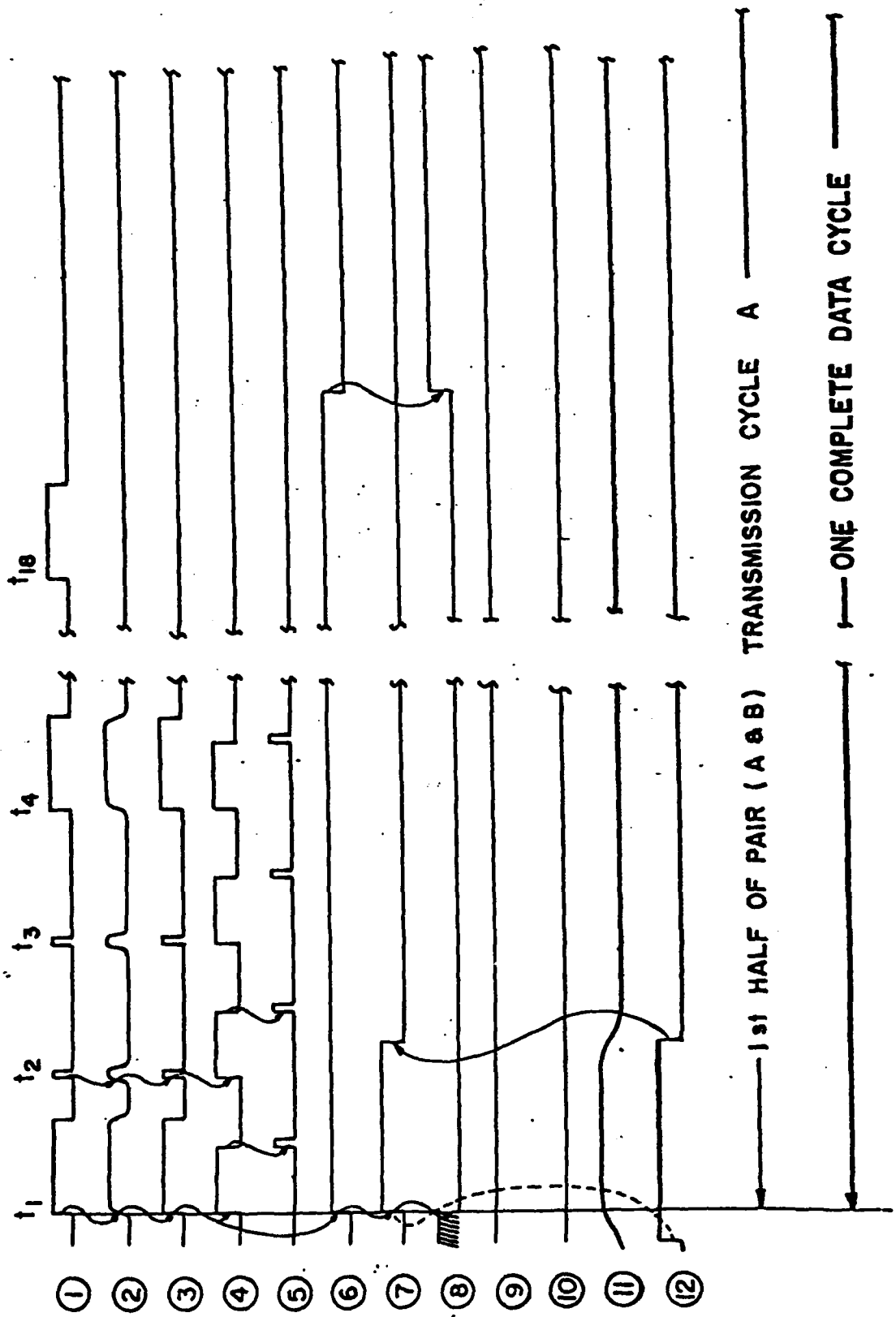
t18
t4
t3
t2
t1
1 2 3 4 5 6 7 8 9 10 11 12
1st HALF OF PAIR (A & B) TRANSMISSION CYCLE A
ONE COMPLETE DATA CYCLE

FIG - 3B

# PULSE-WIDTH DEMODULATOR AND INFORMATION STORAGE DEVICE

## BACKGROUND OF THE INVENTION

1. Field of the Invention

The present invention relates to a pulse-width demodulator and information storage device and more particularly to a pulse-width demodulator and information storage device that converts and stores pulse-width modulated data into digital data and can distinguish between the words of pairs of received words.

2. Description of the Prior Art

One type of prior pulse-width demodulators and information storage devices have had the disadvantage of attempting to use a single clock for controlling the transmitted data and for controlling the recorder and the clocking out of the stored data to the recorder. The difficulty encountered with these type devices has been in attempting to synchronize these two controls to a single clock. Other prior systems have used dual clocks to control the dual systems and a serial buffer to store the binary data. The disadvantage with these systems has been that the buffer often contains much unwanted data and the readout to the recorder includes both the wanted data and the unwanted data. In addition, other systems have been generally very complex.

The present invention overcomes these difficulties by providing a relatively simple system that employs a pair of asynchronous clocking systems. One clocking system is used for controlling the transmitted data and the other independent clocking system is used for controlling the recorder and clocking out the stored data to the recorder. In addition, the storage and readout system provides for readout of only wanted data and eliminates the readout of unwanted data.

## SUMMARY OF THE INVENTION

Briefly, the present invention comprises a pulse-width demodulator and information storage device including a data processing clocking system and an independent data readout and recorder control clocking system. The data input may comprise a pair of words for each data collection cycle. By means of an index signal, which is synchronized with the data input, the device distinguished between each word of the data pair being processed. The device converts each pulse-width modulated word into digital format and stores each pair of words alternately in one of a pair of shift registers. The readout is alternately from the other of the pair of shift registers to the recorder on command from the recorder.

## STATEMENT OF THE OBJECTS OF THE INVENTION

An object of the present invention is to provide a relatively simple pulse-width demodulator and information storage device;

Another object of the present invention is to provide a highly reliable pulse-width demodulator and information storage device;

Still another object of the present invention is to provide a pulse-width demodulator and information storage device that employs a pair of asynchronous clocking systems, one for controlling the transmitted data and the other for controlling the recorder and clocking out the stored data to the recorder;



A further object of the present invention is to provide a pulsewidth demodulator and information storage system that stores and reads out only wanted data;

A still further object of the present invention is to provide a pulse-width demodulator and information storage device that converts and stores the pulse width modulated information into digital information;

Other objects, advantages and novel features of the present invention will become apparent from the following detailed description of the invention when considered in conjunction with the accompanying drawings wherein:

## BRIEF DESCRIPTION OF THE DRAWINGS

FIGS. 1A and 1B are together a schematic diagram of the pulse-width demodulator and information storage device of the present invention;

FIG. 2 is a timing diagram that shows one type of information that may be received and processed by the pulse-width demodulitor and storage device of FIG. 1; and

FIGS. 3A and 3B are together a timing diagram illustrating the operation of the pulse-width demodulator and information storage device of FIG. 1 when it is receiving and processing the type of information shown in FIG. 2.

## DESCRIPTION OF THE PREFERRED EMBODIMENT

In FIG. 1 is shown a schematic diagram of the pulse-width demodulator and information storage device 101 of the present invention. In FIG. 2 is illustrated a timing diagram that shows one type of information that may be received and proessed by the pulse-width demodulator and storage device 101. In FIG. 3 is illustrated a timing diagram illustrating the operation of the pulse-width demodulator and information storage device 101 when receiving and processing the information shown in FIG. 2.

It is to be understood that any type of pulse-width modulated data and an accompanying index or reference signal (referred to as signal 11 in FIGS. 1 and 2) may be procesed by the pulse-width demodulator and storage device of the present invention. Frequently, data is pulsewidth modulated when it is desired to transmit binary data such as 1's and 0's. That is, a 1 is represented by a long pulse and a zero is represented by a short pulse or vice versa. The present invention is illustrated as processing 18-bit words; however, it will be obvious to one skilled in the art that it may be readily modified to process shorter or longer binary words.

The primary function of the pulse-width demodulator and information storage device 101 of the present invention is to receive pulse width modulated information, convert the pulse-width modulated information into digital information, store the digital information and then read out the stored digital information to a recorder or other device upon demand by the recorder or other device.

One of the major difficulties encountered in transmitting information from a remote sensor to a recorder is the required synchronizing of the clock pulses that control the processing of the sensor information with the clock pulses that process the information for readout to the recorder and for controlling the recorder. One of the unique features of the present invention is that it permits the processing of the sensor information by one clock timing system and the processing of the

information for readout to the recorder and for controlling the recorder by a separate clock timing system. Typically, other type systems that employ a dual clock system have stored the digital information in a serial buffer. Therefore, when the recorder reads out this serially stored information it must read out all of the stored information, much of which may be undesirable or unwanted information. One of the unique aspects of the present invention is that it employs a dual clock system that reads out, on demand of the recorder, only the wanted or desired information. Therefore, the problems associated with synchronizing a single clock system are avoided and the problem of obtaining unwanted information in a dual clock system are also avoided.

In order to more fully understand the pulse-width demodulator and information storage device 101 of the present invention, a description will be first given of one type of input information it may be used to process. A detailed description of one type of input information that may be processed by the present invention is completely shown and described in co-pending patent application Ser. No. 486,035, filed July 5, 1974, entitled Electric Field Measuring Device by Peter B. Wagner et al; copending patent application (Navy Case Number 58,393) Ser. No. 592,852, filed July 2, 1975, entitled Analog Signal Processor by Peter B. Wagner; and copending patent application (Navy Case Number 58,394) Ser. No. 592,851, filed July 2, 1975, entitled Digital Signal Processor by Peter B. Wagner.

Before considering the details of the schematic diagram of FIG. 1 it is considered desirable to describe the nature of the information that may be received by reference or index receiver 103 and data receiver 105. In general, the index signal is used to identify a particular word or pairs or words received by data receiver 105. Although the present invention may be used on any type of indexed pulsewidth modulated incoming information, FIG. 2 shows it use with an electric field measuring device (such as shown in Ser. No. 486,035) or other rotating type devices where information is desired to be known at at least one or two different positions in one 360° revolution. More particularly and in the present example the index signal 11 is used to distinguish when a revolution of information is taken from a 0° starting position as compared to when it is taken from a 90° starting position. These 0° and 90° starting positions are frequently used for measuring and analyzing atmospheric electric fields. However, it will be understood that the reference or index signal will not be required if it is not necessary to know the particular orientation being measured.

In the more general sense, it is to be understood that the present invention may be used to process pairs of pulse-width modulated information wherein one pair makes up a complete cycle of information. The pair may comprise a data word A and a data word B. It is to be understood that the information contained in data words A and B may be from any two sources such as temperatures sensors, pressure sensors and the like.

As illustrated in FIG. 1 the data output to the recorder 106 is shown as having a hard line connection which means that the recorder will serially record binary 1's and 0's. It is to be understood that the binary data output may be applied to the input of many different types of devices for further processing. One example would be the transmission of this binary data to a digital to analog convertor for transmission to an analog recorder, for example. The binary data output may be also connected to telemetry equipment, where it may be pulse-width modulated, or frequency or phase modulated, for radio transmission to remote locations.

In the specific example of FIG. 2, three complete 360° revolutions of data collection and processing are shown. Together these three revolutions comprise one data collection cycle. This data collection cycle is then repeated. Each data collection cycle is illustrated as including a pair of 18-bit words A and B. The 18-bit word A represents data starting from 0° (or 360° or 720°, etc.) and the other 18-bit word B represents data starting from 450° (810°, etc.). In the FIG. 2 example, the analog signal is being integrated from 0° to 360° for the first word A. The maximum value $V_{out}$ of the integrated analog signal is then held and converted into an 18-bit digital word and during the dump period the $V_{out}$ signal is returned to zero and the 18-bit digital word is converted into a 18-bit pulse-width modulated word A that is transmitted serially by a light beam, for example, to data receiver 105 of FIG. 1. Many different types of digital to pulse-width modulated processor are known that may perform the above described function. However, the Digital Signal Processor described in co-pending patent application Ser. No 592,851, filed July 2, 1975, has been found to be particularly suited for this purpose. This transmitted light beam signal is shown as light data signal 1 in FIGS. 1, 2 and 3 and includes pairs of 18-bit pulse-width modulated words A and B. It should be noted that the index signal 11 occurs during the beginning of the dump and transmit period of the 18-bit word A and does not occur during dump and transmit period of the 18-bit word B. This is done to distinguish between the A and B words where the A word starts at 0° and the B word starts at 90°. This operation will be hereinafter more completely described.

During the second revolution of the three revolution cycle, the analog signal is being integrated from 450° to 810° (that is, 90° displaced from the first word A). The maximum valve $V_{out}$ of the integrated analog signal is then held and converted into an 18-bit digital word and during the dump period the $V_{out}$ signal is returned to zero and the 18-bit digital word is converted into an 18-bit pulse-width modulated word B that is serially transmitted by a light beam, for example, to data receiver 105 of FIG. 1. At the end of this dump and transmit period the process is then repeated. It should be noted that the dump and transmit period for the B signal is 180° longer than for the A signal so that the next data collection cycle starts at 1080° or 0°.

The pulse-width demodulator and information storage device 101 of the present invention will be now described primarily by reference to FIGS. 1 and 3. Referring to FIG. 1, the light index signal is received by light receiver 103. In FIG. 1 is schematically illustrated one technique for generating this index signal. That is, a rotating index light will impinge upon a stationary index light receiver and thereby generate an index signal once each revolution of the rotating index light. Light receiver 103 provides an output index signal 11 which is applied to the input of schmidt trigger circuit 107. The function of schmidt trigger circuit 107 is to shape and amplify, if desired, the index signal 11. This shaped and amplified signal is shown as index signal 12 in FIGS. 1 and 3 and is applied to one input of AND gate 109 for reasons which will be hereinafter described.

The transmitted pulse-width modulated light signal 1, containing the data as previously described, is applied

to the input of data receiver 105. The output data signal 2 of data receiver 105 is applied to the input of schmidt trigger circuit 111 the output signal 3 of which is applied to one input of latching retriggerable one-shot multivibrator 113. The function of schmidt trigger circuit 111 is to shape and amplify, if necessary, its input signal as shown by comparing signal 2 and signal 3 of FIG. 3. The output of schmidt trigger circuit 111 is also applied to one input of AND gate 115 and to one input of AND gate 117. The output of schmidt trigger circuit 111 is also applied to the input of one-shot multivibrator 119 the output signal 4 of which is applied to the input of one-shot multivibrator 121. The output signal 5 of one-shot multivibrator 121 is a clock signal for the FIG. 1 device and is derived from and synchronized with the data signal 1. Referring to FIGS. 1 and 2 it should be noted that the leading edge of signal 1 starts signal 2, the leading edge of signal 2 starts signal 3, the leading edge of signal 3 starts signals 4 and 6 and the trailing edge of signal 4 starts signal 5. This is depicted in FIG. 3 by the curved arrows interconnecting signals 1 through 5. The time constants for one-shot multivibrators 119 and 121 are selected to provide pulse time durations approximately as shown in FIG. 3. From this it can be seen that the system is provided with a clock pulse signal 5 that is synchronized with the data signal 1. However, it should be noted that pulses of clock signal 5 occur during the long pulses of data signal 3 but do not occur during the short pulses of data signal 3. It should be also noted that clock signal 5 is independent from recorder clock signal C which is independently derived in recorder 106. Clock signal 5 is applied to one input of AND gate 123 and to one input of AND gate 125.

Latching retriggerable one-shot multivibrator 113 provides an output signal 6 that is applied to one input of AND gate 109, to the clock input C of flip-flop circuit 127, and to the clock input C of flip-flop circuit 129. Each of flip-flop circuit 127 and 129 have two data inputs (J an K) and two outputs (Q and $\overline{Q}$). A B+ power source is connected to both data inputs of flip-flop circuit 129. The Q output of flip-flop circuit 127, having a state that is opposite from the state of the Q output, is not used. The Q output signal 8 of flip-flop 127 is connected to both of the J and K data inputs of flip-flop 129. The Q output signal 9 of flip-flop circuit 129 is connected to one input of AND gate 131, to one input of AND gate 115, to one input of AND gate 123 and to one input of AND gate 133. The $\overline{Q}$ output signal 10, having a state that is opposite from the Q output signal 9, is applied to one of the inputs of AND gate 135, to one input of AND gate 117, to one input of AND gate 137 and to one input of AND gate 125.

External recorder 106 provides a recorder clock sigal C, having a series of 36 clock pulses, that is applied to one input of AND gate 133 and to one input of AND gate 137.

The output of AND gate 115 is connected to the data input D of 36-bit shift register 139. The output of AND gate 117 is connected to the data input D of 36-bit shift register 141. The outputs of AND gates 123 and 137 are connected to the respective inputs of OR gate 143 the output of which is connected to the clock input C of shift register 139. The outputs of AND gates 133 and 125 are connected to the respective inputs of OR gate 145 the output of which is connected to the clock input C of shift register 141.

The output of shift register 139 is connected to one input of AND gate 135. The output of shift register 141 is connected to one input of AND gate 131. The outputs of AND gates 135 and 131 are connected to the respective inputs of OR gate 147 the output of which is connected to the data input D of recorder 106. The output of OR gate 147 will be the binary data being shifted out of data shift register 139 or the binary data being shifted out of shaft register 141.

## OPERATION

Referring to FIGS. 1, 2 and 3, the shaped pulse-width modulated data signal 3 is continuously applied to the inputs of AND gates 115 and 117 when data is being received. Data signal 3 contains in series the A word containing 18-bits of pulse-width modulated data and then the B word containing 18-bits of pulse-width modulated data which together make up a complete data collection cycle as previously described. As shown by the curved arrows of FIG. 3, the leading edge of the data signal 3 turns on latching retriggerable one-shot multivibrator 113 thereby providing an output signal 6. This output signal 6 stays on until after the termination of the 18-bit A word pulse train. Signal 6 is normally terminated by selecting an appropriate internal time constant after the 18th bit has been received. The trailing edge of signal 6 toggles and therefore reverses the states of Q and $\overline{Q}$ of flip-flop circuit 127. The trailing edge of signal 6 also toggles the Q and $\overline{Q}$ state of flip-flop circuit 129 when signal 8 is on.

Referring to FIGS. 1 and 3 the coincidence of shaped index signal 12 and signal 6 will provide a reset signal 7 through AND gate 109 that is applied to the reset output of flip-flop circuit 127. This will turn off the Q output signal 8 from flip-flop circuit 127. This is necessary to correct an error if the initial state of the Q output of flip-flop circuit 127 is on at the start of the A period of operation. This is illustrated by the hatched lines at the start of signal 8 in FIG. 3. This also functions to distinguish the A data from the B data since signal 8 must be off for the A data and on for the B data.

Referring to AND gate 123 it should be noted that when the clock signal 5 is on and the Q output signal 9 is on that the clock signal 5 will be applied through OR gate 143 to the clock input C of shift register 139. Therefore, the output of AND gate 115 will be shifted into shift register 139. If data signal 3 is on and the Q output signal 9 is on then the pulse-width data on data signal 3 will be shifted into shift register 139 in binary form. Referring to FIG. 3 it can be seen that the clock pulse 5 will shift a 1 into shift register 139 when a long data pulse on signal 3 occurs because the clock pulse 5 occurs simultaneously with the long data pulse. However, the clock pulse 5 will shift a zero 0 into shift register 139 when a short data pulse on signal 3 occurs because the clock pulse 5 does not occur simultaneously with the short data pulse. Therefore, when the clock signal 5 and the data signal 3 are being applied to shift register 139 a series of 36 bits of 1's and 0's, corresponding to the long and short pulses of data signal 3, will be shifted into shift register 139. This 36-bit group consists of the A and B words of one complete transmision cycle. It should be noted that the A word is first shifted in which is then followed by the B word. This is essential for proper data evaluation. However, it would be equally acceptable if the B word was always first shifted in and then followed by the A word. This would require system modifications which would be obvious to one skilled in the art. During the period when the data signal 3 is being shifted into shift register 139, data signal 3

will not be shifted into shift register 141 because the $\overline{Q}$ output signal 10 will be off.

Conversely, when the data signal 3 is on and $\overline{Q}$ output signal 10 is on then AND gate 117 will present the pulse-width data of data signal 3 to the data input D of shift register 141. When this occurs 36 bits of corresponding digital 1's and 0's will be shifted into shift register 141 because clock signal 5 will be on and the $\overline{Q}$ signal 10 will be on and both will be applied to the input of AND gate 125 which therefore provides a clock signal 5 through OR gate 145 to the clock input C of shift register 141.

In summary, while a data signal 3 is on the corresponding 36-bit binary data (words A and B) will be shifted into either shift register 139 or shift register 141 depending respectively on whether the Q signal 9 is on (and Q signal 10 is off) or $\overline{Q}$ signal 10 is on (and Q signal 9 is off).

When the recorder clock signal C is on, which is started upon recorder demand at any point in time during a data cycle, it is applied to the respective inputs of AND gates 133 and 137. Therefore, when the $\overline{Q}$ signal 10 is on the recorder clock signal C will be applied through AND gate 137 and OR gate 143 to the clock input C of shift register 139. At this time the output of AND gate 115 will provide no output signal, or will be at ground G, and the clock signal C will provide 36 clock pulses and shift out all of the binary data stored in shift register 139 and shift into shift register 139 a group of 36 0's in series. The binary data from shift register 139 will be shifted through AND gate 135, since the $\overline{Q}$ signal 10 is on, and through OR gate 147 to the data input D of recorder 106. It should be particularly noted that the output shift rate of shift register 139 corresponds to and is synchronized with the operation and control rate of recorder 106 since they are both controlled by recorder clock signal C.

Conversely, when the Q signal 9 is on, the recorder clock signal C will be applied through AND gate 133 and OR gate 145 to the clock input C of shift register 141. At this time the output of AND gate 117 will provide no output signal, or will be at ground G, and the clock signal C will provide 36 clock pulses and shift out all of the binary data stored in shift register 141 and will shift into shift register 141 a group 36 0's in series. The binary data from shift register 141 will be shifted through AND gate 131, since the Q signal 9 is on, and through OR gate 147 to the data input D of recorder 106. It should be particularly noted that the output shift rate of shift register 141 corresponds to and is synchronized with the operation and control rate of recorder 106 since they are both controlled by recorder clock signal C. Digital words A and B, 18 bits each, normally represent a pair of signals related in time or in other ways. It is desirable to preserve the relationship between the two words by grouping them in one 36-bit word as held by shift register 139 or 141. Thus the 18 bits of the A word is the first series of bits entered in shift register 139 or 141 and followed by the 18 bits of the associated B word.

Referring to FIGS. 1, 2 and 3, shaped signal 12 is in coincidence with signal 6 at the beginning of the A word transmission cycle only. The resulting output of AND gate 109 resets flip-flop circuit 127 thereby starting the counting process. The process results in flip-flop circuit 129 changing state only after completion of transmission of the B word.

The time duration of the L signal is selected to be about the same as the time duration of the 36-bit recorder clock pulse train C. The L signal is applied to the latch input of latching retriggerable one-shot multivibrator 113. Therefore, when data is being clocked out of either shift register 139 or 141 by recorder clock signal C then the L signal will be applied to the latch input of latching retriggerable multivibrator 113 and will assure that signal 6 will be on for the full time duration of clock signal C even though the 18th bit of signal 3 had previously terminated. It should be noted that this condition will arise only when the recorder clock signal C occurs during the time period shown by the C and L curves at the bottom of FIG. 3. At other selected readout times by recorder 106 the L signal will have no effect. It should be noted that signal L, by itself, will not initiate signal 6. This is done to prevent flip-flop circuit 129 from changing until the data transmission to the recorder is complete.

In view of the foregoing it can be seen that a unique pulse-width demodulator and information storage device is provided. It will be obvious to those skilled in the art that various modifications can be made and still be within the scope of the present invention. Some of the modifications have been previously mentioned. However, it should be noted that the present invention may be used to process more than 2 groups of words that together make up a complete data collection cycle. For example, 3 words A, B and C may comprise the group. Moreover, the bit length could be more or less than 36 bits. The basic modifications that would be required would be in expanding the counter (now consisting of flip-flops 127 and 129) to a larger number that would be responsive to the number of words in the data collection cycle. It should be also noted that the present invention can process an A word having a bit length of from 1 bit to 35 bits and a B word length of from 35 bits to 1 bit, without change to any of the circuits. However, it would be necessary that the combined length of the A and B words equal 36 bits. If not, it would be only necessary to change the length of the shift registers to correspond to the combined bit length.

What is claimed is:

1. A pulse-width demodulator and information storage device for processing a series of at least a first pair and a second pair of pulse-width modulated words comprising:
   a. first data means for receiving said pairs of pulse-width modulated words;
   b. a first clocking means responsive to the output of said first means for generating first clock signal pulses that are synchronized with the pulses of said pairs of pulse width modulated words;
   c. a first shift register;
   d. a second shift register;
   e. second means responsive to the output of said first data means and to output of said first clocking means for alternately shifting said first pair of words into said first shift register and then shifting said second pair of words into said second shift register; and
   d. third means for alternately shifting said first pair of words out of said first shift register and then shifting said second pair of words out of said second shift register.

2. The device of claim 1 wherein:
   a. said pulse width modulated words are comprised of long pulses and short pulses; and

b. said first clock signals are coincident with said long pulses but are not coincident with said short pulses.

3. The device of claim 2 wherein:

a. said first clocking means including a first one-short multivibrator responsive to the output of said first data means and a second one-shot multivibrator responsive to the output of said first one-shot multivibrator;

b. said first one-shot multivibrator being responsive to the leading edge of both said long pulses and said short pulses of said pulsewidth modulated words;

c. the time constant of said first one-shot multivibrator being less than said long pulses and more than said short pulses; and

d. said second one-shot multivibrator being responsive to the trailing edge of said first one-shot multivibrator.

4. The device of claim 2 wherein:

a. said second means includes a third multivibrator responsive to the output of said first data means;

b. the output of said third multivibrator being connected to the respective clock inputs of first and second flip-flop devices; and

c. one output of said first flip-flop device connected to the two data inputs of said second flip-flop device.

5. The device of claim 4 including:

a. an index signal;

b. said index signal coincident with the beginning of said first pair of pulse-width modulated words but not coincident with said second pair of pulse-width modulated words;

c. an index AND gate;

d. said index signal being applied to one input of said index AND gate;

e. the output of said third multivibrator connected to the other input of said index AND gate; and

f. the output of said index AND gate connectedto the reset input of said first flip-flop device.

6. The device of claim 4 wherein:

a. said second flip-flop device has first and second outputs wherein when said first output has a signal said second output has no signal and when said second output has a signal said first output has no signal;

b. a first AND gate and a second AND gate;

c. said first output of said second flip-flop device being connected to one input of said first AND gate and said second output of said second flip-flop device being connected to one input of said second AND gate;

d. the output of said first data means connected to the other input of said first AND gate and to the other input of said second AND gate;

e. the output of said first AND gate being connected to the data input of said first shift register; and

f. the output of said second AND gate being connected to the data input of said second shift register.

7. The device of claim 6 including:

a. third and fourth AND gates;

b. the output of said first clocking means connected to one input of said third AND gate and to one input of said fourth AND gate;

c. said first output of said second flip-flop device being connected to the other input of said third AND gate and the second output of said second flip-flop device being connected to the other input of said fourth AND gate; and

d. the output of said third AND gate being connected to the clock input of said first shift register and the output of said fourth AND gate being connected to the clock input of said second shift register.

8. The device of claim6 including:

a. fifth and sixth AND gates;

b. a second clocking means;

c. the output of said second clocking means connected to one input of said fifth AND gate and to one input of said sixth AND gate; and

d. the second output of said second flip-flop device being connected to the other input of said fifth AND gate and the first output of said second flip-flop device being connected to the other input of said sixth AND gate.

9. The device of claim 8 wherein:

a. the number of pulses in said first pair of pulse modulated words, the number of pulses in said first clock signal, the number of pulses in said second clock signal, the number of bit storage in said first shift register, and the number of bit storage in said second shift register are all the same.

10. The device of claim 7 wherein:

a. said third multivibrator is a latching retriggerable one-shot multivibrator;

b. a latching signal means for generating a latching signal having about the same time duration as the time duration of said second clock signal; and

c. the output of said latching signal means connected to the latching input of said latching retriggerable one-shot multivibrator.

* * * * *

# Letter Discussing Principles and Operation of Field Mill

July 21, 1975

# THE FIELDMILL

## Discussion of Principles

Because of the need to make these measurements from above the fog a new field mill was designed to extend forward from the nose of a twin-engine aircraft. This involves unique features and has resulted in three Navy patent applications covering the special features of the design. Briefly, the design carries miniature operational amplifiers and digital conversion circuitry within the rotating section carrying the charge detection plates. In this way there are no brush problems which can introduce noise in transmitting the low level signals. The digital signals are carried out to the recording circuitry through an axial photo emitting diode and photo diode detector, thus completely avoiding brush noise in the signal path. Automatic ranging of the digital circuitry allows a wide dynamic range to be covered without losing sensitivity and the amplifier range being used is transmitted as part of the signal. Power is transmitted to the unit via brushes but because extensive filtering and regulation can be applied to the voltage supply lines no brush noise enters the circuitry this way. Separate brushes not carrying current provide the instrument ground. Finally the charge detecting plates are inside a glass dielectric cylinder and this provides easy cleaning and small likelihood of conductivity changes in the actual amplifier circuitry.

Our device was designed to work in low fields without any precipitation being present. I have not considered in any detail how raindrops splashing on the glass will affect the device, or snow crystals, but it does seem optimistic to me to expect it to work well under these conditions. It will however,

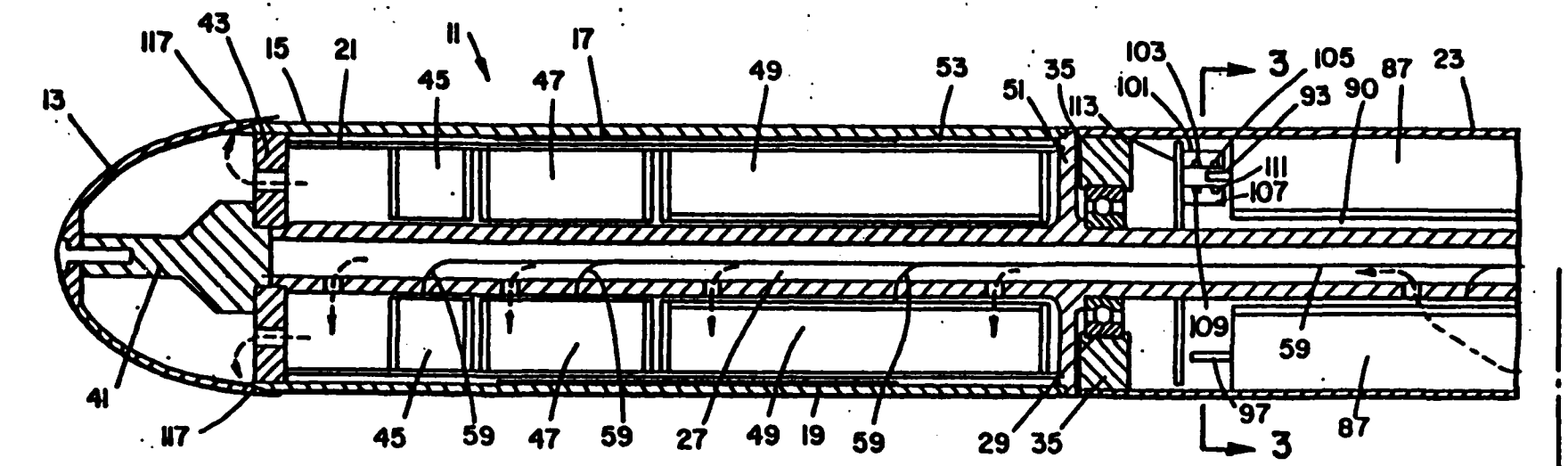


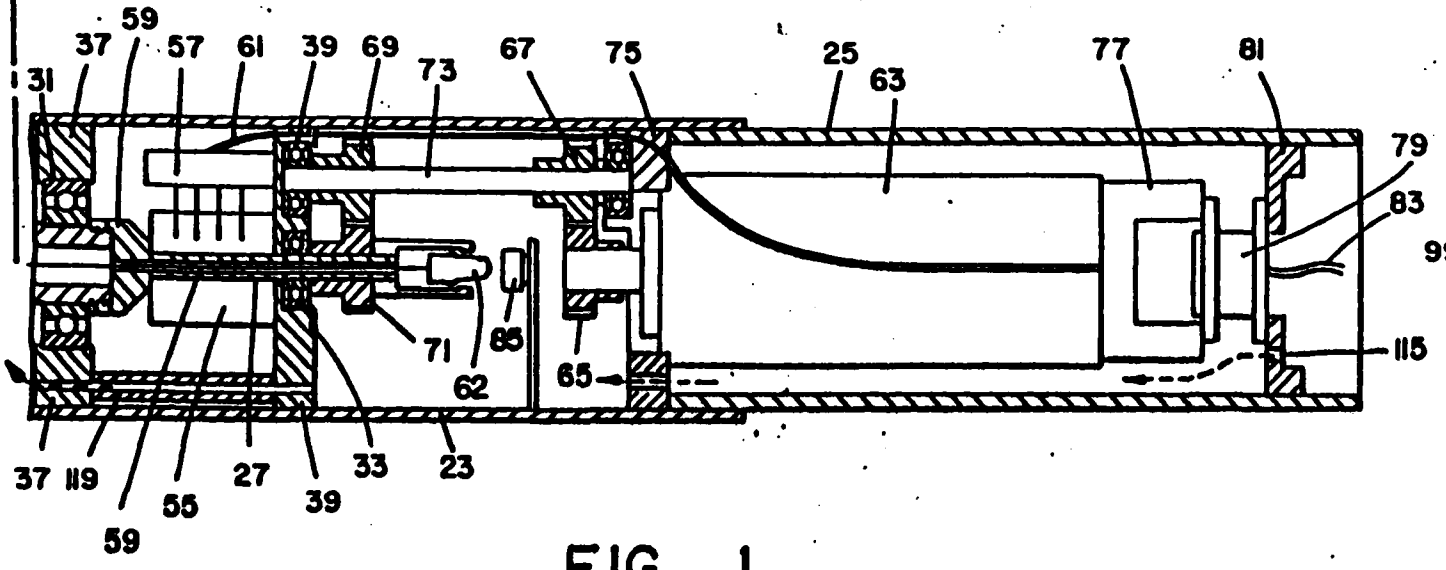


FIG_1

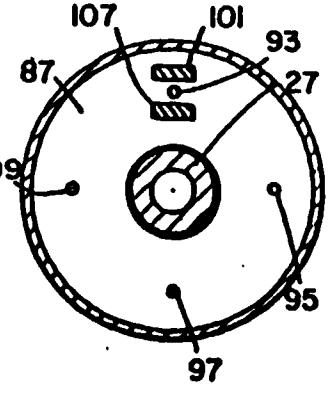


FIG_3

U.S. Patent Nov. 4, 1975 Sheet 1 of 2 3,915,396

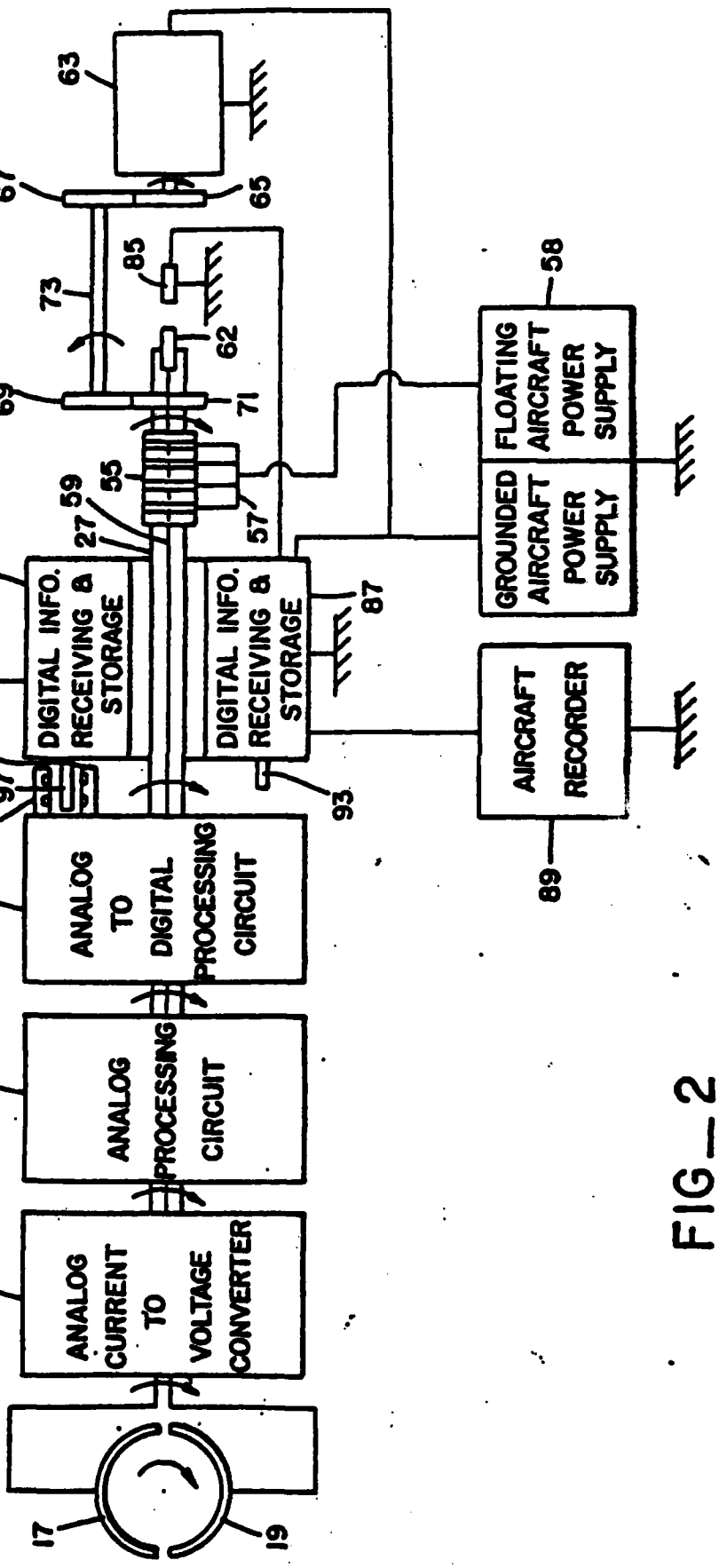
63
67
65
85
73
62
69
71
59
55
27
57
87
87
DIGITAL INFO. RECEIVING & STORAGE
DIGITAL INFO. RECEIVING & STORAGE
107
97
101
93
49
ANALOG TO DIGITAL PROCESSING CIRCUIT
47
ANALOG PROCESSING CIRCUIT
45
ANALOG CURRENT TO VOLTAGE CONVERTER
17
19
58
FLOATING AIRCRAFT POWER SUPPLY
GROUNDED AIRCRAFT POWER SUPPLY
AIRCRAFT RECORDER
89

FIG_2

be no more vulnerable than an external electrode device as I will show below and will recover much faster. The effect of corona will similarly be no worse using the surrounding glass window. We do not expect the mill to survive undamaged in large corona currents or lightning strikes.

My concern that I have failed to communicate adequately the essential feature of our device is illustrated by your Figure 1 which shows two areas, charge accumulation and shielding, and clearly is meant to convey that if one or both these effects are present to a substantial extent the device will not work. I want to emphasize that the device is entirely independent of fixed charges on the window so charge accumulation has no effect on the measurement (see later for varying charges). Most of the other effects you mention such as piezo electric effects are similarly excluded from the signal.

The reason for this is as follows. The device measures the total charge flowing from one plate to the other when the window and the attached plates rotate by 180 degrees. The signal is reversed for the 180° measurement so external fields are seen as positive in both measurements. My discussion of timeconstants in the last letter showed the degree to which the charges needed to be immobilized by the high surface resistivity to have no effect. Exactly the same timeconstant which applies to the charges which provide shielding by neutralizing the induced charges from

the field being measured will also apply to the resident charges left on the glass as generated by other processes. Since electrostatic fields add linearly the field penetrates the glass just as though there were no charged patches on its surface. Any charged area which remains from one measurement to the next, 180° of rotation later, would be included in the integral positively the first time and negatively on the next sample, if the integration of current to charge was performed before rectification, so adding samples in pairs (or smoothing out the fluctuations synchronous to the rotation speed by other means) exactly cancels effects of charges fixed to the glass. We actually rectify before integration, and reset the integral each sample, so no effect of a fixed charge is even processed. The desired field appears with the same sign in each sample so is accurately retained after averaging.

We should consider charge induced in the adjacent structure by charges fixed to the window. When the remaining support and aircraft structure is symmetric about the axis of rotation the induced charge will rotate with the glass (with some phase lag if the conductivity is low) and so cancel as above. We use a probe just behind the mill which is adjusted by rotation and separation to provide cancellation of unsymmetrical features of the aircraft itself.

Before going on to examining to what extent a given rate

of change of surface charge can penetrate the system I would like to state again that effects like piezo-electric charges or work function potentials (Volta effects) on the rotating probe can only affect the measurement if they are changing in synchronism with the rotation so that they are always occurring at the same angular position. This applies to all effects on the rotating parts. I would like to write about other effects later on in this letter. Even then, any sustained synchronous effect will result in a zero off-set which will be nulled out during calibration. The extent to which any synchronous piezo electric effect changes the zero drift between calibrations and so adds to instrumental drift from the electronics, is a matter that will have to be determined by experience. I hope I am not giving the impression that I am dogmatically asserting our device will work. What I am trying to say is that most of the effects you have brought up have been taken care of in principle and that only experience with the device will reveal unforeseen problems from these or other causes.

The functioning of the phase locked electronic sampling device can be discussed as follows. This is the key to rejecting effects of surface charges and other effects which rotate with the front end of the device containing the electrodes. The electrodes are each connected to an amplifier with a feedback loop which maintains the electrode at frame potential (i.e. we

have a zero impedence measuring device) to within a few millivolts. The current into the electrode necessary to maintain zero potential is amplified and integrated to give the charge on the plates at any instant. There are bandwidth limits at this stage. Very rapid changes are not responded to, so a charged drop hitting the glass over an electrode will not be included in the charge circuit until a millisecond or so has passed. Since the electrodes are 0.1 m long, at 100 m $sec^{-1}$ airspeed a charged drop which does not come to rest on the surface will just barely be registered as an individual and could be largely excluded by lengthening this timeconstant to 5 m sec or more. The band pass filtering mentioned later would be a much more effective rejection mechanism. The average effect of charged drops is a real part of the field we are measuring. On the other end of the timescale a charge which sticks to the glass for several seconds will no longer be seen in the measured charge as the integrator acts as a high pass filter and sustained (zero frequency) effects on the rotating parts are removed at this stage. (The system however measured to zero frequency.)

We now need to quantitatively assess the frequencies (or time constants) of charge or field changes to which the system is sensitive. Our device samples the charge magnitude essentially instantaneously at 90° intervals so spectral density analysis and the concepts of aliasing apply directly. If we average

every third successive 180° pair of measurements we have 7/3 samples per second so clearly the frequency foldover is 1.17 Hz and changes in the real field at higher frequencies than this will appear as slower frequencies in the data.

However changes due to the charges rotating with the glass are the important item in terms of errors. Assume we have a small metal plate fixed to the outside of the glass above an electrode and that we can feed this plate with a sinusoidal potential. We will first consider the case where the glass has no leakage. Since we assume a charging mechanism it is exactly equivalent to charging the plates directly with no glass present. How will this charge appear in the output?

The actual procedure used in our field mill first takes the current to the electrodes, amplifies it, rectifies and integrates it across one full revolution. This gives the difference between the charges gathered on each plate over this period with a reversed connection half way through. This resulting current integral is thus averaged, measured and the integrator reset once each cycle. The next cycle is devoted to measuring the other component 90° away. Thus we get one sample of each field every third revolution.

If we apply a charge to the plate of,

$$q = a \sin(2\pi t/T_E),$$

this will induce a current,

$$i = dq/dt = (2\pi a/T_E)\cos(2\pi t/T_E).$$

We now integrate i from $t_s$ to $t_s+T/2$, and then reverse the sign of i and continue integrating from $t_s+T/2$ to $t_s+T$. T is the rotation period. Thus the resulting mean charge Q is,

$$Q = \int_{t_s}^{t_s+T/2} (2\pi a/T_E)\cos(2\pi t/T_E)dt - \int_{t_s+T/2}^{t_s+T} (2\pi a/T_E)\cos(2\pi t/T_E)dt$$

$$= 2\pi a/T_E \int_{t_s}^{t_s+T/2} [\cos(2\pi t/T_E) - \cos(2\pi t/T_E + \pi T/T_E)]dt$$

$$= 4\pi a/T_E \int_{t_s}^{t_s+T/2} \sin(2\pi t/T_E + \pi T/2T_E)\sin(\pi T/2T_E)dt$$

$$= (4\pi a/T_E)\sin(\tfrac{\pi}{2}T/T_E)\left[\frac{-T_E}{2\pi}\cos(2\pi t/T_E + \tfrac{\pi}{2}T/T_E)\right]_{t_s}^{t_s+T/2}$$

$$= 2a \sin(\pi T/2T_E)[-\cos(2\pi t_s/T_E + \pi T/2T_E + \pi T/T_E) + \cos(2\pi t_s/T_E + \pi T/2T_E)]$$

$$= 2a \sin(\pi T/2T_E)[2\sin(2\pi t_s/T_E + \pi T/T_E)\sin(\pi T/2T_E)]$$

$$= 4a \sin(\pi T/2T_E)\sin(\pi T/2T_E)\sin(2\pi t_s/T_E + \pi T/T_E).$$

For successive readings, $t_s = t_0 + 3nT$.

Thus,

$$Q = 4a \sin^2(\pi T/2T_E)\sin(6\pi nT/T_E + 2\pi t_0/T_E + \pi T/T_E).$$

Converting time to frequency, $T/T_E = f_E/f$, and $f_E = 1/T_E$.

$$Q = 4a \sin^2\left(\frac{\pi}{2}\frac{f_E}{f}\right)\sin\left(2\pi\frac{3nf_E}{f} + 2\pi t_0 f_E + \frac{\pi f_E}{f}\right).$$

If the charge rotates around the glass in the opposite sense to the rotation of the glass it simulates a stationary constant external field.

Thus $f_E = f$.

Thus,

$$Q = 4a \sin^2(\tfrac{\pi}{2}) \sin[2\pi(3n) + 2\pi t_0 f + \pi]$$

$$= -4a \sin(2\pi t_0 f).$$

$t_0$ controls the phase of the applied charge signal and is equivalent to the angle the field makes to the sampling index. Since both $t_0$ and $f_E$ are constant we have a constant signal output representing the constant field responsible for the charge on the electrodes.

Whether the external field is slowly rotating around the field mill or varying sinusoidally with time makes no difference to the signal. If the frequency of this variation is $f_1 \pm \ell f$ and the rotation frequency f we may say, for the frequency of variation of the charge on the rotating electrode,

$$f_E = mf \pm f_1,$$

where $f_1 < f/2$, and $\ell$, m and n are integers, or the frequency in fixed space is,

$$f_s = f_E \pm f = (m \pm 1)f \pm f_1.$$

Then,

$$Q = 4a \sin^2\left(\frac{\pi}{2}\frac{f_1}{f}+m\frac{\pi}{2}\right)\sin\left(2\pi 3n\frac{f_1}{f}+2\pi t_0 f_1+m\pi+m2\pi t_0 f+\pi\frac{f_1}{f}\right)$$

$$= (-1)^m 4a \cos^2\left(\frac{\pi}{2}\frac{f_1}{f_2}+\frac{(m-1)\pi}{2}\right)\sin\left(2\pi n\frac{3f_1}{f}+\phi\right),$$

where $\phi = 2\pi t_0(f_1+f) + \pi f_1/f$ is a constant phase angle.

Thus the amplitude of the signal varies as $\cos^2\left[\frac{\pi}{2}\frac{f_1}{f}+\frac{(m-1)\pi}{2}\right]$. Thus if f is small and $f_s$ is nearly an odd multiple of f (m even) then the signal varies as $\sin^2\left(\frac{\pi}{2}\frac{f_1}{f}\right)$. For $f_s$ an even multiple of f the signal varies as $\cos^2\left(\frac{\pi}{2}\frac{f_1}{f}\right)$.

Thus in the case where $f_s = 0$, 2f, etc. the signal is passed through the system at maximum gain. An external slowly varying field is composed of very low frequency components which are transferred according to a $\cos^2$ gain factor and so are almost unattenuated.

On the other hand slowly varying components of charges on the glass which rotate with the glass give m = 0 and the gain factor is $\sin^2\left(\frac{\pi}{2}\frac{f_1}{f}\right)$ so very little signal error arises from this source.

Thus the rectification, integration and sampling procedure in the instrument severely attenuates slowly changing effects on the glass. External fields changing more rapidly than $t_E = t/2$ = 3.5 Hz are indistinguishable from charges on the glass changing more slowly than this. This is the typical folding frequency

effect found in repetitive sampling in measurements. In addition we only take every third value so our folding frequency is actually 3.5/3 = 1.17 Hz. Thus no signal of a frequency larger than this (or more than 1.17 Hz from an even multiple of 7 Hz) can be distinguished from real signals at less than this frequency. This problem can be avoided by a filter in front of the integrator in the current amplifier circuit. If we only amplify frequencies between (7-1.17) Hz and (7+1.17) Hz we have everything that can be unambiguously detected and only charges rotating with the glass that vary in this frequency range will leak into the signal. This effect will be the same whether or not a glass window is present as if its resistivity is high enough to work it will transmit charges to the plates at these frequencies just as effectively by induction as by conduction. We have not done this extra filtering as yet because we did not anticipate needing to make measurements in rapidly charging fields but it is a simple modification to add.

This analysis bridges the gap from the absolute statement that unvarying charges on the glass have no effect to real cases where the charge on the glass is changing.

To put this in perspective we have postulated the glass over one plate (actually we have analyzed it as though charging the plate itself) only being charged first one sign and then the other in periods of a few seconds. Symmetric charging

around the whole cylinder will affect the result in proportion to the time derivative of the charge at the same frequency so much greater attenuation will follow. Furthermore we must stress that this analysis applies to the plates without windows covering them or equally well with a non-conducting window.

Indeed we can now reach the conclusion of my first letter that the window makes virtually no difference if its surface resistivity is high enough. Any charging mechanism affects plates behind a window in the same way as exposed plates. In a rotating cylinder field mill (without external stationary shielding metal windows as used in flat field mills) a window rotating with the electrodes makes no difference. Charged volumes of air affecting one side of the probe and not the other are indistinguishable from comparable changes in the overall electric field whether the charge is deposited on the glass or the metal electrodes or just blows past. Finally the charge leakage around the glass acts exactly the same way as the low frequency cut off of the front end amplifiers and while it can be used to attenuate fluctuating charge effects it will attenuate the true signal in the same way. In any case a fixed charge on the window or an electrode has no effect and the result is the same whether or not a window is present.

The question is now whether the mill itself produces charging mechanisms. I do not know whether a water drop bouncing

off glass will leave more charge than bouncing off a metal electrode but I would be surprised if difference in this effect was crucial. Slow build up of charge has little effect on the measurements and if the build up is symmetrical around the rotation of the cylinder as one would expect, the effect is reduced again by a factor proportional to the time constant. Symmetric overall charging effects both electrodes and so has no effect. In any case removing the window has no effect on performance.

There remains the wetting of the metal front end of the field meter and water drops breaking away over its rear edge at the front of the glass cylinder. The ambient field will charge these drops by induction to tend to produce a neutralizing space charge in the spray of drops. This could be much reduced by a very thin external concentric cylinder shielding the back lip of the cap where the water will be shed, although work function potentials give some symmetrical charging which will not be detected. We have not built this modification as yet, and indeed the rate of drop shedding may be too small to warrant the effort.

The drops shed will be very much bigger than cloud drops and so much fewer in number and so may blow past the electrodes too quickly to disturb the charge measurement if they are sparse enough. It may be possible to drain the water into holes in the cap so it discharges behind the electrodes. This would solve this problem.

Before going on to answer specific questions raised by your letter I feel I should say I am still of the opinion that the answer to this problem cannot be properly obtained by arguing in terms of absolutes without quantitative evaluation of the performance of the device concerned. I believe my discussion has shown we have a solution to the problems involved and extensive field use is the only final way to establish the instrument's performance.

I would be interested to hear where you think I might find a journal interested in a detailed explanation of this instrument and which would reach an interested audience.

Of your list of problems A through G, Section 2, we must remember that only charges on the moving plates between at about 5 and 9 Hz in frequency are likely to be a problem. C, the insulation, I discussed in my previous letter. I think F, the Volta effect and photo electric effects, etc. will filter out unless there is some effect related to the earth's magnetic field I have missed which is not visible in circling at low

field strengths (our estimates say $10^{-3}$ v $m^{-1}$). As I have mentioned, the water dropper effect is a potential problem which can be fixed if indeed it proves actually to be a problem (i.e. if the water comes off the nose in a fine enough spray). In regard to high fields, A, we believe we have a very satisfactory configuration as all the exposed metal parts can be polished and are very rounded in contour. The internal electrodes prevent protruding edges of metal foil or wires being lifted by the airstream so they do not protrude to create high fields.

The frequency response, B, is another problem. The special quality instrumentation metal to metal brushes we used are the only reason for keeping the rotation rate low, however. If we changed to carbon brushes and they were satisfactory we could rotate the probe at, perhaps, 100 revolutions per second, giving a response from 0 Hz to 12.5 Hz (i.e. the folding frequency). However I am not convinced that a stationary plate (possibly configured as our instrument, but not rotating) would not be a better investment for field changes at frequencies above 1 Hz. The two instruments could be calibrated and the outputs blended for a smooth response up to any desired frequency, although we would clearly then detect the passage of a charged particle if it had a large enough charge.

The comment about the measuring of fields in cloud, G, shows we are facing problems similar to the other meteorological

problems of measuring velocity and temperature in clouds where we need to interprete the fluctuations in terms of dynamics. It is a very interesting challenge which I feel should be met by obtaining good measurements which make the effort of interpretation worthwhile and the use of new hypotheses justifiable.

Our use of the dry airstream around the glass is primarily to keep the surface dry but I suspect it will keep small cloud drops from actual impact as you suggest. However it will not stop a drizzle drop or a raindrop. As discussed above the use of a window makes no difference to the transient effect of collecting a charged drop. They may have small enough charges to ignore however as Mapleson and Whitlock postulate. To have appreciable effect through the filter a charged drop would need to attach to a plate cover and then detatch 180° later.

In your section 3 you discuss charges on the glass. As I proved earlier we have essentially a filter which only registers charges which have a rate of change that after band pass filtering between 5 and 9 Hz can still leave an appreciable component (i.e. charges which adhere to the glass above an electrode for a 180° revolution and then are removed). Thus the sharp change in charge on impact will mostly be filtered out and blowing off or leaking off will similarly usually be largely masked out. Charge attraction by the very small dipole formed across the millimeter of glass or across the gap between the electrodes

will similarly be filtered out unless it comes on and off again 180° later. I could quantify this argument by looking at the frequency transform of the step up and decay of an impacted charge in terms of frequency components if you think it necessary.

There is no doubt that the conduction current will produce some effect although it will largely be determined by the conductivity of the drying air we put out over the glass. The airspeed is about 100 m $sec^{-1}$ so little electrode effect will be present and the ions will not move far in the millisecond spent near the electrodes. When we measure conductivity at the same time, as we plan to do, we will get a better idea how serious this effect is. Two cylindrical field mills, far enough apart not to influence each other, would rotate the field effects of conduction current oppositely if they turned in opposite directions and this suggests that if the ion current is easily detectable it could be measured in this way, although previous experience shows this is very difficult.

The problem with designs like your Figure 2 is that at aircraft speed the cloud will circulate through every opening and deposit water throughout its accessible interior. I do not believe any practical amount of dry air forced out from inside could guarantee to keep it free of particles, water, salt, etc. and it would be <u>very</u> hard to clean.

Your remark 6 is a misunderstanding as you suspected. The glass surface leakage is very high but the measuring resistance is low, say $10^{-3}$ volts with whatever current can be induced, say $10^{-9}$ amps. If this resistance has any meaning it would be $10^{6}$ Ω. The requirement is of course that the input current to the amplifier itself (i.e. the FET component) be much less than the current through the feedback resistor, and this design need is adequately met. Since the input current is not linearly related to the input voltage in these FET amplifying devices the old idea of input impedence is not very precise. The dynamic input impedence due to the feedback loop depends on gain and is about 1,000 Ω (I said it was zero earlier which is relatively true). Our design solves a number of instrumental problems (electronic) not mentioned here which makes the old discussions of vacuum tube amplifiers seem quite quaint.

I am afraid this explanation has become somewhat involved as I am not sure which details need to be written out. I think I can only deal with this specific device as the discussion has shown analysis of other instruments, including the flat vane field mill, is totally different as regard many effects (i.e. windows and Volta effects).

We agree with your discussion of the meaning of a field in various circumstances and this has always fascinated us.

# THE MEASUREMENT OF ATMOSPHERIC ELECTRIC FIELDS FROM AIRCRAFT

Peter B. Wagner and James W. Telford

## ABSTRACT

A small, new cylindrical electric field mill is described for airborne use. The electrodes and most electronics are enclosed within a rotating dielectric case allowing use in wet conditions. Special care in arrangement of power supply and grounding leads and the use of digitally coded optical ouput minimize noise in output and measurement electronics. The basic configuration minimizes effects of a wet environment as well as extraneous effects of contact potentials and self charging. This is shown by mathematical analysis which also justifies the use of a dielectric window around the electrodes. Initial field measurements are described along with a simple analytic model of electric fields near the edge of an extensive fog bank.

## 1. Introduction

Aircraft instrumentation usually presents difficulties not found in laboratory use. Mechanical and electrical noise is high, temperature extremes occur over times of a few tens of minutes, the device must function in an airstream of perhaps 100 m $s^{-1}$, it may become covered with ice and it should, ideally, function in the heavy fog like conditions encountered in clouds. The weight and bulk of the device must both be kept small and the device usually needs a rapid time response because of the large distance the aircraft travels in a short time. It also needs to have good long-term stability so it can show accurately changes in conditions on returning to the same area, after having sampled large variations of the measured variable.

These requirements are particularly difficult to meet with the classical instruments for electrostatic measurements. The use of vacuum tubes failed to provide an adequate solution. Even discrete semiconductors pose problems in size, stability and construction. However, the capability of the integrated semiconductor devices has progressed to the stage that with good design there remain few instrumental restrictions to acquiring reliable data.

The field mill described in this paper was designed so that the effort was centered on simplifying most of the problems in the anticipated measuring program by a careful initial design, so that the data gathering phase could concentrate on scientific aspects. Since we expected the atmospheric electric field to

be just as variable and apparently random as other meteorological variables like temperature and moisture, we designed an instrument which could take measurements in close proximity to other instruments. Thus we built it as small as reasonably possible, so it could be placed near the angle of incidence sensors of a velocity measuring system as well as near thermometers, with as little disturbance of the airstream as possible. The best mounting position for all such instruments is on a probe extending into the undisturbed airstream ahead of the aircraft along its centerline. This is a good position for measuring electric field because of symmetry.

## 2. The Design

A frequently used field mill design employs the well known principles of the instrument described by Gathman and Anderson (1965). Their design uses a rotating shutter to alternatively shield and expose a flat electrode to the field to be measured. This approach was particularly valuable for use with vacuum tube electronics as the signal alternates in time with the chopping (rotation) rate and this permits amplifying with vacuum tubes. Direct current vacuum tube amplifiers and early solid state amplifiers, too, posed major problems which chopping the direct current input signal partly resolved.

However this approach does not use the chopping modulation principle to maximum advantage. It does not discriminate in

the chopping process against work function potentials (Volta effects), allow discrimination against fields due to charges on the instrument itself or permit the use of a dielectric window with an acquired charge resident on it. The cylindrical rotating electrode mill design provides a solution to these problems.

Cylindrical field mills have been advocated by Kasemir (1972) and Gathman (1972). Kasemir showed how they could be used to advantage on an aircraft while Gathman built a technically simplified device for a balloon. Winn and Moore (1971) have also used this principle for a rocket instrument. Kasemir stresses that the cylindrical field mill measures two components of the field perpendicular to its axes, that it cancels symmetric fields due to charges on its own structure (and hence of the aircraft on which it is mounted, when properly compensated) and that it largely overcomes the problem of work function potentials. These effects are very sensitive to variations in the surface cleanliness, etc. of the components. He points out the advantage of mounting the amplifiers in the rotating part but mentions difficulties with range changing. In his design capacitive coupling from the rotating head avoids brush noise.

The field mill described here mounts most of the electronics within the rotating sensor head and the only rotating contacts are those which take power to the instrument and the separate brushes which ground the instrument case. The power supply

floats so the return current does not flow through the grounding brushes. The output signal path is through optical pulses along the rotating axis which stops brush noise interfering with the digital pulse stream as well as isolating the instrument from the recorder. The gain changing is automatic and thus the signals consist of two serial, digitized, floating point numbers representing the two field components at each sample time. These signals are converted to analog form for display but recording can be in either direct digital or analog form.

The use of digital techniques avoids a smoothing time constant exceeding ten or so chopping cycles as in the traditional chopper stabilized D.C. amplifier. All field mills which chop the measured field with a shutter produce frequency aliasing which can only be removed by a band pass filter before rectifying. We designed for a maximum saturation field, frequency response and aliasing (which all can be easily changed), appropriate to our interest in slowly changing small fields over fogs.

The analysis below shows that the electrodes of the field mill perform as satisfactorily electrically if glued inside the rotating glass cylinder as they would on its outside. This configuration is particularly suited to aircraft work as the electronics are now totally protected from the outside environment, leaks and condensation being prevented by a slow internal flow of filtered dry air. The smooth glass exterior surface is easy to clean and keep in a hydrophobic, highly resistive state with a silicone coating.

Mechanically the device is streamlined on the outside, so reducing the disturbance it creates in the airflow and the likelihood of corona currents, as can be seen in Fig. 1. This device is proving reliable in service and there is much to recommend this form of design in other applications.

## 3. The Electrical Requirements

The electronic design shown in Fig. 2 follows regular procedures and will not be discussed in detail although some aspects are subject to patent applications. The field effect amplifier front end allows the sensitivity, common mode rejection and freedom from drift which makes this design possible. The open loop input impedence is about $3.2 \times 10^{8}$ Ω capacitive, with negligible resistive current. This impedence is mostly due to $30 \times 10^{-12}$ F attributed to stray capacities and $40 \times 10^{-12}$ F due to the protecting diodes across the input. The input capacity to the amplifier is $3 \times 10^{-12}$ F. The input resistance is $10^{12}$ Ω and the diodes again dominate with an effective resistance of $5 \times 10^{10}$ Ω. The closed loop input impedence is about 1000 Ω which is negligible in practical terms and the error due to the finite open loop input impedence and finite open loop amplifier gain is about 0.001%, which is negligible. The input voltage effect is less than $10^{-3}$ volt and since we are dealing with what is effectively an infinite impedence current source (i.e. a charge source) this is also negligible. The amplifier

front end noise in the sensed bandwidth, and the thermal variations of the overall device are not detectable from -25°C to 30°C. On the most sensitive range this is $\pm 0.1 \cdot V\ m^{-1}$ (i.e. 1 bit change).

This amplifier is a current amplifier and its output is amplified and integrated so the output of the integration is a measure of charge on the plates. Before integration we invert the current in phase with a photo-electric input pulse taken from a fixed, optical interrupter pin. Thus the output of the integrater measures charge change from the initial reset to the current inversion at 180°. The second 180° of the cycle subtracts the charge change in this second interval. This difference is the integrater output at the 360° mark, which is then digitized to 10 bits, and the cycle repeated 90° later for the other perpendicular component of the field. Thus in three complete revolutions we get one sample of each of the two perpendicular fields measured. This cycle was chosen so the numbers output from the digitizer represent the fields without any necessary arithmetic. By not using current rectification but sampling the integrater (without ever reseting it but using a long time constant D.C. restore) with the digitizer, each 90°, and taking the second difference of the odd and the even samples we could get both fields twice each revolution. This arithmetic could be done in a computer, or with a microprocesser if direct readout from the device is considered essential.

As each charge is digitized the magnitude of the number is checked logically to see if a gain change is needed. We provided two successive gain changes of a nominal factor of 16 each. Thus using our 10 bit converter we always have at least five significant bits even just after changing down in gain (i.e. always read to better than 3%, remember one bit is needed for sign). The most sensitive range is up to 50 V $m^{-1}$ maximum with a resolution of 9 bits and sign, so the increment is 0.1 V $m^{-1}$. The next range is 700 V $m^{-2}$ and then 9,800 V $m^{-1}$ maximum (the actual gain changes are nearer 14 than the nominal 16). Larger fields would be easy to accomodate with further gain steps if needed.

## 4. Performance Analysis

### a. The Glass Window

If it is granted that the electronics perform as stated the instrumental performance must be considered in terms of the resistivity of the glass window and the response of the measurements to charges on the glass, etc. It is intended to use this device in fog whenever the opportunity occurs and the instrument was designed to make in-fog measurements if at all possible. Hence moisture leakage is important.

It is clear that if the glass were a good conductor surface currents would always redistribute the induced surface charge so as to shield the inside electrodes. A good estimate of its performance can be made by assuming the inside electrodes are

exactly covered by external foil electrodes. In an external electric field a charge will be induced on the outside electrode with an equal and opposite charge on its inside. Since the circuit keeps the inside electrode at ground potential an equal charge will be induced to flow onto the inner electrode through the circuitry, which will measure it.

If the surface of the glass leaks the charge away the timeconstant of this leakage is that of the capacitor formed by the inner and outer electrodes and the resistance. The plates are formed of aluminum foil 12.2 cm by 6.4 cm and the glass is about 2 mm thick. With a dielectric constant for the glass of five this gives a capacity of $170 \times 10^{-12}$ F for each half. In 1/20 of the time constant 5% of the charge is lost. The mill rotates seven times per second so for less than 5% charge leakage in 1/2 revolution the leakage resistance between the plates needs to exceed $1.6 \times 10^{10}$ Ω. This resistance estimate is too high by perhaps a factor of three or four, because the average leakage path is much longer than the narrow gap between the two inner electrodes. The resistance, measured using a General Radio Co. type 544-B megohm bridge, was found to be greater than $10^{12}$ Ω when dry. When under a large beaker with a wet wad of cotton it stabilized at $2 \times 10^{10}$ Ω. Breathing directly onto the glass produces a much lower resistance which however dries out to greater than $10^{10}$ Ω in about ten seconds, as the condensation evaporates. This test was done without treating the glass surface

with any hydrophobic silicone preparation to repel water. Thus if the surface is kept dry by a continual flow of dry air over the glass through the ring of small holes at the front edge of the glass cylinder, as this design provides, it appears we should have no problems. Additional surface silicone treatment will give a larger margin of safety. The design also allows the drying air to be heated although we do not feel this to be necessary. In the laboratory a light spray of water on the glass produces no detectable effect although a contiguous wet film from a heavy spray naturally prevents the device from functioning.

Thus charges cannot flow around the glass fast enough to allow any shielding of the external field and likewise a charge deposited on the glass will stay there for some considerable time.

To analyze the etfects of charging process rotating with the glass we need to look at the frequency characteristics of the device. Since the device separately measures the two perpendicular components of the electric field an alternating field in one direction or a field rotating at the same frequency around the axis of the rotating electrodes will have an identical effect on one given field component.

It should be noted at this stage that the arguments stated above apply also to external electrodes. With external electrodes an advantage is gained as the low impedence inputs to the amplifiers will reduce the potential on the plates generating the leakage currents. However leakage paths are shorter so that

conditions causing problems with the interior electrodes will be aggrevated with exterior electrodes. Furthermore the exterior electrodes expose the sensitive front end amplifier to direct discharges in handling the mill. However, even if an improvement of 10 or so in leakage timeconstant was possible in this way the surface of the glass tends to be either of adequate high resistivity or unsatisfactorily low, and so the performance would not be noticeably improved as the marginal conditions seldom occur. Other dielectrics may prove to be of value as a material for the cylinder.

The advantages in having a smooth exterior surface include easy cleaning as the metal edge is not present to curl up and fray the cleaning rag or harbor contaminants such as air borne salt particles and adhesive. No frayed metal edge exists as a source of possible corona or of charging by shedding of water drops in fog. No hole is needed in the glass for connections and construction with a smooth flush interior electrode is far easier as it uses a simple, easily replaceable, glass tube.

b. The Frequency Characteristics

Assume we have a small metal plate fixed to the outside of the glass above an electrode and that we can feed this plate with a sinusoidal potential. We will first consider the case where the glass has no leakage. Since we assume a charging mechanism it is exactly equivalent to charging the plates directly with no glass present. How will this charge appear in the output?

We apply a charge to the plate of,

$$q = a \sin(2\pi t/T_E),$$

where t is time, a is an amplitude, and $T_E$ is the period of the extraneous charging mechanism. This will induce a current,

$$i = dq/dt = (2\pi a/T_E)\cos(2\pi t/T_E).$$

We now integrate i from $t_s$ to $t_s+T/2$, and then reverse the sign of i and continue integrating from $t_s+T/2$ to $t_s+T$. The starting time reference is $t_s$ and T is the rotation period of the instrument. Thus the resulting charge Q at the end of a full revolution is,

$$Q = \int_{t_s}^{t_s+T/2} (2\pi a/T_E)\cos(2\pi t/T_E)dt - \int_{t_s+T/2}^{t_s+T} (2\pi a/T_E)\cos(2\pi t/T_E)dt$$

$$= 4a \sin^2(\pi T/2T_E)\sin(2\pi t_s/T_E+\pi T/T_E).$$

For successive readings, $t_s = t_0+3nT$.

Thus, the output measured at successive samples, given by the counting integer n, is,

$$Q = 4a \sin^2(\pi T/2T_E)\sin(6\pi nT/T_E+2\pi t_0/T_E+\pi T/T_E).$$

Converting time to frequency, $T/T_E = f_E/f$, and $f_E = 1/T_E$.

$$Q = 4a \sin^2\left(\frac{\pi}{2}\frac{f_E}{f}\right)\sin\left(2\pi\frac{3nf_E}{f} + 2\pi t_0 f_E + \frac{\pi f_E}{f}\right).$$

If the charge rotates around the glass in the opposite sense to the rotation of the glass so it remains stationary in

aircraft coordinates it simulates a stationary constant external field.

Thus $f_E = f$, and,

$$Q = 4a \sin^2(\tfrac{\pi}{2}) \sin[2\pi(3n) + 2\pi t_0 f + \pi]$$
$$= -4a \sin(2\pi t_0 f).$$

$t_0$, the initial time, controls the phase of the applied charge signal and is equivalent to the angle the field makes to the fixed optical index. Since both $t_0$ and $f_E$ are constant we have a constant signal output representing the constant field responsible for the charge on the electrodes. This is the usual measuring condition.

Whether the external field is slowly rotating around the field mill or varying sinusoidally with time makes no difference to the signal as discussed above. If the rotation frequency is f we may write, for the frequency of variation of the charge on the rotating electrode,

$$f_E = mf \pm f_1,$$

where $f_1 < f/2$, and m and n are integers. The frequency in fixed space, $f_s$, is then,

$$f_s = f_E - f = (m-1)f \pm f_1.$$

Then,

$$Q = 4a \sin^2(\frac{\pi}{2}\frac{f_1}{f} + m\frac{\pi}{2}) \sin(2\pi 3n\frac{f_1}{f} + 2\pi t_0 f_1 + m\pi + m2\pi t_0 f + \pi\frac{f_1}{f})$$
$$= (-1)^m 4a \cos^2(\frac{\pi}{2}\frac{f_1}{f_2} + \frac{(m-1)\pi}{2}) \sin(2\pi n \frac{3f_1}{f} + \phi),$$

where $\phi = 2\pi t_0(f_1+f) + \pi f_1/f$ is the phase angle. Thus, with

changes in frequency, the amplitude of the signal varies as $\cos^2[\frac{\pi}{2}\frac{f_1}{f} + \frac{(m-1)\pi}{2}]$. If $f_1 < f/2$ and $f_s$ is nearly an odd multiple of f (m even) then the signal varies as $\sin^2(\frac{\pi}{2}\frac{f_1}{f})$. For $f_s$ near an even multiple of f the signal varies as $\cos^2(\frac{\pi}{2}\frac{f_1}{f})$.

Thus in the case where $f_s = 0, 2f$, etc. the signal is passed through the system at maximum gain. An external slowly varying field is composed of very low frequency components which are transferred according to a $\cos^2$ gain factor and so are almost unattenuated.

On the other hand slowly varying components of charges on the glass which rotate with the glass give $m = 0$ and the gain factor is $\sin^2(\frac{\pi}{2}\frac{f_1}{f})$ so very little signal error arises from this source.

Thus the rectification, integration and sampling procedure in the instrument severely attenuates slowly changing effects on the glass or elsewhere on the rotating cylinder. External fields changing more rapidly than $t_E = t/2 = 3.5$ Hz are indistinguishable from charges on the glass changing more slowly than this. This illustrates the typical folding frequency effect associated with discrete sampling. The complementary effect of charges on the glass changing at near 7 Hz in frequency and so being mistaken for stationary external fields is the only way charging effects on the glass, volta effects or piezo-electric effects can influence the measurement (unless an external fixed field is generated by these effects).

Thus even harmonics of the rotation frequency are passed through this discrete sampling system as though they were steady fields. All these frequency folding effects apply to flat field mills with or without rotating windows, as well, and also will appear if we used a smoothing circuit instead of digital sampling, and resetting of the integrator. All these frequencies except the fundamental frequency can be removed by a filter in the current amplifier which passed only frequencies between say 4 Hz and 10 Hz although we have not done this as we are not interested in rapidly changing fields at present. These frequencies cannot be removed after sampling however as they are then indistinguishable from the desired data. Sampling every third revolution imposes another sampling window which aliases frequencies above 7/3 Hz so we should filter out all frequencies except those between 5.25 and 8.75 Hz if we need to be absolutely sure of the output.

We should mention that unsymmetric charges on the rotating glass cylinder will induce charges on the surrounding aircraft structure which will vary in synchronism with the rotating field mill if the structure is not symmetric. This will introduce errors, so a movable asymmetric metal collar on the shaft of the instrument is adjusted so such effects are cancelled for the two perpendicular field measurements the instrument makes. This also removes effects due to aircraft charging.

Another extraneous effect, that of the earth's magnetic

field, cannot be detected with this device as it is too small.

Thus, to reiterate, in this instrument the external fields produce a signal changing at the rotation rate of the instrument and this results in charging effects rotating attached to the glass being completely eliminated from the output. Thus charges on the glass, piezo electric effects, and Volta effects (work function potentials at the metal surfaces) are eliminated, except as these effects influence the stationary surroundings to generate non-symmetric stationary external fields. To have a significant effect a charge must attach to the glass at one point and detach 180° later and even so the charges on drizzle or cloud particles are likely to be too small to matter. In this regard the enclosed electrodes behave the same as external metal electrodes (if the glass is actually moist both schemes equally fail to operate).

## 5. Measurements in the Field

As already implied, the ideal fog for initial airborne study is slowly moving, uniform and stable in time. Such an example was found on 24 October 1973 off the Cape Cod coast of the eastern United States. This extensive fog grew from a rather patchy fog in the vicinity of Nantucket Island earlier in the day to a quite extensive fog moving northwest at about 5 km/hr. The fog, about 80 m deep, had a rather straight, well-defined edge extending 150 km or more northeasterly from the southern Cape Cod landfall. Measurements were taken about 80 km from the

cape by traversing the fog edge at various altitudes as shown in Fig. 3. The fog lay in a stable, hazy and near saturated boundary layer some 160 meters in depth. An appreciable decrease in measured field strength was observed beneath the boundary layer.

Figs. 4 and 5 show the fields observed at various altitudes during straight and level flight. There generally appears to be an increase in field strength (more negative) over the clear region adjacent to the fog at lower altitudes. At the same time, there appears to be considerable variability in the data below the maximum altitude of 1.2 km. The source of variability was not determined. Its presence, however, requires considerable care in the data analysis as discussed below.

In order to test whether the fog can be likened to a slab of low conductivity material with a constant potential top we constructed an analytic model for comparison to the data. Even when the field is approximately vertical, as in the undisturbed fair weather field, there is a large change in field strength with height. So it is clear that there is a substantial charge distributed throughout the air itself. In principle a knowledge of the vertical component of the field found by flying perpendicular to the edge of the fog (we would assume the measured horizontal component along the fog averages to zero although this is not necessary to solve the equations) will let us construct equi-potential surfaces. If we have the potential change from the

equipotential sea surface, or can assume a constant potential at the maximum height run, we then know the height of each equipotential surface at each position. So we can map the potential and hence the electric field potential gradients. Thus we would have calculated the electric fields and the charge densities, everywhere. The assumption of no changes with time would then lead to relative current densities and conductivities both scaled with an unknown constant. In practice the measurements show great variability (see Fig. 5) and one level run probably does not relate directly to another level run in either time or space in regard to the detailed variations. So proceeding on these lines would appear to be creating problems by using inconsistent details.

The other approach is to construct a very simple model for the field and see how it resembles the data when adjusted to give the best fit. The fitting procedure matches the vertical electric field component averaged over six seconds. We have no detailed wind information and we have assumed there is no current due to charge transport by the wind. If we then assume the conductivity is constant at each height, except in the fog, we can take a two dimensional model with horizontal equipotential planes at the maximum sampling level, the sea surface and a semi-infinite equipotential horizontal plane representing the fog top. The alternative, of solving Poisson's Equation $\nabla^2 E = \rho$, involves a similar procedure of postulating a charge distribution which

keeps the equipotential surfaces unchanged, if we are to use our simple solution of Laplace's Equation as a model. It has a form suitable for quick calculation. This model is explained in the appendix. Using steepest descent methods we used the model to calculate a current density at each point. At each level the conductivity needed to produce on average the same current as given in the model was calculated. Then minimizing the mean square of the remaining departures of the data from the model values gives the position of the semi-infinite sheet representing the fog, and its potential. Since the actual fog top is not an infinitely conducting current sink the current tubes are not discontinuous at this surface. The assumption of uniform conductivity at each height used above the fog would imply most of the current flow above the fog drained away in the half plane at fog top level. Consequently the current tubes must be interpreted as experiencing a discontinuous conductivity change at fog top to maintain a continuous current through the fog top. Hence all current tubes from underneath the half plane representing the fog top, down to the surface, are in a medium of lower conductivity. This represents the actual conditions within the fog.

The result of this model is shown in Figs. 4 and 5. It is clear that while there is a general consistency wherein the measured field increases over the fog there are other influences which affect the field as much as the organized influence of the

AD-A146 546 STUDIES OF THE OCEAN SURFACE AND THE COUPLING BETWEEN THE SEA AND THE ATMOSPHERE(U) NEVADA UNIV RENO DESERT RESEARCH INST J W TELFORD 01 OCT 84 N00014-75-C-0598 2/3

UNCLASSIFIED F/G 4/2 NL

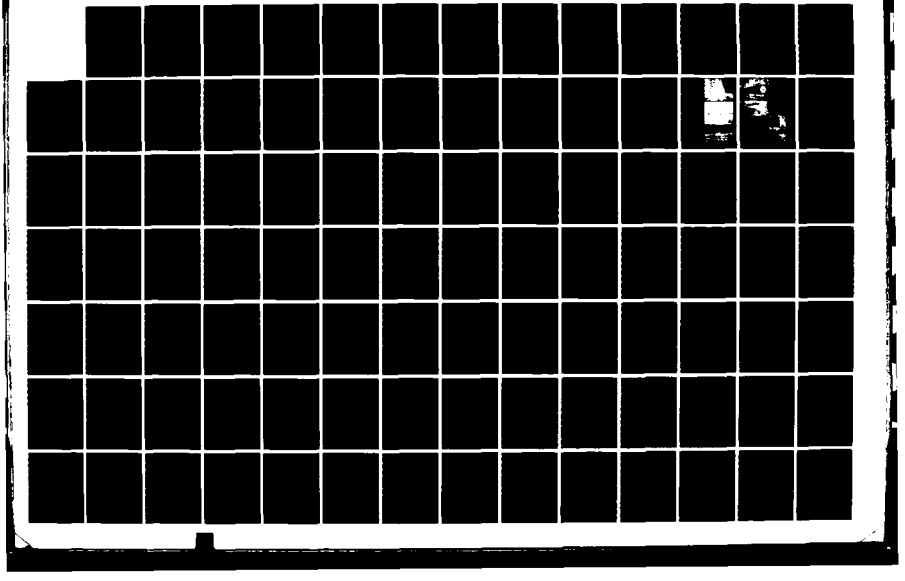

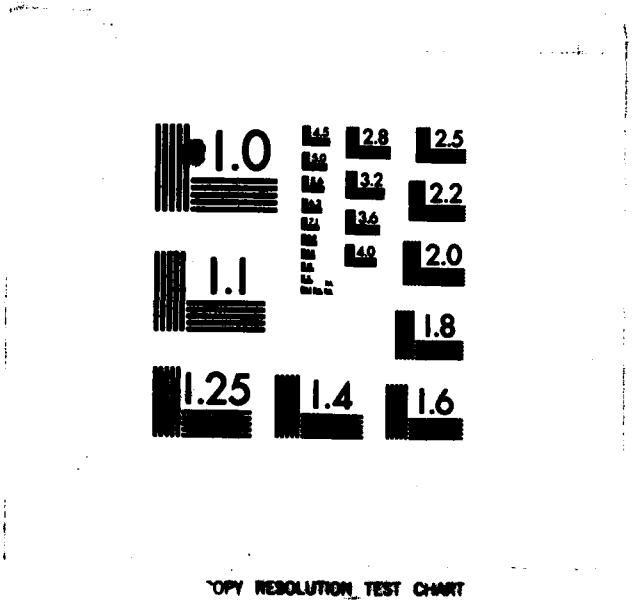

fog, but on a much smaller scale. It is interesting that the field discontinuities at the edge of the fog in the model due to charge concentration on the edge of the half plane representing the fog top, do appear in several places to match corresponding variations in the measured field. The conductivity decreases with decreasing height to 150 m but increases unexpectedly below this level to the fog top as is shown in Fig. 6. It is possible this unexpected behavior is related to unsymmetric aircraft charging within the haze layer.

## 6. Conclusion

A rotating tube field mill has been built with electrodes, amplifiers and digitizers internal to a rotating glass tube. Analysis suggests this design should overcome many problems likely to be encountered with airborne field mills.

The instrument was used to measure the fields over a sea fog. The measurements are consistent with the hypothesis that the top of the fog is a region of charge accumulation where the fog produces an abrupt change of conductivity. There is also some evidence of a charge accumulation at the fog edge as a simple slab model for the fog would suggest. The substantial variability in the field from place to place up to some hundreds of meters above the level of the fog top suggest substantial variability in conductivity. This variability may be an indicator of mixing and changes in airborne particle counts.

## 7. Acknowledgements

We would like to acknowledge the efforts of the NCAR Research Aircraft Facility in providing support for our flying. The funding for this research has been made available from the Office of Naval Research, contract no. N00014-75-C-0598.

## REFERENCES

GATHMAN S.G. and ANDERSON R.V. 1965 *Rev.Sci.Inst.* 36, 1490.

GATHMAN S.G. 1972 *Rev.Sci.Inst.* 43, 1751.

KASEMIR H.W. 1972 *Meteorologische Rundschau* 25,

WINN W.P. and MOORE C.B. 1971 *J:Geophys.Res.* 76, 5003.

## CAPTIONS

Fig. 1. The rotating end of the cylindrical electric field mill. Electrodes are aluminum foil glued to the inner surface of the glass tube. Dry air passes from the stationary body, through the rotating body, and out through the exhaust holes near the leading edge of the glass tube.

Fig. 2. Basic electric field mill circuit contained within and moving with the rotating glass envelope. Space required is approximately 4 cm diameter by 15 cm in length concentric about a 1.3 cm diameter support shaft.

Fig. 3. Measurements were made in level flight at various altitudes and normal to the edge of the fog.

Fig. 4. This is a composite of measured and modeled electric field component in the vertical direction at 60 m altitude, just above the fog top. The irregular line is the measured field. The natural variability of measured field is evident here and in similar plots in Fig. 5.

Fig. 5. Similar to Fig. 4, plots of modeled and measured vertical electric fields at all flight altitudes are shown here. Altitudes in meters are shown inset.

Fig. 6. Relative air conductivity as obtained from the field model are calculated for various flight altitudes. Mean measured fields at each altitude are combined with calculated relative current densities to obtain the conductivity values except in the fog. The reduced conductivity in the fog is obtained from the modeled field jump across the fog boundary. The model indicate a conductivity change by a factor of 3.7 across the fog boundary. No absolute values are possible since neither current density nor conductivity were measured in the 1973 experiment.

## APPENDIX

## The Analytic Model

The analytic model with the semi-infinite conducting plane between two parallel infinite planes has been programmed on a computer. The formulae are as follows (see Korn and Korn, p. 7.9-5)

$$z = k \ln\frac{k}{1-k} + \ln 2(1-k) + i\pi - k \ln(z'+1) - (1-k)\ln(z'-1)$$

$$z' = \coth(w/2).$$

The potential of the intermediate plane when the infinite planes are both at zero potential is v in the relation,

$$w = u + iv,$$

where $z = x + iy$ is the coordinate between the two planes. The height of the intermediate plane is k times the height of the top plane from the bottom plane.

In this part of the transformation the top and bottom planes are both at the same potential.

An arrangement where the top and bottom planes have a potential difference contains the intermediate plane as an equipotential surface where its potential is k times that of the top plane, given a zero potential bottom plane. Thus this is also a solution meeting our boundary conditions and we can add such a solution to the one given by the first formulae.

By writing a program in Fortran using complex arithmetic and a simple Newtonian approximation loop we can find the w for a given coordinate position z.

When $z = x + iy$ we then add the potential v and $yV_T$ to give the final potential at (x,y).

$$V_{xy} = v + yV_T,$$

where $V_T$ is the potential on the top plane and $V_{xy}$ is the potential at x and y. v can be scaled to provide any desired potential on the intermediate plane.

By modifying the iteration loop we can find the y for a specified x and $V_{xy}$. This gives us points on an equipotential surface at successive values of x. The vertical component of the electric field is of course simply the real part of the complex differential,

$$\frac{dw}{dz} = \frac{\partial v}{\partial y} + i \frac{\partial v}{\partial x}$$

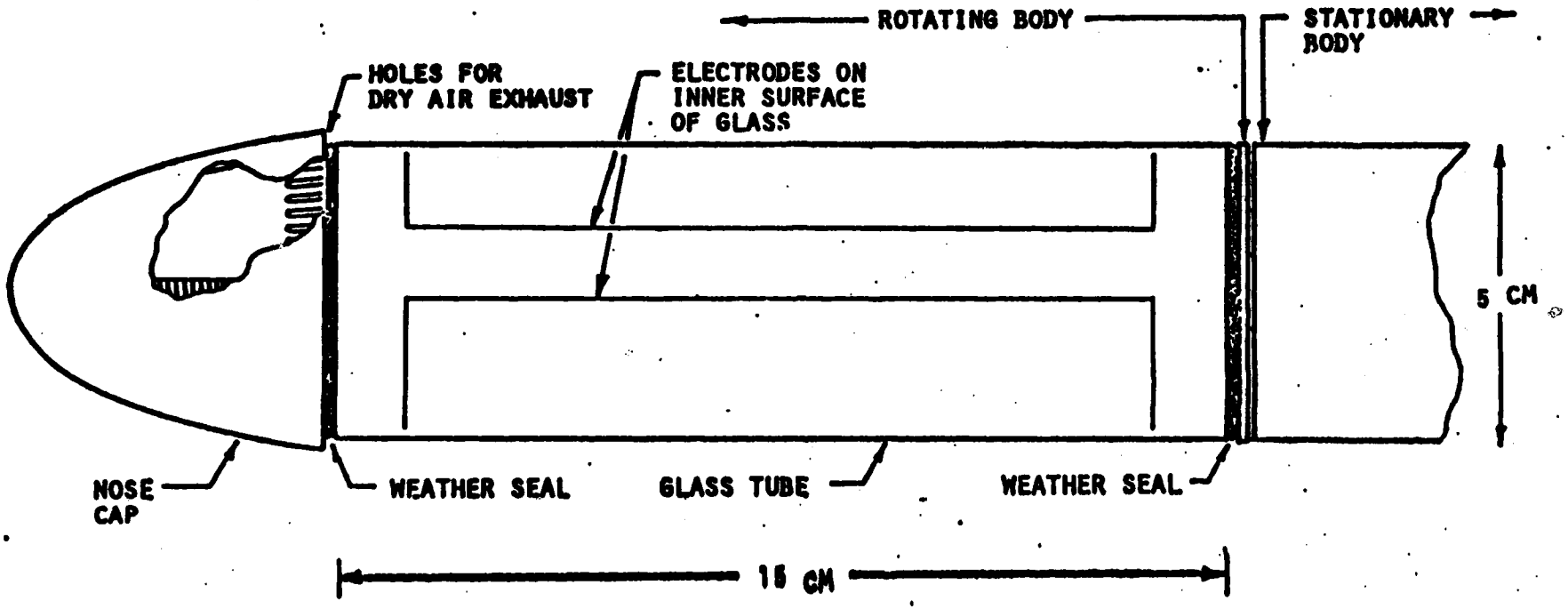
ROTATING BODY
STATIONARY BODY
HOLES FOR DRY AIR EXHAUST
ELECTRODES ON INNER SURFACE OF GLASS
5 CM
NOSE CAP
WEATHER SEAL
GLASS TUBE
WEATHER SEAL
15 CM

Fig. 1

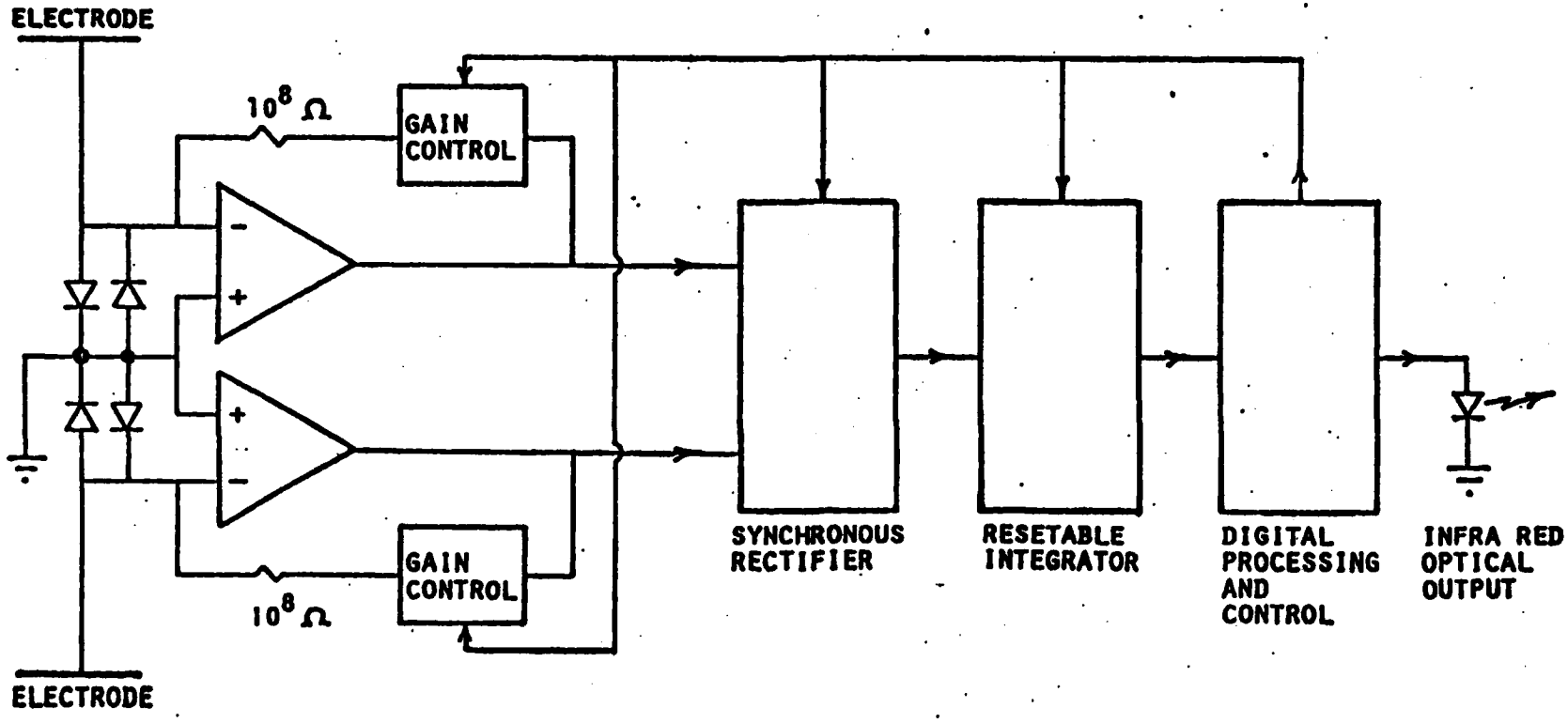
ELECTRODE
$10^8\ \Omega$
GAIN CONTROL
GAIN CONTROL
$10^8\ \Omega$
ELECTRODE
SYNCHRONOUS RECTIFIER
RESETABLE INTEGRATOR
DIGITAL PROCESSING AND CONTROL
INFRA RED OPTICAL OUTPUT

Fig. 2

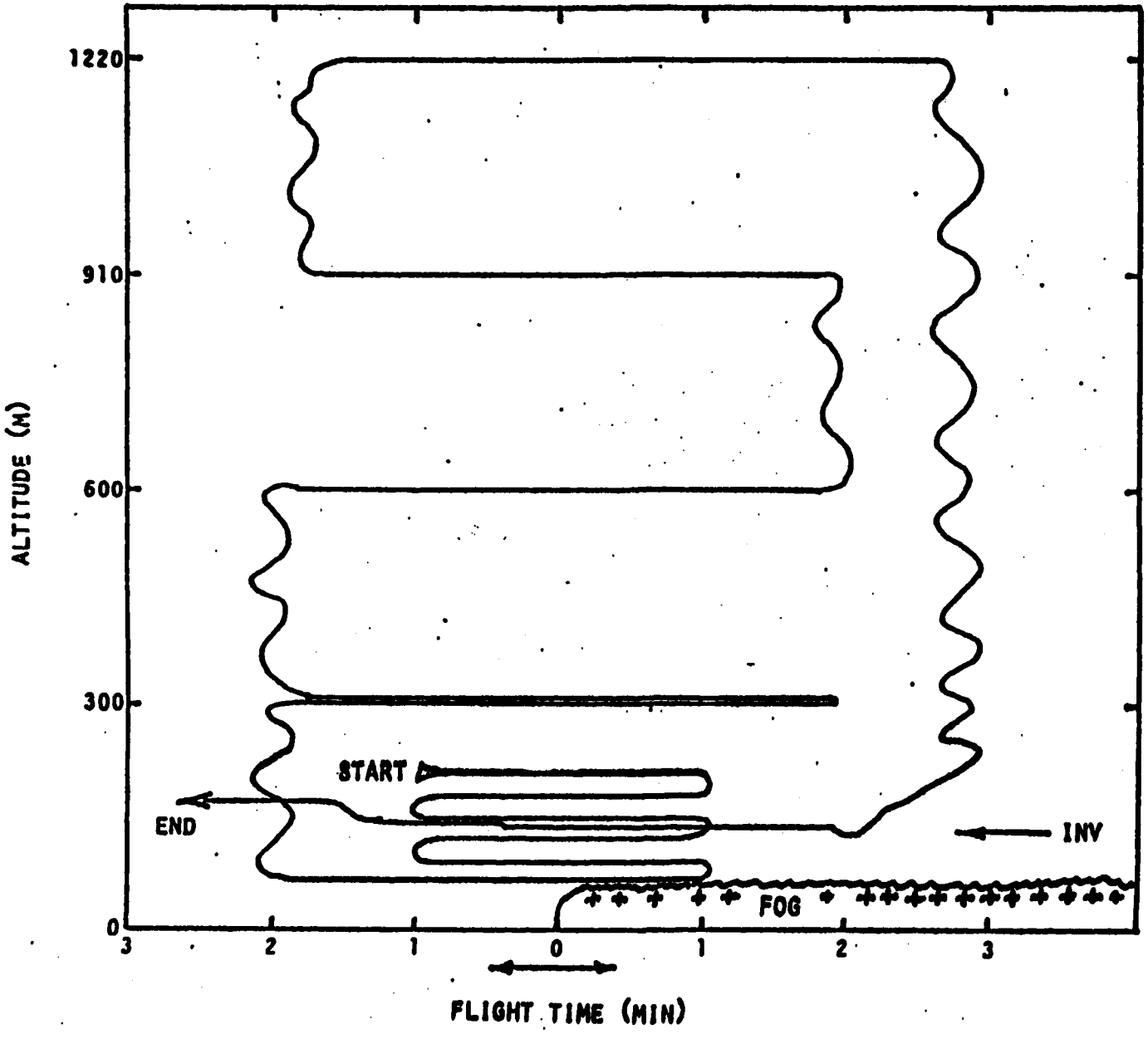
1220
910
600
300
0
ALTITUDE (M)
START
END
INV
FOG
3
2
1
0
1
2
3
FLIGHT TIME (MIN)

Fig. 3

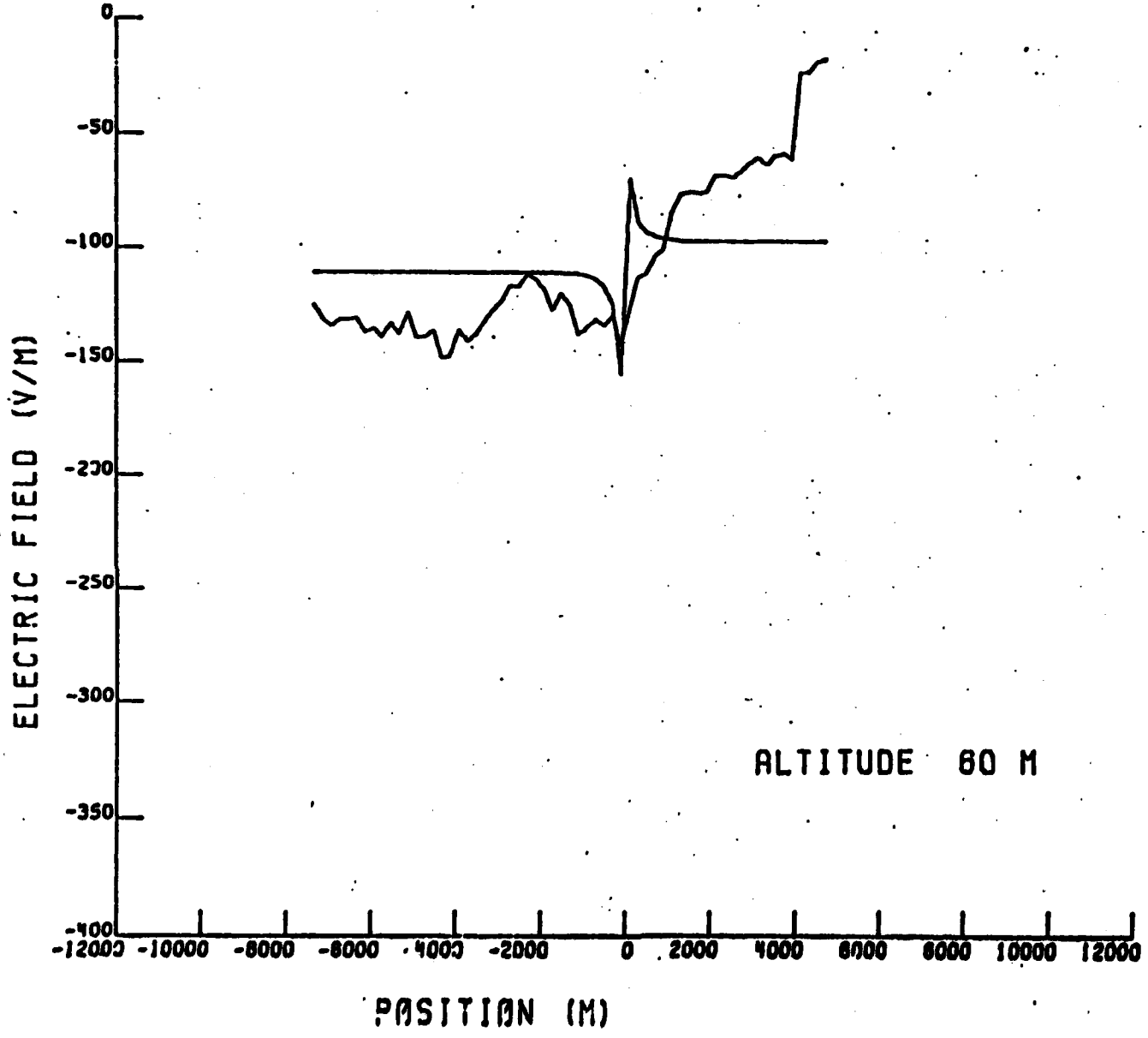
0
-50
-100
-150
-200
-250
-300
-350
-400
ELECTRIC FIELD (V/M)
-12000 -10000 -8000 -6000 -4000 -2000 0 2000 4000 6000 8000 10000 12000
POSITION (M)
ALTITUDE 60 M

Fig. 4

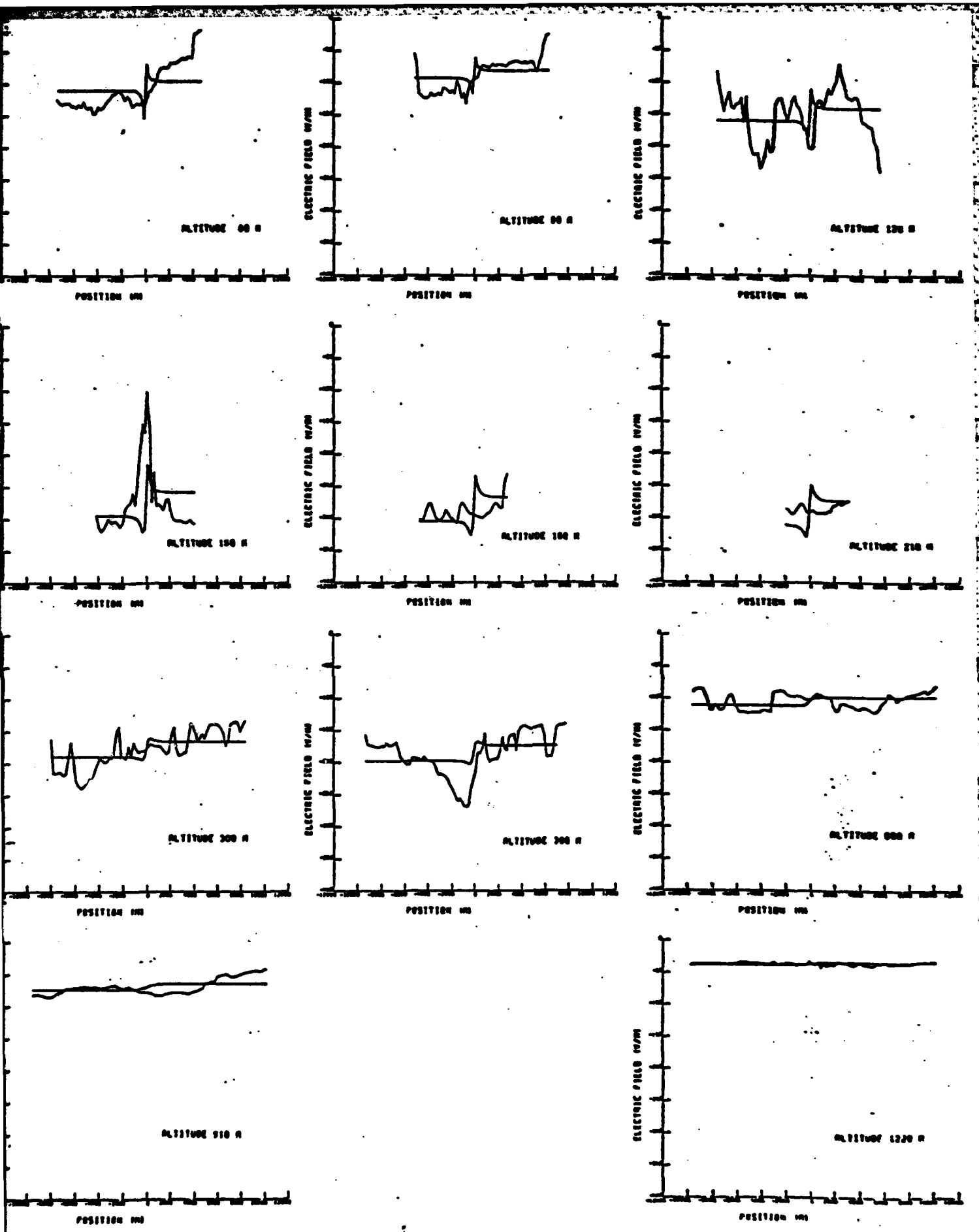


Fig. 5

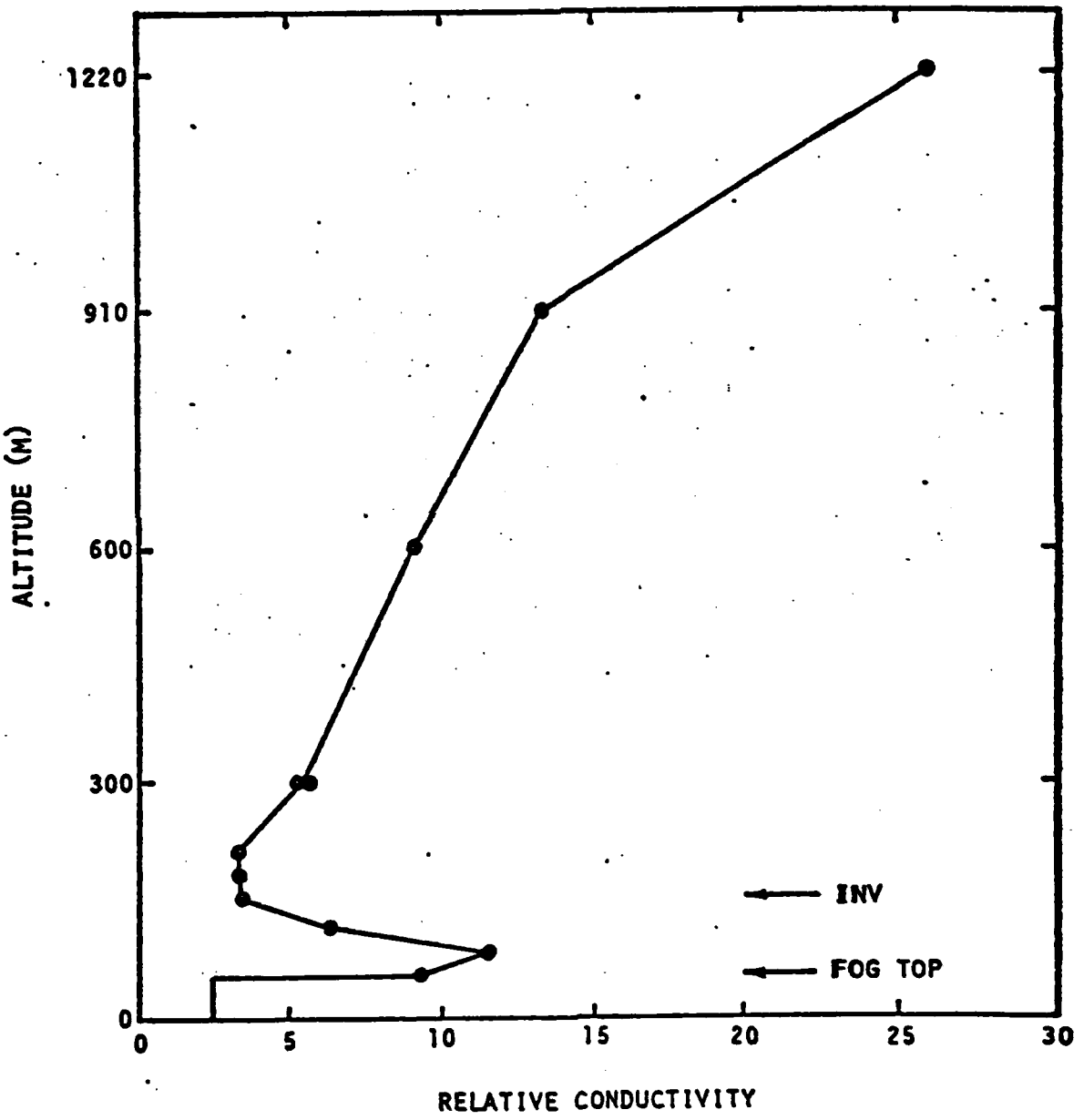
1220
910
600
300
0
ALTITUDE (M)
0
5
10
15
20
25
30
RELATIVE CONDUCTIVITY
INV
FOG TOP

Fig. 6

Summary After Year 1976

December 17, 1976

TABLE OF CONTENTS

## ABSTRACT

This proposal discusses the likely physical processes of fog formation and concludes that the most likely mechanisms involve convective overturning of the fog either in response to radiative cooling of the fog top or an increasing sea surface temperature as the air in the fog moves downwind. This implies that the air is cooler than the water. It is pointed out that the most practical way to seek evidence of how often this mechanism is involved is by measuring the electric fields just above the fog which are determined by the charges on the fog droplets and so on the time the droplets have been exposed at fog top.

Information about the actual charges on the fog droplets continues to be important from the point of stability of the fog against forming drizzle.

The past history and progress of the proposal is reviewed and the capability of this project relative to the problems of obtaining a representative picture of the fog, as compared to spot samples, is stressed. This broader information is essential in studying the mechanisms of fog formation, sustenance and decay.

## 1. Background, History and Accomplishments of Project

The interest of the Atmospheric Motion Group at the Desert Research Institute in electrical effects has a background of long standing. Dr. Peter Wagner became interested in the study of electrical phenomena during his thesis when he studied the propagation of the lightening discharge. Dr. James Telford has been studying such phenomena since his wind tunnel experiments (Telford, Thorndike and Bowen, 1955) and calculations which showed the very substantial changes in collection efficiency which could be induced by electrical charges on the drops. He directed a major project in electrical cloud seeding in the mid 1950's which met the usual problems of statistical sampling in establishing significant changes due to modification procedures.

Many designs have been explored to find ways to measure the charges on individual cloud droplets, one of the outstanding crucial problems in cloud physics. However such direct individual measurements are extremely difficult if not impossible to achieve in a definitive way which would be free of instrumental criticism.

There has been much work associated with the strong fields of electrically active clouds. However this work is attempting to understand a cloud in its mature, fully active condition, whereas any attempt at modifying a cloud or dissipating a fog must be aimed at the earliest stages in the development of an intrinsic physical effect, such as a drop charging mechanism, where a small trigger effect can be expected to multiply.

Thus we believe the real interest in electrical effects in clouds should be concentrated on studying small fields as charging influences begin to modify the fair-weather field as the buildup begins.

There are numerous charging mechanisms postulated for cumulus clouds, some related to water droplets and several depending on ice. They all are weak however in their explanation of how the charges are to be separated to give the overall charge distributions observed. This type of research suffers from the problem that only the overall thunderstorm is observed electrically, together with laboratory experiments which deal only with a few particles. The former is too complex to be interpreted securely and the latter is too simplified to provide a real model. Joining the two seems to need a mathematical model but the problem of accurately modeling the turbulent motion in a thundercloud is formidable indeed. This modeling task is a problem which has not yet been solved even for a small isolated cumulus (see Telford, 1975).

## 2. The Formation and Decay of Fogs

The problems of how a fog forms and dissipates seem to have been rather elusive; possibly due to the difficulties of being able to find a fog when one needs to study one. In many ways the microphysics of drop formation and growth by condensation has received far too much emphasis. As in the

case of cumulus clouds the motion in the cloud has largely been treated by invoking unrealistic conjectures, designed apparently to make it a non-problem: because it is extremely difficult to obtain either measurements or understood them when they are at hand. However this is not good enough when we now have the technology to make studies never before possible.

In fog formation even physical processes which results in supersaturated air are not understood. Mixing is a term commonly used without serious consideration of the resulting effects in supersaturation. Indeed many years ago Emmons (1947) pointed out that warm air flowing over warm water lost its moisture to the sea surface just as rapidly (not exactly but nearly so) as it lost its heat. Thus cooling warm moist air by contact and stirring against a cold saturated surface such as the sea will not obviously provide a theoretical explanation of fog formation.

It is well known that mixing almost saturated air at a cooler and a warmer temperature will produce saturation in the air, however for even 10% or so subsaturation mixing cannot produce saturation without temperature differences exceeding 10°C.

Even when such air with the needed high humidity and warmer temperature is available within ten meters or so of the sea surface the regular forced convection stirred up by the wind does not seem adequate to bring air saturated at the sea

surface directly into contact with the cooler nearly saturated air lying above. This is necessary to achieve saturation by the mixing process. Any gradual process in which air diffuses up and down to the sea surface will not allow the air to become supersaturated since the repeated contacts with the water surface reduce supersaturation to just 100% saturation and the excess supersaturated vapor condenses to the sea.

Furthermore the nature of the turbulence is such that the stable lapse rate takes energy from the turbulence and so the cold air tends to move up a certain distance until a temperature inversion forms on top. Here a strong shear surface is likely to develop with the surface air moving much slower, so the turbulence will tend to diminish. Indeed we are left with a possible explanation that the formation of this cool shallow layer against the sea surface is a necessary preliminary to fog formation. If, after this layer is established, the air then moves from the coldest spot over the sea surface to a region of increasing sea surface temperature convection will set in which is well able to saturate this shallow layer, which is a necessary precondition to fog formation. Perhaps radiation losses complete the process.

Indeed calculations show that the convection which occurs when the wind blows along an increasing sea surface temperature does produce a condensation level which descends as the convective mixing proceeds.

In addition to this process driven purely from the sea surface radiation clearly may play a role. This will result in a cooling of the fog top; assuming most of the sunshine is reflected while the long wavelength thermal radiation from the fog top continues to take heat away. This cooling must also be transferred downwards by convection.

Thus it is very difficult to believe that any sensible method designed to predict the onset and continuity of fog will not be primarily associated with the motion of the air, the sea surface temperature and the role played by radiation. The question is how to best make the observations which can define the roles of the various phenomena we can put into a model. In this context it is quite difficult to see how the microphysics of the condensation process is of much use at this stage in the study although when the role of radiation is better defined the drop size may become a needed parameter.

It is in this context that electrical fields, drop charging and air motion measurements can be seen in the full importance of their role.

## 3. The Role of Electrical Field Measurement in Interpreting The Theories of Fog Formation

From the forgoing discussion it is clear that the "mixing" process must be better understood and the electrical charges carried on the droplets provide a vital diagnostic tool to

be able to let us find where the air is turning over. In addition the knowledge of the electric charge pattern in fog is necessary preliminary information to direct attacks on fog dissipation by electrically induced droplet scavenging. This latter process will be discussed later.

To return to the problem of giving an overall understanding of fog formation, which is necessary for fog prediction since empirical approaches are frequently based on misinterpreting the often scanty data. Only a coherent physical model will allow a consistent interpretation of the observations. The discussion has shown the importance of convective transfer in the process. From the point of view of air transport the substantial size of the organized motion in this sort of mixing is far more effective and totally distinct from the relatively small scale turbulence set up in stable air from surface related drag.

To study this motion with extended flights through fog is not possible because of aircraft control problems. Observations of the fog structure from land based towers on islands is fine if the primary observation is to be concentrated on microphysical details. However the overall view of the fog so necessary to see how and why it is forming is impossible to obtain in this way.

An aircraft observation platform is ideal for obtaining the overall conditions; the edge of the fog can be examined,

the movement of the fog edge can be seen, patchiness in the fog can be noted, the fog top height can be discerned, and there is the possibility of radiation measurements. When we add electric field and conductivity measurements to the observations of air motion now available on the research aircraft supporting this work we have a tracer which can show where fresh foggy air is reaching the fog top, with little charge, and where the fog top has spent a substantial dwell time exposed to the overlying ion-current from the clear air above. This pattern can thus provide the crucial information about the mixing motion.

A large scale variation in the electric field close to the fog top can only occur if there is a large scale variation within the fog changing the foggy air so the more highly charged top layer, which our previous work has established exists, is convected downwards into the bulk of the fog towards the surface where it will loose its charge, due to the residual conductivity in the foggy air.

It is essential to settle this question in a definitive fashion because the presence of convection shows the air must be slightly cooler than the water so both heat and moisture are entering the air. Only when we are quite positive that this is, or is not, the principle condition of fog formation in the areas of interest, can we seriously sort out the detailed preconditions necessary to predict the onset of fog.

## 4. Instrumentation

The goals and methods of this project have been carefully reviewed by the Aviation Panel of the National Center for Atmospheric Research which has again granted aircraft support for the coming summer (valued at $61,140 from NSF funds). The aircraft again involves a full recording system and meteorological instrumentation which includes an air motion measuring system. This is, of course, invaluable in determining the air circulation at the edge of the fog where it is forming or dissipating, as well as providing precise inertial platform position in detail throughout each fog encounter. The value of the program however lies in the new and innovative field measuring devices developed, constructed and mathematically analyzed (see appended correspondence and paper) to make these measurements possible. Electric fields have been a classical study with a long tradition of curous techniques developed early in the century before modern solid state electronics. We have invented and built (and patented under Navy support) extremely sensitive, stable and rugged devices for aircraft use which make regular measurements in low field conditions a routine and relatively trustworthy procedure, fit to be considered in the same class as temperature measurements. This is not to say, of course, that the observer does not need to be knowledgeable to get good results.

With this instrumental background, generous additional support from NSF (via NCAR) and experience to date, we request support to continue our well equipped attack on the

Electric field mill which was flown in past years on a nose boom: This tail mounting proved satisfactory despite some vibration. Lower supports mounted in rubber provided added stiffness and dampening.


Close-up of rotating cylindrical electric field mill: Note glass enclosed capacitive plates and compensation probe beneath cylinder to offset effects of the aircraft tail. The writing pen provides a size reference.

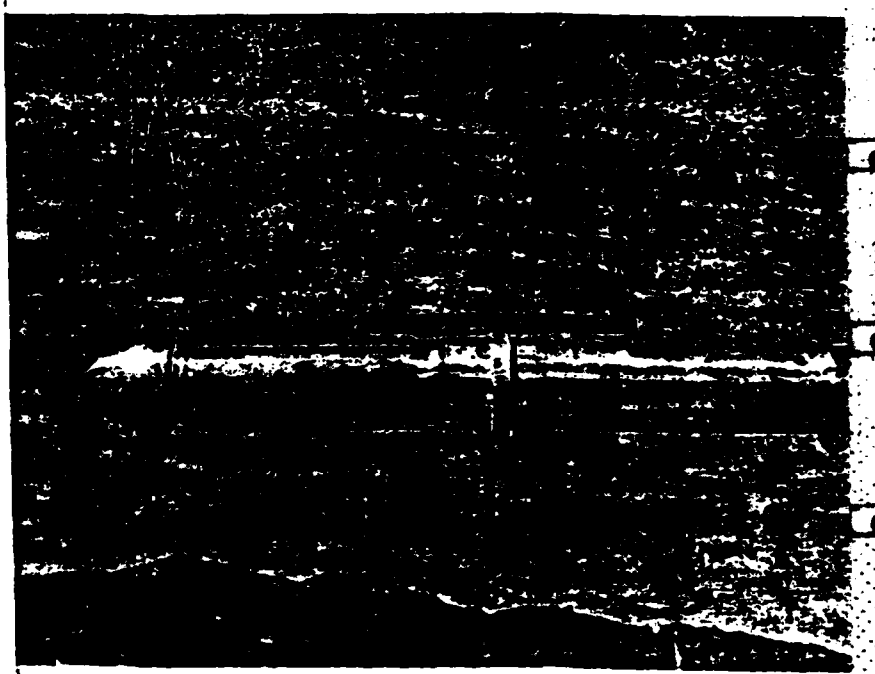

Electricalconductive cell: This Gerdian-type cell is capable of measuring both ionic components of electrical conductivity as well as total small ion population. Air turbine at the rear of the tube measures flow rates. An electrometer amplifier and other electronics are the housing above the tube.

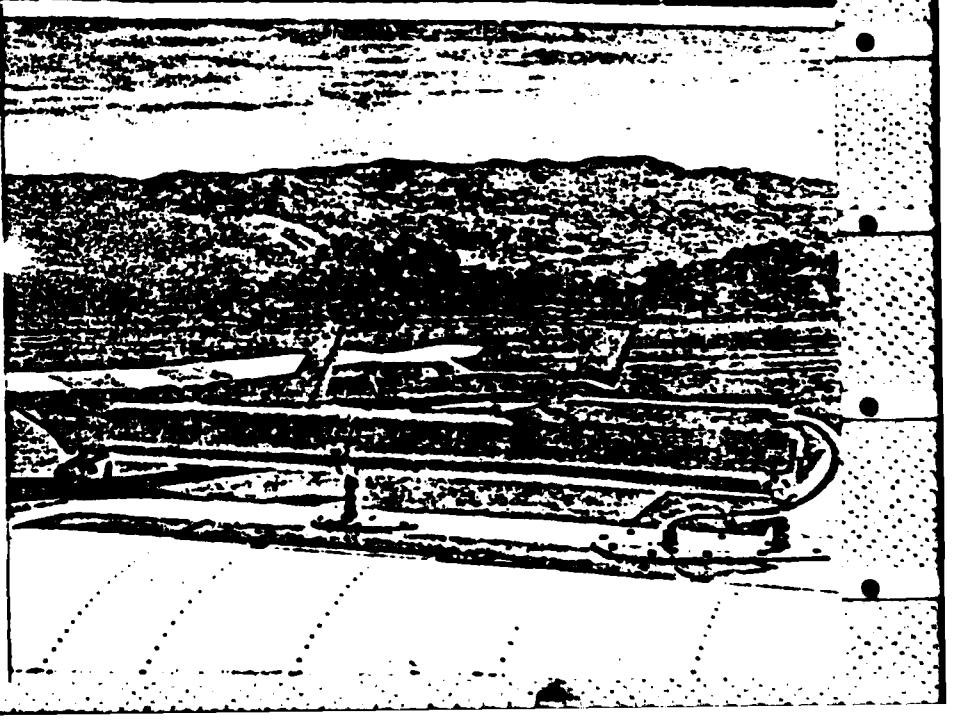

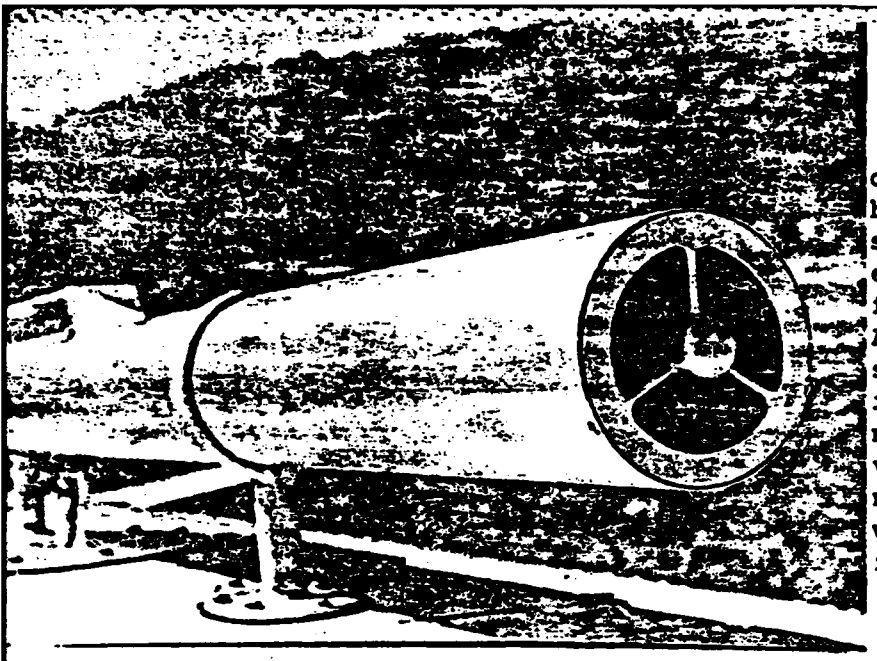

Front view of conductivity cell: The large difference between inner and outer shell sizes is utilized to minimize effects of fringing electric fields in the electrode area. An electrical problem which surfaced in 1975 during fligh in rain has been solved. A mechanical problem caused by vibration of the new roof mount was noted this year and will be corrected before further use.

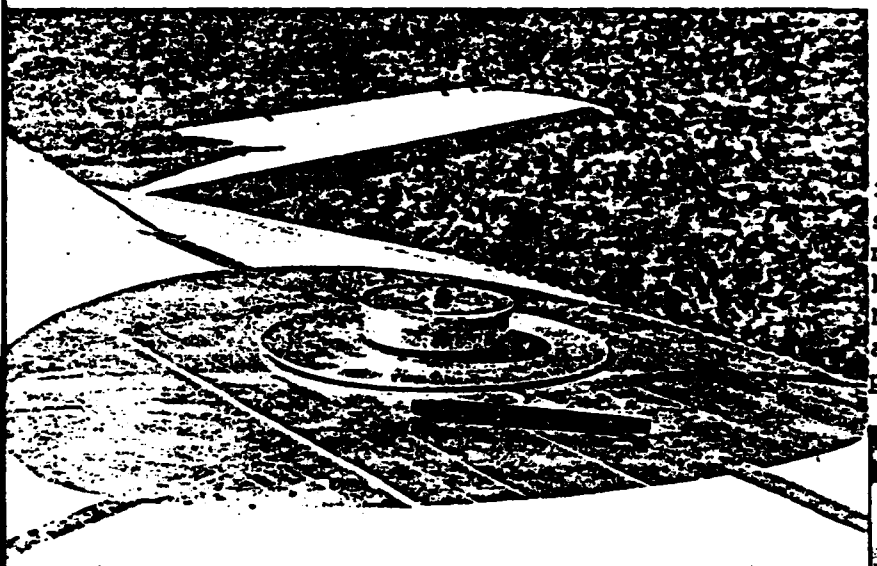

New vertical electric field mill: Functionally similar to the rear mounted mill, this mill measures the horizontal field components. Note the taped ground plane and glass enclosed capacitive plates.

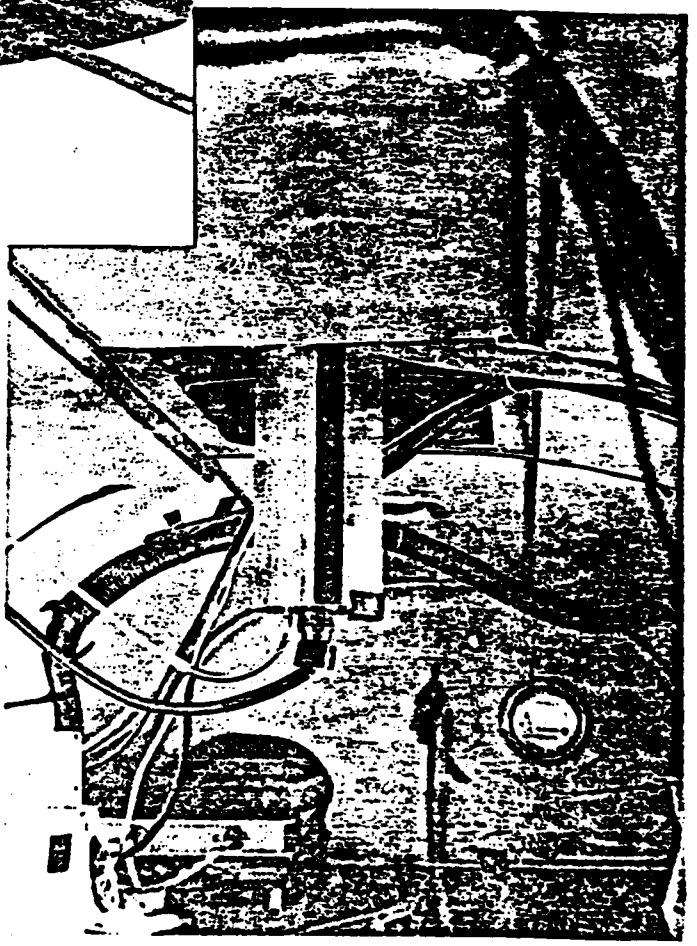

Interior projection of new mill:
ring the 1976 experiment this mill
rformed credibly in overcast conditions
d in fog, however it proved to be
nsitive to sun angle in bright sunlight
is effect was unexpected and is perhaps
effect of the sun on the aircraft
int and skin charging beyond the
ound plane. No further explanation
known, and more investigation will be
cessary. Note the clear tube for dry
r. Circulation of dry air has proven
be an excellent way to maintain
ectrical integrity of all the above
struments in wet conditions.

fundamental nature of sea surface fog. We propose a transfer of our efforts previously to data analysis and a further year's field work. The last year's field program was highly fruitful (the previous year was plagued by aircraft failures) and a list of past accomplishments is given in the appendix.

## 5. Some Detailed Considerations of the Measurements

The aims of this program for the electrical study of fog are to obtain a reliable and detailed understanding of the role played by electrical effects in the stability of fogs, the remote indication of fogs, and as an indicator of the mechanisms in the dynamical and microphysical development of fogs. By this means we intend to evaluate techniques for modifying fog, predicting fog and furthering research to these ends. The program to date has shown there is a clearly defined influence above the fog which corresponds to the influence which would be expected from a uniform potential across the fog top, caused by a charge accumulated at the sudden change in ionic mobility on entering the region where the fog drops fill the air. There are large place to place variations in the measured field however which will be discussed below. It also appears that some of the space charge giving rise to the field change lies in the clear region just meters above the fog. Whether this is due to reduced conductivity or mixing of charge upward on

diffuse droplets (or aerosols from evaporated droplets) is not yet determined.

Data obtained two years past from penetration of fog in flight provided the initial indication of the distribution of charge within the fogs encountered. The data from this year's experiment largely confirms the same general pattern. However with the addition of conductivity and wind measurements made this year for the first time we expect to determine to a new degree the relative roles of conduction and bulk transport in charge transport near the fog. The field experiment in 1975 gave results which were disappointing because aircraft failures limited the experiment time, and no actual fog data was obtained.

The added measurements of wind and conductivity provide the type of physical measurements in which the electric field variations can be cross-checked against conductivity measurements. Further understanding of these factors is necessary if we are to explain the detailed field variations. It would seem likely that the vertical current would be fairly uniform over horizontal distances of a mile or so within an area above a fog of twenty or so miles across, except for changes near the fog edge. Thus if the conductivity varies in step with the large variations we know already exist in the electric field we may be able to test the hypothesis that the current does indeed tend to be relatively uniform. Substantial variations in the current would imply

substantial effects over vertical distances exceeding the horizontal dimensions of the variations.

If there is the expected variation in the current measurements of vertical airmotion such as we have now obtained, it may provide an explanation of the relationships between conductivity and electric field. When convection is occurring we may well find convective transport of charge provides an important role. While it is not clear how convection can be of importance in east coast advection fogs, data just obtained (1976 field experiment) will throw a lot of light on the matter.

Our efforts in the coming year will be divided between data analysis and preparation for an August field experiment. We have been granted use of an NCAR aircraft for continued field work in 1977. We intend to study the fog off the northern California coast in August 1977. Preparation for this work will consist mainly of refurbishing and recalibration. A second conductivity cell, partially built when the first was constructed, will be completed. Minor modifications to cell design will be made to improve some suspected problems of mechanical vibration in both new and old conductivity cells. Our equipment will then consist of two airborne electric field mills and two conductivity cells, all of field proven design (One conductivity cell this year). The second conductivity cell will allow measurement of both polar conductivities simultaneously. At present we alter-

nate measurements of positive and negative conductivity. It is not expected that there will be any need for further similar hardware.

Since our instrumentation is largely complete, the field work and preparation will consume less effort than in the past. We shall emphasize data analysis. This year's field work on the west coast encountered larger cloud and fog systems than found in previous years on the east coast and we found a greater variety in air types as combinations of marine and continental air. We flew extensively in stratus clouds whenever fog could not be found. In our case we observed the continuous spatial transition of stratus over warm water into fog over colder water at some distance. In fog and stratus the liquid water profiles as well as electric field profiles at the tops show clear similarities.

Drizzle from low stratus may well be a contributing mechanism in transferring water substance into the unsaturated air below cloud base down to the surface, although this remains to be proven. This transfer would result in the lowering of cloud base if the mixing ratio is not dominated by vapor transfer at the sea surface. If the region is well mixed by convective stirring such a mechanism may be largely ineffective because if drizzle forms in a low stratus layer it may imply that there is very little convective overturning, since such stirring may inhibit continued growth of the drops by condensation which one

expects in still air. Although this argument needs qualitative study it is reasonable to expect that if the droplets are evaporated every few tens of minutes in a convective cycle into the clear air below base that continued growth will be interrupted.

Once the fog reaches the sea surface the situation is different. The drops will never completely evaporate even with total stirring. Thus the formation of drizzle from low stratus layers may also suggest it can occur within convective fogs. The electrical effects will play a role in drizzle formation which may well provide vital clues as to how to induce drizzle and a consequent increase in fog visibility. In any case the confirmation of a substantial change in the overlying electric field as observed from place to place would be a major contribution to other studies of fog history because the aircraft mobility in examining a substantial area would give information about in-fog circulation.

An additional reason for extending our fog investigations to conditions where convection in the surface layer is present is the program of theoretical work in progress under another grant. This work is in modelling the convective plume boundary layer with the inclusion of both heat and evaporation from the sea. Postulating a horizontal pressure gradient in the direction of an increasing sea surface temperature the model calculates the fluxes of both heat and moisture assuming both components

are transported similarly in turbulent air parcels. As a check the model can be run when the surface vapor pressure only is increasing but not the temperature, buoyancy being derived from the lower density of the water vapor alone. The formulation of the condensation process in the rising air currents has now been included in the calculation. This model should give indications of two convective features which can be related to the measuring program. Firstly it should give the conditions under which convective plumes should exist in the fog and secondly it should show whether or not, and at what rate, the stratus cloud base will descend towards the surface.

We observed very strong vertical motion associated with low stratus cloud boundaries for reasons not yet determined. These may or may not be pertinent to this modelling effort. Accompanying these were large electrical conductivity and electric field perturbations. Since these were penetrated repeatedly in flight some explanation may be obtained. Although this work would be secondary to fog study it may yield in addition some insight into the use of electrical conductivity of air as a short term tracer in plume studies.

## 6. Discussion of Fog Stability

Fog over water often persists long enough to create operational problems for ships and aircraft. Although the temperature profiles may not indicate large vertical stability, a fog usually does appear to be contained beneath a stable over-lying layer. Mixing upward of parcels containing appreciable liquid water will probably be slowed by evaporative cooling. Downward mixing cannot be too vigorous or the fog would dissipate naturally. Hence, natural mixing across the upper fog boundary is probably restricted by the drier overlying air being considerably warmer; a locally intense inversion is possible.

Fog basically is of two forms, "steam fog" when the air is cooler than the water and "advection fog" when the air is flowing over a colder sea. Steam fog will involve substantial and continuing convection and is an extension of the convective field in clear air being studied as a major goal in this laboratory (Telford, 1968, 1970, 1972 and 1975). Advection fog is much more uniform in structure (often described as "milky") and forms when the mechanical mixing due to the wind driven turbulence mixes air with sea surface temperature and saturation mixing ratio. If the warmer overlying air is reasonably moist, then due to the almost exponential increase of saturated water vapor mixing ratio with temperature, the mixing of the cold surface air into the air above gives an excess of moisture for the

average temperature resulting. This releases moisture which condenses into the fog droplets.

Radiation from the fog top may cool the fog and produce some downward convection in both cases. This cooling will also stabilize the top of the fog layer against mixing in of the drier air above.

In any attempt to clear away a marine fog for an appreciable period, the experimenter must face the problem of the existing stability. Mechanical mixing by helicopters of overlying drier air downward to the surface is practical on a small scale for temporary clearing. This has been well demonstrated. (AFCRL, ASL, 1970). However, due to the stability discussed above, evaporation may not cool the transported air sufficiently for it to remain in the lower region. The surrounding fog may still be denser and force the mixed air upward and back into the clear overlying layer. It may be for this reason that clearing fog by helicopter downwash is usually not as effective as might be wished.

Another possible source of fog stability aiding any inversion effects is a net positive electrical charge captured by fog droplets from natural electrical conduction in the air. At least initially, normal fair weather current is likely to penetrate any fog which is laterally extensive. However, since air conductivity is significantly reduced within the fog, a positively charged region will occur near the upper fog boundary.

It is possible that most of the net space charge can be captured by fog droplets. Then charged droplets will settle and any convective mixing within the relaxation period of this charging process will help disperse these droplets throughout the fog. Charge removed from the top layer would probably be replaced to some extent as the downward current continues to flow into the top of the fog. As the net charge accumulates the whole fog attains a positive potential. The intensity to which this effect would be extended in a steady state condition would most likely be dependent upon many parameters, including the fog density, depth and lateral developments.

Should the charging and dispersal mechanism described above be realistic, it could significantly enhance the natural colloidal stability in a fog composed of small droplets. This, of course, would significantly diminish any possibility of natural fog dissipation through fallout of drops growing by coalescence.

If the effects above indeed do occur in nature and contribute to fog stability, then a countering effect could be produced by release of negative ions. This would produce opposing charged drops, induce coalescence, and likely produce more rapid fog dissipation by fallout. As a fog dispersal mechanism, this is attractive in principal because clearing fog by liquid water removal is not frustrated so much by the tendency of any stable temperature profiles to return the fog to the cleared area. To speculate further on this process as a method of dissipating

fog, local charge release, say on board ship by point discharge, would likely create a region of negatively charged fog droplets. These upon mixing into surrounding regions of positively charged droplets would encourage massive coalescence between oppositely charged droplets (Telford, 1955; Davis, 1965; Sartor, 1954). The resulting larger droplets would have improved chances of falling out with normal collection enroute and producing a clearing effect.

An alternative, perhaps more effective since it could be applied at the fog top, is the release of equal but opposite charges from an aircraft at spacings with wing-tip separation. Mixing would be dynamic due to wing tip vorticities and the natural coulomb attractions would gain every opportunity to produce coalescence. Since collection is expected to be important in clearing fog, it is probable that the higher the level of initial interaction, the larger the droplets would grow before reaching the surface. Thus, more of the smaller droplets would be swept from the fog near the sea surface.

## 7. Summary of Proposed Work

Our upcoming work will be principally in data analysis and continued field study. We expect the considerably experimental data now available (mostly from this year's field trip) will be usable and well able to answer some of the questions posed above of conditions than encountered previously. The field

work and the necessary preparation for the next field trip will thus become less prominent in our efforts as the load is shifted to data analysis.

We have for the first time rather complete measurements, including wind and electrical conductivity, with which to work. This will be analyzed with a view of obtaining information about fog convection. We should now also be able to make more complete analysis of charging currents with fogs and clouds encountered, in rates of charging and mechanisms of charge transport. Comparison of low stratus clouds and fog types will be made where such analysis may aid our understanding of the relation between the two or in an understanding of the roles of electricity in the natural stability of these marine cloud types.

In particular the pattern of variability of the electric field near the fog top will be studied with a view to answering the crucial questions of cell size and circulation within the fog.

# Summary After Year 1977

December 1, 1977

# TABLE OF CONTENTS

# Combined Theoretical and Analytical Fog Studies

## Abstract

Analysis of the considerable data obtained in the past airborne measurement efforts will be used to test and refine theoretical studies of turbulent mixing in the marine environment. Measurements of surface temperature and air temperature profiles in and adjacent to fog will provide a good reference for modeling the formation and dissipation of marine fog.

## 1. THEORETICAL STUDIES

The main object of this research is to study the initial onset of fog in sufficient detail to enable us to qualitatively determine the factors necessary to allow us to predict fog formation.

This is the most critical problem. Also, efforts on a somewhat smaller scale will be directed to studying growth and maintenance, or conversely, dissipation of fog (probably due to radiative heat losses from the fog top). These are, of course, important problems too.

Our studies will concentrate upon the first fifty meters above the water surface. The approach will be to explore the physical theory of turbulent mixing being developed in this laboratory. This theory attempts to describe the final stages in the turbulent mixing, wherein molecular diffusion changes the water vapor mixing ratio and temperature in the vicinity of fog droplets, or potential fog droplets. hus, we will be able to estimate what volume proportion is to be found in the mixture for each possible ratio of moist and dry air, and how large these small, but essentially uniform volumes are, on an individual basis. This will give us the variability in the water vapor saturation and liquid water mixing ratio, and hence, the drop size distribution. We will also be able to decide how effective the curve of the water vapor saturation-pressure diagram is in giving supersaturation, as is commonly suggested. We have field data which will be analyzed to see how the role of air and surface temperature, and their variation, affect real fog formation.

The progress to date has been in laying the groundwork for the mixing problem, which now seems to present an attractive line for a profitable attack. In particular, a mechanistic treatment is being developed for the surface boundary layer, which works well for many

rough surfaces (eg.10 m trees) and should be transferable to the relatively low roughness surface presented by the sea afterfurther work. This model should be helpful background for the more intimate study of the details in the mixing which are our ultimate goal.

The theoretical convective boundary layer model has been integrated for a heat loss out the top of the cloud, attributable to radiation, when the lowering stratus flows over colder water (and hence, has little flux from the surface). We believe this is relevant in some circumstances.

## 2. FIELD STUDIES

Marine fog field studies under U.S. Navy sponsorship at the Desert Research Institute have been divided into two areas.

The first is microphysical, where investigation of droplet nuclei has been the major interest.

The second area is a study of electrical and dynamical fog properties, wherein considerable measurements have been made from aircraft. This report concerns the second area in regards to data collected and analysis to be done on these data.

These latter studies were planned to support continued boundary layer. theoretical development. Present theory can only be extended to the surface layer aspects of fog formation by proper choice from among alternate hypotheses. Adequate real data are necessary for this selection.

## 3. FIELD PROGRAMS COMPLETED

In addition to the direct Navy support for airborne study of fog (somewhat less than for the microphysical studies), DRI has successfully solicited full aircraft support from the National Center for Atmospheric Research, with partial instrumentation support, for each of the five

years of study. DRI has developed electric field and air conductivity instruments particularly suited to the wetting incurred during flight in cloud or in fog. As these instruments were developed and proven with time, NCAR's aircraft became more capable, particularly so with installation of inertial navigation equipment, and direct wind measurement capability. So without neglect of electrical instruments, we gained in the later field programs capability for dynamical measurements in fog. Table 1 is a list of measured parameters in the last two years of work.

The earlier measurements were made offshore from Cape Cod, Massechusetts. However, the experiments in the last two years were conducted off the northern California coast near Cape Mendicino. The Pacific measurements were the most fruitful, in terms of both the more comprehensive measurements and the occurrance of suitable meteorological conditions. A total of 18 marine fog situations were found there in our allocated experimental time (about three weeks each year) and 27 stratus cloud situations were investigated. Sufficient flight time was available to study low stratus clouds in absence of fog. Similarities between the two are evident. Indeed, cases of stratus clouds lowering to the surface (fog) were encountered. There were also cases of fog changing to low stratus.

The attached appendix is an abbreviated synopsis of the situations investigated in the past two seasons. About one third as many situations were investigated in earlier experiments.

Figure 1 shows typical vertical profile of flights in fog (an actual profile from Aug. 31, 1977).

4. DATA ANALYSIS

Until now analysis has been rather limited, the instruments and

field programs have received emphasis. This is an undesirable mixture in general, but one we felt necessary in view of the support available.

We have, however, developed a numerical model of the electrical fog charge distribution capable of being fitted t' field measurements measured at various altitudes. We have analyzed examples in east coast fog and shown them to contain a net positive electrical chare in its upper most layer (several meters). Inixial views of west coast fog show strong correlation to field strength and vertical velocity within the fog.

Now, with considerable data collected, particularly that of the past two field experiments, we feel it is time to redress the past imbalance between experiment and analysis with a year of intensive analysis and no field work. We expect to obtain significant progress towards understanding the relationships of fog and low stratus to the first 500 meters of atmosphere.

In particular, we hope to address the relationship of surface water temperature. We have measured water temperature profiles on several occasions each year as a function distance from the coast in the experimental region. Not surprisingly, where fog-stratus transition was found, it was gradual and the fog lay over the colder water.

The relationship of the cloud-forms to winds, windshear and the sometimes enormous overlying temperature inversion must be investigated. Finally, we hope to complete the electrical model with emphasis on dynamical charge transportation. The charge distribution (in top layer only) noted on the east coast does not appear to be universal. Clearly, mixing occurring on the same time scale as the atmospheric time constant is going to perturb the simple picture of top layer charging by bringing the net charge down into the cloud body. This seems to occur frequently.

Admittedly, these are ambitious undertakings. However, we believe that the data are largely of good quality, and sufficiently comprehensive to support these undertakings. We expect to obtain significant advances in understanding the relationship of marine fog to stratus cloud, to each other and to their environment.

## 5. SUMMARY

These data will directly serve to confirm or refute the theoretical aspects of this program which will be studied concurrently. The goal of this work is to identify a clear model for predicting the occurrance, persistance and dissipation of fog over the ocean. The approach taken is to study the temperature of the air relative to the water along horizontal traverses entering the fog edge so the effect on the fog of the temperature changes with time, relative to the underlying water surface, can be thoroughly explored. Wind, turbulence, vertical motion and liquid water content are all to be studied. The theoretical concepts advanced will be tested against measured data.

TABLE 1: Instruments and measured parameters

Wind

Liquid water mixing ratio

Vapor mixing ratio (dew point)

Temperature

Static pressure

Electric field

Air conductivity (both polarity components, alternately)

Upward infrared radiation (surface temperature at low altitudes)

Aircraft velocity, altitude and ground track (inertial navigation)

Altitude (radio altimeter)

Downward looking time lapse camera (16mm)

Hand-held 35mm camera

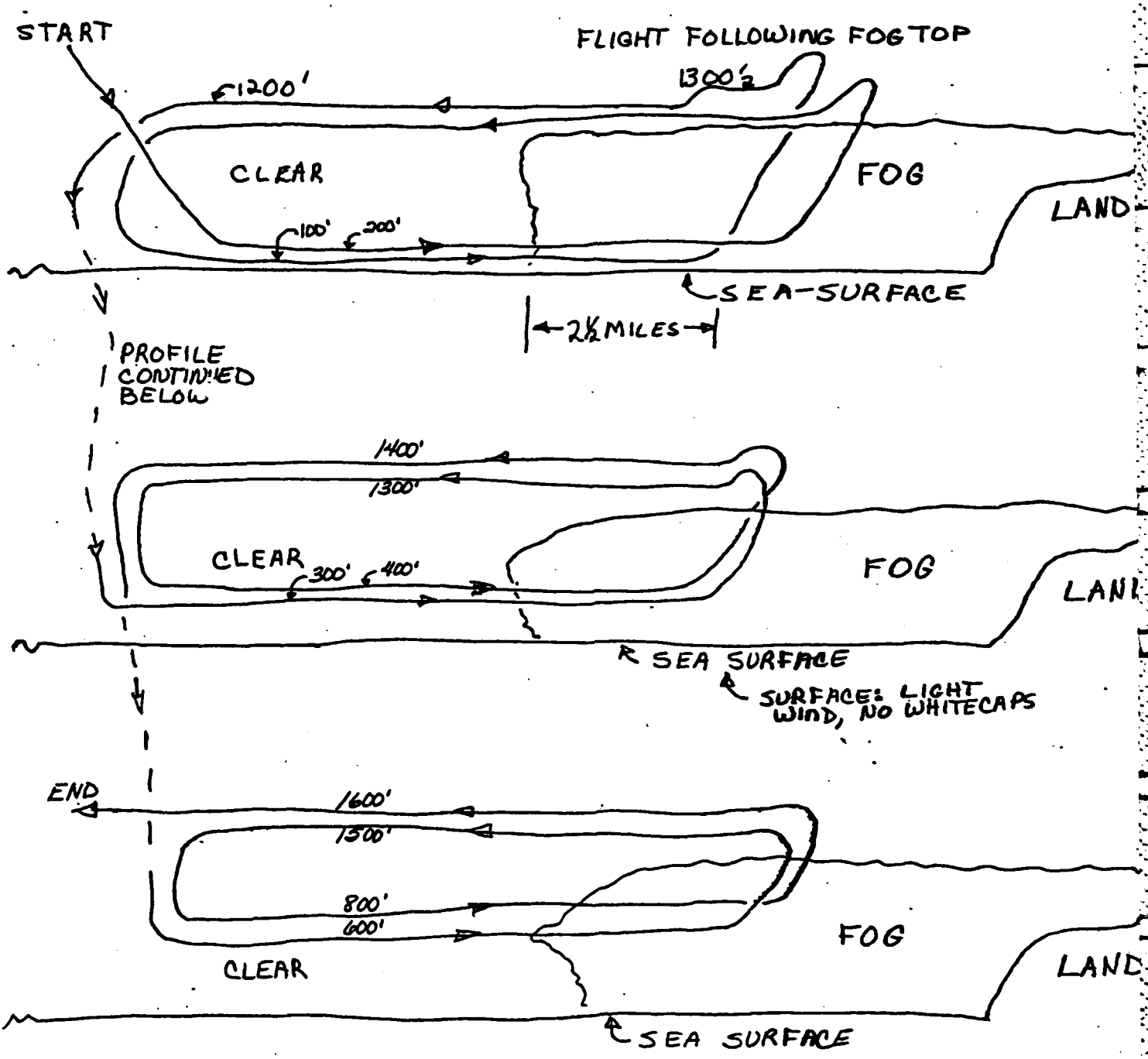


NOTE: FOG EDGE HAS MOVED EASTWARD (TOWARD SHORE) ABOUT 3/4 MI DURING INVESTIGATION

Figure 1. Drawing of approximate flight profile made while investigating a thick fog bank south of Pt. Arena on the California coast. This is taken from a drawing made as flight progressed.

# Flight Summary 1976, 1977

# APPENDIX
## 1976 Fog Trip Synopsis

| FLT # | DATE | SIT. # | DESCRIPTION |
|---|---|---|---|
| 76-1 | 9/17/76 | 1 | Extensive low stratus - near coast, work from clear area below Cape Mendicino - multiple passes clear to cloud. |
| | | 2 | Similar - worked a finger of stratus cloud extending S from second bank 30-40 mi. to sea., outside wide bank along coast. |
| 76-2 | 9/18/76 | | Stratus lowering to fog towards shore, N.S. edge, multiple fts E.W. all levels, noted clear area at shore ∿3 1/2 mi. wide. Bank ∿40 mi. wide. Worked W edge then E edge, all levels - noted wave structure of top on W edge, along wind. |
| 76-3 | 9/21/76 | | Stratus w/haze or fog or drizzle beneath ∿350 to 500 ceiling 2700' tops, top and base lower in north than south. |
| 76-4 | 9/21/76 | | High stratus - somewhat unstable lower cloudy at W edge. Worked area near lower convective clouds, & sounded to 4000' on flt to shore. Flew at 300-200' to get water temp profile. |
| 76-5 | 9/22/76 | | General stratus - usual hole S of Cape Gordo - Worked S edge, noted stationary rolls of pts of land. Thick fog S of hole. Worked this area. Flts. 100-1000' in 50' increments. |
| 76-6 | 9/23/76 | 1 | Stratus worked both sides of usual hole - flts mainly over hole from top upward. |
| | | 2 | Multiple flts thru stationary rolls off Cape Mendicino. |
| | | 3 | Fog - penetrated at to 3 different distances and climbed thru tops - short on time here. |
| 76-7] | 9/24/76 | | FM developed problem (power supply) - NCAR called this Flt 76-7 and I did not, hence subsequent numbering discrepancy. |
| 76-7 | 9/25/76 | | Hi stratus - conductivity cell out (shorted due to vibration) - tops 2000', noted reversed field at cloud edge. |
| 8 | 9/26/76 | | Fixed cond. cell. Stratus - edge along wind "good" measurements? |

76 Continued

| T # | DATE | SIT. # | DESCRIPTION |
|---|---|---|---|
| -9 | 9/29/76 | 1 | Best fog situation - multiple penetrations to different distances w/returns (to clear area 300-4-5-600 ft.) |
| | | 2 | Similar to #1 above. Note error in tape times. |
| | | 3 | Later same fog bank - opposite side, has lifted from water - multiple flts similar to #1 and 2 above. |
| -10 | 9/30/76 | 1 | Stratus cloud/extreme haze - patterns as on 76-9 |
| | | 2 | Similar to 1. |
| | | 3 | Fog - dense, multiple runs, somewhat limited in penetration due to low visibility. |
| -11 | 9/30/76 | | Stratus - 300' to 2000' erroded cliff appearance - pictures. Multiple penetrations thru cld. edge at various levels. |
| -12 | 10/3/76 | | Clear day, several soundings 50' to 5000'. |
| -13) | 10/5/76 | | Bust - use number later. |
| -13 | 10/7/76 | | Stratus - multiple runs beneath w/penetration on climb in 10 sec increments. Pictures (Recording difficulty?) |
| -14 | 10/8/76 | | Last day - Solid fog bank, winds diagonal to edge Multiple penetrations 100' & 50' to different distances (probable recording problem). |

# 1977 Fog Trip Synopsis

| Flt # | DATE | SIT. # | DESCRIPTION |
|---|---|---|---|
| 7-1 | 8/22/77 | 1 | Stratus band, 200' to 900', ~6 mi wide. flts over under to 100' and thru, plus soundings to 4500' and 2000'. |
| | | 2 | Later - second stratus band, 200-700', similar flt patterns, soundings to 1200'. |
| 7-2 | 8/23/77 | 1 | Fog bank 400 to 700' deep, flts in (to 50') and above w/sounding (down) from 4500 over fog. Short soundings to 1000' over fog, fog edge and clear area. Sounding up to 2000', on departure. Fog apparently lifted during investigation to stratus formation, low runs before and after. Top surface showed structure - pictures taken. |
| | | 2 | Stratus cloud - wave structure on top & edge flts near edge, in, beneath and above cloud, sounding to 3500', pictures. |
| 7-3 | 8/24/77 | | Overcast day, 15,000 base, stratus clouds beneath. 1500 base, 2500 top - flts. in, above & beneath (to 50' MSL). Cloud began to break up during investigation - weather preceeded front. Noted slight fog occurring at beach only. |
| 7-4 | 8/25/77 | | Thick cloud, IFR flt only, could not get clearance to descend. |
| 7-5 | 8/26/77 | 1 | Light fog, patchy and dissipating. Flt. over and in (to 100') a "finger" bank 1 to 2 mi. wide. |
| | | 2 | Wave later fog bank - 20 mi. to sea, dissipating. |
| | | 3 | Light fog bank with soundings. 5 mi from coast Flts. crossing fog N-S and E-N. in (at 70') - on top and in (at 50'). |
| 7-6 | 8/27/77 | | Stratus cloud 40 mi. from shore - run to shore @ 200' with several short soundings on route & extensive soundings at shore line. |
| 7-7 | 8/29/77 | | Clear air flt. to sea with repeated (5) soundings (sfc to 2000') to shore line. |
| 7-8 | 8/30/77 | 1 | Thin stratus 2000'-2500', flts in, beneath and thru, below - sounding to 1100' to 4500' |

- continued

| # | DATE | SIT. # | DESCRIPTION |
|---|---|---|---|
| | | 2 | 8 mi. wide stratus band - moving with wind. |
| | | 3 | Similar to 2 - clouds developing to extensive stratus deck from shore to 20 mi. seaward. |
| | 8/31/77 am | | Flt in heavy haze, 2 soundings only. |
| 0 | 8/31/77 pm | | Deep fog (~1000') banked against coastal mountains South of Pt. Arena. Flts in & above fog thru edge. |
| 1 | 9/1/77 | | Stratus band 20 mi. wide (to shore line). Flts in above & below (to 150'), 2 soundings near edge 100' to 2000 & 3500 ft. respectively. |
| 2 | 9/2/77 | | Stratus as on 9/1/77, but lowering to fog toward land. Flt. in, above & below stratus (& on into fog at 100' - twice) Sounding to 2000' over tops. Multiple soundings top sfc to 1500' on trip home. |
| 3 | 9/3/77 | | High thin stratus hanging along coast. Flt. in above, sfc and climbs & descends thru cloud (100' sfc rm). |
| 4 | 9/5/77 | 1 | Cloud - multiple up & down penetrations. |
| | | 2 | Fog (500') multiple penetrations - level flt. from 100' up - climbing out at end run and descending back in for reverse run. |
| | | 3 | Later, same area, fog more cloud-like and drifting rapidly S. Flts along edge to show drift rate. |
| | | | Cloud further north, multiple flts as usual w/ soundings sfc to above cloud & 2 tracks along edge to mark drift. |
| 5 | 9/6/77 | 1 | Fog, 300' multiple runs to 50' and soundings over tops - tape difficulty occurred - returned home. |
| 5 | 9/6/77 | 1 | After correcting recording problem (bad tape itself) returned to sea. Heaviest fog 350-400', multiple runs 50' and 100'. |
| | | 2 | Fast receeding fog, multiple flts. |
| | | 3 | 3rd fog, 200-350', multiple flts to 50' - to 1500'. |

Reprinted from Preprint Volume: Conference on Cloud Physics and Atmospheric Electricity, July 31-August 4, 1978, Issaquah, Wash. Published by The American Meteorological Society, Boston, Mass.

6.6

# ON THE FORMATION OF CONVECTIVE MARINE FOG

Steven K. Chai and James W. Telford

Desert Research Institute
University of Nevada System
Reno, Nevada

## 1. INTRODUCTION

We usually say that fog is formed by warm air flowing over cold water. Text books often say that since warm air can carry moisture it will be cooled down by the cold water surface and finally reach its dew point to form fog. However, since the moisture is also extracted by diffusion to the cold water, saturation cannot be reached this way in most cases.

Petterssen (1938) says that marine fog on the eastern Pacific Ocean near San Diego is convective. The temperature distribution in the fog is unstable. This means that the fog is formed by cold air flowing over a warm sea surface instead of what is usually the case, warm air flowing over a cold sea surface.

Furthermore, from the observations made by Emmons (1947), he concludes that warm air flowing over cold sea with a dew point below the sea-surface temperature usually does not form fog. Thus, convection may be an important mechanism in the marine fog formation. This paper introduces a numerical model to simulate the convective marine fog.

One of the authors (Telford, 1966, 1970, 1972, 1975) introduced a plume model covering a conective field. His model considers only the dry plumes over land and ignored moisture over the sea, and it works well. This work will be an extension of this model. Telford's plume model has been modified to include the water vapor content and the condensation process.

## 2. THE CONVECTIVE FIELD

Our model is to simulate a field of identical plumes over the sea surface. The new model is controlled by three parameters: The height of the convecting layer, z ; the constant horizontal pressure gradient, VP; and the constant surface temperature gradient, VT. The air flows at a speed u, which is generated by the horizontal pressure gradient. We assume that the horizontal pressure gradient as well as the wind speed is uniform throughout the convecting layer. The surface temperature gradient is measured along the direction of the wind. Thus, the time rate of change of temperature is uVT. Since the bottom of the air in the model is heated up continuously by this time rate of change of temperature, convective plumes can be expected to occur. The air will go upward in a plume-like shape and the surrunding air will go downward by continuity. The environmental air has a temperature inversion that starts from $z_i$. The ascending air cannot penetrate this stable boundary and will turn over and start to decend at the inversion base. We have to notice that the bottom of the convecting layer is not the sea surface, since there is a super-adiabatic disorganized layer beneath the plumes.

In the super-adiabatic layer no organized air motion is present. The height of this layer depends on the surface roughness, surface temperature and the wind speed. The decending air will then turn to horizontal convergent motion and re-enters the plume. As the air re-enters the ascending plume, some surface air with recent surface properties will be mixed in. Thus, the plume air gets warmer and wetter. Finally, the air reaches its saturation point at the top of the convecting layer and a stratus cloud is then formed. Since the vapor is continuously being added at the bottom, the cloud base moves downward and eventually forms a sea fog over the ocean surface.

## 3. THE CONSERVATION EQUATIONS

The plume radius is b, its total density $\rho_{t,p}$, density of water substances $\rho_{w,p}$, temperature $T_p$, updraft velocity $w_p$, rms turbulent velocity $i_p$ and dry air pressure $P_{a,p}$. The downdraft velocity is $w_s$, total density $\rho_{t,s}$, density of water substances $\rho_{w,s}$, temperature $T_s$, rms turbulent velocity $i_s$ and dry air pressure $P_{a,s}$. The radius of the convecting cell is a constant c. $\rho_t$ is the rate of change of total density which depends both on heat and vapor fluxes. The vapor flux is not a constant, which will decrease as the moisture content in the convective layer increases. The total pressure is $P_T$.

The five conservation equations for the plume are as follows:

Volume

$$\frac{\partial}{\partial z}(b^2 w_p) = 2ab(i_p - i_s) + b^2 J_p w_p \frac{\partial P_T}{\partial z}, \quad (1)$$

Total Mass

$$\frac{\partial}{\partial z}(b^2 w_p \rho_{t,p}) = 2ab(i_p \rho_{t,s} - i_s \rho_{t,p}) - b^2 \dot{\rho}_{t,p}, \quad (2)$$

Mass of Water Substances

$$\frac{\partial}{\partial z}(b^2 w_p \rho_{w,p}) = 2ab(i_p \rho_{w,s} - i_s \rho_{w,p}) - b^2 \dot{\rho}_{w,p}, \quad (3)$$

Momentum

$$\frac{\partial}{\partial z}(b^2 w_p^2 \rho_{t,p})$$

$$= - b^2 \frac{\partial P_T}{\partial z} - g b^2 \rho_{t,p}$$

$$+ 2ab(i_p w_s \rho_{t,s} - i_s w_p \rho_{t,p})$$

$$- b^2 w_p \dot{\rho}_{t,p} \quad , \qquad (4)$$

Turbulent Kinetic Energy

$$\frac{\partial}{\partial z} (b^2 w_p \rho_{t,p} i_p^2)$$

$$= 2ab\left\{ i_p \rho_{t,s} [(w_p - w_s)^2 + i_s^2] - i_s \rho_{t,p} i_p^2 \right\}$$

$$- b^2 i_p^2 \dot{\rho}_{t,p} - \frac{A}{2} b \rho_{t,p} i_p^3 \quad . \qquad (5)$$

where

$$J_p = \left( \frac{L r_{v,p,sat.}}{T_p} \right.$$

$$- \frac{\varepsilon}{\varepsilon + r_{v,p,sat.}}$$

$$\times c_{v,mix,p}$$

$$- \frac{\varepsilon L}{P_{a,p}}$$

$$\left. \times \frac{dP_{v,p,sat.}}{dT} \right)$$

$$\times [P_{a,p} c_{p,mix,p}$$

$$+ L(\varepsilon + r_{v,p,sat.})$$

$$\left. \times \frac{dP_{v,p,sat.}}{dT} \right]^{-1} \quad ,$$

$$c_{p,mix,p} = c_{pa} + r_{v,p} c_{pv} + r_{w,p} c_w \quad ,$$

$$c_{v,mix,p} = c_{va} + r_{v,p} c_{vv} + r_{w,p} c_w \quad ,$$

and the subscript "sat." denotes saturation.
The last term in (5) is the dissipation term and A=1 by experiments.
The five conservation equations for the downdraft are as follows:

Volume

$$\frac{\partial}{\partial z} [(c^2 - b^2) w_s]$$

$$= 2ab(i_s - i_p) + (c^2 - b^2) J_s w_s \frac{\partial P_T}{\partial z} \quad , \qquad (6)$$

Total Mass

$$\frac{\partial}{\partial z} [(c^2 - b^2) w_s \rho_{t,s}]$$

$$= 2ab(i_s \rho_{t,p} - i_p \rho_{t,s}) - (c^2 - b^2) \dot{\rho}_{t,s} \quad , \qquad (7)$$

Mass of Water Substances

$$\frac{\partial}{\partial z} [(c^2 - b^2) w_s \rho_{w,s}]$$

$$= 2ab\,(i_s \rho_{w,p} - i_p \rho_{w,s}) - (c^2 - b^2) \dot{\rho}_{w,s} \quad , \qquad (8)$$

Momentum

$$\frac{\partial}{\partial z} [(c^2 - b^2)\, w_s^2 \rho_{t,s}]$$

$$= - (c^2 - b^2) \frac{\partial P_T}{\partial z} - g(c^2 - b^2) \rho_{t,s}$$

$$+ 2ab(i_s w_p \rho_{t,p} - i_p w_s \rho_{t,s})$$

$$- (c^2 - b^2) w_s \dot{\rho}_{t,s} \quad , \qquad (9)$$

Turbulent Kinetic Energy

$$\frac{\partial}{\partial z} [(c^2 - b^2) w_s \rho_{t,s} i_s^2]$$

$$= 2ab\left\{ i_s \rho_{t,p} [(w_s - w_p)^2 + i_p^2] - i_p \rho_{t,s} i_s^2 \right\}$$

$$- (c^2 - b^2) i_s^2 \dot{\rho}_{t,s}$$

$$- \frac{A}{2} (c^2 - b^2)^{1/2} \rho_{t,s} i_s^3 \quad , \qquad (10)$$

where

$$J_s = \left( \frac{L r_{v,s,sat.}}{T_s} \right.$$

$$- \frac{\varepsilon}{\varepsilon + r_{v,s,sat.}}$$

$$\times c_{v,mix,s}$$

$$- \frac{\varepsilon L}{P_{a,s}}$$

$$\left. \times \frac{dP_{v,s,sat.}}{dT} \right)$$

$$\times [P_{a,s} c_{p,mix,s}$$

$$+ L(\varepsilon + r_{v,s,sat.})$$

$$\left. \times \frac{dP_{v,s,sat.}}{dT} \right]^{-1} \quad ,$$

$$c_{v,mix,s} = c_{va} + r_{v,s} c_{vv} + r_{w,s} c_w \quad , \text{ and}$$

$$c_{p,mix,s} = c_{pa} + r_{v,s} c_{pv} + r_{w,s} c_w \quad .$$

From these ten conservation equations we can have a set of ten simpler differential equations for ten variables: b, $P_T$, $\rho_{t,p}$, $\rho_{t,s}$, $\rho_{w,p}$, $\rho_{w,s}$, $w_p$, $w_s$, $i_p$, $i_s$. Two more differential equations were added in to handle the temperature profiles for

both plumes and surroundings. They are

$$\frac{\partial T_p}{\partial z} = -\frac{\dot{T}}{w_p} + \frac{2a}{bw_p} i_p \frac{T_p}{T_s}(T_s - T_p) + (R_a T_p + r_{v,p,sat.} L) \times [P_{a,p} c_{p,mix,p} + L(\epsilon + r_{v,p,sat.}) \times \frac{dP_{v,p,sat.}}{dT}]^{-1}, \quad (11)$$

and

$$\frac{\partial T_s}{\partial z} = -\frac{\dot{T}}{w_s} + \frac{2ab}{(c^2-b^2)w_s} \times i_s \frac{T_s}{T_p}(T_p - T_s) + (R_a T_s + r_{v,s,sat.} L) \times [P_{a,s} c_{p,mix,s} + L(\epsilon + r_{v,s,sat.}) \times \frac{dP_{v,s,sat.}}{dT}]^{-1}. \quad (12)$$

Now, we need twelve boundary conditions for those twelve differential equations. They are

At the top

$$w_p = -\frac{(c^2-b^2)w_s}{b^2}$$

$$T_p = T_s = T_0$$

$$\rho_{t,p} = \rho_{t,s} = \rho_{t0}$$

$$\rho_{w,p} = \rho_{w,s} = \rho_{w0}$$

$$i_p = i_s$$

At the bottom

$$i_p = i_s = I_0$$

$$b^2 = c^2/2$$

$$\partial \rho_{t,s}/\partial z = 0,$$

where $T_0$, $\rho_{t0}$, and $\rho_{w0}$ are given and $I_0$ is the surface turbulent velocity.

## 4. SOME SOLUTIONS

Figure 1 shows the properties associated with a set of typical conditions. In this figure no liquid water presents. Figure 2 shows the cloud base half way down the convecting layer. The liquid water content at the top boundary is .0002 kg/m$^3$. Figure 3 shows that the cloud base down to the bottom of the convecting layer and marine fog is formed. The liquid water content at the top boundary in Figure 3 is .0004 kg/m$^3$.

## 5. CONCLUSIONS

From the illustrations shown in last section we can see that the plume convection can form stratus clouds under an inversion and then lower the cloud base by continuous evaporation at the sea surface.

The cloud base lowering speed predicted by this model is somewhat slow. However, there are some other effects, not considered in this paper, which can enhance the convection. First of all is the radiative cooling at the cloud top. The radiative cooling not only produces a downward convection from the top, but also cools the whole layer down and increases the air-sea temperature difference. Thus, the heat flux is continuously added in from the sea but the plume air remains cooler than the sea surface. Therefore, the radiative cooling gives two effects: Decreasing temperature and increasing vapor flux. Both can increase the cloud base lowering speed (Leipper,1948).

Another factor is the entrainment of overlying dry air at the inversion base. This can also enhance the vapor flux from the sea surface and thus increase the cloud base lowering speed. Both of these factors will be considered in the near future by the authors.

## 6. ACKNOWLEDGEMENTS

This work was mainly supported by the National Science Foundation Grants GA-32206 and GA-42636. Other aspects were supported by the National Science Foundation Grants DES 75-10003-A01 and ATM 77-10646 and the Office of Naval Research Contracts N00014-75-C-0598 and N0004-75-C-0598.

## 7. REFERENCES

Emmons, G., 1947: Vertical Distribution of Temperature and Humidity over the Ocean between Nantucket and New Jersey. Papers in Physical Oceanography and Meteorology, Massachusetts Institute of Technology and Woods Hole Oceanographic Institute, Vol. X, No. 3, 89 pp.

Leipper, D. F., 1948: Fog Development at San Diego, California. J. Marine Research, Sears Foundation, Vol. 7, No. 3, 337-346.

Pettersen, S., 1938: On the Causes and the Forecasting of the California Fog. Bull. American Meteor. Soc., 19, 49-55.

Telford, J. W., 1966: The Convective Mechanism in Clear Air. J. Atmos. Sci., 23, 652-666.

Telford, J. W., 1970: Convective Plumes in a Convective Field. J. Atmos. Sci., 27, 347-358.

Telford, J. W., 1972: A Plume Theory for the Convective Field in Clear Air. J. Atmos. Sci., 29, 128-134.

Telford, J. W.,1975: The Effects of Compressibility and Dissipation Heating on Boundary Layer Plumes. J. Atmos. Sci., 32, 108-115.

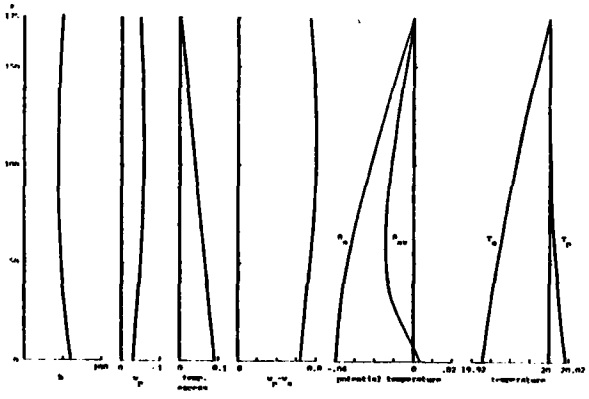

Figure 1 The properties of a convective field over the sea before a stratus cloud is formed. The height of the convective layer is 175 m, the horizontal pressure gradient is 0.25 mb/100 km and the surface temperature gradient is $2^{\circ}C$/100 km. The Temperature curves are the temperatures of plumes and surroundings after taking out the adiabatic lapse effect. $\theta_{av}$ is the average potential temperature and $\theta_s$ is the potential temperature of the surroundings.

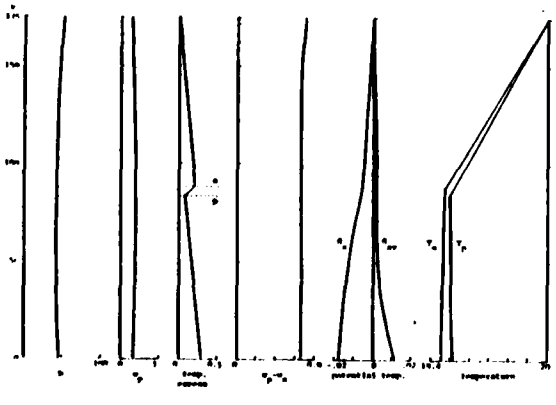

Figure 2 The same convective field as in Figure 1 but with .0002 kg/m$^3$ liquid water content at the top boundary. The discontinuous layer on the temperature excess curve shows the cloud bases. The cloud base in the plumes is about 4.6 m lower than that in the surroundings. The cloud base lowering speed is 0.11 m/min. in the plumes and 0.12 m/min. in the surroundings.

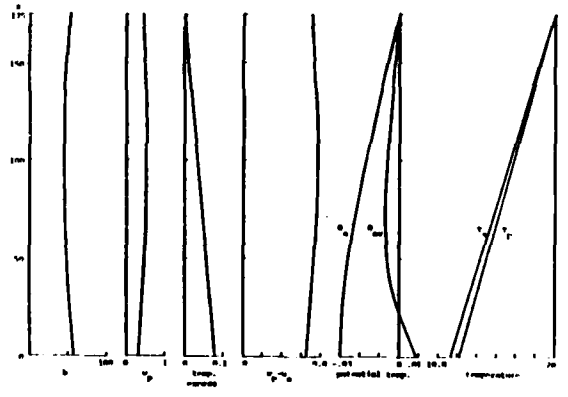

Figure 3 The same convective field as in Figure 1 but with .0004 kg/m$^3$ liquid water content at the top boundary. The cloud bases reach the bottom of the convecting layer and a marine fog is formed.

Reprinted from Preprint Volume: Conference on Cloud Physics and Atmospheric Electricity, July 31-August 4, 1978, Issaquah, Wash. Published by The American Meteorological Society, Boston, Mass.

6.5

# DISSIPATION OF MARINE STRATUS

Peter B. Wagner and James W. Telford
Atmospheric Sciences Center Desert Research Institute
University of Nevada
Reno, Nevada

## 1. INTRODUCTION

An aircraft carrying multiple meteorological instruments was flown in fog and in stratus clouds off the northern California coast in August 1977. The purpose was to measure extensively the environment of these cloud forms especially during their formation and dissipation.

Measurements included inertial wind finding, temperature, pressure, liquid water, upward infrared radiation from the sea (surface temperature), and electrical parameters (field strength and conductivity, not discussed here). The aircraft was a twin Beechcraft operated by the National Center for Atmospheric Research (NCAR). Only the authors' electrical instruments were added to the instrumentation supplied and calibrated by NCAR.

## 2. MEASUREMENTS

One example of decaying morning fog and stratus is given where the decaying edge is essentially stationary geographically in winds on the order of 10 m sec$^{-1}$ at cloud height. This stratus layer originated in fog formed upwind earlier and which lifted somewhat with advancing time. The stratus grew thinner towards its edge and terminated in organized rows of cloud form as sketched in Figure 1.

This obviously periodic structure is more organized than is usually observed at the decaying stratus edge. Generally there is well defined boundary at this edge marked by a thinner region, terminated in either scattered or banded thin clouds drifting away from the thicker cloud body and dissipating. The present case of highly organized bands were observed while flying at 600 m over a stratus layer which had tops at 200 to 300 m. A clear-air descent was made over them adjacent to the banded region. Figure 2 is a plot of temperatures, dew point and winds from this sounding. The straight line is the lapse rate of -5.1 C km$^{-1}$, a rate which is appropriate under these conditions (at 1000mb, 12C) for saturated wet adiabatic ascent. Figure 3 shows potential temperature and vapor mixing ratio. There the straight line is the same fixed saturated lapse rate as in Figure 2, converted to potential form along with the temperature. In both Figures 2 and 3, the plotted winds are the same. The wind is represented in two ways: first as a graph of magnitude versus height, and second as vectors in the direction of airflow.

In Figure 4 a second sounding made later and somewhat closer to the cloud is presented. It shows that the vertical structure remained nearly constant with only a slight lowering of the inversion.

In Figure 5 another sounding was made 20 Km to the east, somewhat south of a true upwind position of the last sounding, showing slightly wetter air with similar temperature profiles up to the inversion as in in Figures 1 and 2, but with a much lower inversion level. This sounding was made through cloud or fog below the inversion and upwards into clear overlying air.

Of special interest for the following discussion is the Figure 6. This is obtained by flight through the periodic cloud form essentially from east to west, from clear air towards a region of substantial stratus and fog. Penetration of the banded cloud forms moving towards the fog at about 215 m. The obvious periodic structure is displayed in nearly all measured parameters in Figure 6.

The next section discusses the way the unusual features of these observations probably came about.

## 3. DISCUSSION OF RESULTS

These measurements tend to support a consistent picture of the mechanisms controlling the dissipation of the stratus clouds over the Pacific Ocean in the area described above. Care must be taken in interpreting the data because temperature differences of one tenth of a degree and velocities of less than one meter per second can be extremely important. The instrumental accuracy is not adequate for absolute comparisons. Two thermometers differ by up to 0.5C. The dew point instrument appears to have a similar accuracy since it sometimes exceeds the actual temperature by about this order, and the sea surface temperature measured by the radiometer presents similar anomolies. The air motion measurement error may also exceed 1 m sec$^{-1}$ although this is about its expected R.M.S. accuracy. Thus we cannot be sure there is no surface counter-wind flow when we measured a near surface flow of less than 1 m sec$^{-1}$.

However, by carefully considering the data as a whole, and making deductions based on relative differences and equating wet bulb and dry bulb temperatures when in cloud, we are able

to draw a consistent picture of what is happening.

In general the picture we find is that the stratus cloud begins upstream of our measurement area. The sea surface is about 12C both beneath the cloud where it was down to the surface and in the clear air well beyond the cloud edge. Also from these soundings our surface air temperature under the cloud was 12.6C and in the clear air about 13.4C. Thus we conclude that dissipation is associated with a cooler sea surface temperature, which will preclude of course any addition of heat and moisture by convection from the surface.

Let us refer to Figure 3. On this diagram it can be seen that we have plotted a wet adiabatic lapse rate next to the potential temperature profile. The potential temperature gradient tends to average about the same as the wet bulb potential temperature gradient, and this raisesthe question as to why this occurs. The sounding is in clear air so any stirring in the vertical would establish a constant potential temperature. The likely explanation is that the proximity of the stratus cloud layer a few kilometers away establishes a vertical pressure gradient associated with its own cloud density, and that this pressure distribution consequently generates horizontal pressure gradients which encourage air from near the cloud top so flow out over the colder air at the surface beyond the stratus edge.

The wind vectors in Figure 3 are at about 30° to the right of the normal to the cloud edge. In Figure 3 the north direction for wind vectors has been rotated so north is towards the left, and the wind vectors show the direction of air travel. Thus the wind flows away from the fog at near cloud top level much more rapidly than near the surface, with a much reduced wind in almost the same direction above the inversion. This wind structure is unusual, as is also the mixing ratio maximum just below the inversion. The usual soundings taken in other circumstances tend to show a slow decrease in mixing ratio up to the inversion with a rapid fall off above it, and a continuing increase in wind speed with a rapid increase above the inversion.

Thus the explanation for Figure 3 is as follows; the density induced flow of the higher level cloud out across the cloud edge, over the clear air, is accompanied by mixing in of dry potentially warmer air from above which evaporates the cloud and warms the air. This action is promoted by the convective instability induced by the evaporation, which produces instability down towards cloud base. This air is stable in the clear air below cloud base, since it is then potentially warmer, being a mixture of surface air and air from above the inversion. This action leaves clear air potentially warmer than the surface air under the cloud as it moves outwards.

Now the increase of mixing ratio with height in Figure 3 can only be produced by adding colder moist air to the mixture and this can only come from air which has been in long contact with the cooler sea mixing upwards to cool it. This

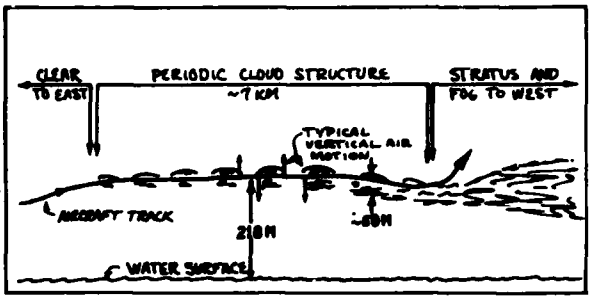


Figure 1. This sketch shows with exaggerated height scale the flight trajectory through banded clouds downwind from a low marine stratus layer.

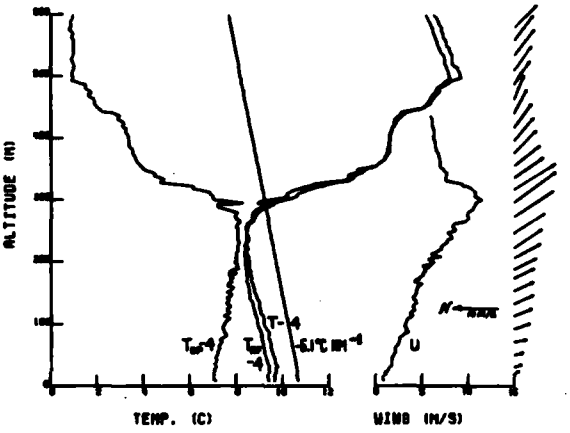


Figure 2. This sounding showing temperature, dew point and winds was made just prior to the the flight track shown in Figure 1. The straight has slope -5.1C/km, the approximate saturated adiabatic lapse rate for conditions below the inversion (specifically 1000 mb and 12C).

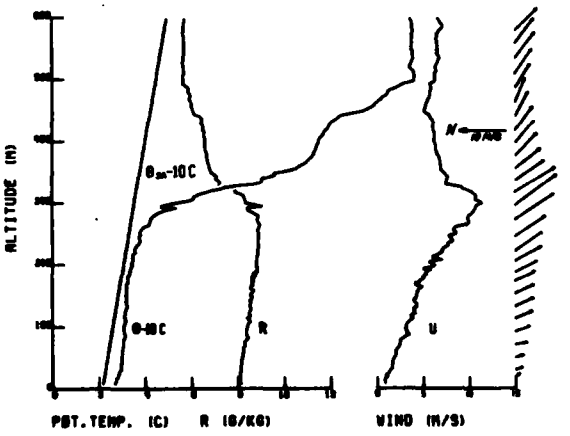


Figure 3. The temperatures in Figure 2 are transformed here to potential form. Winds in Figures 2 and 3 are duplicated.

will reduce both the mixing ratio and the temperature of the air originating from within the fog and then diluted by mixing with a component of overlying air.

To maintain this condition as a steady state would require a continuing supply of cooler air saturated at the cooler sea surface temperature downwind and would have to be both cooler and drier than the air which presumably is initially saturated by a warmer water surface somewhat further upwind. If there is no reversed flow at the surface the cooler and drier air below the evaporated cloud flow will slowly be taken away in cooling the overflowing air and so removed. However since our measurements do not map out a time sequence for the process the phenomenon may be short enough in duration that the cooling seen in Figure 6 (discussed below) as the air flows away from the cloud, cannot be maintained to continue over a long period of time.

Figure 4 is another sounding taken in the same area and the same temperature structure, and moisture structure persists. Figure 5 was obtained in cloud and shows an almost constant mixing ratio with height even when about 0.3 gm/kgm liquid water content is allowed for.

We have argued that the only way the cloud can evaporate is by the entrainment of warm dry air from above the capping inversion and that the density established in the cloud produces a rapid outflow near cloud top which advects this warmer evaporated cloud mixture over the adjacent air downstream.

If we now look at Figure 6, it supports the presence of mixing of potentally warmer overlying air into the stratus. It is also of interest as an example of roll clouds stretched parallel to the edge of low stratus.

The aircraft track (also shown in Figure 1) was chosen to pass through the banded clouds normal to their long dimension at about their middle altitude. The aircraft rose to meet the first visible cloud noted by the event mark at 2.5 Km (Figure 6). The aircraft then flew essentially level until penetrating the slopping inversion at 10 Km, and thereafter it descended.

Figure 6 shows the cloud bands on this track by their liquid water profile. The accompanying vertical velocity profile shows updraft on the upwind side of the cloudy air (to the right in Figure 6) and downdrafts on the downwind side of the cloudy air.

Explanation of these vertical motions is aided by the temperature and dew point graphs and the realization that the liquid water content of the cloudy air is inconsistent with condensation due to lifting over their rather shallow depth. Air with a lifting condensation level at the cloud base could not release sufficient water to match that measured. Therefore these bands must have originated from the upstream stratus cloud,being air parcels previously forming the main bank of cloud until they mixed as they were carried downstream. The whole field of roll clouds was nearly dissipated about ten minutes after we observed them.

Since there was vertical motion within the cloud as well as in the clear intervening areas, rotation within the cloud in the direction of the overlying wind direction and a counter-rotation in the clear areas is possible. Thus the cloud liquid water would be conserved during rotation and be evaporated due to mixing only at its boundaries. The clear areas between the clouds exhibit increased temperature and dewpoint (though not saturated). This implies that warmer air from above must be mixing down into these regions.

The wavelike visual appearance of these clouds suggest wave-action to be accompanying the suggested rotation. Such a wave would have to exist in the overlying inversion, however, but it cannot be producing the clouds by an action similar to mountain waves, since this could not release enough liquid water in the height available. Most likely the vertical motion at the flight level is being produced by vertical instability due to cooling caused by mixing and evaporation in cloudy air in conjunction with horizontal momentum entrained from the wind shear.

## 4. CONCLUSIONS

The dissipation of fog is probably related to radiative heating to some extent and radiative cooling is likely to be important in fog and stratus formation. However the mixing of drier overlying air down through the inversion is a substantial mechanism which these observations appear to show is actually playing an important role.

The data shows that the mixing downwards is much more active when cloud is present than when mixing occurs down into clear air. Thus the mechanical energy released when parcels of cloud evaporate and are cooled can help overcome the high stability which the potential temperature shows to be present at the inversion.

## 5. ACKNOWLEDGEMENTS

This work was supported by the NCAR Research Flight Facility and the cooperation of Clay(Pete) Orum as the project pilot is especially appreciated. The research reported here was funded by the Office of Naval Research.

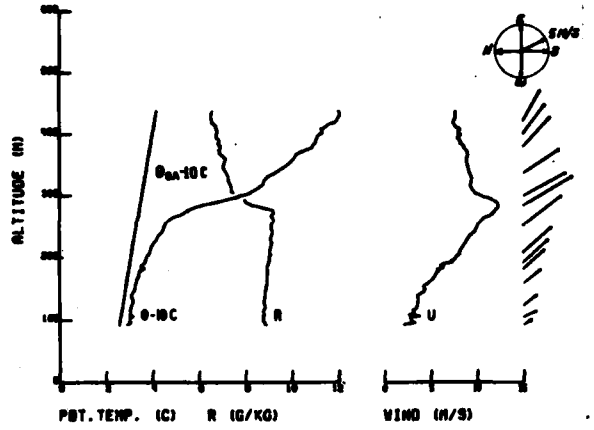


Figure 4. A second sounding in clear air, made after that in Figure 1, shows and somewhat closer to the stratus clouds, shows similar winds and temperature profiles but a lower inversion.

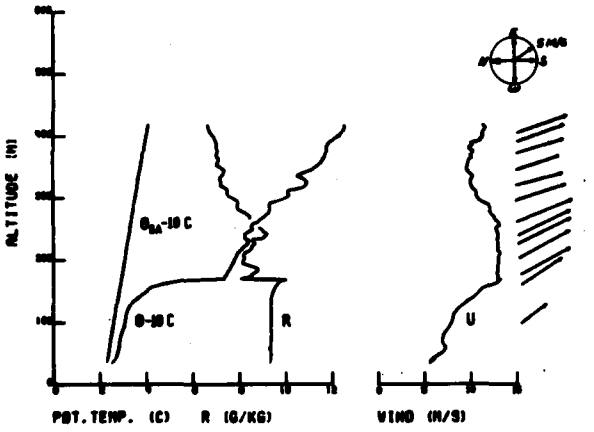


Figure 5. The last sounding was taken 30 minutes after the first sounding in stratus somewhat south of a true upwind position from the earlier work. Marked lowering of the inversion is noted along with increased winds aloft, a trend begun much earlier in the day.

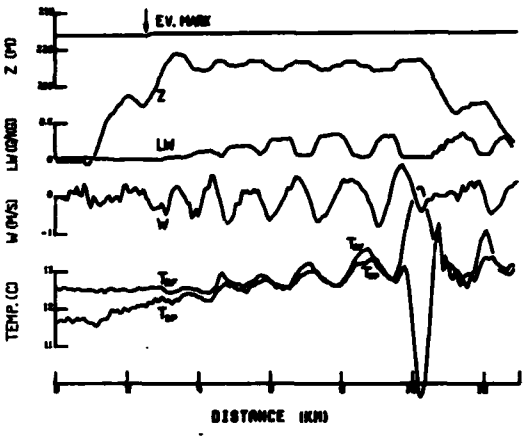


Figure 6. This plot shows parameters measured during a traverse of a group of banded clouds as a function of horizontal distance travelled. From the top down, the parameters are; an event mark on which a level change indicates penetration of the first visible cloud; altitude Z is the flight level; LW is the liquid water which clearly marks the cloudy regions; vertical air motion W correlates with LW, the liquid water, and temperatures as discussed in the text; $T_{rf}$ is temperature as measured by a "reverse flow" thermometer and corrected for air speed; $T_{db}$ is the dewpoint temperature.

# The Airborne Atmospheric Electricity and Fog Dissipation Program

# THE AIRBORNE ATMOSPHERIC ELECTRICITY AND FOG DISSIPATION PROGRAM

Desert Research Institute

P.B. Wagner and J.W. Telford

## Section I

The original objective of this program was to investigate fog from the point of view of relating electrical effects to fog stability, and, likely, to prediction or dissipation techniques. As the program developed it became clear that there were no sufficiently distinct changes anywhere in the fields, such as at its edge, to enable a program to focus on strong electrical effects in one small region, which might possibly exert a large influence. Thus, the problem became one of relating the electric fields to other phenomenon active within the fog. In the last two years, we were able to obtain aircraft support from the National Center for Atmospheric Research with an aircraft able to measure liquid water content and air motion. This combination let us attack the problem of entrainment through the fog top, convection within the fog, and determine how this continual renewal of the upper fog surface could be related to electric fields.

## Section II

(a) This work has resulted in reliable and sophisticated electrical field measuring equipment which works well in fog and rain. (We are the inventors on four Navy patents on this device). A reliable conductivity cell has been developed. The field measurements have shown that the electric field tends to be carried down stream of the fog in the

overlying shear layer, and this may be of importance in detecting the onset of fog.

In addition, we have a clear case where the edge of the fog could be shown to be evaporating by the mixing in of dry overlying air. There is a large collection of data which we believe is worth further study.

Wagner, P.B. and J.W. Telford, 1974. A new electric field mill for aircraft use. Second Annual Conf. on Marine Fog. Naval Postgraduate School, Monterey, CA. Jan. 8-9.

Wagner, P.B. and J.W.Telford, 1974: Airborne measurements of electric charging of marine fog. Proceedings, Fifth Int. Conf. on Atmos. Electricity. Garmisch-Partenkirchen, W. Germany, Sept. 2-7.

Wagner, P.B. and J.W.Telford, 1975: Natural marine fog charging. Third Annual Conf. on the Physics of Marine Fogs, Naval electronics Laboratory Center, San Diego, CA, Jan. 7-8.

Wagner, P.B., 1976 Measurements of charge in marine fog. Fourth Annual Marine Fog Program Review. Reno, NV. Jan. 6-7.

Wagner, P.B. and J.W. Telford, 1978: Dissipation of marine stratus. Preprints, AMS Conf. on Cloud Physics and Atmospheric Electricity, Issaquah, Wash., July 31-Aug.4.

Wagner, P.B. and J.W. Telford, 1977: The electric and velocity fields near and within the tops of fog layers of the west coast. Fifth Annual Marine Fog Progress Review, Buffalo, NY, April 5-7.

(b) This work has contributed to the understanding of fog formation and dissipation in the following way:

(1) It has stimulated concurrent theoretical work under ONR funding which indicates that there are strong reasons for believing that fog onset may be related to the air passing over a minimum in sea surface temperature so that convection over an increasing sea surface

temperature initiates fog.

(2) It has similarly resulted in the conviction that radiative cooling of the fog top plays a crucial role in fog consolidation and maintenance.

(3) It has shown directly that the most important factor in fog dissipation is entrainment of dry air from above.

In this regard it has shown that counter flows induced by the vertical pressure gradients in the fog relative to the clear air, induce counterflows under the dissipating fog edge, which must greatly modify fog processes once the fog begins to dissipate.

(5) It has given evidence that electrical effects can and need to be further studied in relation to the above phenomenon, as means of verifying them and using electric fields to estimate the state of the fog in its cycle between formation and dissipation.

(6) It has stimulated theoretical studies related to the surface boundary layer over the ocean, which is necessary in explaining the water input into the fog.

(7) It has shown how the results of entrainment in modifying the condensation drop sized spectrum in cumulus clouds should be applied to marine stratus and fogs. This gives larger drops as the air recycles.

Section III

Theoretical studies are sponsored by ONR to model the convective overturning of the fog, and we are now studying the way entrainment modifies the droplet spectrum.

Theoretical work sponsored by ONR is now addressing the coupling between the surface layers of the ocean and the surface boundary layer in the air.

A substantial n. nsored program is underway to study sea stratus from the drop size and radiation characteristics as related to albedo and climate. Since fog is often lowered stratus, there is a lot of this data which could be related to fog. Our aircraft has up and down, clear and infra red radiometers, a radiometer seasurface temperature, liquid water, three axis air motion, temperature, etc. measurements at 5 samples per second. This program could relate fog onset with sea surface temperature, for example, if additional support was available. Related papers from work under other funding include.


Chai, S.K. and J.W. Telford, 1976: Model of Convective Fog. Presented at Fourth Annual Marine Fog Investigation Program Review, January 6-7, Reno, NV.

Chai, Steven and J.W. Telford, 1977: The Lowering of the Cloud Base in the Convective Flow Over Increasing Sea Surface Temperature. Proceedings, Fifth Annual Marine Fog Investigation Program Review Meeting, Buffalo, NY, April 5-6, 1977.

Chai, S.K. and J.W. Telford, 1978: On the Formation of Convective Marine Fog. Preprints of the Conference on Cloud Physics and Atmospheric Electricity, July 31-Aug. 4, 1978, Issaquah, WA.

Telford, J.W. and P.B. Wagner, 1979: Electric Charge Separation in Severe Storms. Pure Appl. Geophys., In Press.

Telford, J.W., 1975: The Effects of Compressibility and Dissipation Heating on Boundary Layer Plumes. J. Atmos. Sci., 32, 108-115.

Telford, J.W., 1975: Turbulence, Entrainment and Mixing in Cloud Dynamics. Pure Appl. Geophys., 113, 1067-1084.

Telford, J.W., 1977: Dry Air Entrainment into Convective Clouds. NASA Conference Publication 2029. Third National Aeronautics and Space Administration Weather and Climate Program Science Review held November 29-30, 1977 at NASA Goddard Space Flight Center, Greenbelt, Maryland. P. 1-5.

Telford, J.W. and J.D. Presley, 1979: The Surface Boundary Layer as a Part of the Overlying Convective Layer. Pure Appl. Geophys., 117, 664-689.

Telford, J.W. and S.K. Chai, 1979: A New Aspect of Condensation Theory. Pure Appl. Geophys, In Press.

Telford, J.W. and P.B. Wagner, 1979: The dynamical and liquid water

structure of the small cumulus as determined from its environment. Pure Appl. Geophys., In Press.

Section IV

The current objectives are related to the role of sea surface temperature and radiative cooling of fog tops. These measurements could be obtained from additional work added to the NSF Sea Stratus program with benefits related to NSF funded equipment and background support. In particular, the NSF study of entrainment and drop sizes will support a NAVAIR fog program.

These objectives would test, expand and develop our present conclusions to the point where they could be used as operational tools. With additional funding, lidar (or other techniques) wave height profiling would be very valuable in relating our work to sea state. As operational use is approached, the coupling to satellite data would seem to be necessary.

Pageoph, Vol. 117 (1979), Birkhäuser Verlag, Basel



# Electric Charge Separation in Severe Storms

By J. W. TELFORD and P. B. WAGNER[1])

*Abstract* – This paper proposes a new model for thunderstorm electric field generation which directly utilizes the dynamic turbulent motion to separate the charges. Postulating a microphysical charge separation mechanism, such as is commonly accepted in most other theories, and which places a negative charge on the larger particles with a positive charge on the smaller ones, it is described how evaporation and cooling at the tops of small cumuli will release the positive charges as ions. These ions migrate to the surrounding cloud as the cooled parcel, with negatively charged particles in it, sinks down through the cloud. Since the sinking parcel contains mostly ice, it will be more buoyant than its surroundings when it reaches rising regions of water cloud, and hence should come to rest near the −10°C level. Thus the cloud will acquire an accumulation of negative charge at about this level before substantial hydrometeors begin falling out of it.

**Key words:** Thunderstorm; Cloud electricity; Clouds – electric charge separation in.

## *1. Introduction*

Because the lightning and thunder are so easily observable by any scientist on the ground, many have been stimulated to speculate as to the mechanism. Simple and apparently relevant laboratory experiments at the microphysical level are also fairly easy to perform and so most explanations advanced have tended to concentrate on these aspects of charge separation. Models involving very idealized dynamic circulation have also received a lot of attention in recent years.

However, the process of electrical charging of a thundercloud is still not well understood despite nearly a century of inspection and theories. Numerous theories of cloud and precipitation charging have been proposed, laboratory tested, and apparently can contribute to the charging process. However, applying laboratory test results to real clouds has been difficult and in some cases misleading. Direct measurements of this process are handicapped by the immense size and violence of the thundercloud compared to most other cloud forms. Some measure of success has been obtained in numerical modelling of the charge separation zone of thunderclouds (ILLINGWORTH and LATHAM, 1977; ZIV and LEVIN, 1974; SCOTT and LEVIN, 1975).

[1]) Atmospheric Sciences Center, Desert Research Institute, University of Nevada System, Reno, Nevada 89507, USA.

These models incorporate varying degrees of realism in both geometry and microphysical processes, and have produced some promising though partially contradictory results involving the precipitation and cloud particles in explaining the charging process. Recent work on the dynamics of small cumulus clouds have shown that their life cycle is dominated by turbulent mixing with overlying dry air (TELFORD, 1975, TELFORD and WAGNER, 1976).

This paper describes how this mixing process can also carry opposite electrical charges in opposite directions. Furthermore it also explains how the negative charge may accumulate within the thundercloud at the $-10°C$ level, as has been observed.

This new approach depends upon the developing theory of turbulent mixing and transport. Hence, the theory as presented here is in qualitative physical form rather than being a fully mathematical description. Nevertheless, it is clear that the mechanisms will work and are consistent with observations.

## 2. *Charge separation theories*

Recently models have been employed to test various precipitation charge transport theories. The most recently reported model (ILLINGWORTH and LATHAM, 1977) incorporates ice–ice collision mechanisms to achieve theoretical breakdown field strengths. As the authors state, it is primarily a qualitative approach based on numerical estimates of various processes. However, opposing or dissipating mechanisms have not been fully included, despite model times which appear to be a little too long. These results rely on heavy rainfall extending below cloud base, and apparently lead to considerable negative space charge below the cloud before the lightning can occur.

It has been repeatedly observed that the initial discharge center commonly occurs at the $-10°C$ level, well up into the typical thundercloud (ILLINGWORTH, 1978). This observation has physical significance in discriminating between mechanisms of charge transport.

In review of past literature, such as the recent survey articles of MOORE (1974) (and subsequent debate: MASON (1976) and MOORE (1976)) or ILLINGWORTH (1978), there appears general acceptance that thunderstorm charging is dependent upon, or at least accompanies, precipitation formation. The storm appears usually to utilize ice or the freezing process, where it exists, as an integral part of the process. The early radar observations by WORKMAN and REYNOLDS (1949) still seem to provide an adequate general picture of the single-cell thunderstorm with precipitation echoes on radar also beginning at the $-10°C$ level. However, we must keep in mind the observed lightning in warm clouds (e.g. MOORE, *et al.* 1960), and charge separation which is observed in other non-lightning clouds and reported by ANDREEVA and EVTEEV (1974) and IMYANITOV, *et al.* (1972). In warm clouds the charge separation is often more than an order of magnitude greater than could be expected from charge accumulation in the fair weather field acting on the reduced in-cloud conductivity alone.

Thus, a complete charge transport theory must be suitable for a wide range of clouds, warm and cold, with wide variations of convection, the thunderstorm being the extreme case, and lightning the ultimate indicator of effective electrical charge separation. It is clear from the following discussion that the mechanism also must be effective during the 'growing' stages of thunderstorms, prior to lightning or visible precipitation below the cloud.

### *3. Electrical activity preliminary to a thunderstorm*

As pointed out by MOORE (1974), rain and sudden enhancement of the radar reflection follows the initial lightning stroke. Moore also noted at the time that measurements of charge on precipitation particles at cloud base showed small charges which tended to reduce the thunderstorm charge. Subsequent measurements of precipitation charge near cloud base (GASKELL, *et al.*, 1978) obtained significant charges of both signs, though predominantly negative.

Strong correlation is seen between intensity of convection as judged from cloud type and degree of electrification, as reported by IMYANITOV, *et al.* (1972).

It has been shown long ago that growing thunderstorms transport considerable low-level momentum upward through the growing stage and maintain on the average a shear less than their environment. BYERS and BRAHAM (1949) indicate a maximum mixing of environmental air, or entrainment, of 100% per 500 mb in order to maintain growth.

In studies of cloud dynamics TELFORD and WAGNER (1974) show cumulus clouds vigorously growing at one edge and randomly decaying elsewhere after mixing with overlying dry air. Although the small cumulus is a poor model for latter stages of thunderstorm development, it is reasonable to expect similar mixing at the top of the clouds as turrets rise up into the clear overlying air.

Finally, electric field, temperature and aircraft acceleration measurements by IMYANITOV, *et al.* (1972), indicate average zones of inhomogeneity on the order of 100 m within the cloud at this stage. It is significant that the size of the electrical inhomogeneity is smallest in growing cumulo-nimbus and increases with advancing stages of the storm. This indicates that the best vertical mixing in the flow exists at times when the initial separation of charge is proceeding rapidly before the first lightning strike.

In summary, effective convective charge transport theories must cope with the results of convective turbulence and its inhomogeneities. With this in view, such theories usually fail to consider the action of this continual mixing on their proposed charge separation mechanism, which also results in the inhomogeneities as observed by Imyanitov. Thus we must describe how positive charges rise or negative charges descend, or both, if we are to form some approximation to the observed classical Wilson dipole charge structure seen prior to lightning activity.

### 4. *Discussion of theory*

We have discussed observational data and some of the theories of thunderstorm electrification, and they seem to fall short of providing an adequately energetic means of separating the charges over the depth of the cloud. While it is perfectly clear that to allow a mechanism for thunderstorm electrification to be possible, we must first separate charge on a micro-scale, this is insufficient to produce large-scale separation, and gravitational fall separation previously invoked appears inadequate. Furthermore, the thunderstorm is known for its turbulence as much as for its thunder. Updrafts and downdrafts continually compete in its interior, making aircraft penetration hazardous. It is difficult to see conceptually how, in these conditions, the steady downpouring of negatively charged particles needed in most theories can act consistently enough to produce the prodigious charge separation observed.

Furthermore in gravity settling theories there is the problem of preventing neutralization of larger-particle charges once they are obtained. In the course of growth by accreting a large number of cloud particles of predominately neutral or opposite charge, significant net charge must be lost by neutralization. Of course the induction or other charging by inter-particle collisions may dominate accretion but this is little more than another uncertainty.

We should stress however that the mechanism proposed here does not specifically attempt to invalidate gravitational settling in each air parcel, which, when the theories are quantitatively evaluated, may prove to be a complimentary process in the bulk charge separation budget. However, gravitational separation carries on whether the turbulence is upward or downward in velocity, or repeatedly turning over the air parcels. The common view, often implicitly built into models, is that almost every upward motion observed is part of an updraft with a life time comparable to the cloud life, but this is simply not true. Except on the growing edge, or in the echo-free vault, we must expect that updrafts become downdrafts soon after they are found, and vice versa; they are part of the turbulence induced by the descending air currents and are not in any sense sustained steady-state flows persisting for long periods. All turbulent motion includes rotation, and when an air parcel is turned over, the gravitational separation processes reverse. The same reversal of charge separation applies to turning over when low level cloud is carried up toward cloud top again.

This continual mixing process is occurring in all turbulent clouds, but seems to be omitted from most gravitational charge separation theories. All of the mixing cloud is unstable since a parcel experiences the same externally derived vertical pressure gradients as is experienced by the initial growth (at least for the early stages of the cloud growth) and hence nothing can ever come finally to rest until the cloud totally evaporates. The fact that this turbulent motion can become a source of eddy charge flux, rather than providing only a remixing process, is considered below as the charge separation mechanism.

The alternate explanation for charge separation now proposed here appears to be

more effective, since the process does not depend on balanced rates of accretion relative to induction charging and separation relative to turbulent mixing. Convective transport of parcels 100 m or more across can convey differently charged air parcels past each other with reduced opportunity for charge neutralization compared to that for negative particles falling through rising positive clouds. Thus this alternative process could not only transport more (by reduced neutralization) negative charge on particles to lower cloud levels but it would speed up the charge separation by transporting bulk charges at speeds exceeding 1 or 2 m/s. In addition it may enhance accretion between negatively charged particles of the same sign thereby increasing the range of negative charge on the individual emerging precipitation particles. This is potentially an explanation for the existence of the occasional exceptionally high drop charges observed by GASKELL, *et al.* (1978).

Finally, the electrical noise characteristics of the storm need to be considered. The pulsed noise mentioned above at low frequencies is unexplained by current theories but appears to originate within the cloud. In the theory presented here it may arise from discharges between oppositely charged air parcels as they are turbulently mixed in the growing thunderstorm. In general, proliferation of thunderstorm theories makes it clear that some feature is probably missing from all of the previous theories.

Much of the energy released in a thunderstorm is located in its irregular turbulent motion, and it would seem that unless a theory is based intimately on coupling to this apparently random process it will have difficulties. We propose such a theory in this paper.

## *5. The present theory*

Let us postulate that we have one of the microphysical mechanisms for charge separation in action in the cloud so we have, say, a population of frozen water drops carrying negative charges with a similar positive charge on a population of much smaller ice splinters, all mixed in together. Any other mechanism which generates a negative charge predominantly on the larger particles with the complementary positive charge on smaller particles, will act similarly.

Now, recent work (TELFORD, 1975; WAGNER and TELFORD, 1976; TELFORD and WAGNER, 1976) has shown beyond much doubt that most of the dry air mixed into a small cumulus cloud comes from above cloud tops. Consider what happens when we add dry air to a cloud of frozen drops, or other larger ice particles, and splinters. The sudden reduction in vapor mixing ratio will begin rapid evaporation of the ice. The small splinters will evaporate first and although the equilibrium state, after the mixing is complete, depends on the details of the mixing operation, we can be sure that many splinters will evaporate leaving their charge as positive ions in the air, while the negative charge remains attached to the larger particles. This air parcel is also considerably chilled by the latent heat used in evaporating the ice splinters and hence is much denser than the surroundings, and so it begins to sink down throught the cloud beneath.

The question of the evaporation of the splinters to ions is worth some comment. It seems possible that the ions resulting from the evaporation of charged ice splinters may be quite mobile. This has two possible causes, firstly the charge concentration due to size reduction and secondly the reduction in the size of the remaining salt particles by the process itself.

The splinters are likely to have grown by some freezing process and hence will not usually contain solid bits of original condensation nuclei. The small fraction of the soluble salt from the condensation nuclei in the drop from which the splinter originated will probably be concentrated in the freezing splinter tip, in front of the advancing ice–water interface as the splinters freeze (zone refining mechanism). Thus, as such a splinter evaporates, the surface field will rise until the charge leaves the particle, either as an intermediate ion, likely formed on a fragment of dry solute, or perhaps as a small ion similar to those found in a nuclear physics expansion chamber.

The fragments of solute leaving an evaporating splinter are not likely to be as large as those remaining from an evaporating water drop, of equal volume, since there can be no solute movement within or on the ice particle. One might imagine a tenuous layer of solute powder left on the ice surface. Thus, the ions formed from the evaporation of the ice splinters are likely to have substantial mobilities, both because of a higher than usual charge after concentration by evaporation, and because of smaller salt carriers than those which usually make up the largest ions.

We should remember, however, that a water drop induction mechanism could result in a similar concentration of positive charge on small evaporated droplets. These might not be as mobile as those left from evaporating ice splinters, and so lead to a less efficient, but still viable mechanism. Hence electrification of warm clouds may proceed to some degree by the mechanism described in this paper.

At the cloud top, we initially have electrical conditions approaching a fair-weather field, since the cloud surface is continually overturning and so cannot develop a charged sheath. Thus the ions in the air will migrate downwards and out of the partly evaporated mixed parcel into the normal cloud beneath; thus leaving a negatively charged region of air, perhaps a hundred meters or so across, with the negative charge still immobilized on the remaining larger cloud particles as when they were first separated. Any additional mixing through the cloud sides will act in a similar way, also incorporating, as indicated by VONNEGUT (1955), any sheath charge into the cloud interior.

As this cooler, drier region sinks downwards through the bulk of the cloud, largely uncharged cloudy air will slowly mix in with it, so partially restoring its mixing ratio and warming it. In small cumuli, this sinking process stops at a certain level lower in the cloud (TELFORD, 1975, TELFORD and WAGNER, 1976), because the mixture comes into hydrostatic equilibrium with the surrounding air. This process is illustrated in Fig. 1. The thunderstorm also probably has an equilibrium level attainable by each mixture, but because of the horizontal accelerations, this may not be completely determined by the surrounding air density and may change through the cloud cycle.

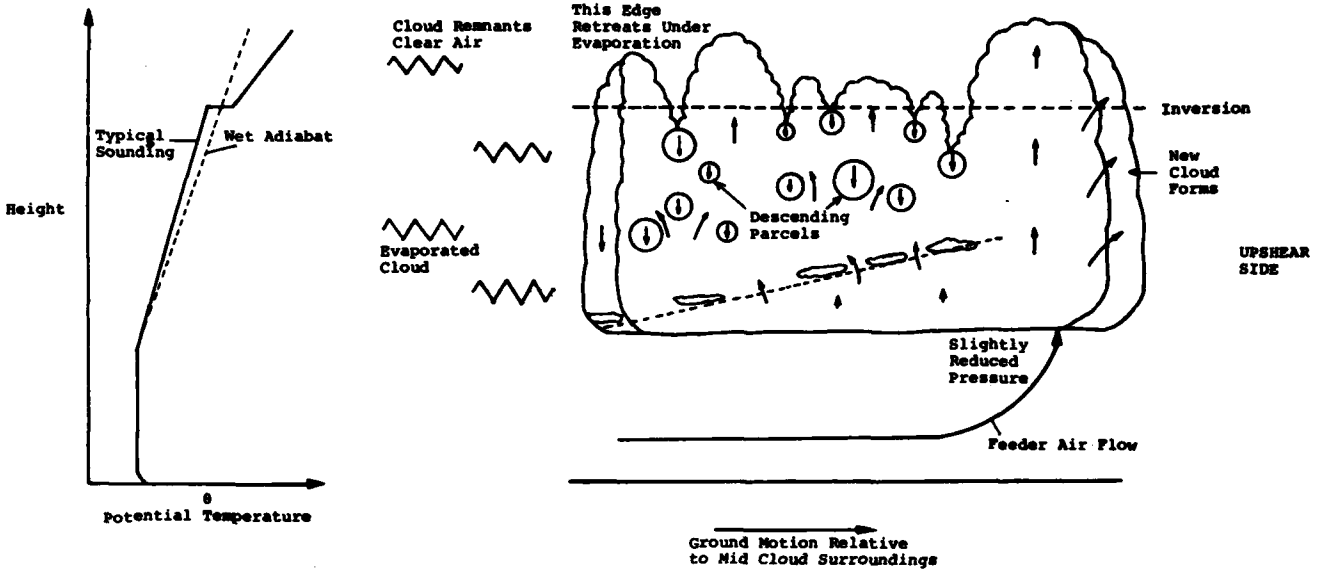


Figure 1

This diagram is a simple conceptual two-dimensional presentation of the motion of the air associated with a small cumulus. The feeder air flows beneath the cloud and rises on the upshear side, as the cloud drifts downshear, which is downwind when the air motion has a constant direction and increasing velocity magnitude with height. The new growth is largely adiabatically expanded unmixed air, and the mixing from the top down starts near this edge and mixes deeper into the cloud as time passes, until, on reaching cloud base on the downshear side, the whole column sinks and evaporates. Spent thermals are shown as flattened blobs resting on the sloping dashed line. The new growth is very buoyant, relative to the surroundings, and this excess buoyancy diminishes as the mixing proceeds. The buoyancy of the newly formed side of the cloud provides the pressure reduction underneath it which is necessary to accelerate the feeder air onto its upward path, and to reduce its relative horizontal velocity. Larger storms probably obey similar principles except that the pressure drop beneath the updraft is large enough to over-ride the simple shear flow and draw in air from the upshear side of the cloud as well. This illustration does not show the ice phase as described in the theory, but does depict the basic dynamics. The temperature structure in the surrounding air is also shown.

Now we have a mechanism in which the charge on the larger microphysical particles is mixed through the cloud at a rate proportional to cloud liquid water dilution in the greater part of the cloud depth below the top regions, where the small particles left their charge on ions which then migrated into the surrounding cloud particles not presently experiencing the dilution and the subsequent sinking motion.

Thus the turbulent motion can be seen to be no longer a totally random statistical phenomenon as it at first appeared, but the up and down motion is directly correlated with a net negative charge in the descending air, and with a net positive charge on the remaining rising cloud, so giving a powerful charge flux or current, directly analogous to turbulent heat fluxes, for example. This separation mechanism functions by directly tapping, for its energy source, into the density differences which give the whole mechanical energy source for the cloud.

Once charging starts, the fields acting on the ions from the charged regions in the various parcels at the top of the cloud which have been mixed in with dry air, or have just risen up, will sweep out a portion of the mobile ions into the surrounding cloud regardless of the electric field directions. The direction of charging depends only on the sign of the charge on the larger particles and the direction of gravity.

## 6. *Other considerations*

The theory we have outlined is very much in line with the picture we have recently established for small cumulus clouds, where the vertical growth is much smaller and less vigorous. In small cumulus clouds, measurements have shown the cloudy air is not moving relative to the clear air in which it is embedded, but its outline moves forward by new growth on the upshear side, followed by dissipation resulting from dilution with overlying drier air and evaporation on the downshear side.

For large cumulus clouds, from their mature stage descriptions by FRITSCH (1975) and BROWNING (1977) for example, it is fairly clear that the pressure deficit accelerates air from the downshear side (i.e. downwind side) of the cloud in the lower layers towards the cloud without waiting for the cloud to pass overhead first, before the feeder stream of air begins to rise. In all these models, there is a large bulk of cloud outside the strong updraft and it appears that it can be, in these large clouds, on either side of the updraft. This cloud is apparently much less buoyant than air in the updraft, because it would otherwise be an updraft region itself. The less buoyant cloudy air must have been diluted by mixing with drier surrounding or overlying air, as occurs in small cumuli, in order to be found where it actually is.

This lower buoyancy certainly appears to be true in downdraft areas where the weight of the precipitation cannot be the factor controlling the air density (and hence buoyancy) since it scarcely compares (i.e. 3 gm/kgm is about a 1°C temperature decrease in terms of density) with the buoyancy excess of more than 3°C or so reported (SCHMETER, 1969, Table VII.1.) for higher buoyancies, which must be associated with

undiluted cloud. The continued downdraft below cloud base is probably the result of further increase in air density due to cooling by evaporation from the precipitation particles.

It is difficult, from the mature storm studies, to deduce how the cloud builds up to begin with, but a reasonable picture is as follows.

The first cloud probably starts off as a small cumulus with vertical growth limited by mixing of drier air in between the turrets. This cloud air is partly evaporated and forms a spreading cloudy area of almost neutral buoyancy, with diluted portions sinking and the more protected areas still rising. There will also be a large region of totally evaporated cloud with a much higher mixing ratio than that in the overlying air, surrounding the cloud top. As the supply of moist air continues from below, the new turrets are protected from dilution, so that they pass through the earlier cloud until they too suffer drying and evaporation and cooling as they penetrate up through the mixed air into the drier air above. ANDERSON (1962) observed by time-lapse photography consistent 1- to 2-minute periodicity to cloud top growth rate in building thunderstorms. Although he attributed those higher frequency pulsations to 'turbulence', perhaps they are due to the somewhat more organized growth process described here.

When this growth reaches a temperature such that freezing mechanisms begin, the internal mixing resulting from the descending cooler mixed parcels will rapidly distribute ice into the rising currents so that the cloud tops are filled by particles from any ice activated charge separation mechanism. Thus, evaporation of these particles will tend to leave the negative charges in the descending or slowly rising air parcels while those regions with more ice or water continue rising.

The fresh updrafts now have so increased the total cloud buoyancy as the cloud approaches its maximum, that the updraft core beneath the cloud tends to draw across the cloud base in the down shear direction, moving across the cloud bottom as upwind air is scavenged from further and further ahead of the cloud, downwind. This follows from SCHMETER (1970) who observed such a change in position of the feeder updraft as the cloud matures.

Thus the cloud turrets continue to penetrate to greater and greater heights always spreading out over the lower levels of cloud as dilution with the drier air above reduces their buoyancy, and brings them more or less to rest. Thus, the bulk of the cloud grows layer by layer, always with cooler negatively charged regions moving down through their surroundings while the less diluted intervening cloud continues to rise and carry the positive charge with it. Thus, the cloud is formed of moist updraft air mixed with dry air at successively higher levels as the general cloud builds itself up. This dilution with air of different horizontal momentum also accounts for the fact that the intermediate levels of the cloud exhibit horizontal motion partly between that of the surface layers and that of the same level outside the cloud.

As a larger and larger depth of cloud becomes dominated by negatively charged particles and the positive charge moves higher and higher, the electrical potential rises, and eventually discharging lightning strokes begin. On this picture the fully developed

cloud will become electrically active primarily by using up stored charge since now the newly formed negatively charged regions will have to sink down through the bulk of the cloudy depth in order to transport the charges through the whole depth, a process a good deal slower than the initial action during growth of the tops of the clouds.

It is worth mentioning that since the charge which can be carried on cloud particles is proportional to their area, the theory given here is more efficient in generating charge than the theories needing larger precipitation particles for charge transport. The reason is that this theory utilizes small negatively charged particles which do not need to coagulate to larger sizes, of reduced total area, in order to fall rapidly, since they are carried to the lower cloud levels by the downdrafts.

A further question of interest is that, as the negatively charged regions sink through the cloud, there will be a substantial reversal of buoyancy resulting from stability due to a change in the surroundings at some height above the 0°C level. This stability arises from the delay in the freezing of the water drops in the rising parts of the cloud, which will be most important in regard to its effects on the descending ice cloud parcels as we will now explain.

Figure 2 is a plot of potential temperature versus altitude for air adiabatically rising and descending through a large convective cloud. The curve labeled 'updraft' is the ascending air curve which shows a cloud base below the freezing level and delayed freezing to the −10°C level. Above the −10°C level the cloud follows the ice adiabat. It is assumed for simplified presentation that all droplets freeze at this one level. At the cloud top the cloudy air is mixed with drier air and then descends along the 'downdraft' curve. For simpler presentation mixing within the cloud is ignored. When the descending air full of ice particles passes the −10°C level, it becomes positively buoyant with respect to the ascending wet air and will thus tend not to descend much below this level.

Freezing of droplets in the rising air over a band of temperatures, from −10°C to −20°C say, depending on the process in action and mixing during parcel descent, will modify this effect but not substantially alter it. Hence, the descending parcels containing ice will tend to produce a negative charge accumulation where they come to rest near the level where the temperature is somewhere from −10°C to −20°C say, as has been observed.

To reiterate, if the droplets in the rising air remain unfrozen water until reaching the −15°C level, say, as observations in clouds show could easily happen, then the descending ice-filled air, with a slight negative buoyancy at say −20°C, will find itself positively buoyant after descending until surrounded by water cloud lower down below the −15°C level. For two air parcels of similar density when frozen, the ice filled parcel will be the more buoyant one when the other parcel still contains only water particles.

Assuming that the likelihood of a cloud being totally unfrozen is initially about one half at the −15°C level and allowing for an average density comprised partly of water and partly of ice cloud, we might expect the descending parcels to come to rest a little below this height. The picture will be complicated by the fact that the descending

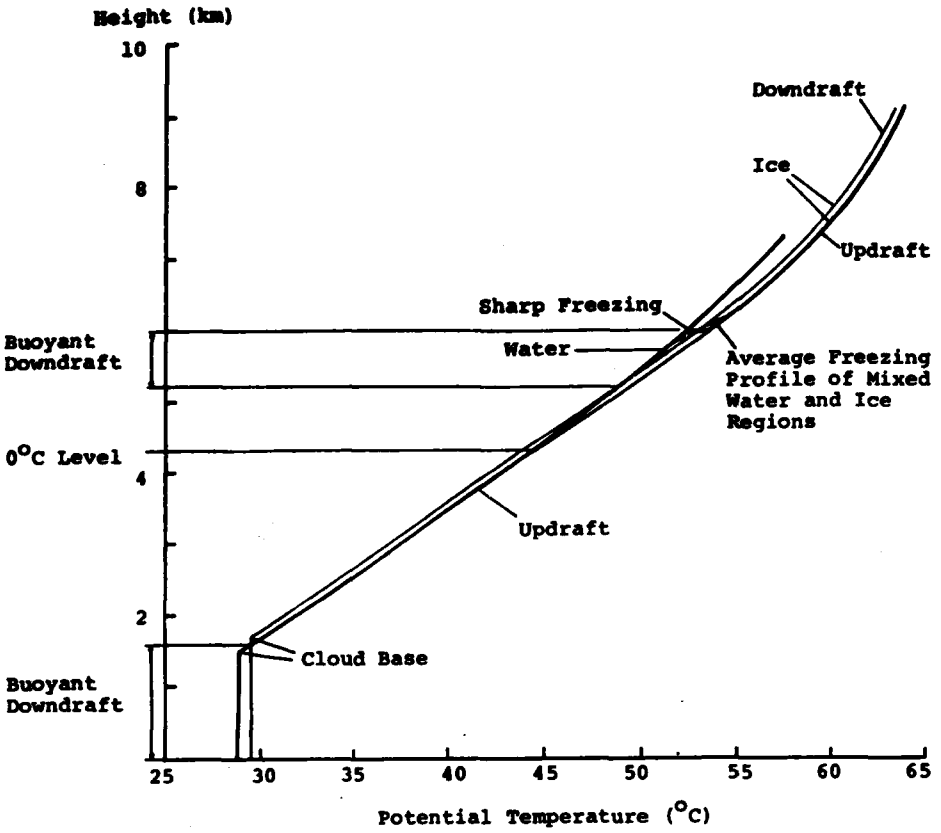


Figure 2
Adiabatic diagram for air parcels without mixing, except at top. The delayed freezing in the updraft makes the downdraft positively buoyant in this region.

parcels will seed the water cloud in the updrafts with ice, and so lower the ice level as the process continues, but it is clear that the $-10°C$ level is a reasonable first approximation.

One limitation of this theory which may be open for checking is that in order to be able to evaporate the cloudy mixture of charged particles the temperature cannot be too cold, since cold dry air will not hold much water vapor and so is not as effective in evaporating drops; and in so separating the charges, or in cooling the air. The water vapor pressure is reduced by a factor of about two for each 10°C temperature decrease. Thus, we might expect this mechanism to work more effectively when the mixing occurs at intermediate levels rather than when the storm has reached the tropopause at $-55°C$ to $-65°C$.

Thus this explanation indicates that given circumstances may produce lightning at summer temperatures but are less likely to do so at winter temperatures. Furthermore

warmer, lower based clouds, would be expected to be more electrically active than higher based cooler clouds, in the same season, since the negative buoyancy in the downdrafts is likely to be larger when the water content is larger to begin with, at a given height (low base), and the evaporation is enhanced by the entrainment of warmer or drier overlying air.

## 7. Summary

This paper discusses the role played by the entrainment of drier air into the tops of cumulus clouds in promoting charge separation. The mixing with drier air from above cumulus tops will evaporate the smaller, positively charged, particles, as well as cooling the air through the latent heat absorbed by evaporation. The positive charge will thus tend to be left on ions which can be swept out by any local field, at least to some extent. These positive charges will soon attach to the surrounding cloud which has not yet been diluted by mixing, leaving the cooler mixed region, with the remaining negatively charged particles, to sink downwards. This process creates a current of positive charge upwards and negative charge downwards.

At the lower levels, but still above the 0°C level, the negative buoyancy will be much reduced, or reversed, when the sinking parcels reach the level of rising, unfrozen, water cloud. Thus, there will be an accumulation zone at about the $-10$°C level where the sinking parcels with excess negative charge are brought to rest.

## 8. Acknowledgements

The authors would like to acknowledge the continued funding support from the Office of Naval Research, and the personal encouragement of Mr. James Hughes of that office, both of which were needed to make this paper possible.

## References

ANDERSON, C. E. (1962), *Observational evidence of kinematics of growing cumulus and thunderstorm clouds*, Trans. N.Y. Acad. Sci. *24*, 898–943.

ANDREEVA, S. I. and EVTEEV, B. F. (1974), *The potential gradient of the electric field in nimbostratus clouds*, GGO Trudy No. 277. ('Studies in atmospheric electricity') translation, U.S. Dept. of Commerce, TT.

BROWNING, K. A. (1977), *The structure and mechanisms of hailstorms* AMS Met. Mono. *16*, 1–43.

BYERS, H. R. and BRAHAM, R. R. *The Thunderstorm* (U.S. Government Printing Office, Washington, D.C. 1949).

FRITSCH, J. M. (1975), *Cumulus dynamics: local compensating subsidence and its implications for cumulus parameterization*, Pure appl. Geophys. *113*, 851–866.

GASKELL, W., ILLINGWORTH, A. J., LATHAM, J. and MOORE, C. B. (1978), *Airborne studies of electric fields and the charge and size of precipitation elements in thunderstorms*, Quart. J. roy. Met. Soc. *104*, 447–460.

ILLINGWORTH, A. (1978), *Charging up a thunderstorm*, New Scientist, *78*, 504–506.

ILLINGWORTH, A. and LATHAM, J. (1977), *Calculation of electric field growth, field structure and charge distributions in the thunderstorms*, Quart. J. roy. Met. Soc. *103*, 281–295.

IMYANITOV, I. M., CHUBARINA, YE. V. and SHVARTS, YA. M. (1972), *Electricity of clouds*, NASA Technical Translation F-718.

MASON, B. J. (1976), *In reply to a critique of precipitation theories of thunderstorm electrification by C. B. Moore*, Quart. J. roy. Met. Soc. *102*, 219–225.

MOORE, C. B., VONNEGUT, B., STAIN, B. A. and SURVILAS, H. J. (1960), *Observations of electrification and lightning in warm clouds*, J. Geophys. Res., *65*, 1907–1910.

MOORE, C. B. (1974), *An assessment of thundercloud electrification mechanisms*, Proceedings of Fifth International Conference on Atmospheric Electricity, Garmish-Partenkirchen, F.R. Germany.

MOORE, C. B. (1976): *Reply* (to B. J. MASON – see MASON (1976)), Quart. J. roy. Met. Soc. *102*, 225–238.

SCOTT, W. D. and LEVIN, Z. (1975), *A stochastic electrical model of an infinite cloud: charge generation and precipitation development*, J. Atmos. Sci. *32*, 1814–1828.

SCHMETER, S. M. (1970), *Structure of fields of meteorological elements in a cumulonimbus zone*, CAO, Trudy No. 88, translation U.S. Dept. of Commerce, TT 70-50020.

TELFORD, J. W. (1975), *Turbulence, entrainment and mixing in cloud dynamics*, Pure appl. Geophys. *113*, 1067–1084.

TELFORD, J. W. and WAGNER, P. B. (1974), *The measurement of horizontal air motion near clouds from aircraft*, J. Atmos. Sci. *31*, 2066–2080.

TELFORD, J. W. and WAGNER, P. B. (1976), *The interaction of small cumuli with their environment*, Preprints, International Conference on Cloud Physics, July 26–30, 1976, Boulder, Colo. 283–287.

WAGNER, P. B. and TELFORD, J. W. (1976), *The measurement of air motion in and near clouds*, Preprints, International Conference on Cloud Physics, Boulder, 669–672.

VONNEGUT, B. (1955), *Possible mechanism for the formulation of thunderstorm electricity*, Proc. Conf. Atmos. Elec., Geophys. Res. Papers *42*, AFCRL-TR-55-222, 169–181.

WORKMAN, E. J. and REYNOLDS, J. E. (1949), *Electrical activity as related to thunderstorm cell growth*, Bul. Am. Met. Soc. *30*, 142–144.

ZIV, A. and LEVIN, Z. (1974), *Thundercloud electrification: cloud growth and electrical development*, J. Atmos. Sci. *31*, 1652–1661.

(Received 6th November 1978)

*J. Rech. Atmos.*, 15 (1981), n° 2, pp. 97-120.

# CLOUD DYNAMICS AND AN ELECTRIC CHARGE SEPARATION MECHANISM IN CONVECTIVE CLOUDS

by

P.B. WAGNER and J.W. TELFORD
*Atmospheric Sciences Center*
*Desert Research Institute*
*University of Nevada System*
*Reno, Nevada 89506, U.S.A.*

## *RÉSUMÉ*

*On émet l'hypothèse que le mélange avec de l'air sec au sommet des nuages donne naissance à des structures thermiques descendantes dont on examine en détail les caractéristiques probables. Ces panaches d'air nuageux refroidi se forment au sommet des cumulus puis descendent à travers les nuages et réduisent la teneur en eau liquide pour produire la composition de l'air observée. En supposant que le front tranchant de ce type de panache est de nature semblable à celle des autres thermiques (ascendants ou descendants) étudiés dans l'atmosphère, on montre ensuite qu'il se produira un mécanisme de séparation des charges si la conductivité est plus élevée dans le thermique descendant.*

*La diminution du nombre de particules de nuage dans les volumes d'air formés par mélange avec l'air sec supérieur caractérise ces volumes qui, après refroidissement par évaporation, donnent naissance à des thermiques négativement instables. Une réduction importante du nombre des particules suffit à changer la conductivité si on considère les concentrations d'équilibre en ions engendrés par les rayons cosmiques. Avec des nombres de particules de quelques centaines par centimètre cube, une diminution par dix suffit à augmenter le nombre d'ions par quatre, ce qui semble convenable pour produire une séparation de charge de l'orage. La diminution nécessaire du nombre de particules est probablement causée en général par l'initiation de la phase glace, mais l'évaporation après mélange aux sommets des nuages peut également être une cause possible dans les nuages chauds. L'évaporation de poussières d'ammoniaque ou d'autres particules exotiques, telles que des gouttes d'acide sulfurique, peut opérer de la même façon dans d'autres atmosphères.*

*Une théorie approchée montre que la production de charge et de champ doit être une fonction exponentielle du temps, avec une constante de temps de l'ordre d'une ou deux minutes.*

## *ABSTRACT*

*This paper hypothesizes that the mixing of dry overlying air into clouds gives rise to descending thermal structures and discusses in detail their likely character. These plumes of cooled cloudy air form at the tops of cumulus clouds then descend through the clouds to ultimately reduce the liquid water content and produce the air composition observed. Assuming that the sharp front of such plumes is similar in character to other buoyant (buoyancy can be up or down) thermals studied in the atmosphere, it is then shown that a charge separation mechanism will operate if the conductivity is higher in the descending thermal.*

*Reduction of cloud particle counts in the air parcels formed by mixing with the drier overlying air characterizes these parcels, which having been cooled by evaporation generate the negatively buoyant thermals. A marked reduction in particle count is sufficient to give the needed conductivity changes when we consider the equilibrium concentrations of cosmic ray generated ions. With particle counts of hundreds per cubic centimeter, reduction by a factor of ten is sufficient to increase the ion count by a factor of four, which appears to be adequate to produce thunderstorm charge separation. The necessary reduction in particle count is probably usually caused by the initiation of ice formation, but evaporation after mixing, at cloud tops, may also be a possible cause in warm clouds. Evaporation of ammonia dust or other exotic particulates, such as sulphuric acid drops, could possibly also operate in this way in other atmospheres.*

*An approximate theory shows that the charge and field build up will be exponential in time, with a time constant of about a minute or two.*

## 1. — INTRODUCTION.

Recent advances have provided a new framework for understanding cloud dynamics. It is thus an appropriate time to examine how these new concepts affect the established approaches and directions of research in cloud microphysics. This paper will take a new look at the separation of electric charge in thunderstorms, and we begin with a review of the role of entrainment in clouds.

Measurements by Telford and Wagner (1974) showed how a small cumulus cloud progresses through the air by growing on the upshear (upwind, when the wind increases with height in the same direction) side, entraining dry air from above, and finally becoming so diluted that it completely evaporates on the downshear edge. These measurements showed that the cloud moves through its embedding air mass by growing and decaying in this way. The cloud is like a balloon trailing a small sea anchor ; it approaches the surface observer tail first with the wake passing overhead before the cloud itself. Thus, the « front » of the cloud is its downstream side in this sense. The well-known formation of precursor

clouds ahead of approaching clouds is an observation of new clouds forming in the wake of the main cloud, in air where there is a mixture of subcloud and above cloud air which is substantially moister than other non-cloud air at that level. This air has previously been through the cycle of cloud formation by adiabatic updraft, entrainment dilution, and evaporation.

The actual directions in which the clouds move through the air, when seen from the ground, depends, of course, on the wind shear. Reversals of these directions, from upwind to downwind (Telford and Wagner, 1974), and cloud orientation across wind (Wagner and Telford, 1976), have been reported. When aircraft samples are taken up and down the direction of wind shear (not up and down the wind direction) the undisturbed air behind the approaching cloud as viewed from the ground under the usual conditions, where the wind increases with height without changing direction, is clearly as yet unaffected by the cloud. In contrast, the air on the other side, preceeding the cloud as it drifts overhead, is very variable in potential temperature, mixing ratio, and all three components of velocity (Wagner and Telford, 1976 ; Telford and Wagner, 1980). The mixing takes some time to achieve total uniformity even after complete evaporation of the cloud particles has occurred and the direct driving force of the entrainment process has ceased to act.

This general pattern also agrees with more recent observations of much larger cumulus clouds by Bennetts *et al.* (1980) with aircraft penetrations, and Lhermitte (personal communication) with radar, who have observed evidence of a very similar pattern in clouds which developed substantial precipitation and electrical activity.

The vertical cycling of the air parcels in the cloud under the influence of entrainment of overlying air, has been shown very elegantly in a paper by Paluch (1979). There she has shown, from the composition of the air in samples taken from within large cumulus clouds, that the observed parcel is a mixture of air from below cloud base and air from the environment taken at several kilometers above where the samples were actually collected.

The conclusion is that the subcloud air flows beneath the cloud and rises up just beyond the upshear side to form new cloud columns. This new cloud is almost adiabatic in composition as sideways entrainment is relatively small in this rapid updraft region. The microphysical processes begin in this « protected core », which is the feeder flow for the whole cloud. In small or growing cumulus this updraft rise is limited by a capping inversion or stable layer. In bigger clouds the rise is stopped by dilution by the drier surrounding air near its top. As this growth is brought to rest it is superseded by the next surge of air from below cloud base, which comes up beside it, the negatively buoyant blobs resulting from the continued entrainment at its top then begin their next phase of diluting the column as it matures through its microphysical cycle. The Bennetts *et al.* and Lhermitte observations lend weight to this picture by showing the observed location of electrical and precipitation activity more towards the down shear side. Mossop also reports (private communication) a similar disposition of the ice structure in his small cumulus cloud observations. Supercooled water is found on the new growth side with increasing maturity in the ice phase, towards the evaporating side. Similar distributions within the cloud are reported by Heymsfield *et al.* (1978). This systematic development of the time cycle in the microphysics for warm clouds, from newly formed drops to parcels showing

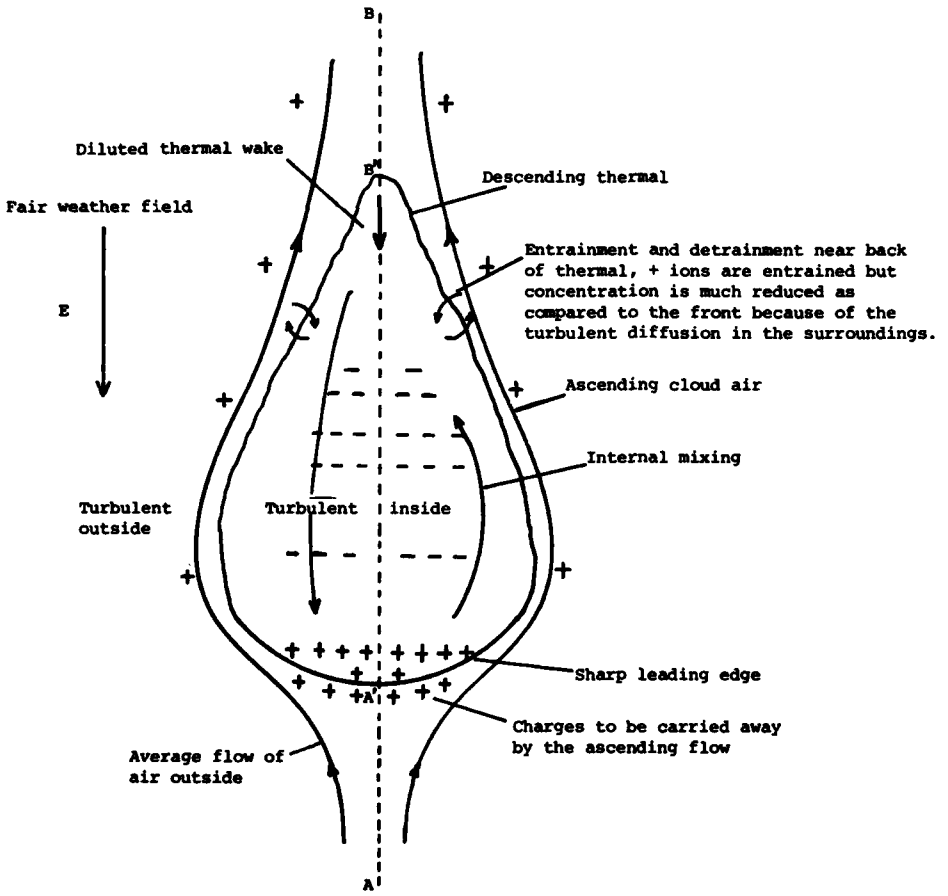


FIG. 1. — The descending thermal, with sharp leading edge, contains far fewer particles than that in the ascending cloud and the ion concentration in the thermal is higher than in the updraft. Due to the sharp leading edge of the descending thermal, the ion concentration has its maximum right behind the leading edge. Thus, when a downward field, which can be the fair weather field, is applied, the ions are separated into positive and negative regions, where some of the positive ions will move out of the leading edge of the thermal and be carried away by the ascending flow. This process will then leave the thermal negatively charged.

effects of multiple vertical excursions and mixing, is presented in the description of the dynamical structure given by Telford and Wagner (1980).

In this paper we explore some electrical consequences on this conceptual basis. Quantitative estimates are developed in section 5, for ion concentration, section 6, for conductivity differences, and section 8 develops an analytical model for charge separation, based on charge migration near a thermal (we think these thermals are blobs in shape), as shown in Figures 1 and 2. These blobs are about 100 m across. The following sections discuss the cloud physics basis for the model, problems with precipitation theories, and how electrical effects can arise.

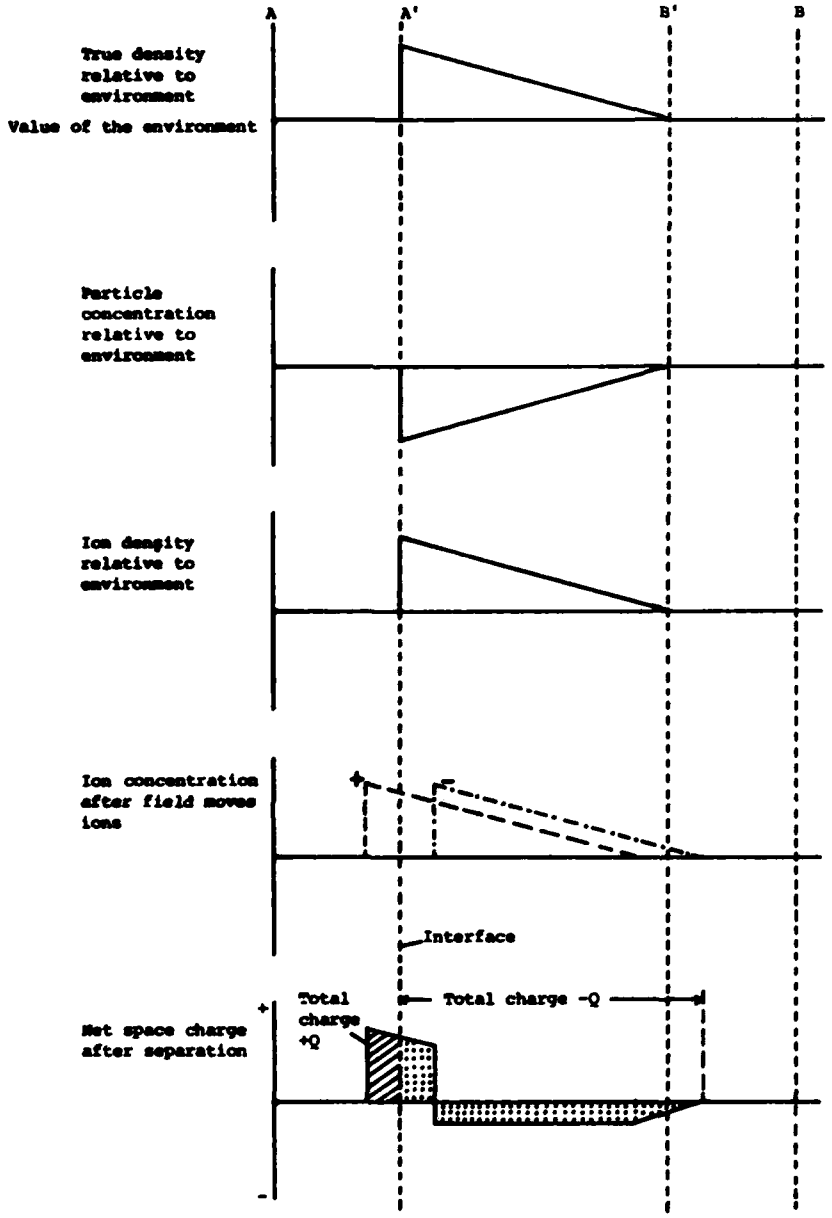


FIG. 2. — The true density and the particle concentration distributions of the thermal relative to environment and the relative ion distribution before and after charge separation.

## 2. — MICROPHYSICAL IMPLICATIONS.

The growth cycle described has major implications in regard to the integration of microphysical studies into a useful framework applicable to the real atmosphere, and to the development of real clouds. A start on this integration of microphysical studies into a practical framework has been made by Telford and

Chai (1980). In that paper it was shown that the vertical cycling of the air which is necessary to produce its observed composition, has a profound effect on the droplet spectrum. As it develops under the condensation cycling, both very small and large drops are rapidly formed in a way quite different to that found in more or less uniform updrafts previously used as a basis for calculations, and the result is in accord with observations of droplet spectra. This suggests that the appearance of particles large enough for further growth to begin by coalescence may be more affected by the nature of the inversion, or the environmental temperature and moisture structure in general, than by the condensation nucleus spectrum as previously thought, a conclusion remote from that reached by using uniform updrafts.

It has also been shown by Telford (1975) and Telford and Wagner (1980) that a quasi-equilibrium in the dynamics of the vertically moving blobs is sufficient to determine the observed liquid water content for small cumuli. If we note that the cloud parcels following the wet adiabat must be unstable relative to the environment, then this instability also applies to each parcel, descending after cooling by entrainment, or cycling upwards again. It is likely that exchange by entrainment between the up and down drafts modifies this stability by diluting the negative buoyancy in the downdrafts so that they tend to come to rest and to dwell at a height where they are almost neutrally buoyant, before starting upwards again. In smaller clouds this level is determined by the environment which sets the in-cloud vertical pressure gradient, averaged horizontal accelerations being negligible for small clouds. The mixing process is one of intense vertical transport but with negligible mixing across the horizontal, as opposed to the assumption of horizontal blending on which other one dimensional models appear to be based.

Using this framework of thermal elements this paper seeks to examine a new possibility for the thunderstorm charge separating mechanism.

## 3. — CHARGE SEPARATION IN THE TURBULENT CLOUD.

The thunderstorm charge generation problem has justified continuing interest in experimental cloud microphysics on the implicit assumption that if a charge separation mechanism can be demonstrated in the laboratory with water or ice particles, then nature will take care of producing lightning. Here we will present a case for charge separation without any particle charging mechanism, by the action of the dynamical mechanisms we have just described, on the cloud particles and ions. The result is that there seems little justification for not considering it further at this stage, and the theory described here explains facts recently observed. Whether a combination of effects is essential in an adequate theory remains to be determined.

Studies of the separation of electric charge in thunderstorms have generally been focussed on measurements of electric fields near severe storms, and charges on rain, etc. Surface based measurements study the end product of the charging process. Recent airborne measurements are closer to the heart of the matter with measurements of charges on particles in clouds (e.g., Gaskell *et al.*, 1978). A comparable effort has also been focussed on microphysical charge separation processes, which is where charge separation begins. The gap between microphysical particle charge separation, and macrophysical storm charge

effects, has been somewhat neglected however. Usually falling precipitation has been allocated the macro charge separation role.

Here we need to draw a clear distinction between separating positive and negative charge on different particles, which will be called charge generation in this paper, and the separation of these charged particles by many hundreds of meters, with charges of the same sign mostly moving in the same direction.

For many years Vonnegut (1955) has advocated a mechanism of charge separation which utilizes circulating air currents around the storm to drive a charge from cloud top towards the base. However the continuing downward flow in the circulation, required for the model, does not seem to occur in real clouds. Besides, numerical models based on convection and ionic conductivity gradients (Chiu and Klett, 1976), have not succeeded in demonstrating that strong electrification occurs. We believe that our mechanism has not been considered previously.

The concept we wish to explore relates to a charge separation process (Telford and Wagner, 1979), in which the entrainment at cloud tops produces downdrafts within the cloud which carry a net negative charge.

A number of performance criteria for charge separation must be met in any thunderstorm theory. We will deal with the more obvious from our point of view.

*a)* Sufficient charge must be generated. This is a rather variable quantity, but should be of the order of a coulomb per second.

*b)* The electric field must build up rapidly enough, say, in 20 to 30 minutes.

*c)* The charge separation mechanism must account for its success in the face of the extremely large vertical mixing, with velocities of perhaps 5 to 10 m $sec^{-1}$, upwards as well as downwards. This requirement has been neglected in many modeling efforts based on charge separation by falling particles, where it has been assumed that the particles will fall with their average terminal velocity relative to the « average » air motion regardless of turbulent fluctuations. Illingworth and Latham (1977), for example, derive some interesting results for a cloudy region where the velocity is constant and vertical over the entire charge generating volume of relevance. A typical turbulent motion is a cylinderlike swirling motion, which, when its axis is horizontal, leaves the lowest drops on top after rotating 180 degrees, and vice versa. The fact that rain falls out of the bottom does not mean that the drops have not been swirled up and down until those of raindrop size close enough to the lower regions of the cloud escape where the local updraft is small enough. In such conditions bigger cloud drops fall back and forth amongst the smaller droplets.

*d)* The negative charges usually accumulate at an altitude between −10 °C and −20 °C, with a positive charge above (Krehbiel *et al.*, 1979). Any lower positive charge, at, or below, cloud base, can probably be explained by secondary processes and so need not be considered at this stage. It is not sufficient to generate charge at this level as some ice-water interaction theories propose, and then let the negative charges fall down. The negative charge carriers must come to rest at this level, while the positive carriers must reside much higher up.

This requirement would seem to exclude any particle charge separation mechanism requiring supercooled liquid water for its operation, since charge generated at this level can only give a negative charge center lower down as the

falling particles continue downwards. It should be recalled that the observational data imply that there can be no sustained updraft in the vertical mixing region where the microphysics matures. The downdrafts cannot move downwards in the updraft feeder flow. The downdrafts are only effective where the average updraft is zero, with the downdrafts separated by updrafts of about the same volume flux. It is the resulting mixing and transport up and down which grows big drops and ice crystals. Indeed, precipitation does eventually fall from most thunderstorms so that in a gravitational settling theory the alternative of suspending the negative charge generating particles at a constant height, while they grow and acquire negative charge, seems to be excluded, unless some new dynamical mechanism to achieve this delicate balance is forthcoming.

This consideration is particularly significant since the theory proposed here provides a simple explanation for this observation.

In addition, on some occasions, lightning has been seen in clouds which are everywhere warmer than freezing (Moore *et al.,* 1960), so that charging can occur without ice particles being present.

*e)* The observation that radar echoes show an enhancement after the first lightning (Moore *et al.,* 1964), is likely to be explicable in terms of rapid coalescence since the ionized air following a discharge charges the cloud particles and newly charged positive particles coalesce with the negatively charged ones. This implies that the microphysics is controlled by the electrical forces at this stage in the storm, rather than that the microphysics is providing the electrical effects.

The argument has been made that the microphysical processes reach electrical maturity at this stage, so that the electrical lightning generation only reaches its full efficiency after the first strike and hence can accommodate any such loss of charged particles without much loss in effectiveness. However this sudden coalescence activity needed to give the rapid increase in the observed radar echo intensity would occur at the same time as the lightning continues to build up, when both the discharge and the loss of charged particles must be accompanied by considerable reduction in the available charge without incapacitating the primary charge separation mechanism. One might suspect that the reverse argument is equally valid. That is that the release of ions improves the efficiency of the process and hence the sudden discharge of the system by lightning makes it more efficient by providing fresh ions.

It should be mentioned that experiments with radar chaff needles spread below storms shows that these continuous sources of corona reduce the lightning by conducting away the charge. This was reported in Holitza and Kasemir (1974) and Kasemir *et al.* (1976). However there is a big difference between having adequate ions in the cloud to support the process we are discussing and the almost unlimited ions resulting from the chaff needles.

It should be noted that Christian *et al.* (1980a) report that they observed « strong correlations of cloud electrification with convection, and weak correlations with the intensity and location of precipitation ».

*f)* The first lightning comes before much precipitation falls out of the cloud. It is observed that the negative charge center does not fall below the −10 °C level, seemingly eliminating the falling particles as the charge carriers to drive the primary separation process. This is true whether there is a lot of cloud below the −10 °C level, or very little.

Many of these points have been made by Moore (1974, 1976), but without the advantage of the interpretation given here.

Let us deal with the requirement (*a*) immediately, and the other points later, after the theory is developed. The present point of view suggests that the charge is first generated by cosmic rays. At heights of 6 km or so cosmic ray ionization generates about 30 ion pairs $sec^{-1}$ $cm^{-3}$. This value is conservative since at 8 km we have 75 ion pairs $sec^{-1}$ $cm^{-3}$, and at 10 km the number is 125 (Israel, 1973, pp. 575-576). Consider the total charge released per second in a volume 1 m square, 1 km in vertical depth. If this charge were separated then it would provide a current per unit area of A h R e, where A is the horizontal area, h is the vertical height, R is the pair production rate in ions produced per $cm^3$ per second, and e is the charge on the electron, e = $1.6\ 10^{-19}$ coulombs.

$i = (100)^2\ 10^5\ 30\ 1.6\ 10^{-19} = 4.8\ 10^{-9}$ amp. per $m^2$ per kilometer depth.

If the area of the storm is 5 km square and the total depth is also 5 km, and we have charge accumulated for 15 minutes, then the total available, without needing any corona to develop to release new charges, is,

$$Q = 4.8\ 10^{-9}\ 10^6\ 125\ 15\ 60 = 540\ C.$$

This appears to be of the right order of magnitude to allow a reasonable margin for producing the first lightning stroke.

In a 15 second period this ionization rate would generate, upon separation, a charge of 9 C. Once again this charge is of an appropriate order of magnitude, if a little low, but since this assumes no storage, it is not an unacceptable value, even without the help of charge released by the corona which will remove this limitation.

If the storm is smaller, with a horizontal dimension of, say, only 2 km square, then only 1.4 C is available for each 15 second period which is too small to maintain some observed lightning rates, which, however, were probably associated with larger clouds.

While there is no doubt that any process is less than one hundred per cent efficient, the removal of ions by recombination is relatively slow, requiring many minutes, so that most of the ions released could well contribute to the final available charges if the separation process is reasonably rapid. There is also air being entrained into the cloud from above, which will bring ions with it to increase the conductivity in the downdrafts. The creation of such increased conductivity in the downdrafts relative to the updrafts, by another mechanism, is the basis of the process introduced below.

One final simple check is whether or not the separation of the available charges could generate an electric field of several times 100,000 V $m^{-1}$, capable of initiating breakdown. If we assume a parallel slab cloud, to avoid computational details,

$$E = Q/\varepsilon_o ,$$

where $1/\varepsilon_o = 36\ \pi\ 10^9$, and E is the field strength in volts per meter, and Q represents the charge per square meter on the parallel charged boundary planes.

$E = 542$ V $m^{-1}$ per second per kilometer of cloud depth,
$= 500{,}000$ V $m^{-1}$ in 15 minutes per kilometer of cloud depth.

This test is far more important than the concern for the total charge because the high fields will produce corona, which then generates unlimited charge on ion

pairs, and the rate of the electric field increase appears to be adequate. It is important to note that this is an average field and that local charge variation resulting from turbulent irregularities will produce much higher fields in local regions by moving opposite charged parcels closer together, which may be enough to compensate for loss of charge due to ionic recombination or capture on drops. These local fields will initiate internal ionization and charge release first, which will remove the limitations being discussed, as we have said before.

In all it is clear that, while there are no great excesses of charge to waste, and that this simple estimate does not prove cosmic ray ionization is the source of thunderstorm charge, the estimates are so close to the required performance that there are grounds for further interest.

Few other approaches to thunderstorm electrification appear to satisfy these basic requirements so readily. The key to such a theory, however, lies in having a mechanism for charge separation, and this will be presented in the following sections.

## 4. — THE NEW MECHANISM.

We will begin by describing briefly what is known about atmospheric thermals as a basis for postulating a thermal structure appropriate to the interior of cumulus clouds. It is hoped this paper will serve to show the need and usefulness of a successful model for this phenomenon, as a matter requiring serious attention. The detailed specification of a numerical model is of no interest in this paper since, once the physical principles are decided upon, the rest is a coding problem (perhaps formidable, but a separate problem). Here it is hoped to demonstrate physical reasonableness.

In the previous paper Telford and Wagner (1979) discussed charge separation on the basis of a mechanism whereby the microphysical processes generated the negative charge on the larger (but still less than 1 mm diameter) particles, with the corresponding positive charge on the smallest particles. The descending blobs then provide the mechanism for separating these opposite charges over cloud sized distances.

We will show here that such initial charge generation on particles is probably unnecessary and that cosmic ray ionization can provide the charges for an adequate separating mechanism.

The mechanism proposed here depends on the sharp interface observed on the leading edge of buoyant thermals. This sharp transition at the leading penetrating edge of buoyant thermal blobs in the atmosphere, is common to all atmospheric thermals which have been studied. The thermal is entraining and hence it internally consists of small parcels ranging in composition from the most buoyant, to parcels with the composition of the surroundings. The internal vertical gradients are unstable in the thermals leaving the buoyancy source, and are stable in the return flow. The buoyancy is increased at the heated surface of the earth, for dry air thermals in the atmospheric boundary layer, as an example where there are adequate observations (e.g., Warner and Telford, 1967), and is decreased at the tops of cumulus clouds where entrainment is cooling the cloud air, which is the case we are considering. Thus, inside the thermals the more buoyant constituent parcels are always rising to the top (or bottom for cooled cloud thermals) of their respective thermal blobs where they replace the previously exposed surface of the blob with fresh buoyant material. Thus, the

interface is always being renewed and a gradual transition region cannot form on the leading edge. See Figures 1 and 2.

This phenomenon of a sharp interface is observed in the sharp edges of clouds, where the observed transition is less than most instruments can resolve on the upshear building side, say a fraction of a meter. This effect is also seen in the sharp outlines of steam and smoke plumes from chimneys, and in the dry air planetary boundary layer plumes, on their upshear side. This sudden transition in moisture and temperature is usually clear. The turbulent properties of the motion show no such transition. No distinction can be made between inside and outside the plumes on the basis of turbulent motion, in the planetary boundary layer. In this case, the return flow between the plumes has a temperature structure which is quite uniform, while the rising plumes themselves have an irregular temperature excess, highest on the upshear edge, but inside everywhere warmer than in the surroundings, so that the temperature structure distinguishes the plumes quite clearly.

We will postulate that a similar dynamical mechanism is at work in clouds. Here the entrainment of the dry overlying air, which evaporates the cloud particles, is the source of negative buoyancy in the cloud blobs.

The studies by Imyanitov *et al.* (1972) show a structure in both the electric field and the temperature, with the most frequent linear dimension of about 80 m, for both.

The dilution of the cloud parcels where entrainment at the cloud top introduced drier and warmer overlying air, results in evaporation of cloud drops and ice particles. In the previous paper (Telford and Wagner, 1979), it was postulated that the smaller ice particles would evaporate before the larger ones. However, recent measurements at the top of stratus cloud layers (Telford *et al.*, 1980) showed that in this case evaporation proceeded by producing a total loss of 90 % of the drops, and the uniform redistribution of the remainder through the now saturated mixture at a tenth of the former concentration. In both cases the number of particles will be greatly reduced.

In addition, there is the likelihood that the parcel which has risen to cloud top and consequently been cooled to a temperature less than, say, −20 °C, will have begun to grow ice particles. Thus, we will postulate that the descending blobs will have a similar water content to the intervening rising air, but with a larger reduction from the hundred or so cloud droplets per $cm^{-3}$ which have now been converted to larger ice particles with a concentration of a few per liter.

The cooler descending parcels have less particle area to absorb cosmic ray ions, and so have a higher conductivity. When an electric field is present the higher conductivity regions can thus give up charge into the rising surrounding cloud. Hence another negatively charged region lower down can provide the electric field to move positive ions across the interface from the descending parcels to the surroundings. The fair weather field can start the process.

If the mixing process behaves with cumulus cloud particles in the same way that the observations show it influences cloud particles in the tops of marine stratus, as observed by Telford *et al.* (1980), then the effect on the particles of mixing dry air into cloud tops is to reduce the particle concentrations. This will occur even when there are no ice crystals present.

Inside the plume the turbulent stirring continually renews the supply of

positive ions to the sharp interface of the leading edge at the bottom of the thermal, and inside the thermal those ions captured on drops tend to be released again as the drops continually evaporate during descent. However, the main effect is the higher ion concentration due to reduced particle concentrations.

Since the fields are created by negatively charged regions lower down below the new descending diluted blobs, and the leading surface of any thermal is sharp and distinct between the thermal and its surroundings, because it is continually renewed by the action of the negative buoyancy inside the thermal, the leading edge becomes an efficient charge separating surface when there is an adequate conductivity difference across it. The trailing edges of the thermal will not present such a sharp interface so that the corresponding current of negative ions out of the thermal on the opposite side of the plume will not occur to an appreciable extent. The negative charges leaving the upper half of a thermal blob will be caught in the trailing, less negatively buoyant, wake, and continue to descend, rather than transferring to the rising surrounding cloud.

A sharp increase in conductivity, followed by a gradual return to low conductivity in the high conductivity parcel, will lead to a strong charge across the interface on the low conductivity side. There will be a distributed compensating charge in the gradual transition region within the thermal (see Figure 2).

## 5. — THE ION CONCENTRATIONS.

The conductivity of the air depends on the particle concentrations as was analyzed by Gunn (1954).

The ionization rate at 8 km is greater than 50 ion pairs $cm^{-3}$ $sec^{-1}$ and the recombination coefficient is 1.6 $10^{-6}$ ion pairs $cm^3$ $sec^{-1}$ (values taken from Israel, 1970, 1973). Thus in cloud free air where the particles in the air are too few to be considered the equilibrium concentration is 5600 ion pairs per $cm^3$, assuming large ion particles exert negligible influence at this altitude.

In a cloud with 2 g $m^{-3}$ water content in the particles, then 100 particles per $cm^3$ have an equivalent mean radius of 17 $\mu$m. The formula from Gunn (1954, eq. 39) gives, for the effective combination coefficient of droplets with the ions, $\eta_a$,

$$\eta_a = 4\pi kTua \,/\, e(1 + Qe/2akT \ldots).$$

If the particles are uncharged, Q = 0. The charge on the electron is e = 1.6 $10^{-19}$ C, and Boltzman's constant k = 1.38 $10^{-23}$ J $°K^{-1}$. The absolute temperature is T = 245 °K, say, the ion mobility is u = 2.0 $10^{-4}$ m $sec^{-1}/V$ $m^{-1}$, and the particle radius is a = 17 $\mu$m.

$$\eta_{17} = 9.0\ 10^{-10} \text{ ion pairs } m^3 \text{ sec}^{-1}.$$

Thus, when we have 100 drops $cm^{-3}$, N is the number of ions per $cm^3$, and $dN/dt$ = 50 ions $cm^{-3}$ $sec^{-1}$ is the ion generation rate from cosmic rays, then

$$\begin{aligned} dN/dt = 50 &= 100\,\eta_a N \\ &= 9\ 10^{-2}\ N \\ N &= 555 \text{ ions } cm^{-3}. \end{aligned}$$

When the opposite signed ions are present in equal numbers

$$\begin{aligned} dN/dt = 50 &= 100\,\eta_a N + \eta_i N^2 \\ &= 9\ 10^{-2}\ N + 1.6\ 10^{-6}\ N^2 \\ N &= 550 \text{ ions } cm^{-3}. \end{aligned}$$

So most of the absorption is on the droplets even if we ignore migration in the electric field.

Let us now estimate the absorption of the ions as they migrate through the cloud droplets in the electric field.

$$\text{Area of drops} = \pi r^2$$
$$= \pi\,(17\ 10^{-6})^2\ m^2$$
$$= 9\ 10^{-6}\ cm^2.$$

If the fraction of the total area obscured per unit length is 1/L, $L = 1/\pi r^2 n = 10^4/9 \simeq 1000$ cm. The inclusion of polarization effects reduces this estimate by a factor of 3.

This is a distance absorption rate constant, L, of 3 m.

With a field of 10 V $m^{-1}$ and a mobility of $u = 2\ 10^{-4}$ m $sec^{-1}$ / volt $m^{-1}$ we can find a time constant, t, for sweeping the ions from the volume as they migrate in the fair weather electric field and are absorbed on the cloud drops.

$$t = L/uE = 3 / 2\times10^{-4}\times10 \simeq 27 \text{ min.}$$

When the field is 1000 V $m^{-1}$, t = 16 sec, so that this effect becomes a large sink for the free ions as the field rises, and will exceed the diffusion rate of the ions to the drops when the field reaches 10,000 V $m^{-1}$, for this population of particles. This absorption does not effect the net charge however. Thus this collection of the drops migrating under the electric field is not rapid enough at low field strengths to seriously reduce the concentration of ions and so reduce the conductivity, but the drops certainly do prevent the ions moving appreciable distances away from where they were produced in the air, since the number of free ions would be down by a factor of e after moving 3 meters.

Let us now postulate that the ice process (or some other process) transfers the 2 g $kg^{-1}$ of water from the 100, 17 $\mu$m radius particles per cubic centimeter, to an equal mass of spherical ice particles at 10 per litre. These particles now have a radius of 370 $\mu$m.

$$\eta_{370} = 190\ 10^{-4},$$
$$N = 2500 \text{ ions cm}^{-3}.$$

Here most of the absorption is between ions, and the particle absorption of ions is much smaller.

The distance absorption constant, L, is

$$L = 1 / 1.25\times10^{-4}\ cm = 80\ m$$

and the time constant at 10 V $m^{-1}$ is t = 11 hours, for this absorption by the migrating ions on the drops.

Another possibility is that if we reduce the numbers of drops by a factor of 10, to give 10 drops per $cm^3$, by evaporation after mixing in of dry air at cloud top (see Telford *et al.*, 1980), the numbers are,

$$N = 3445 \text{ ions cm}^{-3},$$
$$L = 33 \text{ m},$$
$$t = 5 \text{ hours}.$$

Thus the reduction of the particle numbers either by the onset of the ice process, or even by evaporation following mixing if it were ever extensive enough, would raise the ion concentration by a factor of over four, since in both

these cases the collection and hence, loss, of migrating ions in the field by collision with particles is negligible from the local conductivity point of view.

## 6. — THE CONDUCTIVITY DIFFERENCES.

We have described how descending downdrafts begin at cloud top, as a result of the mixing in of dry air from above the clouds which then evaporates and cools cloud parcels. These parcels will be largely ice particle clouds near the tops of large cumuli. The reduction in particle concentrations from a few hundred per $cm^3$ to less than 10 $cm^{-3}$ of the same sized drops, or the conversion of the same amount water to a much fewer number of ice particles, will greatly increase the conductivity of the cooled descending plumes of diluted air.

The rising surrounding cloud will tend to consist of many small drops with the freezing process less advanced and hence will have a lower conductivity.

When this conductivity discontinuity is combined with a dynamic shear discontinuity at the front of a descending in-cloud thermal we shall have the charge separation mechanism.

The first point to note is that the local field at the interface produces the charge separation but since the turbulent motion is several meters per second the charges are rapidly swept away from the interface where they separated and so any neutralizing polarization charge is probably small. Thus every area of interface is generating a charging current at a rate determined by the large scale fields.

With N = 2500 ions $cm^{-3}$ the current per unit area is,

$$\begin{aligned} i &= NquE \\ &= 2500\ 10^6\ 1.6\ 10^{-19}\ 2\ 10^{-4}\ E \\ &= 8.0\ 10^{-14}\ E \text{ amp. } m^{-2}. \end{aligned}$$

If we assume the conductivity in the rising cloud parcels to which the positive charge transfers, arises from N = 550 ion pairs, then this charging current is reduced by the reverse current to,

$$i = 6.2\ 10^{-14}\ E \text{ amp. } m^{-2}.$$

## 7. — THE ROLE OF ICE.

Since the free ion concentration depends on the reduction in particle numbers, the transfer from many water drops to far fewer ice particles is the most important step in initiating charge generation in cumulus clouds.

In a glaciated cloud the parcels descending from above the −20 °C level will be laden with ice particles and no water, since it is observed that most clouds are glaciated at temperatures below about −15 °C. At about the −10 °C level parcels rising up from below the freezing level will still contain many small water drops. Thus near this level descending parcels will embody the latent heat of freezing and tend to be more buoyant than surroundings containing rising liquid water cloud. Hence the descending ice filled parcels will tend to come to rest where they meet the rising liquid drop filled parcels at −10 °C to −20 °C, and if these thermals carry negative charge then this region will become a region of accumulated negative charge. This description agrees with the observations of negative charge accumulation at levels where the temperature is between −10 °C and −20 °C, which have been reported by Krehbiel *et al.* (1979), Christian *et al.* (1980b) and others.

Another role of ice particles may be to encourage ion generation by corona due to the sharp edges associated with the crystal shapes.

## 8. — THE CHARGE SEPARATION MODEL.

In order to formulate a simple model to demonstrate the potential of this mechanism, let us assume that we have a slab of cloud where everything is uniform in the horizontal. Postulate that entrainment introduces negatively buoyant blobs at the top surface which proceed downwards through the cloud.

Because of the resulting vertical ion concentration gradient the negative ions will increase at any point in the thermal, compared to the positive ions, as the ions move in the field. At the bottom interface (henceforth referred to as the interface) of the thermal the positive ions will cross the interface into the surrounding upward moving cloud and get carried away as shown in Figure 1. The negative charge will try to follow the rising outside positive charge but will either be captured on cloud particles or swirled away from the interface by the turbulence inside the blob.

This turbulent stirring inside the descending plume will redistribute the negative charge relatively uniformly inside the plume like thermal and provide new ions in the descending air at the lower front surface of the plume, so the cycle can repeat continuously. The preponderance of negative ions in the ice growing regions of the downdrafts will charge the growing ice particles negatively and coagulation will lead to a range of charges, but with a few ice particles carrying exceptionally large charges.

The turbulent motion between the blobs will also rapidly spread the positive charges throughout the intervening cloud. Thus the positive charge will be much diluted in the surrounding cloud before any of it becomes entrained back into the blobs. Hence the neutralization effect of the negative charges in the blobs by entrained positively charged surrounding cloud will be small.

Since the field lines are parallel, and all within the slab, because there are no edge effects to consider in the infinite plane geometry we are using, the final fields can be constructed by allowing a succession of infinitesimally thin planes of charge separating interfaces to proceed through the slab from the top down, one after another. Assume that the positive charge left in the surrounding cloud remains fixed at the same height at which it was released, then the charge separation rate at the plane depends only on the total charge above the plane, which, of course, equals the total charge of the opposite sign below the plane, accumulated from the preceding charge separating planes which have reached the lower boundary. Thus, the rate of charge separation on a plane which began at cloud top at times between t and $t + \Delta t$, and which is moving downwards through the cloud at velocity, v, and is presently at distance $z = vt$ below the top surface, depends on the sum of the charges above it, which determines the field across the charge generating interface.

A simple formula for the charging process comes from assuming that a succession of charge separating thermal interfaces descend from the top to the bottom of the cloud, one at a time, while generating negative charges as described above. If the corresponding positive charges all proceed to cloud top but are not included in the field until the corresponding negative charge reaches the lower accumulation level, then the electric fields due to any negatively

charged layer underneath stay uniform with height from the cloud top down to the negative layer. This formulation assumes that the positive charges are carried up at the same rate as the negative charges are moved down, and that these separating charges have no effect until the thermal reaches the bottom.

Assume now that the layers all reach the −10 °C level, say, and come to rest, and that a new set of thermals is released at this time so that only one layer of thermals is descending at one time. If it is assumed also that the depth of cloud is such that the thermal release rate allows on average only enough active surface to just fill the available projected horizontal area at each step, then a very simple estimate can be formulated. This is based on the field increasing by $\Delta E$ wherever a charge $i\Delta t$ arrives at the lower level, so,

$$\Delta E = (i/\varepsilon_0)\,\Delta t,$$

where $\Delta t$ is the time the charge generators in the descending surface take to descend through the cloud.

If $i/E = 6.2\ 10^{-14}$, as estimated above, then

$$E = E_0 \times 2^{t/100},$$

and the field doubles in 100 seconds.

Before considering a more realistic process we can use this formula to show the effects of irregularities in the charging of a cloud. With the same average charge separation rate we could have half the cloud area separating charges at half the average rate and the other half separating charge at one and half time average.

Thus, we use $2 \times 100$ and $2 \times 100/3$ as the time factors so,

$$E_A = E_0\,(2^{t/100})^{1/2},$$

and,

$$E_B = E_0\,(2^{t/100})^{3/2}.$$

Thus, when an average generation rate would allow a field of 1,000 V m$^{-1}$ given $E_0 = 10$ V m$^{-1}$, so that $E_A = 100$ V m$^{-1}$, then the faster half would have generated $E_B = 10{,}000$ V m$^{-1}$. In practice $E_B$ would dominate the condition of the whole cloud, so that it is clear that average conditions can seriously underestimate such cloud electrification processes, and if a small part of the cloud turns out to be appreciably more efficient it will dominate the whole process.

The above approach involved several approximations. If there is more than one charge generating layer in a cloudy column at any one time, it is clear that in reality the second layer does not receive the benefit of the field from the total charge separated on the layer ahead of it, for the whole distance, as this first approximation assumed when the first charged layer was right through the cloud before the second one started. Furthermore, the positive charge will be distributed throughout the active part of the cloud by the turbulence, rather than all of it proceeding directly to cloud top.

A better model can be produced by assuming that the negative charge remains compacted in the moving blobs, but that the positive charge released to the surroundings is evenly distributed throughout the cloud depth when the negative charge reaches the bottom, but having no effect until then. Thus we have assumed a uniform vertical mixing of the positive charge at about the same velocity as the descending thermals carry down the negative charge. This assumption reflects the very substantial turbulence and vertical mixing resulting

from the inherent instability everywhere in the cloud. To simplify this model, it is assumed that the cloud is horizontally uniform with charge separating interfaces following each other from the top to the lower accumulation level.

This formulation is based on the description of the dynamical effects as we know them, and which have not yet been quantitatively modeled, but is simplified to give a description which can be handled analytically. A simple approach is all that seems to be justified to demonstrate the mechanism since the next step is likely to be a detailed numerical model which can only be attempted when an accurate dynamical description has become available.

We have postulated that the uniformly distributed positive charges do not increase as each charge separating surface builds up its charge, but that these charges are released and included in the electric field when each negative charge reaches its lower limit. Thus time delays due to transport are included from the start. At each level as the charge generating surface descends, the electric field driving the charge separating current across it is a linear fraction of the maximum field found at the bottom. If we have m steps in the descent, then when the surface reaches the $j^{th}$ step, the field is $jE_{n+j-1}/m$. Here $E_n$ is the field at the bottom surface as the layer starts its descent at the top. The field increases at each step, so that $E_{n+m-1}$ is the field just inside the bottom surface, at the position of the last of the m height increments after $m - 1$ time steps, when this charge separating surface has moved down and finally reached the bottom step. Since we do not release the positive charge until the negative charge reaches the bottom, the field is a linear function with depth at each step. When the charge on the layer in this particular step has reached the lower surface and is included in the field then the field at the bottom is $E_{n+m}$.

Each charge generating surface carries the active surface area released in the interval between one step and the next. Thus, if the cloud depth, between the top and the negative accumulation level, is $z_0$, and the active generating surface area per unit volume of cloud is s, then the fraction of active surface area per unit area for each of the m layers is $sz_0/m$.

The first layer starts at the top, and moves to the beginning of the second step as it descends from $z = 0$, to $z = z_0/m$ in time, $\Delta t = z_0/mv$. This distance from the top down to the position of the particular surface is z and the average velocity of the charge generating interface is v. At this point, one more charged layer reaches the bottom and the field increases from $E_0$ to $E_1$, and a new charged layer starts at the top. The electric field during this first step starts at $E = 0$ and increases to $E = E_0/m$ as z increases from 0 to z/m, so that its average value is $(1/2)E_0/m$. For the second step the field is $E_1$ and the surface moves from $z_0/m$ to $2z_0/m$ as the field increases from $E_1/m$ to $2E_1/m$, with an average value of $(1 + 1/2)E_1/m$. The third step begins at $2z_0/m$ with field of $2E_2/m$ and finishes with $z = 3z_0/m$ at a field strength of $3E_2/m$, an average field strength of $(2 + 1/2)E_2/m$.

Thus, when the charging rate is i coulombs per second per unit electric field strength per unit area of charge separating surface, the layer generates a charge per unit area at the $j^{th}$ step, of $q_j$, where,

$$q_j = i(j-1/2)E_{j-1}sz_0^2 / (vm^3). \quad (1)$$

Thus, the total charge per unit area after the layer has moved through m steps from $j = 1$ to $j = m$ is Q,

$$Q = \sum_{j=1}^{m} q_j. \tag{2}$$

Now the charges are proportional to the field at every step so that once the initial perturbations have smoothed out, if we scale the charges and fields in terms of the electric field just above the lower negative charge accumulation surface, every step is similar to every previous step. Thus, as each small charge arrives at the lower surface the field will increase by a small fraction of the previous field values, say, a,

$$E_1 = (1+a)E_0. \tag{3}$$

Thus,

$$E_j = (1+a)^j E_0, \tag{4}$$

and,

$$E_j = (1+a)^{j-m+1} E_{m-1} \tag{5}$$

where $E_{m-1}$ is the field active during the $m^{th}$ step.

We also have,

$$E_m - E_{m-1} = Q/\varepsilon_0 = aE_{m-1}. \tag{6}$$

Now, Q can be evaluated.

$$Q = E_{m-1} \sum_{j=1}^{m} i\,(j - 1/2)\,(1 + a)^{j-m} s z_0^2 / (vm^3). \tag{7}$$

Hence,

$$Qv / (iE_{m-1}\, s z_0^2) = [(1 + a)^{-m+1} / m^3] \sum_{j=1}^{m} (j - 1/2)\,(1 + a)^{j-1}, \tag{8}$$

letting $x = 1 + a$,

$$\begin{aligned} &= (x^{-m+1}/m^3)\,[1 + 2x + 3x^2 + \ldots + mx^{m-1} \\ &\qquad - 1/2\,(1 + x + x^2 + \ldots + x^{m-1})] \\ &= (x^{-m+1}/m^3)\,[d/dx\,(1-x^{m+1})/(1-x) - 1/2\,(1-x^m)/(1-x)] \\ &= (x^{-m+1}/m^3)\,[-(m+1)x^m/(1-x) + (1-x^{m+1})/(1-x)^2 \\ &\qquad - 1/2\,(1-x^m)/(1-x)]. \end{aligned}$$

Now we can proceed to a limit as the number of steps, m, tends to infinity. Since $a \to 0$ as $m \to \infty$, let us set $am = k$, where k is a constant.

Now,

$$x^m = (1 + ma/m)^m = (1 + k/m)^m \to e^k$$

$$1 - x = -a = -ma/m = -k/m.$$

Thus, the previous expression in x becomes,

$$\begin{aligned} &= (1+a)e^{-k} / m^3\ [m(m+1)e^k / k + m^2\,(1 - (1+a)e^k / k^2) \\ &\qquad + 1/2\, m(1-e^k)/k] \\ &\to e^{-k}/m\,[e^k/k + (1-e^k)/k^2] \\ &= 1/m\,[(k-1+e^{-k})/k^2]. \end{aligned} \tag{9}$$

Substituting $Q = \varepsilon_0 a E_{m-1}$, since the last field increment was caused by the total incoming charge increment.

AD-A146 546 STUDIES OF THE OCEAN SURFACE AND THE COUPLING BETWEEN THE SEA AND THE ATMOSPHERE(U) NEVADA UNIV RENO DESERT RESEARCH INST J W TELFORD 01 OCT 84 N00014-75-C-0598 3/3

UNCLASSIFIED F/G 4/2 NL

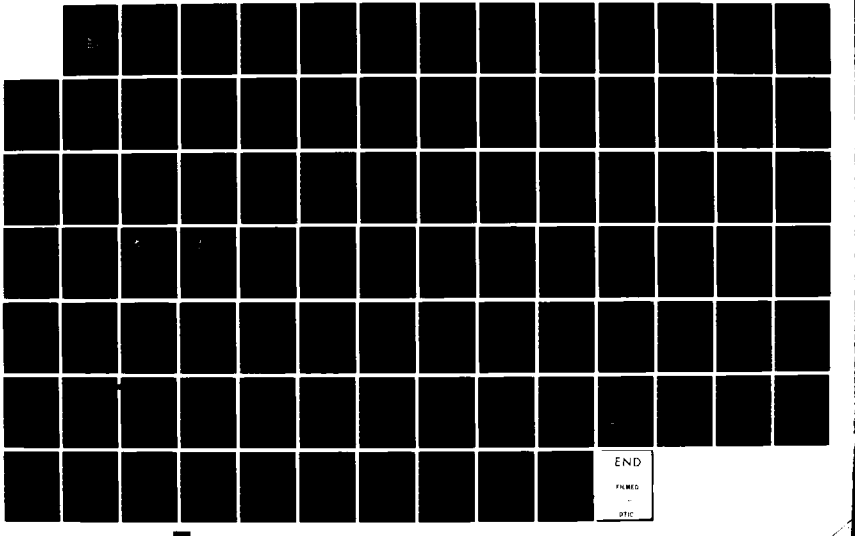

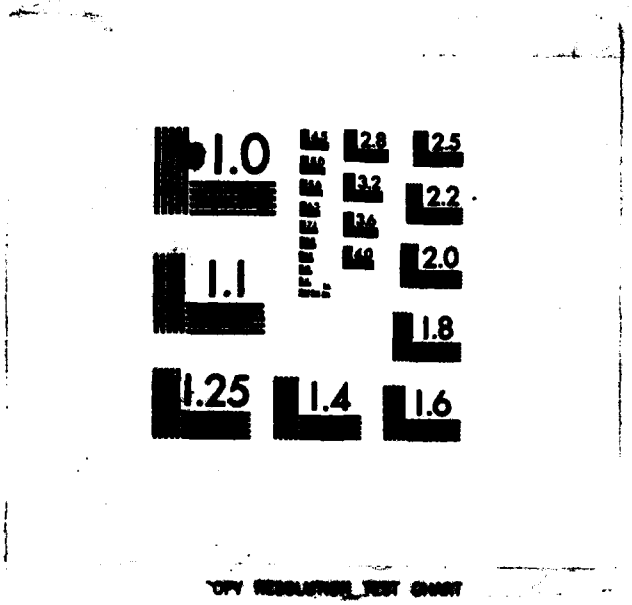
1.0
1.1
1.25
1.4
1.6
1.8
2.0
2.2
2.5
2.8
3.2
3.6
4.0

$$Qv / (iE_{m-1}sz_0^2) = v\varepsilon_0 ma / isz_0^2 m = v\varepsilon_0 k / isz_0^2 m = (k - 1 + e^{-k}) / k^2 m. \quad (10)$$

Thus,

$$k^2 = (isz_0^2 / v\varepsilon_0)\,[1 + (e^{-k}-1)/k]. \quad (11)$$

As used above,

$$\Delta t = z_0/mv, \text{ so,}$$
$$E_m - E_{m-1} = \Delta E = aE = maE/m = kvE\Delta t/z_0. \quad (12)$$

Hence,

$$dE/dt = kvE/z_0 = E/\tau, \quad (13)$$

and

$$E = E_0 e^{t/\tau}, \quad (14)$$

where, $\tau = z_0/kv$.

Now consider the factors in k,

$$k^2 = (i/\varepsilon_0)\,(sz_0)\,(z_0/v)\,[1+(e^{-k}-1)/k]. \quad (15)$$

As before $i/\varepsilon_0 = 1/143$. This value follows because we had $e^{t/\tau_0} = 2^{t/100} = e^{t/100}$. The product $sz_0$ is the area of the charge separating surfaces per unit total area, over the depth of the charge separating region of the cloud, $z_0$. These factors were present in our first simple model where $sz_0 = 1$, by implication. This requirement gives one charge generating surface at some level for every horizontal position between the top and bottom, as we first assumed.

The new factor is $z_0/v$, which is the time taken for the charge generating surfaces to descend through, $z_0$, the depth of the cloud from top to the bottom accumulation level. If this factor were omitted (this implies $z_0/v = 1$ second), as in our first estimate, then k would be small, so that, with $sz_0 = 1$.

$$k^2 = (iz_0/\varepsilon_0 v)\,[1 + (e^{-k}-1)/k] = (iz_0/\varepsilon_0 v)\,[1 + (1 - k + k^2/2 - k^3/6 \ldots - 1)/k] = (ikz_0/2\varepsilon_0 v)\,(1 - k/3 \ldots). \quad (16)$$

Thus, $k \simeq iz_0/2\varepsilon_0 v$,

and so,

$$\tau = (z_0/v)/k. \quad (17)$$

Cancelling $z_0/v$,

$$\tau = 2\varepsilon_0/i = 2 \times 143 \text{ sec.}$$

This is a time constant of twice the earlier estimate, where the numerical factor 2 is due to the redistribution of the positive charge equally at all levels and is a constant. Thus it is clear that the main difference in the new model is the other factor arising from the inclusion of the effects caused by the time, $z_0/v$, needed for the finite velocity of the charge separating surfaces to move down through the cloud.

Since the factor $z_0/v$ is however quite large we need to reestimate k. Let us take $v = 5$ m sec$^{-1}$, say, and $z_0$ is some kilometers, say, $z_0 = 3$ km, so that $z_0/v = 600$ seconds (10 minutes).

The expression $(1 + (e^{-k}-1)/k)^{1/2}$ is about 0.75 for $k = 2$, and tends to 1 for larger k, so that we can approximate,

$$k \simeq (is/\varepsilon_0 v)^{1/2} z_0 \qquad \text{for } k > 2. \tag{18}$$

If we use $s = 5 \times 10^{-3}$, as given below, $v = 5$, and $z_0 = 3000$, then $k = 7.9$. Hence, to a good approximation,

$$\tau \simeq (\varepsilon_0/ivs)^{1/2}. \tag{19}$$

It is necessary to justify the above estimate of s, which is the area of charge separating surface per unit volume of cloud. If the thermals are 100 m cubes and these occupy half the cloud volume then consider first a kilometer cube of cloud. The number of thermals (per cubic kilometer) is $0.5\ (10^9)/(10^6) = 500$ per cubic kilometer. These thermals have a frontal area of $10^4$ m$^2$ each. Thus, the relative area per cubic meter is $s = 500 \times 10^4/10^9 = 5 \times 10^{-3}$.

If $v = 5$ m sec$^{-1}$ is a reasonable estimate for the downdraft velocities,

$$\tau = (143 \times 10^3 / 5 \times 5)^{1/2} \simeq 76 \text{ seconds}. \tag{20}$$

It should be noted that the time constant is independent of $z_0$, so that the charge will separate at a similar rate over smaller distances than the total cloud depth. Even if $z_0 = 500$ m the time constant is not much longer, so that charges separate at the higher levels with about this time constant before the thermals accumulate at $-10$ °C level. Thus the steady state condition on which this model is based is established without appreciable delay near the cloud top, so that there is no need for the whole cloud to be filled with charge generating surfaces so as to ensure that a steady state is reached everywhere before these time constants can be considered reasonable estimates. This condition assumes, of course, that the positive charge is released from the equivalent negative charge reasonably soon after it is generated, say within 500 m, rather than adhering strictly to the assumption that the positive charge was all carried down to the $-10$ °C level, with the negative charge generating surface, before it was released. This assumption was only introduced to simplify the calculation, which it achieves because it keeps the field linear with depth. The next step probably needs a computer.

Thus the field doubles each 53 seconds (i.e. increases by a factor $e = 2.718$ in 76 seconds), which, starting with a fair weather field of 10 V m$^{-1}$ gives, in 13 minutes,

$$E = 270{,}000 \text{ V m}^{-1}.$$

This field growth rate seems sufficient to produce lightning in the times observed. It is perhaps a little confusing that it does not depend on the cloud depth but the reason is that while a deeper cloud produces more charges on each thermal it takes longer for the thermals to cover the distance, and the two effects cancel.

This model simplifies the process rather severely but it does appear to recognize the essential features of the mechanism, except for the likelihood of higher than average growth rates resulting from variations in the growth rate which could provide an advantage wherever the field is greater than the average.

At the average field strength estimated for 13 minutes growth, we should expect internal corona to be starting, particularly if large, sharp edged, ice crystals are present.

## 9. — TESTING THE THEORY.

The most obvious aspect of this thunderstorm charge separation theory is that it does not need larger falling particles to carry the charge downwards. However any particle charge microscale separation mechanism which works as soon as freezing starts, will also give rise to macroscale charge separation by essentially the same mechanism, once entrainment at cloud tops begins to affect a part of the cloud high enough to be cold enough to freeze. Large falling particles are not needed in either case.

Thus measurements directed at the early stages of cloud growth, in the beginning of the thunderstorm development cycle, will be more likely to identify charge separation processes not relying on precipitation. The sudden onset of an electric field change, when the cloud top reaches −15 °C, for example, is quite significant if no precipitation is present for a few thousand feet below the tops. Our initial observations showed electric field reversals in such cloud at about the −8 °C level when the tops reached −15 °C. The fields were about 100 V $m^{-1}$ in magnitude. Numerous observations in stratus clouds, and non raining cumulus, are discussed by Imyanitov *et al.* (1972). These fields seem quite unrelated to any effects which might be expected from the fairweather current and so are possibly attributable to the process advanced in this paper.

The most interesting measurement will be related to the cloud ion conductivity and net charge, as compared to updrafts, air density, air temperature, and ice and water particles, at different positions in the cloud. The measurement of ion concentrations and mobility in cloud is an extremely difficult problem because any bouncing of the particles at the entry into the instrument generates new, and very large, charges by contact electrification. To solve this problem it is probably necessary to remove the particles from the airstream without contact with any surface, so that clear air methods can be used for charge and conductivity measurement.

The measurement of radio noise from clouds, well before the lightning phase, was reported in 1964 by Sartor. He concluded « ... the electrification process, at least in warm clouds, may be related to the smaller scale turbulent and cellular motions in the clouds... ». This type of observation may deserve renewed interest.

There does not seem to be any need to fly in large storms however, or to seek conditions of heavy precipitation, as these elements will just confuse the issue as far as this theory is concerned. Thus, if we concentrate on the early stages of storm development we would appear to have an experimentally practical task, but one requiring a major instrumental advance.

## 10. — CONCLUSIONS.

It is clear that a mechanism such as we have described above will lead to large negatively charged ice particles which have been joined by coagulation, and that positive charges will be found on the smaller particles found in the rising undiluted air currents. Increasing evidence shows that it is in diluted air parcels which have experienced repeated mixing that the large drops are found. This evidence was addressed at a recent conference (Telford *et al.*, 1980). Thus the observations of charges on larger particles give no way to discriminate as to the origin of the charge separation mechanisms, but the initiation of fields near cloud

tops before precipitation begins should be observable. This mechanism relies on free ions being present in clouds at about the free air conductivities near cloud top heights, with higher conductivities in the descending diluted parcels than in the less modified surrounding cloudy updrafts. In these circumstances the dynamics of the descending in-cloud thermals gives interfaces of sudden changes in conductivity at shear surfaces. Here charge separation will give rise to net negative charges in the descending air.

Recent work by Markson (1980), and Markson and Muir (1980), has shown that the ionospheric potential varies with the cosmic ray intensity, and while this may be due to higher conductivity in the air above the storms it certainly fits well with the general idea that more ions will give a higher charging rate in storms. Another interesting relationship was discovered by Bigg (1966) who showed that the radio noise from the planet Jupiter increased, on average, when the moon IO was almost perpendicular to the Jupiter to Sun direction. Since Jupiter is believed to have lightning storms (Lanzerotti *et al.*, 1980) in strongly convective clouds of ammonia particles, and in ice-water clouds also, and the cosmic ray modulation on earth is caused by the magnetic fields carried by the solar wind, it seems likely that the present theory may provide an explanation of these results as well. The ion clouds released by IO's volcanoes interacting with the solar wind, and so affecting the cosmic rays, may be the link in this case.

Thus the theory proposed here seems to be adequate in terms of producing sufficient charge (criterion (a)), at sufficient electric potential, in the time scale observed (criterion (b)). It gives a physical mechanism for relating convective vigor with electrical activity (criterion (c)), and explains the charge concentration at the −10 °C to −20 °C level (criterion (d)).

The charge separation process uses ions in the cloud air to provide the charges so that the ionization resulting from lightning processes could well assist this process rather than acting solely as a dissipating mechanism (criterion (e)). Since the charge is separated by the air parcels rather than the movement of the precipitation through the air the lightning could well precede precipitation (criterion (f)). The charge is negative when the fairweather field starts the process rather than the presence of another storm, which could reverse the field locally. The process gives predominantly negative charges on the precipitation, and can become more active after a sudden increase in the charge-induced coalescence between the precipitation particles. It also shows how, in unusual circumstances, lightning can develop without any ice being present in the cloud.

## 11. — ACKNOWLEDGMENTS.

We wish to acknowledge the continuing support from the Office of Naval Research in turbulence and electrical research, and the personal encouragement of Mr. James Hughes of that office. Dr. Steve Chai was a great help in reading the manuscript and in making the figures. The preliminary observations mentioned were obtained during a field trip to TRIP in 1979. The observations were supported by the Meteorology Program, Division of Atmospheric Sciences, National Science Program on Grant No. ATM-7912430. Dr. Lee Parker was a great help in reading the manuscript and suggesting improvements.

It is with a renewed sense of grief that I also report that my coauthor, Dr. Peter B. Wagner was killed while flying in a supercooled water research program on 2 March 1980. I was writing the first drafts of these ideas for a research

proposal to continue Peter's electrical work, when the aircraft apparently became unstable and entered an uncontrollable vertical dive, and was shattered on impact. Peter was at the height of a scientific career replete with promise, and was my very close friend. I greatly missed his continuing help and critical scientific discussion which would have much improved this paper. We were at the stage of considering the feasibility of these ideas and had discussed the concept in some detail, so I have finished the paper alone.

Dr. William Gaskell, who was one of the most promising young scientists entering the field, was also aboard and died in the impact, together with the two pilots, John Lapham and Gordon Wicksten, both men of extraordinary experience, skill, and dedication.

---

## REFERENCES


BENNETTS, D.A., P. RYDER, J. LATHAM and I.M. STROMBERG, 1980 : The electric field structure of convective cloud. *Abstracts, VI Int. Conf. Atmospheric Electricity,* Manchester, 28 July-1 August, 1980, Paper XI, 6.

BIGG, E.K., 1966 : Periodicities in Jupiter's decametric radiation. *Planet. Space Sci.,* 14, pp. 741-758.

CHRISTIAN, H.J., C.B. MOORE, J.W. BULLOCK, W. GASKELL, A.J. ILLINGWORTH and J. LATHAM, 1980a : Airplane measurements of electric fields inside thunderstorms. *Abstracts, VI Int. Conf. Atmospheric Electricity,* Manchester, 28 July-1 August, 1980, Paper XII, 7.

CHRISTIAN, H.J., M. WEBER, M.F. STEWART and A.A. FEW, 1980b : Balloon measurements of electric fields inside thunderstorms. *Abstracts, VI Int. Conf. Atmospheric Electricity,* Manchester, 28 July-1 August, 1980, Paper XI, 10.

CHIU, C.S., and J.D. KLETT, 1976 : Convective electrification of clouds. *J. Geophys. Res.,* 81, pp. 1111-1124.

GASKELL, W., A.J. ILLINGWORTH, J. LATHAM and C.B. MOORE, 1978 : Airborne studies of electric fields and the charge and size of precipitation elements in thunderstorms. *Quart. J. Roy. Meteor. Soc.,* 104, pp. 447-460.

GUNN, R., 1954 : Diffusion charging of atmospheric droplets by ions, and the resulting combination coefficients. *J. Meteor.,* 11, pp. 339-347.

HEYMSFIELD, A.J., P.N. JOHNSON and J.E. DYE, 1978 : Observations of moist adiabatic ascent in northeast Colorado cumulus congestus clouds. *J. Atmos. Sci.,* 35, pp. 1689-1703.

HOLITZA, F.J., and H.W. KASEMIR, 1974 : Accelerated decay of thunderstorm electric fields by chaff seeding. *J. Geophys. Res.,* 79, pp. 425-429.

ILLINGWORTH, A.J., and J. LATHAM, 1977 : Calculations of electric field growth, field structure and charge distributions in thunderstorms. *Quart. J. Roy. Meteor. Soc.,* 103, pp. 281-295.

IMYANITOV, I.M., Ye.V. CHUBARINA and Ya.M. SHVARTS, 1972 : Electricity of clouds. NASA Technical Translation F-718.

ISRAEL, H., 1970 : *Atmospheric Electricity,* Vol. I, Translated from German, Israel Program for Scientific Translations Ltd., 317 p.

ISRAEL, H., 1973 : *Atmospheric Electricity,* Vol. II, Translated from German, Israel Program for Scientific Translations Ltd., 478 p.

KASEMIR, H.W., F.J. HOLITZA, W.E. COBB and W.D. RUST, 1976 : Lightning suppression by chaff seeding at the base of thunderstorms. *J. Geophys. Res.,* 81, pp. 1965-1970.

KREHBIEL, P.R., M. BROOK and R.A. McCORY, 1979 : An analysis of the charge structure of lightning discharges to ground. *J. Geophys. Res.,* 84, pp. 2432-2456.

LANZEROTTI, L.J., K. RINNERT, E.P. KRIDER, M.A. UMAN, G. DEHMEL, F.O. GLIEM and W.I. AXFORD, 1980 : Planetary lightning and lightning measurements on the Galileo Probe to

Jupiter's atmosphere. *Abstracts, VI Int. Conf. Atmospheric Electricity,* Manchester, 28 July-1 August, 1980, Paper VIII, 1.

MARKSON, R., 1980 : Modulation of the earth's electric field by cosmic radiation. *Abstracts, VI Int. Conf. Atmospheric Electricity,* Manchester, 28 July-1 August, 1980, Paper III, 2.

MARKSON, R., and M. MUIR, 1980 : Solar wind control of the earth's electric field. *Science,* 208, pp. 979-990.

MASON, B.J., 1976 : In reply to a critique of precipitation theories of thunderstorm electrification by C.B. Moore. *Quart. J. Roy. Meteor. Soc.,* 102, pp. 219-225.

MOORE, C.B., 1974 : An assessment of thundercloud electrification mechanisms. *Proc. 5th Int. Conf. Atmospheric Electricity,* Garmish-Partenkirchen, F.R. Germany.

MOORE, C.B., 1976 : Reply [to B.J. Mason — see Mason (1976)]. *Quart. J. Roy. Meteor. Soc.,* 102, pp. 225-238.

MOORE, C.B., B. VONNEGUT, B.A. STEIN and H.J. SURVILAS, 1960 : Observations of electrification and lightning in warm clouds. *J. Geophys. Res.,* 65, pp. 1907-1910.

MOORE, C.B., B. VONNEGUT, E.A. VRABLIK and D.A. McCAIG, 1964 : Gushes of rain and hail after lightning. *J. Atmos. Sci.,* 21, pp. 646-665.

PALUCH, Ilga R., 1979 : The entrainment mechanism in Colorado cumuli. *J. Atmos. Sci.,* 36, pp. 2467-2478.

SARTOR, J.D., 1964 : Radio observations of the electromagnetic emission from warm clouds. *Science,* 143, pp. 948-950.

TELFORD, J.W., 1975 : Turbulence, entrainment and mixing in cloud dynamics. *Pure Appl. Geophys.,* 113, pp. 1067-1084.

TELFORD, J.W., and P.B. WAGNER, 1974 : The measurement of horizontal air motion near clouds from aircraft. *J. Atmos. Sci.,* 31, pp. 2066-2080.

TELFORD, J.W., and P.B. WAGNER, 1979 : Electric charge separation in severe storms. *Pure Appl. Geophys.,* 117, pp. 891-903.

TELFORD, J.W., and S.K. CHAI, 1980 : A new aspect of condensation theory. *Pure Appl. Geophys.,* 118, pp. 720-742.

TELFORD, J.W., and P.B. WAGNER, 1980 : The dynamical and liquid water structure of the small cumulus as determined from its environment. *Pure Appl. Geophys.,* 118, pp. 935-962.

TELFORD, J.W., P.B. WAGNER and S.K. CHAI, 1980 : The modification of drop spectra in sea stratus by entrainment. *Proc. VIII Conf. Int. Physique des Nuages,* Clermont-Ferrand, France, 15-19 July, 1980, II, pp. 353-356, Paper III, 1.12.

VONNEGUT, B., 1955 : Possible mechanism for the formulation of thunderstorm electricity. *Proc. Conf. Atmospheric Electricity,* Geophys. Res. Papers 42, AFCRL-TR-55-222, pp. 169-181.

WAGNER, P.B., and J.W. TELFORD, 1976 : The measurement of air motion in and near clouds. *Preprints Int. Conf. Cloud Physics,* Boulder, pp. 669-672.

WARNER, J., and J.W. TELFORD, 1967 : Convection below cloud base. *J. Atmos. Sci.,* 24, pp. 374-382.

★

*(Reçu le 5 décembre 1980,*
*et, après révision, le 24 mars 1981)*

PAGEOPH, Vol. 119 (1980/81) 0033–4553/81/002278–16$01.50 + 0.20/0


# The Surface Roughness and Planetary Boundary Layer

By JAMES W. TELFORD[1])

*Abstract* – Applications of the entrainment process to layers at the boundary, which meet the self similarity requirements of the logarithmic profile, have been studied. By accepting that turbulence has dominating scales related in scale length to the height above the surface, a layer structure is postulated wherein exchange is rapid enough to keep the layers internally uniform. The diffusion rate is then controlled by entrainment between layers. It has been shown that theoretical relationships derived on the basis of using a single layer of this type give quantitatively correct factors relating the turbulence, wind and shear stress for very rough surface conditions.

For less rough surfaces, the surface boundary layer can be divided into several layers interacting by entrainment across each interface. This analysis leads to the following quantitatively correct formula compared to published measurements.

$$\frac{\sigma_w}{u^*} = \left(\frac{2}{9Aa}\right)^{1/4}\left(1 - 3^{1/2}\frac{a}{k}\frac{d_n}{z}\frac{\sigma_w}{u^*}\frac{z}{L}\right)^{1/4}$$

$$= 1.28(1 - 0.945(\sigma_w/u^*)(z/L))^{1/4},$$

where $u^* = (\tau/\rho)^{1/2}$, $\sigma_w$ is the standard deviation of the vertical velocity, $z$ is the height and $L$ is the Obukhov scale length. The constants $a$, $A$, $k$ and $d_n$ are the entrainment constant, the turbulence decay constant, Von Karman's constant, and the layer depth derived from the theory. Of these, $a$ and $A$, are universal constants and not empirically determined for the boundary layer.

Thus the turbulence needed for the planar model of convection, which resides above these layers and reaches to the inversion, is determined by the shear stress and the heat flux in the surface layers. This model applies to convection in cool air over a warm sea. The whole field is now determined except for the temperature of the air relative to the water, and the wind, which need a further parameter describing sea surface roughness.

As a first step to describing a surface where roughness elements of widely varying sizes are combined this paper shows how the surface roughness parameter, $z_0$, can be calculated for an ideal case of a random distribution of vertical cylinders of the same height. To treat a water surface, with various sized waves, such an approach modified to treat the surface by the superposition of various sized roughness elements, is likely to be helpful. Such a theory is particularly desirable when such a surface is changing, as the ocean does when the wind varies.

The formula,

$$\frac{0.118}{a_s C_D} < z_0 < \frac{0.463}{a_s C_D(u^*)},$$

is the result derived here. It applies to cylinders of radius, $r$, and number, $m$, per unit boundary area, where $a_s = 2rm$, is the area of the roughness elements, per unit area perpendicular to the wind, per unit distance downwind. The drag coefficient of the cylinders is $C_D$. The smaller value of $z_0$ is for large Reynolds numbers where the larger scale turbulence at the surface dominates, and the drag coefficient

[1]) Desert Research Institute, Atmospheric Sciences Center, University of Nevada, Reno, NV 89506, USA.

is about constant. Here the flow between the cylinders is intermittent. When the Reynolds number is small enough then the intermittent nature of the turbulence is reduced and this results in the average velocity at each level determining the drag. In this second case the larger limit for $z_0$ is more appropriate.

## 1. Introduction

In studying methods for deriving the heat and moisture fluxes over the ocean as compared to over land, there is a fundamental difference. Over land the total flux of radiative heat is an input variable since very little solar radiation is stored in the land surface and the temperature rises until the convection takes away almost as much heat as is entering the surface. Over the sea the solar radiation is very slow to change the sea surface temperature, so that the heat (and moisture) flux is a function of the temperature difference between the air and the sea, as the basic input parameter.

Interest in the boundary layer continues as improve airborne measurement techniques allow observations to be extended over the open sea, where the influence of the fluxes on the general atmospheric circulation is clearly of importance. However, these studies are usually related to theory founded on non-dimensional and similarity based relationships, without any mechanistic model to give quantitative formulae; empirical constants appear frequently, and are determined from the measurements. This paper advances previous mechanistic theory for the surface boundary layer (Telford and Priestley, 1978) to include the surface contour, for an ideal case. It provides an explanation of how an ideal surface of equal, randomly distributed, vertical cylinders controls the scale of the turbulent flow, so that the surface roughness height is no longer an empirical parameter, but can, at least in the certain cases discussed here, be calculated from the given surface profile.

The importance of an explanation of how the surface profile relates to the roughness length in the logarithmic wind-height formula, lies in the fact that the logarithmic profile is itself an idealization. If we are to understand flux transfers where the surface is not a uniformly grassed plane with large unobstructed fetch, or where the surface changes with changing wave structure, then we need to understand the mechanism involved. The importance of this understanding has recently been stressed by the study of flux-profile relationships above tall vegetation by Hicks, Hess and Weseley (1979) and the discussion which followed by Raupach, Stewart and Thorn, and Garrett.

Since the equations for the convective plume planetary boundary layer use turbulence, heat flux and layer depth as the determining parameters (Telford, 1972) we need to derive these from more general atmospheric factors. The layer depth depends on the previous history of the air mass which we will take as given at this stage in the research. The turbulence is a function of the surface shear stress which is determined by the layer depth, the horizontal pressure gradient, and the Coriolis forces. Given also the temperature difference between the air and the surface, the heat flux and the wind speed can then be determined if the surface roughness can be

specified. This paper shows how the surface roughness can be calculated for an ideal surface profile.

## 2. *The surface boundary layer and the shear stress*

We will briefly describe the theory as developed by TELFORD and PRESLEY (1978) for the convective layer. Above a height of about 60 m convection is organized into rising plumes of warm air separated by slightly cooler descending regions, while below this height the warmer rising parcels chaotically mingle with the cooler descending parcels.

Until buoyancy becomes very large heat is transferred by parcels in which the momentum essentially stays with the air. At large buoyancy, momentum can be transferred by pressure forces before the heat is deposited at any given level because the buoyancy moves the parcel even after initial momentum is lost. Assuming the momentum and heat are transferred together, we can relate the heat entering the plumes from the subplume layer to the erosion of surface air into the subplume layer. The analogous equations apply to horizontal momentum, or shear stress.

Thus,

$$\tau = \rho w_p \Delta u/2 = \rho v_{av} a i_s$$

The shear stress is $\tau$, $\rho$ is the air density, $w_p$ the plume updraft velocity and $\Delta u$ the difference in horizontal velocity between the descending air and the rising plume. The middle expression in the equation is the vertical transfer of horizontal momentum downwards by the air around the plumes. The horizontal velocity of the layer is $v_{av}$. The right hand expression is the loss of horizontal momentum from the subplume layer to the stationary surface layer, where $a$ is the entrainment constant and $i_s$ is the turbulence in the subplume layer, the erosion rate thus being $ai_s$.

The generation rate of turbulent energy per unit volume in the subplume layer is $\tau v_{av}/D$ joules $m^{-3}$ $sec^{-1}$, where $D$ is the layer depth. The decay rate in this layer, where $1/2\rho i_s^2$ is the turbulent energy density, is

$$\frac{di_s^2}{dt} = -\frac{Ai_s^3}{D},$$

where $A = 1$ has been determined by wind tunnel measurements.

Thus in equilibrium,

$$\frac{\tau v_{av}}{D} = \frac{\rho A i_s^3}{2D}.$$

Thus,

$$v_{av}^2 a i_s = \frac{A}{2} i_s^3,$$

$$i_s^2 = \frac{2a}{A} v_{av}^2.$$

Now $A = 1$, and $a = 1/12$, from laboratory measurements (see TELFORD, 1966, 1970, 1975). There are theoretical reasons for using $a = 1/12$ rather than the measured value which is nearer to 1/13.

Thus,

$$l_i^2 = v_{av}^2/6.$$

Also,

$$\tau = \rho a l_i \left(\frac{A}{2a}\right)^{1/2} l_v$$

and introducing $u^*$, with the defining formula $\tau = \rho u^{*2}$,

$$l_i^2 = \left(\frac{2}{aA}\right)^{1/2} u^{*2} = 4.9u^{*2}.$$

These expressions agree quantitatively with observations over very rough terrain. When $3\sigma_w^2 = l_i^2$, $\sigma_w$ being the vertical component of the turbulence,

$$\frac{\sigma_w}{u^*} = 1.28.$$

Further analysis (see TELFORD and PRESLEY, 1978) gives

$$\frac{\sigma_w}{u^*} = 1.28 \left(1 - 0.945 \frac{\sigma_w}{u^*} \frac{z}{L}\right)^{1/4}.$$

This is in good quantitative agreement with the observations as summarized by MONIN and YAGLOM (1971), Fig. C. Thus the turbulence can be expressed in terms of the total convective layer depth and the horizontal pressure gradient, with a correction for height and stability. This expression is independent of surface roughness.

### *3. The variations in the surface boundary layer*

In developing the last equation, it was necessary to consider several uniform parallel layers of exponentially decreasing depth subdividing the subplume layer. This step introduced the concept of surface roughness, which controls the size of the lower layers and hence the number of layers needed to reach the level of the plumes. Although this subdivision does not enter explicitly into the above formula, it does directly control the windspeed and temperature differences. This is because the difference of these two quantities between adjacent layers is always the same and so more layers give a larger total change to wind and temperature from the surface up.

With several layers the variable $v_{av}$ becomes $\Delta v$, across each layer, so that for $n$ layers the wind speed is $v_n = n\,\Delta v$, where $\Delta v = \tau/(\rho a l_i)$. Similarly the temperature at

plume level becomes, $T = T_s + n\Delta T$, where $T_s$ is the surface temperature and $\Delta T = H/(\rho C_p a i_s)$.

The temperature increment across each layer is $\Delta T$, $H$ is the heat flux, and $C_p$ is the specific heat of air at constant pressure.

Thus the relationship we need between the air temperature and the surface temperature depends on $n$, which depends on the surface roughness. Thus, if we know $n$, and are given $T$, $T_s$ and $\tau$ (from the pressure gradient and the total convective layer depth), we can determine $H$, $i_s$, $v$, and even the moisture flux, if we have the mixing ratio some distance above the surface.

We will now discuss how the number of layers, $n$, relates to the roughness height $z_0$, and will extend the theory to relate $z_0$ to the physical surface structure in a simplified case.

From earlier equations we have,

$$v_n = n\tau/(\rho a i_s), \qquad i_s^2 = (2/aA)^{1/2} u^{*2}.$$

Thus,

$$v_n = nu^{*2}/(a i_s),$$

and so,

$$\frac{v_n}{u^*} = \left(\frac{A}{2a^3}\right)^{1/4} n.$$

From the usual logarithmic profile,

$$\frac{v}{u^*} = \frac{1}{k} \ln (z/z_0),$$

where $k = 0.4$ is Von Karman's constant.

Thus,

$$z_n = 8.77^n z_0,$$

where $z_n$ is the height of layer $n$.

At this point the surface roughness length, $z_0$, is a parameter relating the flow to the surface velocity, usually taken as zero.

We have

$$\frac{v - v_n}{u^*} = \frac{1}{k} \ln \frac{z}{z_n},$$

if we wish to refer to the flow to the air at level $z_n$ moving with velocity, $v_n$.

The task is now to relate $z_0$ to actual surface features in a way which allows for $v_0 = v(z_0) = 0$. We should note that the origin of $z$ has been chosen so that $(dv/dz)_{z_n} = (1/k)u^*/z_n$ at some reference level.

### 4. *The representative layers*

The assumption used in deriving the formulae relating the turbulence, the wind increase for each layer, and $u^*$, given above, was that within a layer the horizontal velocity is uniform. For much of the theory it is sufficient to treat only such representative layers. Thus for a very rough surface only one layer is needed above the trees up to the plumes, and this layer has a constant average velocity, $\Delta v$. Entrainment with a layer of air between the trees, of effectively zero velocity, then completes the model. Such a single layer is independent of the roughness length since its thickness is determined by the flow back from downdraft to updraft in the plumes. When the surface roughness is smaller, however, additional layers are needed, but adding exactly one or two uniform layers is not sufficient. While it is still helpful to think of a set of representative layers beginning at the top of the roughness elements, each with average velocity $\Delta v$ greater than the layer below, we must consider some form of fluctuations in velocity or height to give the average smoothly varying velocity gradients observed. In this way we can also generate a flow field among the roughness elements which would otherwise be in the zero velocity layer.

In the layers themselves the mixing of entrained air from adjacent layers is very rapid over the distance of one layer depth, but mixing beyond that depth is limited by the entrainment exchange between layers. These layers are continually reforming and shifting so that the transition between one layer and the next can be found at any height with appropriate probability over a long time period. If a layer always has the correctly scaled average thickness, and still keeps a uniform average velocity, then a probability can be found such that the velocity averages at a given height as the layers fluctuate in height will give a self-similar velocity profile (as specified by the usual logarithmic profile). In such a distribution no layer needs to move up or down more than half way to the next layer. We will need to consider below such a statistical ensemble of layers to relate quantitatively the average turbulent length scales to the surface roughness.

We need to choose a field of properly scaled layers so that on average they represent the whole ensemble. Thus if $v_n$ is the velocity of representative layer $n$, and $v_{n-1}$ the velocity of layer $(n-1)$, then the transition between these representative layers should occur where the average velocity over all distributions of the layer positions in the ensemble, is $v_{n-1/2}$.

When we refer to layer $n$ we mean the representative layers, where layer 1 starts at the top of the crops, or the smaller roughness elements, and the higher layers join contiguously above this one. The next step in detail is to consider fluctuating heights which are introduced so that while representative layer $n$ extends from $z_{n-1/2}$ to $z_{n+1/2}$ it is allowed to fluctuate up to between $z_n$ to $z_{n+1}$ and down to $z_{n-1}$ to $z_n$ to generate the final flow field.

From the earlier analysis we have, at $z_n = 8.77^n z_0$,

$$v_n = (A/2a^3)^{1/4} u^* n,$$

and so, at $z_{n-1/2} = 8.77^{n-1/2} z_0$,

$$v_{n-1/2} = (v_n + v_{n-1})/2 = (A/2a^3)^{1/4} u^*(n - 1/2).$$

This choice makes the average velocity of two layers above and below their junction equal to the velocity from the logarithmic profile, at this level. Thus the representative layers are matched in velocity to the logarithmic profile height at the levels of the transitions between layers. Furthermore we have taken the equivalent height for the layer itself as the level on the logarithmic profile with the same velocity, so that the self similar profile velocity matches both at a point in the layer as well as at the level separating the layers. Other levels within the layers will be related to the appropriate average velocities as the representative layers fluctuate up and down in height. A point at each height spends most of the time at the velocity of its representative layer, but some fraction of the time is spent in the flow from the adjacent layer as it moves up or down to flow over the point, so that the average velocity at each height is correct when the ensemble of layers over all variations in height is averaged.

### 5. *The surface roughness*

We now need to consider how the representative layers we have chosen relate to the roughness length in the logarithmic formula. On the above basis the layer with velocity equal to 0, lies between the levels where the velocity corresponds to $n = 1/2$ and $n = -1/2$.

If $d_n$ is the thickness of the layer which has a velocity given by

$$v_n = \frac{u^*}{k} \ln\left(\frac{z_n}{z_0}\right),$$

and $z_n = 8.77^n z_0$, then,

$$d_0 = (8.77^{1/2} - 8.77^{-1/2})\, z_0$$

$$= 2.62 z_0,$$

and $d_n = (8.77^{1/2} - 8.77^{-1/2})\, z_n = 2.62 z_n$.

We now need to examine how a standard roughness surface interacts with the lowest layer. The first layer above the roughness elements is layer $n = 1$, which lies between levels $z_{1/2}$ and $z_{1.5}$, while the equivalent stationary surface layer needed to absorb the momentum taken up by the roughness elements lies between $z_{-1/2}$ and $z_{1/2}$.

If we consider the roughness elements as being vertical cylinders of radius $r$, with $m$ cylinders randomly distributed over unit area of the surface and of vertical depth greater than, say, the layer above, then we can calculate the extent to which the moving air of the first layer must penetrate between the cylinders so that the drag is sufficient to exactly balance the shear stress.

These drag cylinders can be regarded, from the point of view of momentum transfer, as extracting moving air from the layer and replacing it with stationary air. This will effect a momentum transfer equal to the actual drag of the cylinders, just as if it was the result of the erosion from an underlying layer of turbulent air. This latter process is the same as the entrainment process transferring momentum between all higher layers. The question is, how does the scale of the roughness elements set the scale of the turbulent layer just above it?

Let us assume the roughness elements lie below the first moving layer of air, where $n = 1$. If we remember our earlier formulation described above, the effective turbules (the word turbule is used to identify a coherent turbulent entity which exists long enough to transfer from one position to another) carried momentum (and heat, etc.) a distance of one layer thickness at each entrainment event, so that the whole depth of this layer exchanges air with the layer between the roughness elements.

However, we must now return to consider the whole statistical ensemble of variations in the heights of the interfaces between layers. The layer of air between the roughness elements would otherwise be a zero velocity layer if we only considered it as one of the representative layers without taking account of their fluctuations up and down.

To simulate the average smooth velocity distribution with height the ensemble of turbulent motions can be divided into subsets as follows. From the total infinite turbulent field select those motions of elements from one level to another where the logarithmic mean of the starting and finishing height lies at level $z_n$. Now take the mean of the distance travelled (actually we need to take the logarithmic average of the height in each category, and take the difference, so as to comply with the requirement for the self-similarity of the motion in terms of scaling in relation to the distance in the fluid from the surface boundary); this distance is the layer depth, $d_n$, for a layer at characteristic height $z_n$. Similar selection can be made from the ensemble of motions about the level $z_{n-1}$, and averaging them defines the next compatible layer, and so the field can be reassembled into subsets of layers. Another subset of layers can be selected at height $z_{n-0.1}$ say, and so on, for all heights not already selected between $z_{n-1}$ and $z_n$.

Now each of these subsets complies with the formulae presented above, so that the formulae always apply, regardless as to which subset the particular motion at a given position at any particular time actually belongs. However, the length of the surface roughness elements is fixed, and does not vary so as to remain similar to the layer depths, from subset to subset, and hence some type of averaging will need to be introduced to match the ensemble with the fixed surface roughness. It is now possible to further subdivide the subsets into velocity classifications, but since the requirement is that the time averaged velocity at each height must match a self-similar logarithmic profile, this distribution can be achieved by using the same average velocity for a given layer, as in the closest representative layer, but allowing the layer to move up and down a half layer depth, to generate the velocities needed for a fuller description of the flow.

Hence the first layer always has velocity $\Delta v$, regardless of its level relative to roughness elements. This is probably the simplest assumption which leads to the correct velocity profile, rather than using more complex assumptions with a range of velocities for each of the layers, as their height varies, between ensemble subsets. The first layer fluctuates in height and for half the time penetrates varying distances into the roughness elements. The top of the roughness elements coincides with the bottom of the first representative layer, $z_1$, which is at height $z_{1/2}$.

This averaging process can be explained as follows. The air at $z_n$ is always in the layer of velocity $v_n$, thus the mean velocity averaged over all subsets at $z_n$, is $v_n$. All heights just above $z_n$ must occasionally be in the layer of velocity $v_{n+1}$, when all ensemble subsets are considered, so that their average velocity will be a little higher, and vice versa, heights just below $z_n$ must occasionally be swept, in other subsets, by the layer below of velocity $v_{n-1}$.

Thus at level $z$, where $z_n \leq z < z_{n+1}$, if the layer $z_{n+1}$ with velocity $v_{n+1}$, is present for a fraction of the time, $f$, then the average velocity is,

$$v(z) = (1-f)v_n + fv_{n+1}.$$

We can determine $f$ as a function of $z$.

$$v(z) = \frac{u^*}{k} \ln \frac{z}{z_0},$$

so that,

$$\ln \frac{z}{z_0} = \ln \frac{z_n}{z_0} + f\left(\ln \frac{z_{n+1}}{z_0} - \ln \frac{z_n}{z_0}\right),$$

and,

$$f = \ln \frac{z}{z_n} \Big/ \ln \frac{z_{n+1}}{z_n}.$$

Thus,

$$v(z) = v_n + \left(\ln \frac{z}{z_n} \Big/ \ln \frac{z_{n+1}}{z_n}\right)(v_{n+1} - v_n).$$

The height $z_n$ is the only level which is always within the limit of variation of the upper and lower boundaries of its representative layer.

In this picture, with constant velocity within layers, the smooth variations of average velocity with height are the result of each layer fluctuating in height about the representative positions. Underneath the lowest layer, where the stationary roughness elements remove the momentum from the air, we place a representative zero velocity layer. The motion within this roughness layer results from the downward displacement of the lowest free air representative layer as it fluctuates in height, and this airmotion provides the drag on the roughness elements needed to absorb the shearing stress.

While the representative layers give a first approximation to the flow field, and their motion up and down gives the second approximation, the actual details of how the flow distributes the drag with depth as it penetrates between the roughness elements well be more complex and need closer study. The differences arise because the drag forces dissipate the turbulence in quite a different way to that occurring in the layers above the surface where the turbulence breaks up its own irregular turbulent motion into smaller scales. The vertical components of the turbulence in a grid of vertical cylinders will be much less damped than the horizontal components, and energy will probably transfer from horizontal turbulence to the vertical component. Thus, the forward motion will penetrate deeper than the self-similarity in the free stream would imply. Most of the momentum will be lost, however, near the top of the layer where the speed is greatest and the modifications to the profile are the least.

### 6. *The drag of the surface elements*

Since the motion between the surface elements has been specified we can now consider the drag. Assume the surface consists of vertical cylinders of radius $r$, all of equal height and high enough so that no significant drag is transmitted to the substrate below them. They are randomly spaced with $m$ cylinders per unit area. Drag is exerted on this array by horizontal air currents so that we need the drag coefficient of each element of the array, and the area of the array per unit area across stream, per unit length along the wind direction. If we call this fractional area $a_s$ then $a_s = 2rm$.

Defining the drag coefficient on an individual cylinder as $C_D = F/((1/2)\rho v^2(2r))$ per unit length, where $F$ is the force, then the total drag force per unit surface area of the boundary becomes,

$$\tau = \frac{\rho}{2} a_s \int_{-\infty}^{z_{1/2}} \times v^2(z)\, C_D(v)\, dz.$$

The drag coefficient is somewhat variable as a function of Reynold's number, $R_e$. At very low Reynold's number ($R_e < 5$ say), the drag coefficient is $C_D = 8\pi/(R_e(\ln(8/R_e) - 0.57722 + 1/2))$. With increasing Reynold's number it then becomes almost constant, at about $C_D = 1.2$ ($C_D = 0.6$ if defined as $C_D = F/(\rho v^2(2r))$), until it drops by a factor of three to about 0.4 when turbulent separation sets in around the cylinder at Reynold's numbers of about $10^5$. A 1 mm diameter cylinder in air moving at 10 cm sec$^{-1}$ has a Reynold's number of about 7, while a 1 m diameter tree top in a wind of 10 m sec$^{-1}$ has a Reynold's number of $7 \times 10^5$.

Let us first estimate the drag using a drag coefficient independent of velocity.

$$\tau = \frac{\rho}{2} a_s C_D \int_{z_0}^{z_{1/2}} v^2(z)\, dz,$$

since $v = 0$ at $z = z_0$, this value of $z$ is taken as the lower terminal for the integration.

Using the velocity for the logarithmic profile described above for the layer between $z_0$ and $z_1$, where the layer velocity at $z_1$ is $v_1 = \Delta v$,

$$v(z) = \left(\ln\left(\frac{z}{z_0}\right) \Big/ \ln\left(\frac{z_1}{z_0}\right)\right) \Delta v.$$

If we assume the velocity is first averaged with time and then squared we find,

$$\int_{z_0}^{z_{\nu 2}} v^2(z)\, dz = (\Delta v)^2 \int_{z_0}^{z_{\nu 2}} \left(\ln\left(\frac{z}{z_0}\right) \Big/ \ln\left(\frac{z_1}{z_0}\right)\right)^2 dz$$

$$= (\Delta v)^2 z_0 \left[\frac{z}{z_0}\ln^2\frac{z}{z_0} - \frac{2z}{z_0}\left(\ln\frac{z}{z_0} - 1\right)\right]_{z_0}^{z_{\nu 2}} \Big/ \ln^2\left(\frac{z_1}{z_0}\right) = 0.209\,(\Delta v)^2 z_0$$

Thus,

$$\tau/(\rho \Delta v^2) = (u^*/\Delta v)^2 = (2a^3/A)^{1/2} = 0.104 a_s C_D z_0$$

and,

$$z_0 = 9.59\,(2a^3/A)^{1/2}/(a_s C_d),$$

$$z_0 = \frac{0.326}{a_s C_D}.$$

Before continuing we can compare this result with work by KONDO (1971, 1972) and KONDO and AKASHI (1976) who obtained a similar result where,

$$z_0 = \frac{4k^2}{C_D 2rm} e^{-1} = \frac{0.235}{C_D 2rm} = \frac{0.235}{a_s C_D}$$

This result was obtained from a solution for the horizontal flow within the drag elements based on the assumption of a constant mixing length and gradient diffusion of momentum. The velocity $u$ and its first derivative, are made equal where the flow matches the logarithmic flow above, at the top of the drag elements. For the exponential solution which results, both these quantities can then be determined from the shear stress and the geometry of the roughness elements. The first derivative of $v$ with height then gives the origin of $z$, and the value of $v$ at this level gives $z_0$. By using this procedure, however, the curvature of the $u(z)$ profile is reversed in sign at the interface. Comparisons of this formula with data from corn crops gave $z_0$'s which were perhaps 50% too high, so that our initial estimate of $z_0$ is too large by a factor of about 2 for this same data. However, as discussed below, if we consider the variation of the drag coefficient and the intermittent nature of the turbulence better results are obtained.

### 7. *Variation of the drag coefficient*

Let us examine a direct comparison with some careful measurements made by THOM (1971), above an artificial crop, consisting of 1 mm diameter rods (14.3 cm long), mounted on a 1 cm grid.

Our formula applies in these conditions at low Reynold's numbers. An average drag coefficient can be derived from $\tau = \rho u^{*2} = 1/2\rho C_D u_{Av}^2$, since Thom gives $u^* = 22$ cm sec$^{-1}$. Then $u_{Av} = (2/C_D)^{1/2} u^*$ and so $u_{Av} = 19$ cm sec$^{-1}$ and $C_D = 2.7$. Note that Thom defines $C_D$ on the basis of $\rho u^2$ rather than $\rho u^2/2$ as in Kondo, and as we do here. Thus we find our formula gives $z_0 = 1.21$ cm. Any more realistic averaging process which weighted the importance of $C_D$ higher, for higher velocity and higher drag regions, would increase $z_0$ by decreasing the average $C_D$, and so improve the estimate.

The measured value Thom reports for the main body of his measurements is $z_0 = 1.37$ cm, which is in encouraging agreement with our simple estimate. However, this justification for using the drag coefficient corresponding to $u^*$ is rather oversimplified, and we will discuss more realistic estimates.

It is now necessary to introduce another important point which can be shown using Thom's measurements. When he changed the velocity of the flow at the top of the cylinders, in his experiment, through the values 25, 50, and 75 cm sec$^{-1}$, $z_0$ changed through 1.57, 1.37, and then to 1.25. Since the corresponding average drag coefficient (as averaged in Thom's paper) changed through 4.6, 3.2, and 2.7 under the same conditions there is clearly another factor needed in the formulae for $z_0$, since this relationship gives changes which are opposite to the measured trend. That is, using the changes in drag coefficients in the same proportion, our formula would give for $z_0$, 0.8, 1.2, and 1.4 cm which shows a variation in the opposite direction to the observed changes.

Thom, in discussing this point, suggested that there is a transition from viscous to turbulent flow as the Reynold's number of the flow increases.

At the lowest speed a better fit is possible if we follow Thom's suggestion and assume that approximately, $C_D \propto u^{-1/2}$ (the actual formula is more complex). We can then numerically integrate the drag including a $C_D$ varying with velocity.

We find,

$$C_D(v) = (v/u^*)^{-1/2} C_D(u^*)$$

so that,

$$\tau = \frac{\rho a_s C_D(u^*)}{2} \left(\frac{u^*}{\Delta v}\right)^{1/2} \frac{\Delta v^2 z_0}{\ln^{3/2}\left(\frac{z_1}{z_0}\right)} \int_{z_0}^{z_1/z_0} \ln^{3/2}\left(\frac{z}{z_0}\right) d\left(\frac{z}{z_0}\right).$$

Since,

$$\int_{z_0}^{z_1/z_0} \ln^{3/2}\left(\frac{z}{z_0}\right) d\left(\frac{z}{z_0}\right) = 1.0940,$$

hence,

$$z_0 = \frac{0.463}{a_s C_d (u^*)}.$$

Taking Thom's values of $u^*$ for the three speeds he uses in his measurements, namely 13, 22 and 30 cm sec$^{-1}$, we find from his Fig. 3 for $C_D$, the values 3.45, 2.5 and 2.15 (his values $\times 2$). From our last theoretical expression we thus calculate for $z_0$ the values 1.34, 1.85 and 2.15. These theoretical estimates are closest to the measurements of $z_0$ (namely 1.57, 1.37 and 1.25 cm) at the lowest velocity, and suggest that more details of the drag coefficient might give a closer fit yet for the lowest $R_e$ value. For example, the regular spacing of the cylinders used in the measurements may reduce the average drag for some wind directions and so increase $z_0$. However, the effect of the Reynold's number of the flow in reducing the measured $z_0$ as the velocity increases, must be understood better if we are to seek much closer agreement.

### 8. *Intermittent turbulence*

Let us consider how a higher Reynold's number would affect our result. In the model presented above we averaged the velocity in the roughness element before squaring it. If, however, we preserve the intermittent nature of the turbulence by assuming the velocity as always being $\Delta v$ in instantaneous magnitude, or else 0, with no intermediate values (as our model asserts), but forming an average value of,

$$v(z) = \left( \ln \frac{z}{z_0} \Big/ \ln \frac{z_1}{z_0} \right) \Delta v,$$

then the drag becomes,

$$\tau = \frac{\rho a_s C_D \Delta v^2 z_0}{2 \ln (z_1/z_0)} \int_{z_0}^{z_{1/2}} \ln (z/z_0)\, d(z/z_0)$$

$$\left( \frac{u^*}{\Delta v} \right)^2 = \left( \frac{2a^3}{A} \right)^{1/2} = 0.289 a_s C_D z_0.$$

So that under this assumption of intermittent turbulent penetration into the roughness elements, as might be expected at higher Reynold's numbers where viscous damping is less important in modifying the free stream turbulence,

$$z_0 = \frac{0.118}{a_s C_D}.$$

This is to be compared with our earlier expression,

$$z_0 = \frac{0.326}{a_s C_D},$$

when the intermittent turbulent action is smoothed over at low Reynold's numbers.

If we include the effects of a changing drag coefficient at low Reynold's numbers then,

$$z_0 = \frac{0.463}{a_s C_d(u^*)}.$$

Thus there is a range of values of 2.8:1 in $z_0$ from changes in the nature of the turbulence at different Reynold's numbers, to help explain the change of 2:1 in the values of $z_0$ measured by Thom at different windspeeds, after we have included the changes due to the drag coefficient.

This reduction in $z_0$ at higher Reynold's numbers would also allow a good fit to data quoted by KONDO (1971) in his Table 2 for plant crops (corn and forest), mentioned above, where our first low Reynold's number formula for $z_0$, using a constant $C_D$, was 2 times too large. A value of $z_0 = 0.16/a_s C_D$ would be about right if we accept the values of $a_s$ and $C_D$ used. This is within the range given for $z_0$.

Thus the formulae for the roughness length generated in the turbulent boundary layer by flow over a surface of equal length cylinders (of sufficient length to avoid drag on the substrate) is given by,

$$\frac{0.118}{a_s C_D} < z_0 < \frac{0.463}{a_s C_D(u^*)}.$$

This range of values in $z_0$ covers experimental values measured in conditions covering a wide range in Reynold's number.

The smaller value of $z_0$ occurs with larger speeds, larger surface elements, a constant drag coefficient, and higher Reynold's numbers. The larger values of $z_0$ occur with lower Reynold's numbers, smaller surface elements, and slower speeds, and a rapidly increasing drag coefficient.

There is a need for more experiments to explore this transition region since this theory now appears to offer an approach to study such variations without introducing empirical parameters.

### *9. Applications to the marine boundary*

The oceans cover a large part of the earth's surface and so constitute a major part of the boundary for any global model of the atmospheric circulation. GARRATT (1977) reviews the various approaches which have been taken to specify and measure surface drag. The subject does appear to be largely empirical in approach with the incorporation of similarity relationships, and the use of constants determined from measurements in similar conditions to those in which the formulae need to apply.

In addition to considering large scale averages of ocean surface conditions, the interest in marine stratus and fog directs us to greater concern about local conditions. The lack of a mechanistic theory of boundary layer turbulent transfer, whereby all

turbulent phenomena can be derived quantitatively by the laws of mechanics from a few unifying assumptions, tends to prevent us using our background knowledge to quantify other circumstances where direct observation is difficult.

The approach taken here tries to avoid analogies between turbulent diffusion and molecular diffusion (gradient diffusion), or rarefied gas mean free path ideas, and to explore the usefulness of analyzing turbulent flow in terms of entraining turbulent layers. To apply these ideas to smoother surfaces, such as the sea, the present relationship between the roughness elements and the flow will need to be extended to describe the coupling of a surface of mixed roughness length elements to the free air. When an adequate method for superimposing the different surface scales is discovered, the effects of changes in sea state will be more easily studied.

Once a good theoretical description of the coupling between the air and the water is formulated the large fetch found over the ocean should make it possible to test accurately boundary layer models involving fog and stratus clouds.

## *10. Conclusion*

We have established a simple physical model for the surface roughness length in terms of equal cylinders randomly distributed over the surface at a given areal density. An important application of this model will be as background to extend these ideas to surfaces of mixed element sizes, and then to derive the equivalent roughness of ocean surfaces which combine viscous drag with that contributed by various sized waves. A determination of the roughness length in this way will then give wind speeds and heat flux, given the horizontal pressure gradient, total convective layer depth, and the temperatures difference between the air and the water surface (also moisture flux, given the mixing ratio of the air). Such an approach allows a recognition of the turbulent nature of the flow, which tends otherwise to limit analytic studies, and it will hopefully lead to a theoretical background for the bulk transfer formula currently in use.

## *Acknowledgments*

This work was funded under Navy contract N00014-75-C-0598 and the encouragement of Mr James Hughes of ONR, is gratefully acknowledged.

## References

Garratt, J. R. (1977), *Review of Drag Coefficients Over Oceans and Continents*, Mon. Weather Rev. *105*, 915–929.

Hicks, B. B., Hess, G. D., and Wesley, M. L. (1979), *Analysis of Flux-profile Relationships Above Tall Vegetation – An Alternative View, With Replies*, Q. J. R. Met. Soc. *105*, 1074–1082.

KONDO, J. (1971), *Relationship Between the Roughness Coefficient and Other Aerodynamic Parameters*, J. Met. Soc. Japan *49*, 1–124.

KONDO, J. (1972), *On a Product of Mixing Length and Coefficient of Momentum Absorption Within Plant Canopies*, J. Met. Soc. Japan *50*, 487–488.

KONDO, J., and AKASHI, S. (1976), *Numerical Studies on the Two-dimensional Flow in Horizontal Homogeneous Canopy Layers*, Bound. Layer Meteor. *10*, 225–272.

MONIN, A. S., and YAGLOM, A. M. (1971), *Statistical Fluid Mechanics: Mechanics of Turbulence, Vol. 1* (The MIT Press, 1971), 769 pp.

TELFORD, J. W. (1966), *The Convective Mechanism in Clear Air*, J. Atmos. Sci. *23*, 652–666.

TELFORD, J. W. (1970), *Convective Plumes in a Convective Field*, J. Atmos. Sci. *24*, 347–358.

TELFORD, J. W. (1972), *A Plume Theory for the Convective Field in Clear Air*, J. Atmos. Sci. *29*, 128–134.

TELFORD, J. W. (1975), *The Effects of Compressibility and Dissipation Heating on Boundary Layer Plumes*, J. Atmos. Sci. *32*, 108–115.

TELFORD, J. W., and PRESSLEY, J. D. (1978), *The Surface Boundary Layer as a Part of the Overlying Convective Layer*, Pure appl. Geophys. *117*, 664–689.

THOM, A. S. (1971), *Momentum Absorption by Vegetation*, Q. J. R. Meteor. Soc. *97*, 414–428.

(Received 12th July 1980)

PAGEOPH, Vol. 120 (1982) 0033-4553/82/040648-14$1.50+0.20/0


# A Theoretical Value for von Karman's Constant

By James W. Telford[1])

*Abstract* – This paper extends the theory of the entity and entrainment model of turbulence to obtain a numerical value of von Karman's constant, $k = 0.37$.

The formula is,

$$k = (2a^3/A)^{1/4} \ln \beta$$

where, $a = \frac{1}{12}$ is the entrainment constant, $A = 1$ is the turbulent decay constant, and $\beta$ is the ratio in height of the successive self-similar layers of the theory, where $\beta$ is evaluated as $\beta = e^2$.

These new values for $k$ and $\beta$ improve the surface roughness length estimates derived from this theory.

Key words: Atmospheric turbulence; Entrainment; Turbulence; Karman constant.

## 1. Introduction

Previous studies of turbulent processes in the planetary boundary layer (Telford and Pressley, 1978; Telford, 1980), have implemented the entity concept of turbulence to explain various aspects of turbulent transfer. In this paper we will extend this theory and deduce a theoretical value for von Karman's constant.

To begin with, this approach using turbulent entities was used to formulate a quantitative description of the plumes in the convective layer above the surface boundary layer (Telford, 1966, 1970, 1972, 1975a).

The assumptions on which the theory is founded were identified after working with extensive airborne observations of the plume structure over uniform surfaces; of trees, or grass, or the sea surface. It was clear that although the layer at a given height was statistically almost the same from place to place in the same area, when considering vertical velocity fluctuations, to the extent that regions of updraft could not be recognized because the turbulent fluctuations masked the updrafts, the regions of rising warmer air were easy to identify in the temperature measurements. Their increased and fluctuating temperature, relative to the uniform level base temperature in the descending areas at the same height in the same convecting field of flow, shows them quite clearly (Warner and Telford, 1967).

[1]) Air Motions Laboratory, ASC, Desert Research Institute, University of Nevada System, Reno, Nevada 89596.

In each contiguous region defined by the temperature trace the vertical velocity fluctuates up and down several times, and since the difference between updrafts and downdrafts in average velocities are no larger in magnitude than the fluctuations due to the turbulence, no clearly defined regions of updrafts or downdrafts can be distinguished. Upward motion correlated, of course, with warmer air, as there is a large upward heat flux, but averages in a particular updraft or downdraft are too statistically variable to show discernible average motion (without data treatments involving filtering or averaging, or some such operation).

In analyzing the behavior of an isolated plume, such as can be seen in smoke or steam from chimneys, it becomes clear that the plume must be treated as a continuing entity which preserves its existence even as it grows by eroding its surroundings (TELFORD, 1967). The turbulent motion within the plume is of such a scale that it always is within the plume boundaries. This motion actually defines the plume boundary, and even though the boundary is irregular, and moving, it provides a clear interface between inside and outside. The plume does not gradually vary in properties from inside to outside to follow a gaussian profile in temperature, for example, as gradient diffusion theories suggest, even though long time averages with fixed probes appear to support this idea when only averages are considered. At any instant there is always a sharp transition between inside and outside, and the edges do not present a gradual transition.

Thus, we can conceptualize a plume as an entity which is well stirred inside, with statistically uniform composition over its cross-section at a given height. Then entrainment across this boundary provides a transfer of material from the surroundings into the plume at a rate proportional to its root mean squared turbulent velocity. This latter velocity is the variance of the velocity within the plume. The constant of proportionality giving the entrainment velocity from the turbulent velocity, was deduced from plume studies in water tanks to be about $\frac{1}{12}$ (TELFORD, 1966, 1975b).

One other constant is needed, to describe the rate of transfer of turbulent energy to smaller wavelengths from the wavelength where it is generated. The maximum wavelength, where the turbulent energy is created by entraining material at a different vertical velocity, from the surroundings outside the plume, is the diameter of the plume, since clearly the very existence of a uniform region of this size shows that plenty of turbulent stirring must be occurring over exactly this dimension.

The energy decay rate is given by,

$$-d(i^2)/dt = Ai^3/D,$$

where $i$ is the standard deviation of the velocity in the plume, $t$ is time, and $D$ is the plume diameter. The kinetic energy per unit volume within the plume is $\frac{1}{2}\rho w^2 + \frac{1}{2}\rho i^2$, where $w$ is the mean updraft velocity, and $\rho$ is the fluid density. Thus, $\frac{1}{2}\rho i^2$, is the kinetic energy per unit volume due to the turbulent fluctuations. The constant $A$ is equal to 1, as indicated by wind tunnel experiments (BATCHELOR, 1960).

Thus, a model of the convective plume field was constructed. It was assumed that the rising buoyant plumes were surrounded by a turbulent return flow downwards, and that the downdrafts entrained plume air by the same mechanism that the plumes entrained air from the downdraft. Equations for volume, mass, momentum, and kinetic energy then lead to a quantitative description of the convective field agreeing quite well with the observations (TELFORD, 1972).

## 2. *The surface boundary layer*

These ideas are now being applied to the surface boundary layer. The first stage was to examine the implications of dividing the surface layers into parallel layers which maintained self-similarity at different heights (TELFORD and PRESLEY, 1978).

The idea is basically the same as used for the plumes, but with horizontal layers forming the entities, though now there is not a clear difference in air temperature observed across the edge of a layer such as has been discerned in the measurements of vertical plumes. It is possible that this is because the layers are continually reforming, so that averaged temperatures do not show the layers. The assumption is that the turbulence still has the same basic structure as in a plume, in that a layer structure exists because within a layer the turbulent swirls are essentially maintaining internal uniformity. Transfer occurs at its upper and lower surfaces by the same turbulent entrainment process that operates through the sides of vertical plumes (TELFORD and PRESLEY, 1978). If these structures continually fluctuate in height to different heights, so that every fixed level has some exposure to each of the two layers normally above or below it, an average can be formed. The layers are subject only to self-similarity scaling in height from the surface, and in thickness of the layer relative to its height. In this way we can construct the average velocity profile observed, and then relate other variables to the height.

Since the magnitude of the turbulence resulting from the energy conservation equations does not depend on layer thickness, we can, as a first approximation, study the turbulence in the boundary layer by taking a fixed height for each of the contiguous layers. This is a first step, in which the fluctuating height of the layers can be ignored.

Such fixed representative layers were the basis of the evaluation of the vertical turbulence as a function of heights given by TELFORD and PRESLEY (1978). This gave the result (using the new value of $k$ as derived below).

$$\sigma_w/u^* = (\tfrac{2}{3}Aa)^{1/4}[1 - 3^{1/2}(D_n/z_n)\,(a/k)\,(\sigma_w/u^*)\,(z/L)]^{1/4}$$

$$= 1.28[1 - 0.919(\sigma_w/u^*)\,(z/L)]^{1/4}$$

Here $k$ is the new value of von Karman's constant, $k = 0.37$, $a$ is the entrainment constant, $a = \frac{1}{11}$, $A$ is the turbulent energy decay constant, $A = 1$. The meanings of $D_n$ and $z_n$ are explained later. The vertical component of the turbulence is $\sigma_w$, $u^*$ is the friction velocity, $L$ is the Obukhov scale length, and $z$ is the height.

### 3. *The surface roughness*

The next theoretical step was to evaluate the surface roughness length, $z_0$, from a given idealized surface of identical, randomly spaced, cylinders (TELFORD, 1980). To do this, it was necessary to adopt a better approximation by using a population of layers randomly varying in height with the correct probability to provide a logarithmic profile of velocity with height. In this way it could be assumed that the velocity of a layer was constant, but that it varied in height. The previous study had given an equal increment in horizontal velocity from one of the fixed height, representative layers, to the next. The simplest way to modify this stepped velocity profile, to match the self-similar smoothly varying average profile, was to keep the velocity of the $n$th layer constant, but allow it random fluctuations up and down, to as far as halfway to the next layer. Thus, at any given point the velocity would be an average from sharing the velocity from two adjacent layers.

When this structure encounters the surface roughness elements, we have a velocity of fluid motion between these elements which creates surface drag. Given the shearing stress, the depth of penetration required for the needed drag then follows, and this depth directly relates the size of the layers and the roughness length (TELFORD, 1980).

This simple assumption about the probability of the given velocity layer being at a particular height gives the following formula for $z_0$ (corrected for the new value of $k$, and using $\int_{z_0}^{z_{1/2}} \ln^{3/2} x\, dx = 0.83484$, where $x = z/z_0$, where $z_{1/2} = ez_0$. Previously the two constants were 0.118 and 0.463, where now we have 0.136 and 0.537).

$$0.136/a_s C_D < z_0 < 0.537/a_s C_D(u^*)$$

where, the surface roughness elements are cylinders of the same height, with radius, $r$, and $m$ cylinders per unit boundary area. Thus $a_s = 2rm$, is the area of the roughness elements, per unit area perpendicular to the wind, per unit distance downwind. The drag coefficient of the individual cylinders is $C_D$.

This new range of values for $z_0$ is in good agreement with observed values from field and laboratory experiments, and fits the data better than values derived using the earlier value of $k = 0.40$. At the lowest Reynold's number he used, THOM (1971) obtained $z_0 = 1.57$ cm experimentally, and our new value is 1.55 cm, rather than the earlier value of 1.34 cm (TELFORD, 1980). Similarly, at high Reynold's numbers $z_0 = 0.16/a_s C_D$ was measured, where our numerical constant comparable to the 0.16 is now 0.136, rather than 0.118 as previously. This aspect is discussed further below.

### 4. *Comparison of turbulent decay in this model with another configuration*

We will now show that, by comparing the turbulent decay rates we would expect for flow in the surface layer as a whole, with the decay rate for the above model, we obtain a value for von Karman's constant $k$, of $k = 0.37$.

The discussion above described how the decay of the motion in the turbulent field had been modeled as though it always represented motion within definite boundary surfaces at the edges of the entities. The turbulent motion behaves as though such surfaces are present in each region of the motion where there is an interfacial surface to a layer. It is then assumed that exchange occurs through these interfacial surfaces. It seems reasonable to believe that where actual impervious solid surfaces are present, then the motion is restrained to always match the real surface in the same way as occurs within the fluid entity, where the in-fluid entraining surface is a boundary appropriate to the motion within the entity in the fluid.

Thus, we assume that the decay of turbulence in the fluid is determined by the thickness of this parallel layer which is being used in describing the surface boundary layer, whether this layer is determined by the fluctuations of the turbulent flow within the fluid or by real boundaries.

Let us now consider how the motion is influenced by a real solid boundary. Since viscosity is assumed to be zero, then perpendicular to the boundary the motion will see an image of itself in the solid wall, so that the wall could be replaced by fluid which exactly mirrored the motion in the actual fluid. Thus, the motion at a given height will be decaying from its larger scales to smaller scales at a rate inversely proportional to its distance from the wall.

In thinking about the motion in this way we are taking a self consistent view based on self-similarity of the motion relative to the boundary surface. Since there is no natural dimension to scale the neutral, surface, planetary boundary layer, every scale is equivalent to every other scale. Thus, a layer several meters deep is indistinguishable, in a description of the motion, from a layer of half that depth, if the scale of distance and time are appropriately adjusted. Turbulent excursions from any reference level to halfway to the surface, for example, occur with identical probability at all scales.

Thus, the breakup of a turbulent swirl of a given size at a given height, into smaller swirls, occurs with the same probability at all scales in a time derived from the turbulent velocity and the scale length.

For the layers representing entities in the bulk of the fluid we have assumed that the turbulent decay at a given height depends on the dimension of the layer thickness, or twice the distance from the nearest boundary to the most remote point in the entity. We assume the rate of turbulent decay, when the whole boundary layer is viewed as one layer controlled directly by the presence of the solid surface, is the decay rate expected when there is a second solid surface at the same distance above the point. The decay rate at the wavelengths in the motion determined by the influence of one solid surface is the same as if the point was halfway between two solid surfaces, insofar as the largest wavelength which can be generated in the motion determines the decay rate.

By describing the turbulent decay in the surface boundary layer in this way, and comparing it to the decay with the multilayer model, we will show that von Karman's constant must be

$$k = 2(2a^3/A)^{1/4} = 0.369.$$

Another way to look at the motion in the self-similar boundary profile is that the presence of the solid wall allows a certain scale of motion where the pressure forces turn a given motion back on itself, so that a particle completes a circuit over a given scale size at a given velocity in a certain time, without any loss of total energy, but with energy going to make smaller turbules all the time. These are the motions characteristic of this height, and for this particular scale of motion the wall could equally be the same distance *above* the level concerned, as below it since it would exercise the same restraint. Thus, the motion could just as well be restrained at the same distance both above and below, and lie in a channel of thickness equal to twice the height. The turbulent motion in the middle of a parallel channel will be essentially the same after the top boundary is removed because of the restraining influence of the lower boundary. As mentioned below, extensive observations show that channel flow is very closely logarithmic in velocity profile, so that this description is borne out experimentally.

This choice of twice the height is the simplest possible assumption for the channel depth. Comparing the boundary layer to flow in a parallel channel with the height itself as the channel depth, is clearly rejected, because no motion in the fluid could occur at the specified height if a solid wall was positioned there. Similarly, if the roof of the channel was closer than the floor then it would add an additional restraint to the motion. Greater depths than twice the height would make little difference to the motion at the level of the chosen height since the distance to the lower boundary would determine possible motion anyhow. A typical turbulent motion is a swirl, so that any swirl centered at a given height cannot reach above twice that height.

It may be worth commenting that these remarks do not apply to large scale two-dimensional motion parallel to the boundaries. Such motion can probably be stimulated in the atmospheric surface boundary layer by variations along the surface. This motion may well decay by a different mechanism, and is not likely to interfere with the decay of turbulent motion which involves vertical components.

### *5. von Karman's constant*

Before formulating the new equations describing the decay of the turbulence with different representations of the layers, let us summarize the theory up-to-date with the aid of graphical representations.

In Fig. 1 we see two layers represented on a logarithmic height scale in the vertical direction. Across the page, three possible vertical shifts of the layers have been sketched with the dotted lines showing the vertical displacements. The first step in the theory examined the turbulence in the representative, or undisplaced, layers whose horizontal velocity was taken to match the logarithmic boundary layer velocity profile at the logarithmic center of each layer (i.e., the geometric average height between the upper and lower surfaces). The layer velocities start with zero horizontal velocity, and increase by a constant step as each higher layer is entered. The zero velocity layer is equivalent

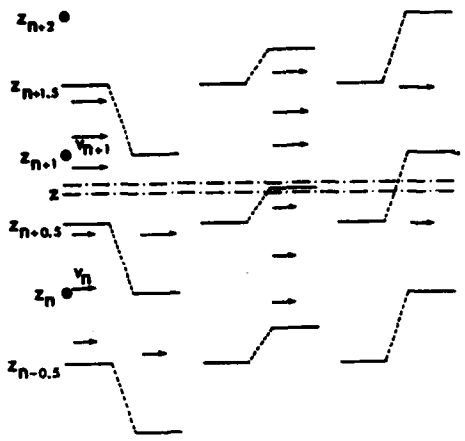


Figure 1

This is a representation of the $n$th, and the $(n+1)$th, layers using a logarithmic height scale. The left-hand, and the right-hand, representation of the layers show the extreme down and up departures of the layers from their nominal heights where their boundaries lie at $z_{n-0.5}$, $z_{n+0.5}$ and $z_{n+1.5}$. The middle representation shows the transition between the $z_n$ and $z_{n+1}$ layers fluctuating upwards to lie between $z$ and $z + \delta z$. The velocity at height $z$ is $v_{n+1}$, when the transition lies below $z$, and $v_n$ when it is above $z$.

to the non-moving surface of the earth. In a specific layer, the organized entity structure in the turbulent air, represented by the layer, is uniformly mixed, so that the turbulence and horizontal velocity are independent of height within each layer.

The next step was to allow the layers to fluctuate up and down by half a layer. The real atmosphere does not sort itself into such neat horizontal layers, but the continually forming and breaking up of the turbules maintains a recurring history of the appropriately scaled motion at each level relative to the surface, and the layer model describes how this regulates transport in the vertical direction across their faces, so that every level, has a layer centered at its given height for some part of the time. Thus any fixed level could find itself in one or two adjacent layers at different times. To reproduce a smooth horizontal velocity profile proportional to the logarithm of the height, then requires that the probability of the lower boundary of a layer being anywhere between half a layer up and half a layer down, is a constant, for constant intervals in the logarithmic height. The probability of the lower boundary of a layer lying between $y$ and $y + \Delta y$, for constant $\Delta y$, is independent of $y$, when $y = \ln z$, and $\ln z_n < \ln z < \ln z_{n+1}$.

On this basis, the lower surface boundary layer can be examined by postulating that the plane lying at the top of the surface roughness elements is the transition between the representative layer with zero horizontal velocity, and the next representative layer up, which carries a horizontal velocity equal to the constant increment in velocity between layers.

This state is represented on a linear height scale in Fig. 2. Allowing these layers to fluctuate in height then provides a measure of the velocity between the roughness

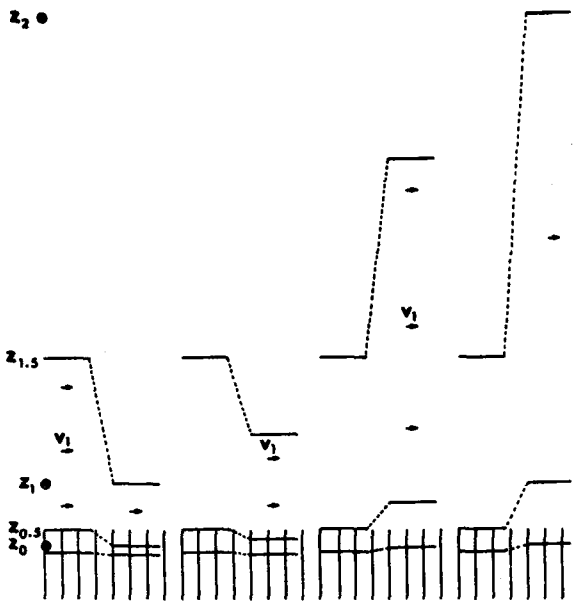


Figure 2

This figure represents the layer heights on the ordinate as directly proportional to the actual height from the model. The four cases represent fluctuations from the nominal layer height with the two extreme values and two intermediate values. The vertical lines in the bottom of the diagram show the surface roughness elements and how the first layer, with its mean horizontal velocity, can dip down into the roughness elements and so generate drag. The bottom layer depicted has zero horizontal velocity in the model (TELFORD, 1980).

elements, which leads, by the calculation of the drag and relating it to the shear stress, to the surface roughness length discussed here, and in the previous papers (TELFORD and PRESLEY, 1978; TELFORD, 1980).

Figure 3 shows this picture again with the wavelength of the turbulent motion indicated. Using the same probability for a layer position as determined earlier to produce the logarithmic velocity profile, the average turbulent decay rate at a given level can be calculated by averaging the decay rate at each wavelength, weighted by the fraction of the time that this wavelength occurs at that level.

By now further invoking the concept of self-similarity, we say that the total flow below a given height is similar to the flow through a parallel trough with fixed floor, and a roof at twice the specified height. This is also similar to the transient entities making up the flow in the fluctuating layers with transient boundaries of which the flow itself is composed.

The postulate is that a turbule is similar to something like a cylindrical swirl, which then breaks up into smaller swirls at a rate which depletes its kinetic energy with time in

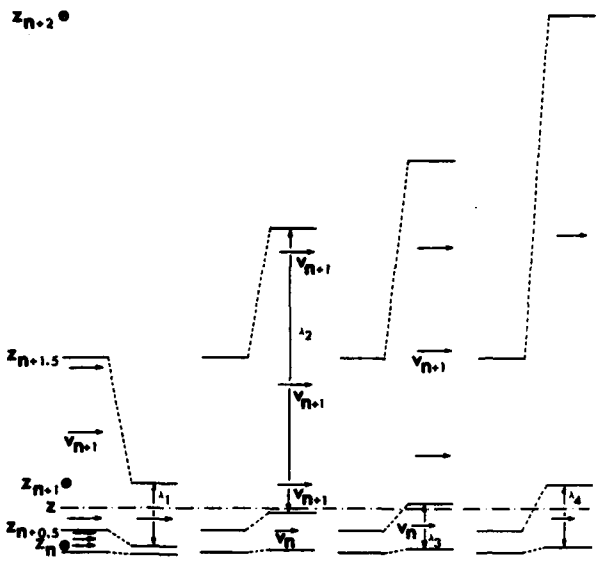


Figure 3

This diagram shows how the fluctuating, rising and falling, layers change the turbulent scale length, $\lambda_1$, at level $z$. With the probability of a layer being at a given level, determined by the logarithmic horizontal velocity profile, the average decay rate for the motion at a set level, can thereby be determined. There is an abrupt change in scale length from $\lambda_2$ to $\lambda_3$ as the transition between the layers fluctuates above and below height, $z$.

proportion to the inverse of its diameter (and the 3/2 power of the internal kinetic energy it carries). In comparing self-similar swirls, the constants of proportion are irrelevant. In a steady state the extremes of the motion in the possible turbules determine the scale, say $\lambda$, of the energy released from the shear forces, and it is this length scale which relates the rate of energy release between the different, but self-similar, representations.

We will now equate the turbulent decay rates at height $z$ evaluated in two ways, from that expected from the self-similar logarithmic profile model involving many entity type layers which are fluctuating in height, and from that derived for the single entity layer model where the scale length is $2z$ ($=D_{Av}$, where $D_{Av}$ is the scale length of the turbulent motion which determines the average decay rate).

In this single entity model,

$$-di^2/dt = Ai^3/2z = Ai^3/D_{Av}.$$

In the multiple entity model we must average the decay rate as it relates to the scale lengths of the fluctuating thickness of the successive layers containing the reference height $z$.

In the multiple entity model (TELFORD, 1980) the self-similar logarithmic profile is obtained at height $z$, between the representative layers of height $z_n$ and $z_{n+1}$, by the following formula,

$$v(z) = (1-f)\, v_n + f v_{n+1}.$$

Here $f$ is the fraction of the time the lower edge of the representative layer nominally at height $z_{n+1}$, with velocity $v_{n+1}$, lies below height $z$, as its height fluctuates. Equating this profile with the normal logarithmic profile, namely,

$$v(z) = (u^*/k) \ln (z/z_0),$$

gives,

$$f = \ln (z/z_n)/\ln (z_{n+1}/z_n)$$
$$= \ln (z/z_n)/\ln \beta,$$

where $\beta$ is defined by $\beta = z_{n+1}/z_n$.

Now, setting, $\Delta v = v_{n+1} - v_n$, continue the discussion of this representation a little further.

$$\Delta v = v_{n+1} - v_n = (u^*/k) \ln (z_{n+1}/z_n) = (u^*/k) \ln \beta,$$

and,

$$\beta = z_{n+1}/z_n = \exp (k \Delta v/u^*),$$

and since, from TELFORD and PRESLEY (1978),

$$\Delta v/u^* = (A/2a^3)^{1/4} \simeq 5.42,$$

then,

$$z_{n+1}/z_n = \exp (k(A/2a^3)^{1/4}) = \beta,$$

or,

$$k = (2a^3/A)^{1/4} \ln \beta.$$

Now to continue with our evaluation of $k$ we need to evaluate $\beta$, by comparing the decay in the single entity representation, to the decay in the many entity layer case.

As before, the representative layer at $z_n$ extends from $z_{n-1/2}$ to $z_{n+1/2}$, so its thickness $D_n$ is (see TELFORD, 1980).

$$D_m = z_{n+1/2} - z_{n-1/2}$$
$$= z_n(\beta^{1/2} - \beta^{-1/2}).$$

The thickness of the layer whose bottom surface lies at $z_{n-1/2}$, is thus

$$D(z_{n-1/2}) = D_n = (\beta - 1)\, z_{n-1/2}.$$

Now, when we consider the fluctuating layers, where $z_n < z < z_{n+1}$, the thickness of those layers whose bottom boundary is between $z$ and $z + \delta z$ is,

$$D(z) = (\beta - 1)\, z.$$

The next lower layer has thickness $(\beta - 1)\, z/\beta = D(z)/\beta$.

The fraction of the time when the edge of the two contiguous layers lies between $z$ and $z + \delta z$, is $(df/dz)\, \delta z$.

Thus, when the turbulent energy decay rate in a layer of depth $D(z)$ is $i^3/D(z)$, which is the decay rate in a layer with its base at the level $z$, an average for the decay rate at height $z$ can be formed over time as the layers containing $z$ fluctuate, and a different thickness for each layer starting below $z$, but containing $z$, gives a different decay rate for a short time. This average is,

$$i^3/D_{Av} = i^3 \int_{z_n}^{z} (df/dz)[1/D(z)]\, dz + i^3 \int_{z}^{z_{n+1}} (df/dz)\, [\beta/D(z)]\, dz.$$

Since,

$$df/dz = 1/[z \ln (z_{n+1}/z_n)] = 1/(z \ln \beta),$$

hence,

$$\begin{aligned} 1/D_{Av} &= \{1/[(\beta - 1) \ln \beta]\} \left[ \int_{z_n}^{z} (1/z^2)\, dz + \beta \int_{z}^{z_{n+1}} (1/z^2)\, dz \right] \\ &= \{1/[(\beta - 1) \ln \beta]\}\, [-1/z + 1/z_n + \beta(-1/z_{n+1} + 1/z)] \\ &= \{1/[(\beta - 1) \ln \beta]\}\, [-\beta/(\beta z_n) + 1/z_n + (\beta - 1)/z] \\ &= 1/(z \ln \beta). \end{aligned}$$

From the single entity model, $D_{Av} = 2z$,

so,

$$1/2 = 1/\ln \beta,$$

and,

$$\ln \beta = 2.$$

Hence, $\beta = 7.39$.

Thus, since $A = 1$ and $a = \frac{1}{12}$, in terms of the universal constants of the theory, and as given above,

$$k = (2a^3/A)^{1/4} \ln \beta.$$

So,

$$\begin{aligned} k &= \ln \beta / 5.42 \\ &= 2/5.42 = 0.369. \end{aligned}$$

The earlier formula for the vertical turbulence can now be rewritten, where $D_n/z_n = e - 1/e$, and $a/k = (aA/2)^{1/4}/2$, as,

$$\sigma_w/u^* = (2/9Aa)^{1/6}\{1 - (9Aa/2)^{1/4}(\sigma_w/u^*)\,[(e - 1/e)/2]\,(z/L)\}^{1/4},$$

or, if

$$x = (\sigma_w/u^*)\,(9Aa/2)^{1/4},$$

$$x = \{1 - [(e - 1/e)/2]\,xz/L\}^{1/4}$$

and $e = 2.71828$ is the base of natural logarithms.

### 6. *The observations*

Numerous studies have been done in pipe flow, including rectangular pipes, which show that the logarithmic (self-similar) velocity profile is a good approximation from just outside the viscous boundary layer right up to the mid-point of the pipe. MONIN and YAGLOM (1971), Figure 31 (from Laufer) gives an example of measurements taken in a rectangular channel. The data fits the formula,

$$u_0 - \bar{u}(z) = -2.5u^* \ln (z/H_1) + 0.65,$$

where $z$ is the distance from the wall, $2H_1$ is the channel thickness, $u_0$ is the average velocity at the channel center and $\bar{u}(z)$ is the average velocity at distance $z$ from the wall.

Thus, our comparison of the self-similar planetary boundary layer flow to channel flow, with an upper and lower plane boundary, seems to be well justified. The big difference seems to be that the factor of 2.5 in the above formula gives $k = 0.40$, rather than 0.37 as we have obtained here.

However, there is the question of whether fully developed turbulent motion can be found in laboratory scale experiments where the viscous range of motion, where energy is removed from the turbulence, is relatively close in scale to the dimensions of the experiment. It is a question of whether the inertial sub-range in the turbulence is fully developed. BATCHELOR (1960), remarks 'The existence of the inertial sub-range requires the Reynold's number to be of the order of the square of that required for the existence of the equilibrium range, and is clearly unlikely to be realized in laboratory wind tunnels.' Since our theory is based on self-similarity, in a comparable way to the arguments used for explaining an inertial sub-range, the self-similarity value of $k$ is likely to differ from the experiment value obtained in laboratory channels.

We are, of course, as in previous studies, assuming that the constants $a = \frac{1}{12}$, and $A = 1$, have these values, and are constants which are fundamental to turbulence. At present, a kinematic derivation for $a = \frac{1}{12}$ is being studied, and $A$ will, hopefully, eventually be derived in the same way from kinematical considerations.

The model presented here assumes the viscous dissipation wavelengths are so small that decreasing them further would produce negligible increase in the total kinetic energy of the turbulence available to drive the entrainment process. The model also ignores buoyancy effects in this derivation.

Careful and extensive field measurements in the atmospheric boundary layer have yielded a value of $k = 0.35$ (BUSINGER *et al.*, 1971) in neutral (no buoyancy) conditions, rather than $k = 0.40$ as is often accepted, since this latter value is usually found in laboratory experiments.

As mentioned above the new value of $k$ leads to theoretical limits of the roughness length $z_0$ (TELFORD, 1980), ranging from high Reynold's number turbulent flow to low Reynold's number flow, of

$$0.136/a_s C_D < z_0 < 0.537/a_s C_D(u^*).$$

This yields $z_0 = 1.55$ cm, in the same conditions as Thom's lowest Reynold's number measured value of $z_0 = 1.57$ cm. The extent to which this agreement is coincidental is difficult to determine. Thom derived $k = 0.41$ in the experiment where he measured these values of $z_0$. He used three airflow velocities of 25, 50 and 75 cm sec$^{-1}$, corresponding to $u^* = 13$, 22 and 30 cm sec$^{-1}$. These velocities gave, for his surface, $z_0 = 1.57$, 1.37 and 1.25, with Reynold's numbers $u^* z_0/\nu$ ($\nu$ is kinematic viscosity of air, $\nu = 0.15$ cm$^2$ sec$^{-1}$) of 136, 201 and 250. Thus, if the Reynold's number were decreased again, $z_0$ may increase further. So the value for $z_0$, at limiting low Reynold's number, may perhaps become higher than our value. However, the Reynold's number based on the roughness element diameter of 1 mm, used by Thom, is less than 10, a value in the viscous flow regime near the region below which inertia in the fluid is no longer significantly contributing to the flow, and hence the $z_0 = 1.57$ may indeed represent something of a limiting value, to be compared to the value 1.55 cm derived from our formula, $z_0 = 0.537/a_s C_D(u^*)$.

In addition, assuming that $k = 0.37$ in Thom's analysis of his data makes only a small difference to his value of $z_0$. He quotes changing from 0.41 to 0.40 as changing $z_0$ from 1.37 to 1.35, so, roughly, $k = 0.37$ should give $z_0 \simeq 1.30$ or so. Thus one might expect $z_0 = 1.57$ to be reduced to $z_0 = 1.48$, or thereabouts, by forcing the new value of $k = 0.37$ in the data analysis. This is a more comfortable value as regards to the theory since it allows for some increase in the measured value for a further reduction in Reynold's number to still lie within the theoretical limits.

It also seems possible that another mechanism, not considered here, may be contributing to the slope of the velocity profile in laboratory experiments, perhaps an influence due to the roof of the tunnel. Such a mechanism may not greatly influence the relative layer depths and so may not change the roughness lengths, but it could still influence $k$ to be 0.41 rather than 0.37.

Further studies in this area might be interesting.

## 7. Conclusions

While it is difficult to assess the accuracy of this theoretical derivation, or, indeed, of the relevant field measurements, it certainly appears that the new theoretical value of $k = 0.37$ presented here is in acceptable agreement with present experimental values of von Karman's constant measured in neutral boundary layer motion at atmospheric boundary layer length scales. The author is aware of no other theoretical deduction of a value for this constant which is based on this type of physical reasoning (rather than approximate solutions to the Navier-Stokes equations).

## Acknowledgments

This study was completed under Navy ONR funding from contract N00014-75-C-0598 and this encouragement, and that of Mr James Hughes of ONR, are gratefully acknowledged.

## References

Batchelor, G. K., *Homogeneous Turbulence* (Cambridge University Press 1960), 197 pp.

Businger, J. A., Wyngaard, J. C., Izumi, Y., and Bradley, E. F. (1971), *Flux-Profile Relationships in the Atmospheric Surface Layer*, J. atmos. Sci. *28*, 181–189.

Lauper, J. (1951), *Investigation of Turbulent Flow in a Two-Dimensional Channel*, Nat. Advis. Com. Aeronaut., Rep. No. 1033.

Lauper, J. (1954), *The Structure of Turbulence in Fully Developed Pipe Flow*, Nat. Advis. Com. Aeronaut., Rep. No. *1174*.

Monin, A. S., and Yaglom, A. M. (1971), *Statistical Fluid Mechanics: Mechanics of Turbulence*, Vol. 1 (The MIT Press 1971), 769 pp.

Telford, J. W. (1966), *The Convective Mechanism in Clear Air*, J. atmos. Sci. *23*, 652–666.

Telford, J. W. (1967), *The Vertical Penetration of Hot Plumes*, Jnl Rech. atmos. *3*, 1–8.

Telford, J. W. (1970), *Convective Plumes in a Convective Field*, J. atmos. Sci. *27*, 347–358.

Telford, J. W. (1972), *A Plume Theory for the Convective Field in Clear Air*, J. atmos. Sci. *29*, 128–134.

Telford, J. W. (1975a), *The Effects of Compressibility and Dissipation Heating on Boundary Layer Plumes*, J. atmos. Sci. *32*, 108–115.

Telford, J. W. (1975b), *Turbulence, Entrainment and Mixing in Cloud Dynamics*, Pure appl. Geophys. *113*, 1067–1084.

Telford, J. W. (1980), *The Surface Roughness and Planetary Boundary Layer*, Pure appl. Geophys. *119*, 278–293.

Telford, J. W., and Presley, J. D. (1978), *The Surface Boundary Layer as a Part of the Overlying Convective Layer*, Pure appl. Geophys. *117*, 664–689.

Thom, A. S. (1971), *Momentum Absorption by Vegetation*, Q. Jl R. met. Soc. *97*, 414–428.

Warner, J., and Telford, J. W. (1967), *Convection Below Cloud Base*, J. atmos. Sci. *24*, 374–382.

(Received 14th December 1982, revised 12 April 1982)

Reprinted from Preprint Volume of Extended Abstracts:
Conference on Cloud Physics, Nov. 15 - 18, 1983.
Chicago, Ill. Published by the American Meteorological
Society, Boston, Mass.

1.2

# FOG, STRATUS AND CUMULUS FORMATION IN WARM AIR OVER COOLER WATER

J.W. Telford and S.K. Chai

Air Motions Laboratory - ASC
Desert Research Institute
University of Nevada System
Reno, Nevada 89506

## 1. INTRODUCTION

There has been somewhat of a mystery in regard to the formation of fog and stratus over the ocean. The problem is that while radiation can cool the air, over land, and hence increase the relative humidity of the air to above its saturated value, and so form fog, this is possible only because the surface temperature of the land falls in step with that of the air. If the surface remains warm, then convection will prevent the air falling appreciably below its temperature; which is the case over the sea.

Thus for fog to form at sea, convection from the surface must add moisture to the air, since the temperature cannot be reduced to the dew point by radiative cooling to below surface temperature.

Convection from the surface, needed to add the necessary moisture to the air, would seem to be impossible unless that air is cooler than the water. Thus, there follows the general conclusion that fog should be able to form when the sea is warmer than the air to promote convection, and evidence has been published to support this claim.

Radiative cooling of the fog near its top has also been promoted as a necessary precondition, mainly on the basis that the inversion at fog top must be undergoing renewal to remain so sharp, and convective energy coming from radiative cooling of the cloud top must be continually supplied so it can be dissipated in supplying the energy needed to bring down the buoyant, above inversion, air into the layer. Radiative cooling would also drive convection down to the surface and hence bring up moisture.

There are doubts however because the radiation entering the fog from above and below is relatively high, since there are warm temperatures above and below, and in addition the sun often heats the air layer during the day.

Measurements confirm such doubts, and cast doubt on that mechanism itself. There is often no buoyancy difference between the cloud, and mixtures of cloud with above inversion air, so no energy is needed to erode the inversion. Furthermore we have an actual case where there is strong convection within the cloud, but calculations show that the cloud is being heated with the sun shining on it (Dr. Twomey is doing this radiation work).

## 2. STABILITY AND ENTRAINMENT

How the temperature of the cloud top decides its stability, because if the wet bulb temperature of the air above the cloud is equal to the cloud temperature, then mixtures are neutrally buoyant in cloud. A cooler cloud is stable to all mixing whereas a warmer cloud is unstable. Such instability can only be stopped if there is sufficient moisture in the convective layer to moisten the whole layer up to where the wet bulb temperature of the overlying air again exceeds the temperature at the cloud top.

This process involves the entrained air sinking down to cloud base where it will come to rest at cloud base temperature, but with cloud drops all evaporated. The remaining cloud will rise upwards along the wet adiabat, and the process will repeat until an increase in the wet bulb potential temperature (hence an increase in wet bulb temperature relative to cloud top) makes the mixtures buoyant again, so they cannot sink. Figure 1 shows this overturning process.

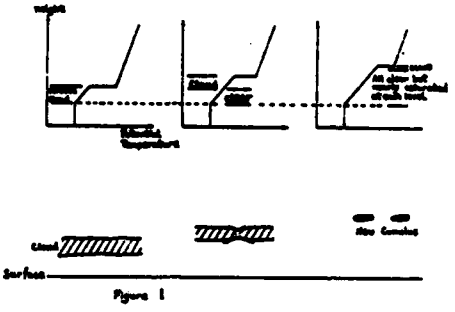

Figure 1

Thus the new dried out air left beneath the cloud will follow the wet adiabat in temperature and will be very close to saturation; this creates a constant wet bulb potential temperature with height, in clear air, in place of this formerly cloudy layer.

Thus a layer cloud which is convecting with heat and moisture coming from below, continues to increase in potential temperature at its top as its base lowers, until it rises above the wet bulb temperature of the air above. Rapid entrainment then brings the mixtures down to below cloud, and so increases the cloud top height again.

If the wet bulb potential temperature of the overlying air is less than before, entrainment is unstable and overturning continues.

If the wet bulb potential temperature of the air above has increased, then the cloud base must lower again before more entrainment can occur. The base can lower to the surface if

the wet bulb potential temperature exceeds surface temperature close to the surface. This is a requirement for fog formation. Figure 2 illustrates this process.

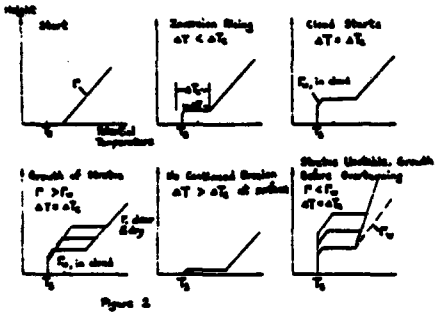

Figure 2

Thus the entrainment process determines the possibility of fog formation, as well as the formation of inversions. The surface temperature, and the wet bulb potential temperature of the overlying air, determines whether there will be fog, stratus or cumulus clouds, once there has been enough time for the processes to approach equilibrium.

## 3. INVERSIONS

However, the air must start off warmer than the water to allow for fog formation since an inversion is needed near the surface so that the layer which has to be moistened is not too deep. Indeed, there are observations of fog forming near cold patches of the sea.

Thus the first point in this paper is that inversions are created by moist surface convection eroding into warmer dry overlying air by the action of condensing droplets near the top of the convection. A fog forms its own capping inversion. The droplets provide the latent heat to cool the overlying air so that mixtures are negatively buoyant, and the additional consequential replacement of a cloud layer by constant wet bulb potential temperature air, gives a constant vertical wet bulb potential temperature profile which crosses the inversions without change.

## 4. CONDITIONS FOR FOG

The second point is that convection from the sea surface can occur when the overlying air is warmer than the water, but not if the potential wet bulb temperature of the air referred to the surface pressure is higher than the surface temperature.

Once condensation forms on haze droplets near the water surface, the dry air can be eroded because the latent heat of the evaporating haze drops makes mixtures cooler than the hazy air. Then the process will begin. This process will occur if the wet bulb temperature of the dry air is below water temperature.

Now the key to the whole process is that convection can occur with the air warmer than the water by a fraction of a degree, because the air descending down to the surface is subsaturated (before the fog forms near the surface), whereas rising air parcels leaving the surface are initially saturated. Since the molecular weight of water vapor is less than that of air, the parcels leaving the surface are buoyant relative to drier descending parcels.

Thus when dry warm air blows out over water the process of inversion formation at a hazy interface begins immediately. Vapor density driven convection continues to add moisture to the air, and the haze at the top of the layer erodes upwards until it reaches a level where the wet bulb potential temperature of the air above exceeds convective air temperature. Cloud begins here, and then grows both up and down. No cooling by radiation is needed, and the sea does not need to have an increasing temperature as the air blows along it, but both would probably help.

Since the same process works for both warm and cold water, other explanations are not needed for fog formation.

If the wet bulb potential temperature increases with height the haze will form a fully saturated cloud layer, and the base will descend until it reaches the surface when the wet bulb potential temperature of the air above the inversion reaches surface temperature.

These are the conditions which give fog.

Fig. 3 shows our theoretical model results for air at water temperature driven by moisture density above with no heat flux. The inversion was set at 250 m with a horizontal pressure gradient of 0.03 mb/100 km. The wind speed is 1.4 m/sec. The cloud base is lowering according to the time schedule given in Figure 4.

## 5. ACKNOWLEDGMENTS

This work was supported by the Navy under contract N00014-75-C0598.

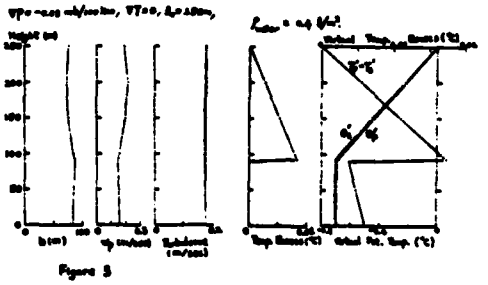

Figure 3

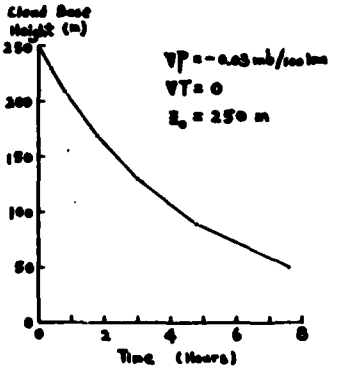


Figure 4

# CONVECTION MODEL FOR STRATUS CLOUD OVER A WARM WATER SURFACE

S. K. CHAI and J. W. TELFORD

*Air Motions Laboratory, ASC, Desert Research Institute, University of Nevada System, Reno, NV 89506, U.S.A.*

(Received in final form 10 February, 1983)

**Abstract.** A numerical model is developed to simulate convective stratus cloud formation over the sea. The model is based on quasi-steady state moist plumes advecting over an area of increasing sea-surface temperature with the sea warmer than the air, but it is also a good approximation for non-steady states whenever the model is matched to air-sea temperature differences. Combining the effects of upward transfer of heat and moisture fluxes as well as adiabatic cooling, stratus cloud forms and spreads downward in this field. The depth of the convective field, the sea surface temperature gradient, the liquid water content at cloud top, and the horizontal pressure gradient are the four controlling parameters for the convective field. Alternatively, the wind speed, air-sea temperature difference, and the mixing ratio of the air, derived variables in this treatment, can be taken, with the depth, as the basic parameters.

The entity type of convective model used here has the advantage that it models the transport and modification of air parcels and hence provides a method for studying drop size development in stratus clouds. It also uses relationships derived from water tank experiments with plumes and tested in dry convection and so needs no parameters specific to each situation. Its most important feature, however, is that the mean motion of plumes, rather than turbulent diffusion, transports the moisture.

The upward growth and erosion of a temperature step increase to produce an inversion can be attributed to liquid water present in haze drops or cloud drops, rather than to turbulent diffusion. Radiative transfer is not a necessary requirement, but may either enhance or slow down the process.

## 1. Introduction

From observations of marine fog on the eastern Pacific Ocean near San Diego, Petterssen (1938) concluded that fog is convective in that area. The vertical temperature structure in fog is observed to be unstable. This implied to him that the marine fog near San Diego is formed by air flowing over a warmer sea surface after it has presumably been cooled by radiation or mechanical stirring to near surface temperature upwind, instead of what is sometimes considered to be the case, based on observations, warm air flowing over a cold sea surface. The latter case would seem to lead to a stable temperature distribution without convection, and hence require a mechanism to cool or moisten the air, such as radiative cooling or mechanical stirring. He attributed a strong role to radiative cooling at the fog top once fog formed.

Observations of the marine fog along the California coast by Pillie *et al.* (1979) showed that the initial fog patches are formed by the passage of cold air over a warm sea surface. The instability created by the warm water generates the convection which produces the initial condensation. Radiation from the fog top may then cool it and so enhance the instability inside the fog, which, in turn, enhances the exchange of heat and water vapor between the sea and air.

*Boundary-Layer Meteorology* **26** (1983) 25–49. 0006–8314/83/0261–0025$03.75.

Recent work by Telford and Wagner (1981) shows details of marine stratus clouds involving the entrainment process.

This paper presents a model of the convective planetary boundary layer over the sea. Since the approach is very different from other models which have been developed, and because the technical implementation of the model involves a large amount of algebra (and computing) which is conceptually irrelevant to the physics we are attempting to describe, the physical background to the formulation of the model will be discussed. The mathematics is essentially an exact description of the physical assumptions involved, since the quasi-steady-state assumption is the only approximation introduced with an aim to facilitate solution of the equations. The equations are based on the reversible mixing of ideal gases, and volume and mass are used to specify density, and hence pressure and temperature.

Furthermore, there is a body of physical observations and conceptual physical restraints which need to be considered if the model is to be understood in the context of explaining the physical world, rather than meeting only a few special basic requirements, as has sometimes been done in the past.

## 2. Background to the Model, and Entrainment from above

The whole problem of boundary-layer modeling can be thought of as one of energy transfer; buoyant gravitational energy transferred to turbulent energy, turbulent energy to gravitational energy in eroding a warmer inversion, and turbulent energy decay to random heat motion. Since these transfers drive the model, the heat and moisture fluxes might be regarded as subsidiary functions until we realize that these determine the energy release. Thus each depends on all the others. It is for this reason that the energy conversion steps need each to be modeled quantitatively, and why an energy balance approach is usually inadequate.

Let us note that turbulent energy dissipated near the surface cannot be used to entrain warmer overlying air. Energy released low down largely supports organized updraft velocities rather than direct turbulent generation and dissipation. Upward moving plumes later generate turbulent energy near the top of the layer, and the transport of heat and moisture in the vertical plumes totally overrides any transport by irregular turbulent motion.

The plume model used here takes account at each height of the energy transferred from the buoyancy, to the mean motion, to the turbulent motion, and concurrently to turbulent dissipation, as well as the other aspects of the dynamics. In such an explicit mechanistic model, it does not make sense to feed entrained air down from above the inversion without considering how the process occurs. Given an increase in the inversion temperature jump in a hypothetical model, with other parameters unchanged, then to maintain the erosion rate, additional free turbulent energy to continue the erosion can only be obtained by lowering the dissipation rate which is removing turbulent energy. To achieve this involves decreasing the turbulent intensity, whereas to continue to bring down warmer overlying air at the same rate would appear to require higher turbulent

velocities to give more kinetic energy to overcome the higher potential energy needed to entrain warmer air from above. Thus a relationship describing a feedback between the turbulent intensity and the entrainment rate would need to be specified by other considerations, relating the turbulent intensity itself to the entrainment rate perhaps, in order to specify how far the turbulent intensity must be lowered to establish a new balance.

When this is done, using the same relationship as governs the turbulent transfer by entrainment through the sides of the plumes, we find that the energy to bring down the now buoyant mixed parcels in the downdrafts must come from the upward kinetic energy of mean motion in the plumes, and not the eddy diffusivity arising directly from the turbulence. This latter process is so slow compared to transport by the plumes that it has negligible effect. Now this retarding buoyancy in regions of downward descending air, after warm air has been added at the top, slows the plumes so much that they spread out and break up by entering the intervening upward plumes.

Thus we find that equations involving the plume structure cannot produce solutions yielding entrainment of air from above, if that air is more than a fraction of a degree warmer. We are quite unable to erode a substantial inversion temperature jump of ten degrees or more. Observations agree with this conclusion in that most substantial inversions in dry air occur over a considerable depth, say 200 or 300 m, and probably involve other considerations. This behavior was studied theoretically by Presley (1976).

In such circumstances a turbulent diffusing layer is likely to develop just above the plumes which prevents them from making direct contact with the warm air above. Advection, and other considerations then need to be included. Now, with such an intermediate layer, the diffusion rate down through the inversion will be much slower than the erosion found when the model assumes a sharp inversion of less than a degree, and the downward heat flux will be limited to much smaller values. Thus the approach given here with encroachment as the means of deepening the layer will be a good approximation in most circumstances.

The conclusion that in dry air, thermal plumes will not appreciably erode upward into the inversion is supported by measurements. Those made by Telford and Warner (1964), and Warner and Telford (1967) show no inversion in typical cases of convection when the air is subsaturated.

In these two examples, the increasing depth of the convective layer occurs because the surface and the whole layer up to the inversion, warm during the morning, and hence the air at greater heights is no longer buoyant relative to the air underneath. Then the overlying air is incorporated into the layer, which deepens. Thus the model for such conditions does not need to include a mechanism to erode or entrain overlying air.

The occasional inversion of a few degrees over land on clear days probably arises by advection of warmer air over the top of the convecting layer, or is due to the action of haze droplets as discussed later. Certainly another mechanism is needed, apart from the strong convection seen in these examples.

This same energy-free incorporation of the overlying air can operate with large inversions over the sea. In the presence of water droplets in haze, mist, fog or cloud,

the wet bulb potential temperature is the parameter which should not show a temperature jump at the inversion, rather than the potential temperature, as in the dry case just discussed. Thus large inversions in true temperature can exist when the overlying air is dry and the air below the inversion is near saturation.

Thus the whole idea of an energy transfer description of the boundary layer without any mechanism to model plumes, where energy is arbitrarily assigned to the erosion process, is open to question. Observations such as those mentioned, show that the convective process itself can proceed without producing an inversion, so we need to look elsewhere to explain the inversions observed over the sea. Since we have an example of strong convection in stratus cloud over the sea where the radiation balance is probably heating the cloud, and certainly not appreciably cooling it, with a large inversion present (Telford and Wagner, 1981, Twomey (personal communication, soon to be published, 1983), radiative cooling is not the explanation.

This paper develops a plume model to describe the marine fog formed by cold air advecting across a warm sea surface. One of the authors (Telford, 1966, 1970, 1972, 1975) introduced a plume theory for a dry convective field. The present work is an extension of that model to include moisture and condensation. For the reasons given above, the model does not include an entrainment process at the top surface (although it has been modeled in detail, Presley, 1976) or the radiative cooling or heating processes near cloud top. The inversions seem to arise from other mechanisms, which are under investigation.

The assumptions of the model are quite simple. It is assumed that turbulent entities occur in convection in the form of plumes with vertical continuity, which have edges through which entrainment occurs at a rate proportional to the level of turbulence. The only other assumptions (apart from the quasi-steady state) are the decay factor for turbulence and the regular mechanics and thermodynamics needed (see Telford, 1966). The apparent complexity of the equations is purely algebraic and numerical, with no other assumptions of importance. The thermodynamics are reversible.

It is shown below that the upward convective transfer may well mostly occur between brief episodes of encroachment at cloud top, and that the time for this upward transfer dominates, with encroachment happening over quite short times. Observations of the intermittent nature of entrainment by Telford and Wagner (1981) support this suggestion. Figure 1 illustrates a condition where surface convection temporarily stops halfway up to the inversion, for example.

The plume structure in the model described in this paper transports properties relatively rapidly in the vertical as compared to random turbulent eddies. In dry air this approach shows the experimentally observed positive potential temperature gradient with height which eddy diffusivity models do not reproduce; most of the other observed features of convection are modeled in quantitative terms.

Furthermore, a matter of major interest relates to the development of the drop-sized spectra of fog and stratus. An eddy diffusivity, or statistical, model of the layer cannot describe the life history of droplets in the way that can be done using an entity plume model (see Telford and Chai, 1980). In particular, recent observations of marine stratus

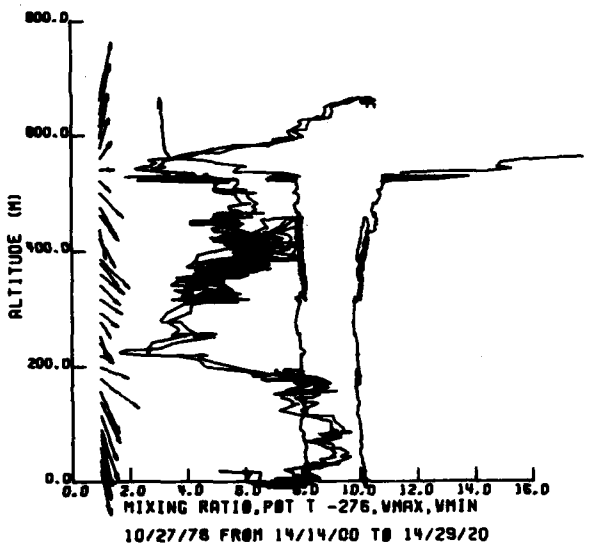


Fig. 1. Aircraft measurements of marine stratus cloud on 27 October, 1978 over the Pacific ocean near Monterey, California. The traces from left to right are wind vectors, maximum and minimum wind magnitudes in m $s^{-1}$, vapor mixing ratio in g $kg^{-1}$, and potential temperature in °C. Measurements within the stratus cloud layer from 320 to 530 m showed strong mixing at cloud top. (From Telford and Wagner, 1981.)

over the eastern Pacific ocean reported by Telford and Wagner (1981) give clear evidence that parcels rise from cloud base to top as relatively intact entities.

Figures from that paper reproduced in Figures 1 and 2, also show that there are unmistakable variations on a meso-scale over about 10 km or so, with relatively short time constants. In Figure 1 the remarkable wind differences at different heights, above and below 180 m altitude for example, suggest that there is little vertical transport of horizontal momentum between layers at the time of the observation. In Figure 2 this effect is much less. The data in Figure 1 were obtained when other data provide clear evidence of active entrainment (see Telford and Wagner, 1981), and the data in Figure 2 were obtained about 10 min later and about 10 km away, during the following ascent. There is no evidence of entrainment in progress in the second case although evidence of recently past entrainment is unmistakable. There is a slight updraft in the region of Figure 1.

An interesting paper by Mahrt and Paumier (1982) discusses observations of the entity structure involved in the entrainment process, and they too remark in a somewhat different context that this entrainment instability occurs intermittently.

These data, which are described in detail in Telford and Wagner (1981), seem to indicate that in the first case a slight overall updraft probably was associated with slightly warmer cloud, or horizontal variations in the temperature of the overlying air, and also

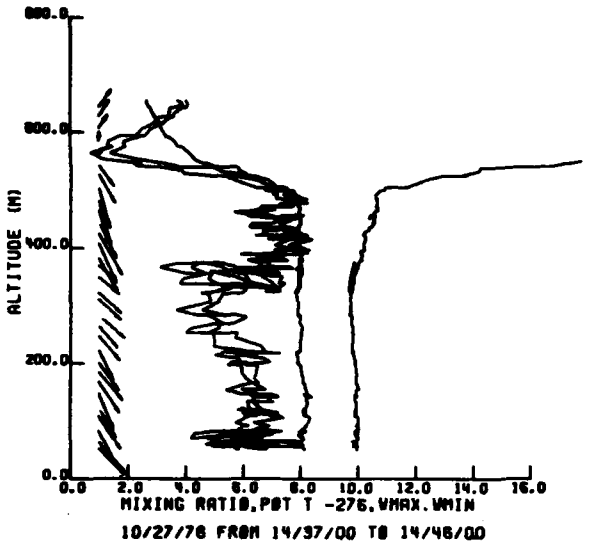


Fig. 2. Data obtained at a location about 10 km away from Figure 1. There is no evidence of cloud top entrainment in progress in this sample. (From Telford and Wagner, 1981.)

with strong entrainment because the temperature jump at the inversion was slightly less, which in turn resulted in downward convection from cloud top, quite separated from ongoing convection upward from the sea surface. This condition may have occurred in the recent past and the entrainment may have just stopped, because the entrainment itself has cooled the cloud at this stage. These two separate sources of buoyancy at top and bottom appear to have separated the layer into two parts, at about the 180 m level. No eddy diffusivity model could predict this without an adjustment of ad hoc values of the eddy diffusivity to fit the data. Stage and Businger (1981b) comment briefly on the possibility of such a division.

In the second case, the entrainment has stopped (the temperature jump at the inversion is probably slightly larger), convection from the surface is reaching cloud top again and the horizontal momentum transported in the plumes is eliminating the wind shear and unifying the two layers again.

It is important to note how the potential temperature and the mixing ratio show, in both cases, the vertical uniformity normally associated with the strong convection in the dry planetary boundary layer. Thus any separation into layers must have been short-lived and had little effect on the mixing ratio and temperature.

Similarly, the second case shows unequivocal evidence of previous entrainment in the drop size spectra. Thus it is difficult to avoid the conclusion that the two processes alternate, with entrainment coming in bursts. This cycling is probably controlled by variations in the temperature of the overlying air. Thus a model which separates entrainment at the cloud top from convection from below may well be the best approach.

## 3. Previous Models

Ball (1960) was probably the first to perform a block energy balance for the layer. He assumed that dissipation of turbulent energy did not go directly into heating; instead, the energy released by the upward heat flux was used to override the buoyancy of the entrained overlying air, mixing it downward. Lilly (1968) greatly improved this approach by including condensation and evaporation effects, but it was again a bulk treatment for the layer with an assumed profile shape and, by implication, some mechanism to maintain it. This would seem to imply some sort of random turbulence with no need for organized plumes or downdrafts, and other restraints about the eddy diffusivity not mechanistically modeled. In that model, the excess energy from the energy expressions used for the energy balance, is used for downward entrainment of warmer overlying air. This lack of a detailed mechanism describing the plumes is cause for concern, because this is the only way cloud parcels can be followed to study the development of the cloud droplet size distributions. This is quite apart from the fact that the observed plume structure should have an explanation.

Lilly considers "radiation off the cloud tops as an essential element", but finds that "several presently used radiation models are in serious disagreement". It is assumed at the start that the wet bulb potential temperature above the cloud top is constant or increases with height (claimed as a prediction in the conclusions).

If the cloud base is to lower with continuing evaporation from the sea surface, then the stability criterion requires that the wet bulb temperature above the cloud must exceed the temperature of the wet adiabat, as Lilly's increasing wet bulb potential temperature ensures. For cloud base to lower, however, there is a additional constraint relating the magnitude of each increase in wet bulb potential temperature above with the magnitude of each corresponding decrease in cloud base height. The wet bulb temperature in the cloud must remain equal to that of the dry air just above, and as it increases a given amount as the mixing ratio increases and the inversion erodes upwards, a corresponding precise decrement in the height of the cloud base occurs at the same time, because the convection maintains the potential temperature at cloud base equal to the constant surface potential temperature.

Furthermore, if the overlying air is less stable than the wet adiabat, then eventually the cloud will become unstable, with entrainment driving downdrafts to produce total overturning, and the usual cumulus growth will follow after the stratus layer breaks up. This is because the entrainment of dry air will result in a decrease of the wet bulb potential temperature just above cloud top as the cloud top erodes higher, giving increasing entrainment rates. Lilly discusses many of the quantities considered here but from a different standpoint, and reaches very different conclusions.

Randall discusses Lilly's model in terms of internal turbulence generation within stratus cloud (Randall, 1980a); then he extends the radiation analysis to consider the cooling at different levels within the cloud (Randall, 1980b). He concludes that lower stability is needed in the overlying air than is given by Lilly's criterion to promote turbulence. In this second paper he concludes that the details of the entrainment assumption are significant except in the special cases reported by Lilly (1968) and Schubert (1976).

Stage and Businger (1981a, b) developed an energy balance model for entrainment into a cloud-topped marine boundary layer. They used the turbulent kinetic energy budget to derive the entrainment rate. They applied their model to a cold-air outbreak which occured over Lake Ontario during the International Field Year for the Great Lakes (IFYGL). Comparisons with other models were also presented. These papers provide extensive discussion of previous models.

## 4. Assumptions

This model simulates a field of identical plumes advecting, with the mean wind, over an increasing sea surface temperature with the sea warmer than the air (in a reference frame moving with the wind). The model is controlled by four parameters: the height of the convective layer, $z_0$; the liquid mixing ratio at cloud top when cloud is present; a constant horizontal pressure gradient, $\nabla p$; and a constant surface temperature gradient, $\nabla T$. The mean wind speed is generated by the horizontal pressure gradient. The effects of the Coriolis force are included in the pressure gradient, since only the surface stress relates to the wind. The change in wind speed in the convective plume layer was shown to be negligible by Presley (1976) and Telford and Presley (1978). The horizontal pressure gradient as well as the wind speed is assumed to be uniform throughout the convecting layer. The surface temperature gradient is measured along the direction of the wind. Thus, the rate of change of temperature is $u\nabla T$, where $u$ is the wind speed. Since the air at the bottom is heated continuously by this changing temperature, convection can be expected to occur. The convective field is capped by a temperature inversion, which the rising air cannot penetrate. Therefore, it must turn over at the inversion base and descend to the surface again. We have assumed here that the overlying air is warm and moist enough to stop entrainment at the cloud top. The prime effect of encroachment into the layer above is to change the rate of lowering of cloud base by reducing the total moisture flux into the layer.

The bottom of the convecting plumes are not at the sea surface however, since there is a super-adiabatic, disorganized layer beneath the plumes. The descending air will undergo horizontal motion at the bottom and re-enter an adjacent rising plume. As the air re-enters the plume, some surface air with recent surface properties will be mixed in. Thus, the plume becomes warmer and wetter. Finally, the air reaches its saturation point at the top of the convective layer and stratus cloud is formed. Since vapor is continuously being added at the bottom, the cloud base moves downward and eventually forms sea fog if these conditions continue.

All variables, except temperature and the densities of dry air and water vapor, are assumed to be in a quasi-steady state. The temperature as well as the densities of dry air and water vapor slowly change with time but the rate at which these changes occur, which is a controlling parameter, itself changes only slowly and other variables do not change at all if the inversion does not rise. Turbulence will transfer not only the heat but also the water vapor upward from the sea surface. This vapor transport causes the density of water substances to change with time. Furthermore, the pressure changes with

time at a rate $u\nabla P$. For all the cases illustrated in Section 8, the values of $u|\nabla P|$ are less than $1.5 \times 10^{-5}$ mb s$^{-1}$. Hence, the pressure can reasonably be assumed to be in steady state.

The recirculation of a parcel of air rising from the bottom of the plume up to the top boundary and then descending in the downdraft region back to the base of the convecting layer takes about 15.5 min when we take $\nabla P = -0.18$ mb/100 km, $z_0 = 175$ m, and $\nabla T = 2.8$ K/100 km. If the initial values of the plume are suddenly changed, the recirculation time will be the time required for the plume to adjust to its new structure.

Indeed this time for recirculation enables us to gain some confidence that other non-steady state solutions will differ only slightly from the case studied here. If changes in temperature are relatively slow compared to this time constant, then the solutions should not show appreciable differences. The fraction of air from the downdraft replaced by surface air to form the next updraft is $2ai_s/w_p$ (see Telford and Presley, 1978), so if $a = 1/12$ and $i_s/w_p = 1$, we get 1/6. Thus the quasi-steady state plume model recirculates once in a single period to reduce its temperature excess over the surface layers to 5/6, or to $1/e$ in 5.48 periods, which is the usual definition of a time constant, and is about 1.4 hr for the above example.

Thus the convective field has an immediate response to a change in boundary conditions involving a surface temperature step, due to the change in temperature of the air entering the base of the plume. As soon as this air has moved up to the inversion and back to the surface again, the buoyancy and hence the driving force and the dynamics will have largely accommodated to the new conditions. Thus, the dynamics of the layer will change in one overturning time approximately, whereas the temperature accommodation will take about 5 times as long. Thus the dynamical solution is approximately stable, with quite small transient components, through the whole temperature accommodation time, and hence will be closely modeled by the quasi-steady state where the surface temperature is changing fast enough to keep the temperature difference between updraft and downdraft unchanged.

The validity of this approximation solution also applies to the case of cool air over a constant warm sea surface, the fields being essentially the same when temperature and mixing ratio differences between the surface and the air are the same, and the wind is the same.

The plume and its surrounding air are assumed to be uniform over horizontal sections. This assumption is supported by the aircraft observations made by Warner and Telford (1967). Their observations showed that the plumes have well defined boundaries and the temperature outside the plume is uniform throughout the field. Temperatures inside the well-mixed plumes are assumed to have stable averages. The mixing process internal to the plumes is rapid. Whenever a parcel of surrounding air is entrained into the plume by turbulence, the turbulence will mix it with the plume air so rapidly that it is hardly identifiable from the plume air with modern measuring techniques. Seldom is the temperature within a plume as low as in the surroundings on each side, and never lower (with an upward heat flux).

The vertical mixing within plumes is so small that it has been neglected without introducing apparent error.

The entrainment rate horizontally through the plume boundary is assumed proportional to the r.m.s. turbulent velocity. As noted in Telford (1966), this model does not need to consider the turbulent energy spectrum.

## 5. Equations

Volume, total mass (dry air + water vapor + liquid water), mass of water substances (water vapor + liquid water), momentum and turbulent kinetic energy must be conserved under convective motion of a moist air parcel without precipitation.

It should be noted that in this treatment, the temperature is specified by the volume and mass equations, which give the air density, and hence the pressure, as a function of height, and in consequence, the temperature and liquid water content at each height. This approach was chosen because it is simpler to represent all parcel changes with height, as exact thermodynamically reversible actions for a perfect gas, using this approach; rather than by starting off with the Boussinesq approximation and thermal averaging during mixing. We know of no way to establish the accuracy of each approximation other than by calculating the result both ways, and since the precise model calculation involves a trivial amount of computer time by present standards, there is no point in studying various other approximations.

The volume conservation equation can be derived as follows. In an air parcel moving upward, adiabatic expansion due to the pressure change can be expected. If the air parcel contains water vapor, the question of whether the air reaches its condensation level or not, must be examined. If it does, the latent heat released from the phase transition must then be considered. Mixing with surrounding air through the boundaries is also continuously taken into account at every stage.

The expansion-condensation proceses can change neither the total mass of air nor the total mass of water substances. The only property to be calculated is the volume, once the pressure is determined. Therefore, in the volume equation, both mixing and expansion-condensation effects must be considered. When the incremental changes are small, the higher order terms in Taylor's expansion can be neglected. Therefore, the volume equation can be written as

$$(\mathrm{d}V)_{\text{total}} = (\mathrm{d}V)_{\text{entrainment}} + (\mathrm{d}V)_{\text{expansion-condensation}} \cdot \tag{1}$$

where $V$ is volume.

In the case of convective marine stratus formation, precipitation is not considered. All the condensate is transported forward. Thus, a reversible process can represent the expansion during atmospheric convection. The reversible ascents of a saturated air parcel and an unsaturated air parcel have been considered separately in the calculation.

For saturated air parcels, the volume change due to expansion-condensation can be expressed as

$$(\mathrm{d}V)_{\text{expansion-condensation}} = JV\,\mathrm{d}P_T, \tag{2}$$

where

$$J = \left[ 2r_{v,\,\mathrm{sat}} L - Tc_{\mathrm{mix}} - \frac{r_{v,\,\mathrm{sat}} L^2}{R_v T} \right] \times$$

$$\times \left[ P_a c_{p,\,\mathrm{mix}} T + L^2(\varepsilon + r_{v,\,\mathrm{sat}})\rho_{v,\,\mathrm{sat}} \right]^{-1}, \tag{3}$$

where $P_T$ is total pressure, $P_a$ is dry air pressure; $T$ is temperature; $L$ is the latent heat due to vaporization; $r_v$ is water vapor mixing ratio; $R_a$ is the gas constant of dry air; $\varepsilon = R_a/R_v \simeq 0.622$; $R_v$ is the gas constant of water vapor; $\rho_v$ is the vapor density; $c_{mix} = c_{va} + r_{v,\,sat}c_{pv} + r_w c_{pw}$; $c_{p,\,mix} = c_{pa} + r_{v,\,sat}c_{pv} + r_w c_{pw}$; $c_p$ is the specific heat at constant pressure; $c_v$ is the specific heat at constant volume; subscripts $a$, $v$, $w$, and sat denote dry air, water vapor, liquid water, and saturation, respectively. Here we use $c_{pv}$ and $c_{pw}$, in $c_{\mathrm{mix}}$, rather than $c_{vv}$ and $c_{vw}$. The reason follows from the derivation. Now, $L = T(s_v - s_w)$, $\mathrm{d}L(T)/\mathrm{d}T \simeq c_{pv} - c_{pw}$ and $\mathrm{d}s_w = c_{pw}\,\mathrm{d}T/T$, where $s$ is the specific entropy. We obtain after substituting these three relationships into the total entropy conservation equation for the derivation of the volume equation, the relation given above.

For an unsaturated air parcel, the $J$ in (2) can be written as:

$$J = -\frac{c_{va} + r_v c_{vv}}{c_{pa} + r_v c_{pv}} \frac{1}{P_T}. \tag{4}$$

For the plume, differentiating (2) with respect to time and setting $V_p = \pi b^2 h$, where $b$ is the plume radius and $h$ is the depth of a slice, we get

$$\frac{\mathrm{d}}{\mathrm{d}t}(\pi b^2 h) = \pi b^2 h J_p \frac{\mathrm{d}P_T}{\mathrm{d}t},$$

where the subscript '$p$' denotes plume.

Using the quasi-steady state assumption and setting $h = w_p \delta t$, where $w_p$ is the updraft velocity and $\delta t$ is a small constant time interval, we get

$$\frac{\partial}{\partial z}(b^2 w_p) = b^2 w_p J_p \frac{\partial P_T}{\partial z}. \tag{5}$$

For the mixing process alone, the conservation of volume implies that the time rate of change of volume of a plume slice is equal to the mixing through the cylindrical boundary, i.e.,

$$\frac{\mathrm{d}}{\mathrm{d}t}(\pi b^2 h) = 2\pi b h a (i_p - i_s), \tag{6}$$

where $i_p$ and $i_s$ are the r.m.s. turbulent velocities in the plume and in the surroundings, respectively, and $a$ is the ratio of mixing velocity to the turbulent velocity.

Using the same techniques as in deriving (5), Equation (6) becomes

$$\frac{\partial}{\partial z}(b^2 w_p) = 2ba(i_p - i_s). \tag{7}$$

Therefore, the total volume change is the combination of (5) and (7), i.e.,

$$\frac{\partial}{\partial z}(b^2 w_p) = 2ab(i_p - i_s) + b^2 w_p J_p \frac{\partial P_T}{\partial z}. \tag{8}$$

The derivations of other conservation equations can be found in Telford (1970).

The five equations for the updraft are as follows:

*Volume*

$$\frac{\partial}{\partial z}(b^2 w_p) = 2ab(i_p - i_s) + b^2 J_p w_p \frac{\partial P_T}{\partial z}, \tag{8}$$

*Total mass*

$$\frac{\partial}{\partial z}(b^2 w_p \rho_{t,p}) = 2ab(i_p \rho_{t,s} - i_s \rho_{t,p}) - b^2 \dot{\rho}_{t,p}, \tag{9}$$

*Mass of Water Substances*

$$\frac{\partial}{\partial z}(b^2 w_p \rho_{w,p}) = 2ab(i_p \rho_{w,s} - i_s \rho_{w,p}) - b^2 \dot{\rho}_{w,p}, \tag{10}$$

*Momentum*

$$\frac{\partial}{\partial z}(b^2 w_p^2 \rho_{t,p}) = -b^2 \frac{\partial P_T}{\partial z} - gb^2 \rho_{t,p} + 2ab(i_p w_s \rho_{t,s} - i_s w_p \rho_{t,p}) - b^2 w_p \dot{\rho}_{t,p}, \tag{11}$$

*Turbulent Kinetic Energy*

$$\frac{\partial}{\partial z}(b^2 w_p \rho_{t,p} i_p^2) = 2ab\{i_p \rho_{t,s}[(w_p - w_s)^2 + i_s^2] - i_s \rho_{t,p} i_p^2\} - b^2 i_p^2 \dot{\rho}_{t,p} - \frac{A}{2} b \rho_{t,p} i_p^3, \tag{12}$$

where $\rho_{t,p}$ (or $\rho_{w,p}$) and $\rho_{t,s}$ (or $\rho_{w,s}$) are the total density (or density of water substances if the alternative formulation is used, since both are conserved) of the plume air and the surrounding air, respectively, $A$ is a constant of proportionality relating the rate of dissipation of turbulent kinetic energy to $i^3/l$, and $l$ is a typical length scale of the turbulent motion. From laboratory experiments, the value of $A$ is of the order unity. We set $A = 1$ in this model.

Similarly, we can derive a set of conservation equations for the downdraft:

*Volume*

$$\frac{\partial}{\partial z}\left[(c^2-b^2)w_s\right] = 2ab(i_s - i_p) + (c^2-b^2)J_s w_s \frac{\partial P_T}{\partial z}, \tag{13}$$

*Total Mass*

$$\frac{\partial}{\partial z}\left[(c^2-b^2)w_s\rho_{t,s}\right] = 2ab(i_s\rho_{t,p} - i_p\rho_{t,s}) - (c^2-b^2)\dot{\rho}_{t,s}, \tag{14}$$

*Mass of Water Substances*

$$\frac{\partial}{\partial z}\left[(c^2-b^2)w_s\rho_{w,s}\right] = 2ab(i_s\rho_{w,p} - i_p\rho_{w,s}) - (c^2-b^2)\dot{\rho}_{w,s}, \tag{15}$$

*Momentum*

$$\frac{\partial}{\partial z}\left[(c^2-b^2)w_s^2\rho_{t,s}\right] = -(c^2-b^2)\frac{\partial P_T}{\partial z} - g(c^2-b^2)\rho_{t,s} + \\ + 2ab(i_s w_p\rho_{t,p} - i_p w_s\rho_{t,s}) - (c^2-b^2)w_s\dot{\rho}_{t,s}, \tag{16}$$

*Turbulent Kinetic Energy*

$$\frac{\partial}{\partial z}\left[(c^2-b^2)w_s\rho_{t,s}i_s^2\right] = 2ab\left\{i_s\rho_{t,p}\left[(w_s-w_p)^2 + i_p^2\right] - i_p\rho_{t,s}i_s^2\right\} - \\ - (c^2-b^2)i_s^2\dot{\rho}_{t,s} - \frac{A}{2}(c^2-b^2)^{1/2}\rho_{t,s}i_s^3. \tag{17}$$

From these ten differential equations, we can derive the following ten equations which describe the field more directly. (Detailed derivations can be found in Chai, 1978.)

$$\frac{\partial P_T}{\partial z} = \left\{2ab(w_p - w_s)\left[i_s\rho_{t,p}^2 w_p^2 - i_p\rho_{t,s}^2 w_s^2 + \right.\right. \\ \left. + \rho_{t,p}\rho_{t,s}w_p w_s(i_p - i_s)\right] - g\rho_{t,p}\rho_{t,s}\left[w_p^2(c^2-b^2) + w_s^2 b^2\right]\right\} \times \\ \times \left\{b^2\rho_{t,s}w_s^2 + (c^2-b^2)\rho_{t,p}w_p^2 + w_p^2 w_s^2\rho_{t,p}\rho_{t,s}\left[b^2 J_p + (c^2-b^2)J_s\right]\right\}^{-1}. \tag{18}$$

$$\frac{\partial\rho_{t,s}}{\partial z} = -\frac{2abi_s(\rho_{t,s} - \rho_{t,p})}{(c^2-b^2)w_s} - \frac{\dot{\rho}_{t,s}}{w_s} - \rho_{t,s}J_s\frac{\partial P_T}{\partial z}. \tag{19}$$

$$\frac{\partial\rho_{t,p}}{\partial z} = \frac{2ai_p(\rho_{t,s} - \rho_{t,p})}{bw_p} - \frac{\dot{\rho}_{t,p}}{w_p} - \rho_{t,p}J_p\frac{\partial P_T}{\partial z}. \tag{20}$$

$$\frac{\partial \rho_{w,p}}{\partial z} = \frac{2ai_p(\rho_{w,s} - \rho_{w,p})}{bw_p} - \frac{\dot{\rho}_{w,p}}{w_p} - \rho_{w,p} J_p \frac{\partial P_T}{\partial z} . \tag{21}$$

$$\frac{\partial \rho_{w,s}}{\partial z} = -\frac{2abi_s(\rho_{w,s} - \rho_{w,p})}{(c^2 - b^2)w_s} - \frac{\dot{\rho}_{w,s}}{w_s} - \rho_{w,s} J_s \frac{\partial P_T}{\partial z} . \tag{22}$$

$$\frac{\partial w_s}{\partial z} = -\frac{g}{w_s} + \frac{2abi_s\rho_{t,p}(w_p - w_s)}{(c^2 - b^2)w_s\rho_{t,s}} - \frac{1}{w_s\rho_{t,s}} \frac{\partial P_T}{\partial z} . \tag{23}$$

$$\frac{\partial w_p}{\partial z} = -\frac{g}{w_p} - \frac{2ai_p\rho_{t,s}(w_p - w_s)}{bw_p\rho_{t,p}} - \frac{1}{w_p\rho_{t,p}} \frac{\partial P_T}{\partial z} . \tag{24}$$

$$\frac{\partial b}{\partial z} = \frac{a(i_p - i_s)}{w_p} - \frac{b}{2w_p} \frac{\partial w_p}{\partial z} + J_p \frac{\partial P_T}{\partial z} \frac{b}{2} . \tag{25}$$

$$\frac{\partial i_p}{\partial z} = \frac{a\rho_{t,s}}{bw_p\rho_{t,p}} [(w_p - w_s)^2 + i_s^2 - i_p^2] - \frac{A}{4bw_p} i_p^2 . \tag{26}$$

$$\frac{\partial i_s}{\partial z} = \frac{ab\rho_{t,p}}{(c^2 - b^2)w_s\rho_{t,s}} [(w_s - w_p)^2 + i_p^2 - i_s^2] - \frac{A}{4(c^2 - b^2)^{1/2}w_s} i_s^2 . \tag{27}$$

The latent heat released by the condensation of water vapor will change the rate of change of densities of both dry air and water substances inside the cloud. Therefore, there are changes in $\dot{\rho}_t$ and $\dot{\rho}_w$ across the cloud base. The dot terms in the clear region below the cloud base are determined by the surface heat, moisture and momentum fluxes. In order to find the dot terms at height $z$ in cloud, we first lift a parcel of air adiabatically from the bottom of the plumes below the cloud base, at $z_1$, up through the cloud base to $z$ at time $t$. Then at $\delta t$ time later, we lift another parcel from $z_1$ to $z$ and compare the property changes within $\delta t$ time interval at $z$ to find the dot terms at that level.

The ten equations, (18) through (27), given ten boundary conditions, can be integrated numerically. A fourth-order Runge-Kutta method was employed for the integration.

## 6. Boundary Conditions

At the top boundary, since the air in the downdraft region has just turned over from the plume, the temperature, turbulent velocity, total density and the density of water substances must be equal to those in the plume. We are not including entrainment at the top surface here, at this stage. We assign the temperature, pressure and liquid water content at the top.

Adding (8) and (13), and using the top boundary conditions as described above, we get

$$\frac{\partial}{\partial z}\left[b^2 w_p + (c^2 - b^2) w_s\right] = \left[b^2 w_p + (c^2 - b^2) w_s\right] J_p \frac{\partial P_T}{\partial z} .$$

If there is no net volume flux at the top boundary, we can set

$$b^2 w_p + (c^2 - b^2) w_s = 0 ,$$

or

$$w_s = -\frac{b^2 w_p}{c^2 - b^2} . \tag{28}$$

Therefore, we have six boundary conditions at the top:

$$P_0, T_0$$

$$\rho_{t,p} = \rho_{t,s}$$

$$\rho_{w,p} = \rho_{w,s}$$

$$i_p = i_s$$

$$w_s = -b^2 w_p/(c^2 - b^2) ,$$

where $P_0$ and $T_0$ are given, and $w_p$, $i_s$, $c$, and $b$ will be determined at the top by iterating the process to meet the four conditions at the bottom.

The lower boundary conditions are the same as in Telford (1970):

$$i_p = i_s = I_0$$

$$b^2 = \frac{c^2}{2}$$

$$\frac{\partial \theta_s}{\partial z} = 0 ,$$

where $I_0$ is the turbulent velocity in the forced convective layer and $\theta_s$ is the potential temperature in the downdraft.

Setting the initial values at the top boundary of downdraft velocity, turbulent velocity in the plume, plume radius and the combined radius of the convective cell, the equations can be integrated downward through the depth of the convective layer. The four initial values are adjusted until the four lower boundary conditions are satisfied. This is done by an appropriate iterative method.

## 7. The Surface Boundary Layer

Telford and Presley (1978) developed a multi-level surface layer model. That model is employed here to calculate the momentum, heat, and vapor fluxes. Based on the observations reported by Priestley (1959), a three-level boundary layer is chosen for application in this sea fog model.

The momentum flux can be expressed by the product of horizontal pressure gradient, $\nabla P$, and the depth of the convective layer, i.e.,

$$\tau = -z_p \nabla P . \tag{29}$$

Assuming that the turbulent energy per unit volume is a constant throughout the boundary and that there is no significant net transport up into the convective plume layer, the following two equations can be obtained by equating the rates of generation and dissipation of the turbulent energy per unit volume. (Detailed derivations of these two equations can be found in Telford and Presley (1978).)

$$\tau = \frac{A\rho_{t,p} I_0^3}{2\bar{u}} .$$

and

$$I_0 = \left(2\,\frac{a}{A}\right)^{1/2} \bar{u} .$$

where $\bar{u}$ is the mean wind velocity at the base of the plume.

Combining these two equations and cancelling $\bar{u}$, yields

$$I_0 = \left(\frac{2}{aA}\right)^{1/4} \left(\frac{\tau}{\rho_{t,p}}\right)^{1/2} .$$

Since $a \simeq \frac{1}{12}$ and $A = 1$, we get

$$I_0 = 2.21 \left(\frac{\tau}{\rho_{t,p}}\right)^{1/2} . \tag{30}$$

Assuming that upward and the downward mixing rates through any interface are equal, yields

$$ai_n = ai_{n-1} = aI_0 ,$$

or

$$i_n = i_{n-1} = I_0 .$$

Therefore, the momentum flux can be expressed as

$$\tau = \rho_{t,p} a(i_{n-1} u_n - i_n u_{n-1}) = \rho_{t,p} a I_0 \Delta u_n .$$

Assuming that $\tau$ is approximately constant, i.e., $\Delta u_n = \Delta u$, the mean wind velocity at the plume base can be expressed as,

$$\bar{u} = n\Delta u .$$

Combining these two equations and cancelling $\Delta u$ yields,

$$\bar{u} = \frac{n\tau}{aI_0\rho_{t,p}} .$$

Since a three-level boundary layer is suitable for our purpose, we set $n = 3$. Therefore,

$$\bar{u} = \frac{3\tau}{aI_0\rho_{t,p}} . \tag{31}$$

The rate of change of potential temperature is then

$$\dot{\theta} = \bar{u}\nabla T , \tag{32}$$

The heat flux is

$$H = \rho_{t,p}c_{p,\,\mathrm{mix},\,p}z_0\dot{\theta} . \tag{33}$$

From (29) through (33), we can infer that the three controlling parameters of the convective field are $z_0$, $\nabla T$, and $\nabla p$.

Using the Telford and Presley model, the vapor flux, in a three-level surface layer, can be expressed as

$$Q = \tfrac{1}{3}aI_0\rho_{t,p}\Delta r_v . \tag{34}$$

where $\Delta r_v$ is the difference between the saturation mixing ratio at the sea surface and the average mixing ratio at the bottom of the plume. Defining $K \equiv \frac{1}{3}aI_0\rho_{t,p}$, Equation (34) becomes,

$$Q = K\Delta r_v . \tag{35}$$

From (31), the momentum flux can be written as

$$\tau = K\bar{u} . \tag{36}$$

Thus, the vapor flux can be calculated in this model by using (29), the momentum flux, and (31), the wind velocity, i.e.,

$$Q = \frac{\tau}{\bar{u}}\,\Delta r_v .$$

The vapor flux brought up by the plume is distributed to the whole convective layer and changes its vapor density. Therefore, the vapor flux can also be defined as

$$Q = \dot{\rho}_v z_0 .$$

Thus, the rate of change of water vapor density can be determined by using

$$\dot{\rho}_v = \frac{Q}{z_0} . \tag{37}$$

The model is now complete. All the conservation equations are formed, suitable boundary conditions are given, and the momentum, heat and vapor fluxes in the convective field have been derived.

## 8. Applications

The model has been applied to a convective field with the values of the three controlling parameters as:

$$z_0 = 175\ \text{m},$$

$$\nabla P = -0.18\ \text{mb/100 km},$$

$$\nabla T = 2.8\ ^\circ\text{C/100 km}.$$

The initial conditions at the top boundary are: $T = 20\ ^\circ\text{C}$, $P_T = 992.867$ mb and $\rho_v = 0.017\ \text{kg m}^{-3}$, where $\rho_v$ is the saturation vapor density over water at 20 °C. The vertical structures of several major properties are shown in Figures 3 to 5. In Figure 3, the air is just saturated at the top boundary and there is no liquid water throughout the convecting layer. Since the liquid water content in the model is specified by the given liquid water content at the top boundary, increasing this given value leads to a lowering of the cloud base (Figures 4 and 5). In Figure 5, the cloud base is about 5 m above the base of the convecting plume layer.

The heat flux is about $17\ \text{W m}^{-2}$, and the temperature difference between the plume base and the sea surface is about 1.5 °C. The vapor flux, the cloud base height and the cloud base lowering speed are shown in Table I as functions of the liquid water content at the top boundary. The vapor flux decreases as the liquid water content at the top increases. The cloud base in the plume is lower than that in the downdraft. This can

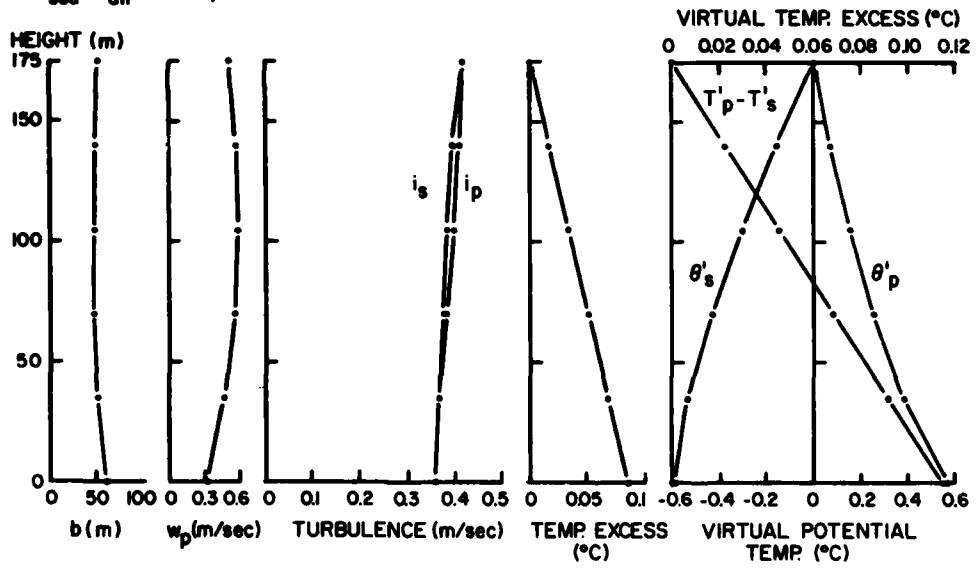


Fig. 3. The calculated model convective field before the stratus is formed. The air is just saturated at the top boundary.

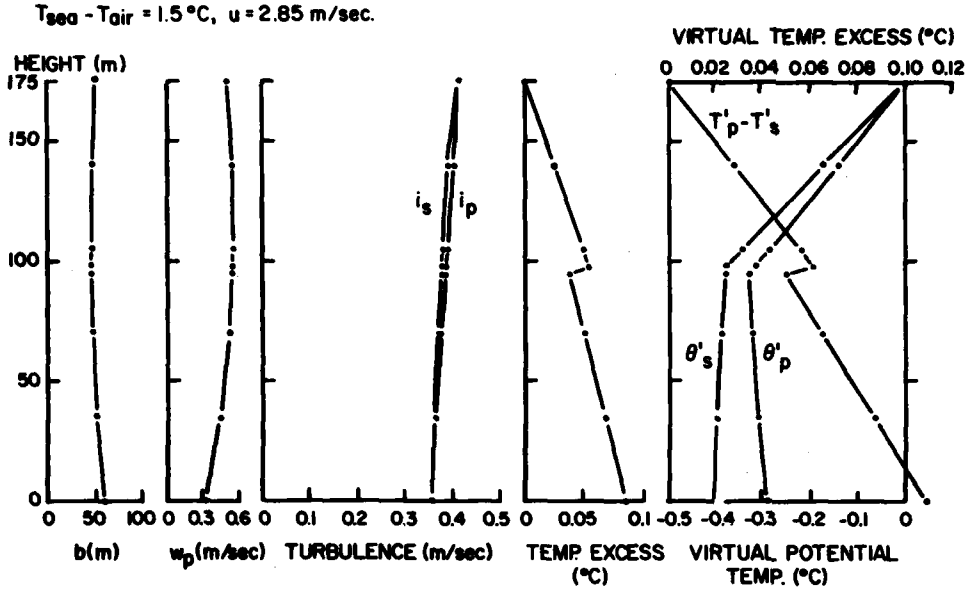


Fig. 4. The convective field with 0.2 g m$^{-3}$ liquid water content at the top. The cloud base in the plume is about 95 m above the surface boundary layer, which is about 3 m lower than that in the downdraft.

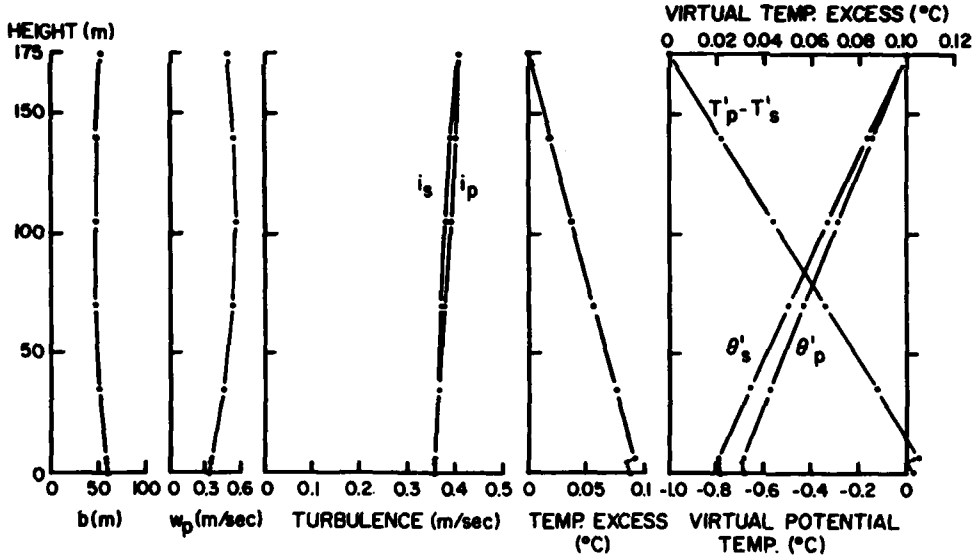


Fig. 5. As in Figure 4 but the cloud base in the plume is about 5 m above the bottom of the convecting plume layer.

TABLE I

The height and the lowering speed of cloud base and the vapor flux as functions of the liquid water content at the top boundary

$\nabla P = -0.18$ mb/100 km, $\nabla T = 2.8$ °C/100 km, $z_0 = 175$ m, $T_{sea} - T_{air} = 1.5$ °C, $u = 2.85$ m s$^{-1}$

| Liquid water content at the top boundary ($\times 10^{-1}$ g/cm$^3$) | Vapor flux (cm day$^{-1}$) | Cloud base | | | |
|---|---|---|---|---|---|
| | | Height (m) | | Lowering speed (m hr$^{-1}$) | |
| | | Plume | Downdraft | Plume | Downdraft |
| 0 | 0.26 | – | – | – | – |
| 1.0 | 0.23 | 134.7 | 136.9 | 106.7 | 100.4 |
| 2.0 | 0.20 | 94.8 | 98.0 | 78.6 | 74.7 |
| 3.0 | 0.18 | 55.3 | 58.5 | 50.7 | 48.9 |
| 4.0 | 0.15 | 16.4 | 18.4 | 23.5 | 23.0 |
| 4.3 | 0.14 | 4.9 | 6.3 | 15.5 | 15.2 |

be explained as follows. Since the air at any position in the convecting cell originally came from the plume base, the air in the plume rises at a later time than that in the surrounding downdraft. Thus, the plume air is warmer and wetter than the surrounding air. From the Clausius-Clapeyron equation and the equation of state, we find that

$$\frac{d\rho_s}{dt} = \left(\frac{L}{R_v T} - 1\right)\frac{\rho_s}{T}\frac{dT}{dt} . \tag{38}$$

where $\rho_s$ is saturation vapor density. This equation gives the rate of change of saturation vapor density as a function of the rate of change of temperature. In our case, the rate of change of temperature is 0.288 °C/hr. This implies a rate of change of saturation vapor density of 0.000 29 kg/m$^3$-hr. The vapor flux from evaporation at the sea surface gives the plume a rate of change of vapor density of 0.000 33 to 0.000 63 kg/m$^3$-hr. Since the rate of change of vapor density from the vapor flux is greater than that from the heat flux, the cloud base in the plume is lower than that in the downdraft region.

The temperature excess curve is very close to a straight line in Figure 3. This is because there is no condensation in the whole convective layer, and the temperature profiles both inside and outside the plume are nearly that of the dry adiabatic profile. They are not exactly dry adiabatic structures because there is a heat flux coming up from the sea surface and because there is mixing between updraft and downdraft. In Figures 4 and 5, there is a discontinuous layer on the temperature excess curve. This is because the vapor in the plume starts to condense above the plume cloud base releasing latent heat while in the downdraft region, the air is still under-saturated. The lapse rate in the plume is nearly pseudo-adiabatic which is quantitatively smaller than the dry adiabatic lapse rate in the surroundings.

The plume radius decreases with height in the lower portion but increases with height in the upper portion. This is caused by the buoyancy force. In the lower portion of the

convective layer, the temperature excess is large. Thus, the updraft rises at an accelerating speed and, by the continuity equation, the radius decreases while it is accelerating. During this rise, mixing with cooler descending air slows the acceleration and finally deceleration begins; then the radius starts to increase with altitude. This mechanism can be seen by comparing the radius curve with the updraft velocity curve.

We should stress here that the base of the convecting layer is not the sea surface. There is a surface layer, beneath the organized plume layer, as mentioned in the previous section. The depth of the surface layer is about $b/2$.

The large slope of the virtual potential temperature curves in the clouds is caused by condensation heating.

The wind velocity in this case is about 2.85 m $s^{-1}$. About 3 hr are required to lower the cloud base from 175 m down to the sea surface (Figure 6).

Figure 6 shows the time required to lower the plume cloud base for three cases. Curve *b* is the case just discussed. Curve *a* is for the same convective layer height but with half of the surface temperature gradient and the horizontal pressure gradient. It takes about 7.3 hr to lower the cloud base from 175 m down to the bottom of the plumes.

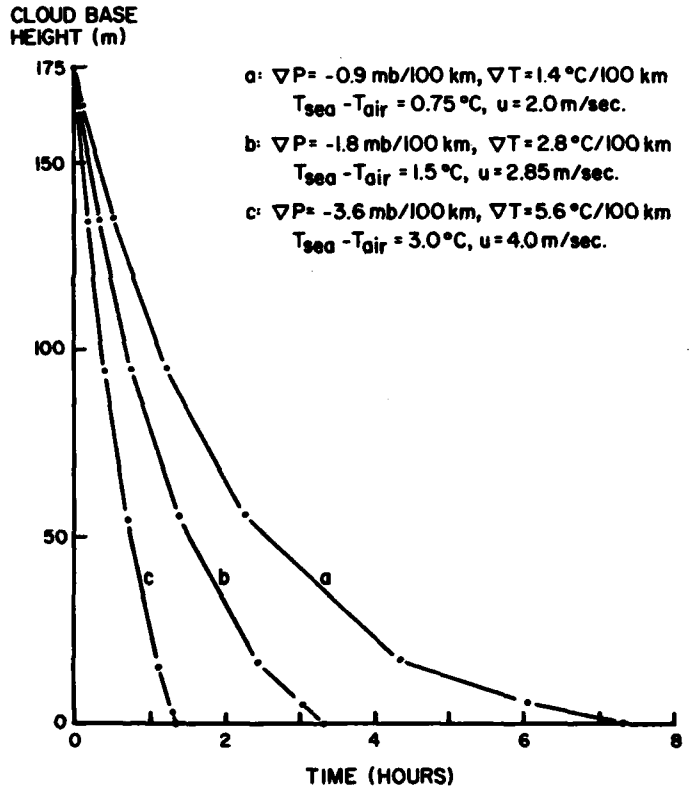


Fig. 6. The cloud base height in the plume layer as a function of time.

Curve *c* shows the case with double the horizontal pressure gradient and the surface temperature gradient. The time required to lower the cloud base from 175 m to the plume base is about 1.3 hr. Thus, higher surface temperature gradients and horizontal pressure gradients can lower the cloud faster.

One point of interest is that in the dry air case, there is a non-dimensional parameter which is equivalent to the ratio of the total convective layer depth to the Obukhov scale length (Telford, 1972). The solutions to the motion field for the clear air case were unrealistic beyond a range of 1 unit to 2.2 units for this parameter.

Converting to $z/L$, where $L$ is the Obukhov scale length we get,

$$z_0/(-L) = z_0 kgH/\rho c_p T u^{*3} .$$

This parameter can be evaluated using the present theory.

From Telford (1983), von Karman's constant $k$, is,

$$k = 2(2a^3/A)^{1/4} ,$$

where $a = 1/12$, $A = 1$, and hence $k = 0.37$.

From Telford and Presley (1978),

$$u^* = (aA/2)^{1/4} i .$$

Thus,

$$z_0/(-L) = (2(2a^3/A)^{1/4}/(aA/2)^{3/4}) z_0 gH/\rho c_p T i^3$$

and from Telford (1972),

$$K^2 = z_0 gH/(\rho c_p T i^3) .$$

Hence,

$$z_0/(-L) = 2(2a^3 2^3/a^3 A^4)^{1/4} K^2$$

$$= (4/A)K^2 .$$

Thus for $1 < K < 2.2$, or $1 < K^2 < 4.8$,

$$-4L < z_0 < -19.4L .$$

As an example, where the turbulence $i = 1\ \mathrm{m\ s^{-1}}$, and the heat flux is $H = 100\ \mathrm{W\ m^{-2}}$, we have,

$$-L = 100\ \mathrm{m, approximately} ,$$

and,

$$400\ \mathrm{m} < z_0 < 1900\ \mathrm{m} \quad \text{(Telford, 1972)} .$$

Since, in this present model,

$$\tau = -z_0\, \partial p/\partial x = \rho u^{*2} = \rho(aA/2)^{1/2} i^2$$

thus,

$$K^2 = (z_0^2 g\, \partial T/\partial t)/(Ti^3)\,,$$

$$\partial T/\partial t = v\, \partial T/\partial x\,,$$

and

$$v/i = n(A/2a)^{1/2}\,.$$

Thus,

$$\begin{aligned} K^2 &= (g/T)(\partial T/\partial x) v z_0^2/i^3 \\ &= (g/T)(\partial T/\partial x) n(A/2a)^{1/2} z_0^2/i^2 \\ &= -(g/T)(\partial T/\partial x) n(A/2a)^{1/2} z_0 \rho(aA/2)^{1/2}/(\partial \rho/\partial x) \\ &= -(nA/2)(\rho g/T) z_0 x(\partial T/\partial x)/(\partial \rho/\partial x)\,. \end{aligned}$$

Thus for $z_0 = 175$ m, $\nabla \rho = -18Pa/100$ km, and $\nabla T = 2.8$ °C/100 km, and using $r = 3$, as we have here,

$$\begin{aligned} K^2 &= (3/2)(9.8/300) z_0 (2.8/18) \\ &= z_0/131\,. \end{aligned}$$

With, $1 < K < 2.2$,

$$131 \text{ m} < z_0 < 635 \text{ m}\,,$$

and the value of $z_0 = 175$ used is within the limits set for cloud-free convection. As the cloud base lowers towards the surface, $K$ decreases in the model by less than 10%. Thus these conditions are those for dry plumes before the cloud forms, and do not change markedly as the cloud lowers.

Convective fields with $-z/L$ beyond these limits imply that other forms of convective transfer are occurring such as horizontal rolls or blobs. As is well known, the convective plume layer often lies below a layer where clear air convection is in the form of blobs (Telford, 1972). This phenomenon has been described by glider pilots such as Woodward (1959). Cumulus clouds also form above the level reached by the dry air convection, as is shown in Figure 2 of Warner and Telford (1967). These cloudy structures are very likely to be blobs rising from the top of the convective plume layer.

These limits on the convective field may also be associated with the observed intermittency as seen in the data of Figure 1, where the convective field has separated into two layers at 200 m altitude.

We should note that layer depth, cloud base height, sea-to-air temperature excess, and wind speed, are equally valid parameters to specify.

## 9. Discussion

The plume model described above can be used to study marine stratus or fog formation. Plume convection, or some alternative form probably involving rolls, is likely to be an

essential part of the mechanism for fog formation. It is concluded that the additional effects of entrainment at cloud top happen rapidly and do not need to be modeled when seeking approximate time estimates. In our model, stratus cloud forms under an inversion without radiation or entrainment, and then lowers as moisture accumulates by continuous evaporation at the sea surface. The model gives a quantitative estimate of the rates at which this takes place. Average encroachment, and heat flux effects at the top of the layer, can both be adequately modeled by choosing appropriate heat and moisture fluxes at the surface to follow the temperature profile in the overlying air as the cloud base lowers. Modified flux values can be found to incorporate the overlying air at a given rate as the air in the layer reaches the same composition as the next slice just above. Alternatively, given the flux, this gives the rate of increase in layer depth.

Extensive measurements have been undertaken by the Air Motions Laboratory at the Desert Research Institute to elucidate this question. While convecting fog has been found over warmer water, the edge of the upstream fog has, until now, been too far west to reach with our aircraft. Furthermore, the sea surface temperature is often relatively constant, with very rapid transitions of a few degrees from one area to the next. Such a situation occurred for several weeks, viz., two degrees centigrade increase flying west in less than one kilometer, about 150 km west of the Golden Gate Bridge, San Francisco. Sea surface temperatures of up to 5 °C warmer than near the coast were observed beyond this transition. Thus, much larger surface temperature gradients are found than would be assumed as average values, and these are also associated with local large horizontal pressure gradients. The model given here provides a tool which should be an adequate approximation by using the temperature difference between the air and water to specify the fluxes.

While radiation cooling is not necessary to form and maintain stratus or fog, it may be an additional factor in marine fog formation once a cloud layer forms from convective activity. Radiative cooling will not only produce downward convection from the top, but also it will cool the whole layer and so increase the sea-to-air temperature drop and hence the surface heat and vapor fluxes.

When heat is continuously added from the sea with the air remaining cooler than the sea, the upward vapor flux continues even though the air may be saturated at the surface, and so more liquid water condenses to make the fog denser.

While radiation may not take an appreciable difference to convecting stratus cloud, when foggy air advects across a sudden decrease in sea surface temperature, and convective overturning temporally stops, it will make the fog more dense due to a lowering of the surface air temperature. As radiative cooling continues after the fog moves over a cooler sea surface, the air near the surface will cool without being immediately warmed again by convection, since the water surface is now cooler, and hence there is no vapor flux to remove its associated supersaturation, so that more liquid water will be released onto the fog drops close to the surface.

This model does not take proper account of the relation of the surface drag to sea surface roughness, which was arbitrarily held constant. This aspect needs more study.

## Acknowledgments

This work was partly supported by the National Science Foundation Grant ATM-8012929 as basis for a stratus cloud model to examine the droplet spectra development by condensation when dry air entrainment is active. Our observations were also made under this grant. Support from the Office of Naval Research Contract N00014–75–C–0598 was related to surface boundary-layer studies incorporated in the model and the application of the model to the formation of fog by lowering stratus.

## References

Ball, F. K.: 1960, 'Control of Inversion Height by Surface Heating', *Quart. J. Roy. Meteorol. Soc.* **86**, 483–494.

Chai, S. K.: 1978, 'Lowering Stratus Cloud in Surface Driven Convection Over the Sea', Ph.D. Dissertation, Univ. of Nevada-Reno, 146 pp.

Lilly, D. K.: 1968, 'Models of Cloud-Topped Mixed Layers Under a Strong Inversion', *Quart. J. Roy. Meteorol. Soc.* **94**, 292–309.

Mahrt, L. and Paumier, J.: 1982, 'Cloud-Top Entrainment Instability Observed in AMTEX', *J. Atmos. Sci.* **39**, 622–634.

Petterssen, S.: 1938, 'On the Causes and the Forecasting of the California Fog', *Bull. American Meteorol. Soc.* **19**, 49–55.

Pillie, R. J., Mack, E. J., Rogers, C. W., Katz, U., and Kocmond, W. C.: 1979, 'The Formation of Marine Fog and the Development of Fog-Stratus Systems along the California Coast', *J. Appl. Meteorol.* **18**, 1275–1286.

Presley, J. D.: 1976, 'Free Convective Plumes in the Atmosphere', Ph.D. Dissertation, Univ. of Nevada-Reno, 162 pp.

Priestley, C. H. B.: 1959, 'Turbulent Transfer in the Lower Atmosphere', Univ. of Chicago Press, 130 pp.

Randall, D. A.: 1980a, 'Conditional Instability of the First Kind Upside-Down', *J. Atmos. Sci.* **37**, 125–130.

Randall, D. A.: 1980b, 'Entrainment into a Stratocumulus Layer with Distributed Radiative Cooling', *J. Atmos. Sci.* **37**, 148–159.

Schubert, W. H.: 1976, 'Experiments with Lilly's Cloud -Topped Mixed Layer Model', *J. Atmos. Sci.* **33**, 436–446.

Stage, S. A. and Businger, J. A.: 1981a, 'A Model for Entrainment into a Cloud-Topped Marine Boundary Layer. Part I: Model Description and Application to a Cold-Air Outbreak Episode', *J. Atmos. Sci.* **38**, 2213–2229.

Stage, S. A. and Businger, J. A.: 1981b, 'A Model for Entrainment into a Cloud-Topped Marine Boundary Layer. Part II: Discussion of Model Behavior and Comparison with Other Models', *J. Atmos. Sci.* **38**, 2230–2242.

Telford, J. W.: 1966, 'The Convective Mechanism in Clear Air', *J. Atmos. Sci.* **23**, 652–666.

Telford, J. W.: 1970, 'Convective Plumes in a Convective Field', *J. Atmos. Sci.* **27**, 347–358.

Telford, J. W.: 1972, 'A Plume Theory for the Convective Field in Clear Air', *J. Atmos. Sci.* **29**, 128–134.

Telford, J. W.: 1975, 'The Effects of Compressibility and Dissipation Heating on Boundary Layer Plumes', *J. Atmos. Sci.* **32**, 108–115.

Telford, J. W.: 1983, 'A Theoretical Value for Von Karman's Constant', *Pure Appl. Geophys.*, accepted for publication.

Telford, J. W. and Chai, S. K.: 1980, 'A New Aspect of Condensation Theory', *Pure Appl. Geophys.* **118**, 720–742.

Telford, J. W. and Presley, J. D.: 1978, 'The Surface Boundary Layer as a Part of the Overlying Convective Layer', *Pure Appl. Geophys.* **117**, 664–689.

Telford, J. W. and Wagner, P. B.: 1981, 'Observations of Condensation Growth Determined by Entity Type Mixing', *Pure Appl. Geophys.* **119**, 934–965.

Telford, J. W. and Warner, J.: 1964, 'The Fluxes of Heat and Vapour in the Lower Atmosphere Derived from Aircraft Observations', *J. Atmos. Sci.* **21**, 539–548.

Warner, J. and Telford, J. W.: 1967, 'Convection Below Cloud Base', *J. Atmos. Sci.* **24**, 374–382.

Woodward, B.: 1959, 'The Motion in and Around Isolated Thermals', *Quart. J. Roy. Meteorol. Soc.* **85**, 144–151.

BOUN 83-88T

# INVERSIONS, AND FOG, STRATUS AND CUMULUS FORMATION IN WARM AIR OVER COOLER WATER

J. W. TELFORD and S. K. CHAI

*Air Motions Laboratory, ASC, Desert Research Institute University of Nevada System, Reno, Nevada 89506, U.S.A.*

(Received in final form 23 January, 1984)

**Abstract.** Two aspects of convection over oceans are discussed and the following conclusions are derived from theoretical considerations.

(1) The air layer over the sea will usually convect even when the water surface is ten degrees or more colder than the initial air temperature.

(2) An inversion at stratus cloud tops is created by the stratus, and is not a necessary preexisting condition. Such inversions persist after subsidence evaporates the cloud.

(3) Radiation heat exchange does not play an essential role in stratus formation or maintenance, and can either be heating or cooling the cloud.

(4) Dry air convection does not erode inversions at the top of the convecting layer. Examples of soundings are discussed.

(5) Fogs are most likely to form at sea where the water is coolest, and need no radiation effects to initiate cooling, or a boost from patches of warmer water, to begin convection.

(6) Both stratus cloud growth, and the evaporation of clouds by cloud top entrainment, readjusts the vertical structure of the air to leave a constant wet-bulb potential temperature with height.

These conclusions are supported by, firstly, a convective model which has been developed and which shows that vapor-driven convection over the ocean will proceed with zero or negative heat fluxes, at rates which saturate the lowest layer of the atmosphere in a few hours to altitudes of many tens of meters. Secondly, the availability of condensed moisture at the top of the surface layer cools the warmer entrained overlying dry air parcels so that when they descend they are no warmer than the sea surface temperature, and this induces downward moving plumes. This occurs if the wet-bulb potential temperature of the overlying air is less than the sea surface temperature, even if it is ten degrees C, or more, warmer in actual temperature.

## 1. Introduction

A major problem in explaining the formation of fog over the ocean has related to the question of how the air reaches saturation. Over land, radiation at night will cool the surface, and air which is in contact with it can apparently also be cooled by radiation or shear stirring to reach saturation without any increase in mixing ratio. Over the sea, radiation cools the water very slowly, so that it changes little in temperature compared to changes due to advection of the air, and so such a process is not likely to work. The air itself cannot cool appreciably by radiation since it cannot drop in potential temperature below the almost steady sea surface temperature.

Thus over the sea, the mixing ratio of the air must increase to allow fog to form. Radiative cooling of clear air itself is very small, so that this could produce very little convective overturning and evaporation, although it results in cooling of the atmosphere as a whole and the gradual subsidence of high-level air dried out by previous high-level cumulus activity over land.

*Boundary Layer Meteorology* **00** (1984) 000–000. 0006–8314/84/0000–0000$00.00.

The idea that two very nearly saturated air layers at substantial temperature differences can give a mixture exceeding saturation, is an interesting one which seems to occur in some conditions (Saunders, 1964; Woodcock, 1982), but there is little evidence to show how such layers can come about in the first place, or how, being stable, they can mix. Such explanations usually postulate a strong inversion close to the surface, and a simultaneous decrease in mixing ratio at this inversion, as a given precondition, without explaining how it occurs. In almost all cases, radiative cooling of the clear air is very small before an inversion forms with an associated sudden decrease in mixing ratio at that level, and may be negligible until cloud actually forms at the inversion.

This paper demonstrates that radiative cooling is not generally necessary to form fog or stratus cloud. It extends the model of Chai and Telford (1983) for stratus formation over a warmer water surface, to the case where the surface is cooler than the air. It shows how the warmer surface air can be cooled by evaporation of condensed drops at the inversion, so that the circulating air at the surface is very close to surface temperature and the convection is then driven by the lower density of water vapor.

From the need for convection, it might be concluded that the sea needs to be warmer than the air, so as the promote convective overturning, and in this way add the necessary moisture to the air. However, fog is often found to form where the water is coldest so that convection from a warmer sea surface does not seem to be a sufficient explanation. There is a discussion of other models in Chai and Telford (1983).

This paper shows that there are two additional physical factors which need to be considered, and which completely change the picture relative to dry convection over land. The first consideration is that water vapor from the sea surface will drive convection, even when the sea surface is slightly cooler than the air. This process is modeled in this paper to give quantitative estimates of the time needed to moisten the air, and to lower the cloud base. This will continue until the surface air is saturated and fog lies on the surface. The model shows that frequently the resulting wet- and dry-bulb temperature excursions and the eddy fluxes may be too tiny to be measured directly, but that in a few hours the cloud base can move down a hundred meters or so.

The second factor is, however, the more important one. We believe this explanation to be new. It involves understanding the role of the latent heat of condensed water in eroding an inversion in warm overlying air. To have the water surface initially somewhat cooler (several degrees) than the air greatly enhances the chances of fog formation, rather than acting to suppress convection and hence stop the water vapor entering the air to saturate it, as might at first be thought. This is because the height where the wet-bulb potential temperature exceeds the water surface temperature is lower for a cooler surface, and the top of the layer cannot erode above this level. This limits the mass of water needed to saturate the layer by limiting the layer depth, but does not stop the convection itself.

There is no question that if the air leaving the water surface were not buoyant it could not rise, and so moisture could not be carried into the air. The question is how can the negative buoyancy due to the temperature excess be overcome? We argue here that the latent heat of mist or haze droplets at the top of a nearly saturated layer will cool any

entrained overlying dry air. As soon as such mixtures become negatively buoyant from the cooling following droplet evaporation, they will descend. Cooling in this way can occur whenever the wet-bulb potential temperature moving over the water is less than that of the air in actual equilibrium with the water (to a good approximation; exact expressions for ideal gases with and without cloud, follow below). Thus the layer grows upward as the air entrained down into the surface layer is cooled to surface temperature, by evaporation of haze drops, whereupon convection driven by the water vapor density alone continues to maintain a saturated top to the layer.

Given time, convection will form cloud and the cloud base will typically lower as its top rises, until fog lies from the surface up to the height where the air above the inversion exceeds the wet-bulb potential temperature in the fog. Evaporation at the top of the fog thus cools the air near the water. The air lying on the sea surface can thus create its own inversion-capped layer where originally there was a layer of dry air warmer than the water. An increasing wet-bulb potential temperature with height in the original dry air provides a maximum possible inversion height where this wet-bulb potential temperature exceeds water temperature, which limits the volume of air which must be saturated by the surface evaporation to give fog. If this height is relatively close to the surface, it reduces the time needed for fog formation, and hence increases the probability that it can occur under specific conditions.

This process would appear to be sufficient, in most circumstances, to explain fog formation over the sea, without recourse to other mechanisms, such as radiative cooling (Telford and Chai, 1982). However, other mechanisms may often contribute.

This new process will also contribute to the formation of inversions over land since thick haze is commonly observed just below such inversions even when no cloud is present. Inversions formed in this way will be preserved during subsidence, since this action does not alter the wet-bulb potential temperature as height changes. Potential temperature of a dry air parcel is also constant during subsidence, so that a potential temperature step at the inversion will remain, but the relative humidity will everywhere drop to well below saturation, leaving a typical inversion. Observational data which illustrate these conclusions can be found in Telford and Keck (1984).

## 2. Some Background

It has always been understood by workers in this area that convection is driven by buoyancy which is determined by temperature and by mixing ratios of liquid water and water vapor. The equation for the virtual temperature of unsaturated moist air was discussed by Guldberg and Mohn (1876). A more recent theoretical evaluation of penetrating downdrafts in cumulus clouds, driven by dry air mixing in at cloud tops, was undertaken by Squires (1958). The sort of virtual temperature involved in such density calculations, which includes liquid water, was discussed as a factor in studying measurements of cumulus buoyancy by Telford and Warner (1962).

Observations of clear air convection over the sea were reported by Warner and Telford (1963) where the sea is apparently warmer than the air but where the wet-bulb

temperature excess in the plumes is two or more times the excess of true temperature at the same point, a situation where a large part of the buoyancy comes from the lower density of the water vapor. One author (Telford) recalls reporting on one occasion in an aircraft that the plumes were cooler than the intervening air, with a large wet-bulb temperature excess. It seems clear that on this occasion the sea was colder than the air and cooling it, and that there was convection present with a negative heat flux. Since we were seeking strong convection in these measurements, we tried to choose conditions with cool offshore winds and hence met few such cases with negative heat fluxes.

The model presented below describes quantitatively this condition where water vapor generates the buoyancy, with a detailed discussion for the case when the heat flux is zero. The concepts of pseudo-wet-bulb potential temperature, wet-bulb potential temperature and wet-bulb temperature are well-known and are used here without much comment, and since the effects due to the density of the liquid water and water vapor are small, they have been ignored to reduce detailed complexity, but are precisely described by mathematical formulae used in the model.

Since the conclusions reached are quite different from those of the other models available, a brief comparison is called for, together with the caution that when the physics of a process is introduced by way of postulates chosen mainly for their simplicity, great restraint should be observed before the models are accepted, and thus alternative approaches such as we have proposed here are worth exploring, and may prove to be more fruitful, realistic or of greater generality (e.g., this model based on entities and entrainment gives a theoretical value of von Karman's constant (Telford, 1982)).

The theoretical study of the boundary layer has followed two different approaches, one starting with Ball (1960) and the other with Telford (1966). In the former case, there are numerous papers, such as Lilly (1968), who added a stratus layer to Ball's model and Randall (1980a); these all claim that radiative cooling near the top of the layer is an essential or important ingredient. Other papers concentrate on defining the entrainment of the overlying air, and it is often assumed that an entrainment rate at cloud top is proportional to the turbulent velocity, as Telford (1966) first assumed for entrainment through the sides of plumes.

The effects of 'entrainment' at the top of the convective layer are distinctly different between the models, which can be seen when the plume model is compared to other models. Deardorff (1983) discusses his position succinctly. The term 'encroachment' is a corollary to the idea of 'entrainment' eroding an inversion at the top of the convective plume layer (i.e., at the top of the observable plume layer, and not the entrainment between plumes and their surroundings). Observations, such as those shown here in Figures5 and 6 convinced the first author (Telford) that no provision for entrainment of warmer overlying air into the plumes at their tops was necessary, and so it was omitted from the model. This approach was confirmed theoretically when Presley (1976) examined this question with a plume model. It is clear that air warmer than about 0.5 to 1.0 °C cannot be carried down in the downdrafts (see Section 5 for more details) and hence entrainment at the top of the planetary boundary layer is not an effective factor

to be considered (although it no doubt occurs right at the top of the plumes, it does not introduce warmer air into the convective field as a whole) unless liquid water has condensed out at the top of the layer.

Recently Manton (1980) has used eddy diffusivity in a boundary-layer model. This approach for treatment of turbulence was rejected when we discovered that large upward heat fluxes were observed in the convective planetary boundary layer where the potential temperature was constant with height, at some level below the center of the layer, and at higher levels it was increasing slightly with height (see Section 6 in Telford and Warner, 1964; Warner and Telford, 1967). This condition demands infinite, and negative, values for the eddy diffusivity, if the observed profiles are to be reproduced. The plume-based theory gives this result directly (Telford, 1970). There are a number of other similar examples where the ideas of gradient diffusion are in conflict with observed behavior of turbulent gases, and we do not see how to obtain trustworthy time estimates without adjusting the diffusivities after the required result has been determined by other means.

All these models ignore the observed plume structure which is the basis of this present approach, and involve other postulates and constants.

Deardorff (1980) (and Lilly (1968) earlier) discuss the instability due to the entrainment of dry air at cloud top and the consequences in terms of their modelling approach. Deardorff points out that continued instability will change a stratus deck to a layer of isolated cumulus clouds. The effects of the modelling assumptions on the damping, and onset, of the instability, are investigated by Randall (1980b). The very large increase in entrainment rate as the parcels become negatively buoyant (because of a negative step in $\theta_E$ or $\theta_w$ at cloud top) is discussed in such papers, and the conclusion that there is a large increase in the entrainment rate when the parcels become negatively buoyant, agrees qualitatively with our argument that the process is very fast, compared with the addition of moisture to the layer from the sea surface.

However, there are restrictions in these models resulting from omitting the role played directly by vertically circulating elements (e.g., plumes), which will descend to cloud base directly from the cloud top, after dilution, and hence rapidly modify the whole layer almost at the same time. Such considerations have led us to reach the conclusions we present here which concern the structure of the atmosphere before and after entrainment has played its role, the relationship between $\theta_w$ above cloud and the sea surface temperature, the formation of fog, etc.

The plume model has been developed with increasing generality for the dry convective layer (Telford, 1966, 1970, 1972, 1975), the surface layer (Telford and Presley, 1978) and surface roughness (Telford, 1981) and has been used to derive a theoretical value of von Karman's constant, $k = 0.37$ (Telford, 1982). The theory has been applied to stratus cloud formed by convection over warm water (Chai and Telford, 1983) and this present paper carries the argument to convection with stratus cloud and fog, over cooler water.

Observational evidence showing that the wet-bulb potential temperature is indeed constant with height in a variety of conditions is presented in Telford and Keck (1984).

The present paper has two distinct parts which are treated differently. Firstly it is

necessary to establish that convection will occur in reasonable times with the sea cooling the air, but with buoyancy from the water vapor (which is entering the air from the sea) driving the process. Our model has been modified by the inclusion of exactly reversible thermodynamics for parcels rising or descending in and out of cloud, to make this possible with the required accuracy. This development follows in Sections 3 and 4.

The restrictions on entrainment at the top of the dry convecting layer when no condensation is present are discussed in Section 5. This shows that whenever the mixtures are buoyant, entrainment will be negligible. This condition will also apply at cloud top, so that erosion will stop once the wet-bulb potential temperature of the cloud falls much below that of the air above. Thus stratus cloud top inversions will be sharp and not spread out in height as one might expect if turbulent erosion were significant in this part of the process.

The other crucial part of the discussion involves the cooling of the top of the layer by entraining warmer overlying air into the top of the convective layer where the humidity is high enough so that liquid water is available on haze or cloud drops just below the inversion. In this discussion, we assume that the mechanism is a stop-go process with the entrainment proceeding rapidly to dilute the whole cloud in a negligible time priod compared to the times required for surface convection to add moisture to the air. This will begin every time the wet-bulb potential temperature in the cloud exceeds that of the dry warm air above. The processes will build up rapidly since there is no flux-limiting mechanism, comparable to the solar radiation making heat available on a land surface, to set the buoyancy transfer rate; the more entrainment, the more buoyant energy to support further entrainment. The process stops when wet-bulb temperature in the cloud becomes less than the dry air in contact with it so that mixtures are no longer negatively buoyant. Observational evidence that such a 'stop-go' process is actually found in marine stratus clouds is given in Telford and Wagner (1981) and discussed in Chai and Telford (1983), but the process could be thought to function continuously if the switching were rapid. In this way, the convective solution described in the earlier sections can be applied stepwise to find approximate times for the process to continue without accounting for time needed in the rapid entrainment phase driven by the unstable entrainment of an eroding cloud top. Such times will provide a reasonable estimate of the actual times required for the whole cycle.

This detailed calculation of precise times is left for later study since we now can discuss (without exact time requirements) the different cloud conditions which will prevail under various temperature and moisture structures in the overlying air. This is done in Sections 6, 7, and 8.

## 3. The Thermodynamics of Transfer Through Cloud Base

In order to model plumes driven by density differences from water vapor variations when there is no heating, the cloud condensation processes must be reversible themodynamically, so that the density of the downdraft may be calculated precisely relative to the updraft.

The basic relationship needed in the model is a formula giving the changes in a parcel from a pressure below cloud base to a pressure above cloud base, and vice versa, which does not introduce the errors of numerical integration procedures, and is physically acceptable. If we use the empirically defined water vapor pressure formula, then the latent heat involves changes in the specific heat of water with temperature, and other refinements which are very difficult to unravel.

In the model, the demand is for self-consistency over different thermodynamic paths, so that errors in temperature in the calculations are maintained to less than about 0.0001 °C. Thus while no serious error occurs if we take the specific heat of water as constant at all temperatures, the empirical vapor pressure (given in the Smithsonian Meteorological Table (1966) as the internationally accepted values) cannot then be used consistently with the simple expression for the latent heat of condensation. The following thermodynamic formulae give the exact expressions for ideal gases, and have been checked by computation in the model discussed above. Such problems become self-evident when checked against simple physical examples by the model, such as when the heat flux is zero, and entrainment between plumes and updrafts is suppressed.

The parcel can be expanded reversibly through cloud base in three stages.

(A) Separate the parcel, and expand both the air and the water vapor in perfect thermal contact (i.e., with no temperature difference to increase entropy), keeping both volumes equal, from temperature $T_1$ to $T_2$, air pressure $p_{A1}$ to $p_{A2}$, and vapor pressure from $p_{v1}$ to $p_{v2}$, where $p_{v2} > e(T_2)$ the saturated vapor pressure at temperature, $T_2$. The vapor is now supersaturated.

(B) Keep the air and the vapor in perfect thermal contact with the temperature constant at $T_2$, compress the air to pressure $p_{A3}$, and expand the vapor until $p_{v3} = e(T_2)$, the saturated vapor pressure at temperature, $T_2$.

(C) Now, again at constant temperature $T_2$, expand the air to $p_{A4}$ as some vapor condenses to water, until the volume of air again equals the volume of vapor, which now has exactly saturated vapor at $T_2$ together with condensed liquid water.

These steps can be described mathematically, using perfect gas theory, and the internal energy concept. We use $U$ for internal energy, $q$ for quantity of heat energy, $T$ for temperature, $p$ for pressure, $v$ for volume, $\rho$ for density and $m$ for mass. Subscript $A$ is for air; where appropriate, $v$ as a subscript also denotes water vapor. Water vapor mixing ratio is given by $r$, the saturated water vapor pressure by $e(T)$ and $L$ is the latent heat of vaporization of water. The subscript $w$ denotes water. Specific heat is denoted by $C$, with the first subscript $p$ or $v$ for constant pressure or volume, and the second subscript $A$ or $v$ for air or water vapor. The gas constant is $R$. The ratio of the molecular weight of water vapor to that of air is $\varepsilon$ and the ratio of specific heats of air at constant pressure to that at constant volume is $\gamma$. The symbol $\delta$ is used to denote a small increment in the following variable.

*Step A.* For air,

$$\delta U = m_A C_{vA} \delta T = \delta q_A - p_A \delta v_A = \delta q_A - (m_A R_A \delta T - v_A \delta p_A),$$

or,

$$m_A C_{pA} \delta T = \delta q_A + v_A \delta p_A ,$$

since, $C_{pA} = C_{vA} + R_A$.

For vapor, similarly,

$$m_v C_{pv} \delta T = \delta q_v + v_A \delta p_v .$$

Since thermal contact is maintained and no heat is supplied to the systems $\delta q_A + \delta q_v = 0$, so remembering that $p = \rho RT$,

$$(C_{pA} + rC_{pv})\delta T = 1/p_A(\delta(p_A + p_v))$$

$$= R_A T \frac{\delta p_A}{p_A} + rR_v T \frac{\delta p_v}{p_v} ,$$

or,

$$\left(\frac{1 + rC_{pv}/C_{pA}}{1 - 1/\gamma}\right) \ln(T_1/T_2) = \ln(p_{A1}/p_{A2}) + \frac{r}{\varepsilon} \ln(p_{v1}/p_{v2}) . \qquad (1)$$

since, $\varepsilon = R_A/R_v$, and $\gamma = C_{pA}/C_{vA}$.

*Step B.* Expand the vapor until $p_{v3} = e(T_2)$, keeping the temperature constant ($\delta T = 0$) by compressing the air.

For the air,

$$m_A C_{pA} \delta T = 0 = \delta q_A + v_A \delta p_A = \delta q_A + m_A R_A T_2 \frac{\delta p_A}{p_A} .$$

For the vapor, note $v_A \neq v_v$ now,

$$m_v C_{pv} \delta T = 0 = \delta q_v + v_v \delta p_v = \delta q_v + m_v R_v T_2 \frac{\delta p_v}{p_v} .$$

Again, $\delta q_A + \delta q_v = 0$, so,

$$\ln(p_{A2}/p_{A3}) + \frac{r}{\varepsilon} \ln(p_{v2}/p_{v3}) = 0 .$$

Since $p_{v3} = e(T_2)$, and combining with Equation (1)

$$\left(\frac{1 + rC_{pv}/C_{pA}}{1 - 1/\gamma}\right) \ln(T_1/T_2) = \ln(p_{A1}/p_{A3}) + \frac{r}{\varepsilon} \ln(p_{v1}/e(T_2)) . \qquad (2)$$

*Step C.* At constant temperature $T_2$, condense water from the vapor at pressure $e(T_2)$ by decreasing the vapor volume and expanding the air volume to absorb the latent heat, until both volumes are equal. For the air ($\delta T = 0$),

$$m_A C_{vA} \delta T = 0 = \delta q_A - p_A \delta v_A = \delta q_A - m_A R_A T_2 \frac{\delta v_A}{v_A} .$$

For the vapor,

$$\delta q_v = L\delta m_v = L\rho_v \delta v_v = \frac{Le(T_2)}{R_v T_2}\,\delta v_v .$$

Then,

$$0 = \delta q_A + \delta q_v = m_A R_A T_2 \ln(v_{A3}/v_4) + \frac{Le(T_2)}{R_v T_2}\,(v_{v3} - v_4), \tag{3}$$

where,

$$v_4 = v_{A4} = v_{v4} .$$

Now replace the volumes by pressures,

$$v_{A3} = \frac{m_A R_A T_2}{p_{A3}} \quad \text{and} \quad v_{A4} = \frac{m_A R_A T_2}{p_{A4}} ,$$

$$v_{A3}/v_{A4} = p_{A4}/p_{A3} , \tag{4}$$

and for the vapor,

$$v_{v3} = \frac{m_v R_v T_2}{p_{v3}} ,$$

since, for this formula, no vapor has yet been condensed.

Now we have,

$$v_{v3} = \frac{m_v R_v T_2}{e(T_2)} ,$$

and

$$v_{v4} = v_{A4} .$$

Thus,

$$v_{v3} - v_{v4} = \frac{m_v R_v T_2}{e(T_2)} - \frac{m_A R_A T_2}{p_{A4}} .$$

So, substituting in the last term of Equation (3),

$$\begin{aligned} \frac{Le(T_2)}{R_v T_2}\,(v_{v3} - v_4) &= L\left(m_v - m_A \frac{R_A e(T_2)}{R_v p_{A4}}\right) \\ &= Lm_A\left(r_1 - \frac{\varepsilon e(T_2)}{p_{A4}}\right) \\ &= Lm_A(r_1 - r_{s4}(T_2)) , \end{aligned} \tag{5}$$

where $r_{s4}(T_2)$ is the saturated water vapor mixing ratio at $T_2$ and $p_{A4}$.

Thus, using Equations (3), (4), and (5),

$$\ln\left(\frac{p_{A4}}{p_{A3}}\right) + \frac{L}{R_A T_2}(r_1 - r_{s4}) = 0 .$$

Subtracting this result from Equation (2),

$$\left(\frac{1 + rC_{pv}/C_{pA}}{1 - 1/\gamma}\right)\ln\left(\frac{T_1}{T_2}\right) = \ln\left(\frac{p_{A1}}{p_{A4}}\right) + \frac{r_1}{\varepsilon}\ln\left(\frac{p_{v1}}{e(T_2)}\right) - \frac{L}{R_A T_2}(r_1 - r_{s4}).$$

Now since,

$$p_{v1}/e(T_2) = \frac{\varepsilon p_{v1}}{p_{A1}}\,\frac{p_{A1}}{p_{A4}}\,\frac{p_{A4}}{\varepsilon e(T_2)} = \frac{r_1}{r_{s4}(T_2)}\,\frac{p_{A1}}{p_{A4}},$$

we have

$$\left(\frac{1 + r_1 C_{pv}/C_{pA}}{1 - 1/\gamma}\right)\ln\left(\frac{T_1}{T_2}\right) = \left(1 + \frac{r_1}{\varepsilon}\right)\ln\left(\frac{p_{A1}}{p_{A4}}\right) + \frac{r_1}{\varepsilon}\ln\left(\frac{r_1}{r_{s4}}\right) - \frac{L(T_2)}{R_A T_2}(r_1 - r_{s4}). \tag{6}$$

Above cloud base we have a pressure $p_4$, a temperature $T_2$, a liquid water mixing ratio $r_w$, and a saturated mixing ratio $r_{s4}$. Then we have $r_1 = r_{s4} + r_w$, which is the same both above and below cloud base, $p_{A4} = p_4 - e(T_2)$, and $p_{A1} = p_1/(1 + r_1/\varepsilon)$, where $p_1$ is the total pressure below cloud. In addition, similar reasoning shows that for exact consistency,

$$e(T_2) = e_0 \exp\left\{-\frac{1}{R_v}\left[(c_w - c_{pv})\ln\frac{T_2}{T_0} + \frac{L(T_2)}{T_2} - \frac{L_0}{T_0}\right]\right\}, \quad \text{and}$$

$L(T_2) = L_0 - (C_w - C_{pv})(T_2 - T_0)$, where $L_0$, $T_0$, and $e_0$ are at 0 °C and $C_w$, $C_{pv}$ are constants.

Thus, given the pressure, temperature, and liquid water content in cloud, we can calculate $T_1$, the new temperature below cloud at pressure $p_1$. This direction for the conversion does not require iteration since $r_{s4}$ is a function of $T_2$, which is given directly. The reverse process follows with some iteration. No numerical integration is present to introduce errors and use computer time. Iteration errors do not accumulate, and the process rapidly converges.

This formula can also be used as the basis for mixing clear and cloudy air if the components are both taken to below cloud base, mixed, and then returned to cloud height. Further analysis shows that $\dot{p}$ and $\dot{p}_w$ in cloud can be calculated from the values given below cloud base.

These functions are essential to formulate the model to the accuracy needed.

## 4. The Model for Moisture-Driven Convection

We have taken the model developed by Chai (Chai, 1978; Chai and Telford, 1983) and upgraded the thermodynamic approximations to achieve consistencies in the calculations of about $10^{-4}$ K, as discussed above. Thus the model can be applied to cases where there is zero or negative surface heat flux, and the convection is driven solely by the lower density of the water vapor from the evaporating sea surface.

The issue we are concerned with is that of self-consistency, rather than the direct comparison with the air temperatures, which, in many relevant cases, cannot be measured to the accuracy necessary. We would need 0.01 °C, to say 5% which is 0.0005 °C accuracy, in a situation where these changes are of the order of degrees, e.g., 2.5 °C from surface to cloud top, and rapidly fluctuating. Meanwhile there is no reason to doubt that accurate calculations with ideal air and water vapor will also represent real air and water vapor to great accuracy.

Using these equations, we have explored several convective situations and will discuss one case here. We have selected conditions in which this model provides a solution.*

We took an inversion at 250 m above the surface layer, and followed a lowering cloud base down to 50 m above the surface layer in successive calculations. The surface layer below the organized plumes is probably quite hazy at this stage since it is likely to be saturated in places, and nearly saturated on average. At 50 m, falling drops and haze probably take the fog right down to the water by other processes. Figure 1 shows the characteristics of the plumes with 20 m of cloud at the top, and Figure 2 has a cloud base at 90 m above the plume base at the top of the surface boundary layer.

These are cases where the water and the clear air are at exactly the same temperature but a virtual temperature difference between the plume and its surrounding is providing the buoyancy.

Inside the cloud, at a cloud base of 93 m, there is a virtual temperature excess of 0.017 °C, much larger than just below cloud, where it is about 0.004 °C. The cloud is controlled dynamically by the latent heat, which, because the liquid water content is increasing with time, increases the temperature of the air more in the updraft than in the downdraft.

The overall effect of these plumes as time progresses can be seen in Figure 3. There we have used the lowering rate of the cloud base to plot the lowering cloud base height as a function of time. In this case, the air above the inversion is assumed to be too high in wet-bulb potential temperature to be eroded. As can be seen, in these conditions with a wind of 1.4 m $sec^{-1}$, an inversion at 250 m, and constant sea surface temperature, the cloud will take about 6 hr to lower to 75 m from 250 m. Other effects such as small changes in sea surface temperature, condensation on haze particles, and the formation

* There are other conditions where the model does not work because the controlling parameters are beyond the range $4L < z_0 < 20L$ ($z_0$ is the layer depth and $L$ is the Obukov scale length) where this model is valid (see Chai and Telford, 1983, for limiting conditions for these models). A differently formulated model may then be needed.

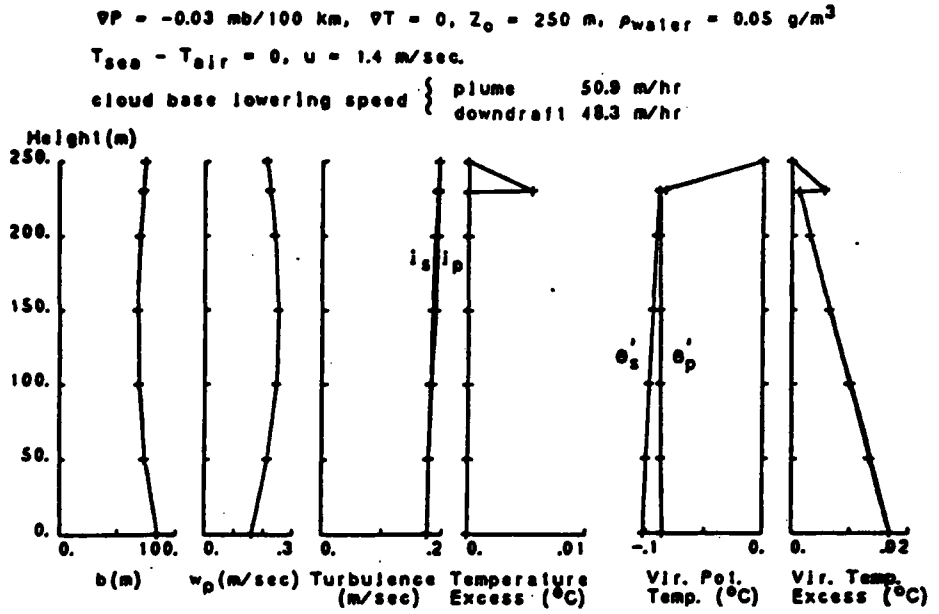


Fig. 1. The convective field with no heat flux coming from the sea surface. The cloud base in the plume is at about 230 m which is about 1 m lower than that in the downdraft.

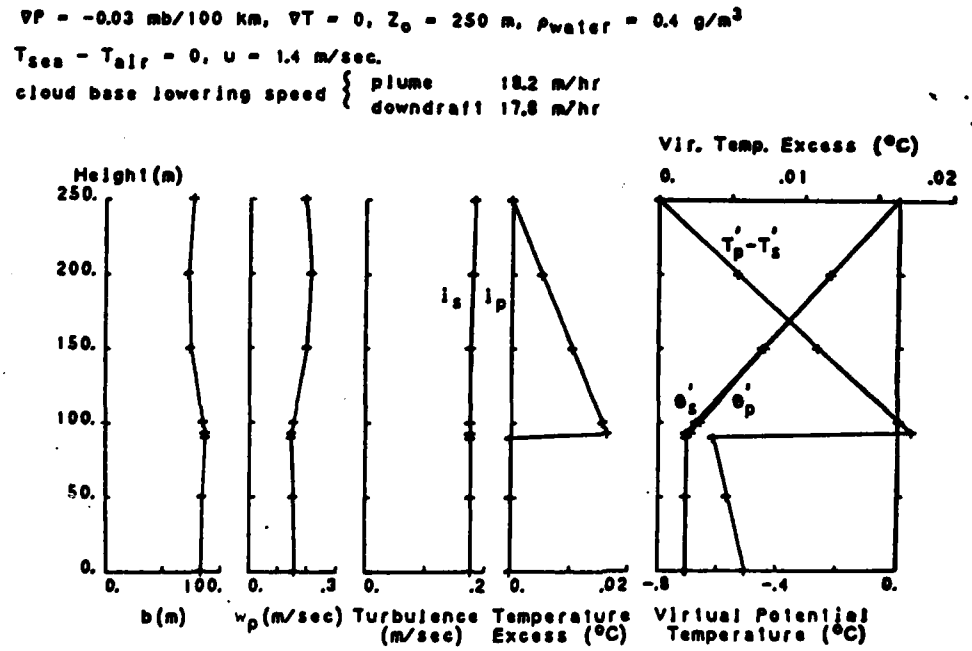


Fig. 2. The convective field with 0.4 g m$^{-3}$ liquid water content at the top boundary. The cloud base in the plume is about 90 m and is about 3 m lower than the downdraft cloud base.

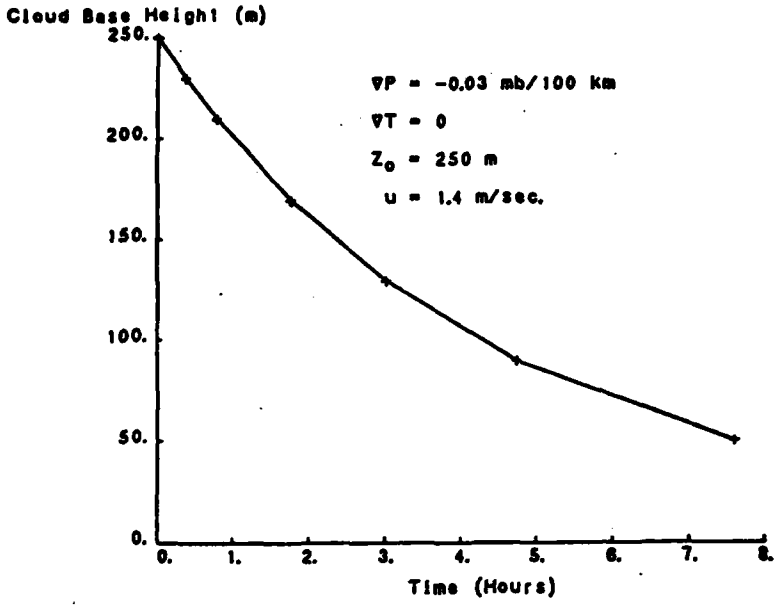


Fig. 3. Cloud base height as a function of time.

of drops big enough to fall out, will introduce other mechanisms which will probably dominate in the lower 50 m or so, and which will probably quickly extend the fog to the surface. In particular, mechanical turbulence from the shear zone will tend to maintain the stirring without free convection for about 10 to 50 m above the surface. This process of buoyant vapor-driven convection slows down as the air begins to saturate near the surface since the subsiding air is then as low in density, from mixed-in moisture, as it can become.

Figure 4 shows additional data from calculations for air warmer than the water. Convection can still continue under the action of the water vapor density until the water is about 0.2 °C cooler than the air. The heat flux then cools the air at about 1 W $m^{-2}$. These cases were with a thin layer of cloud at 250 m, and hence the air was still fairly dry, a condition that supported a relatively large vapor flux. These negative heat flux solutions may be needed when the overlying air is being eroded due to entrainment by the cloudy layer. The figure also shows the vapor flux and the ratio of the heat flux into the water to the vapor flux from the water, as a function of air-to-sea temperature difference.

These calculations indicate that the solution is appropriate in terms of the time required to form fog for the circumstances we have discussed, although, clearly, there are many aspects which need further consideration.

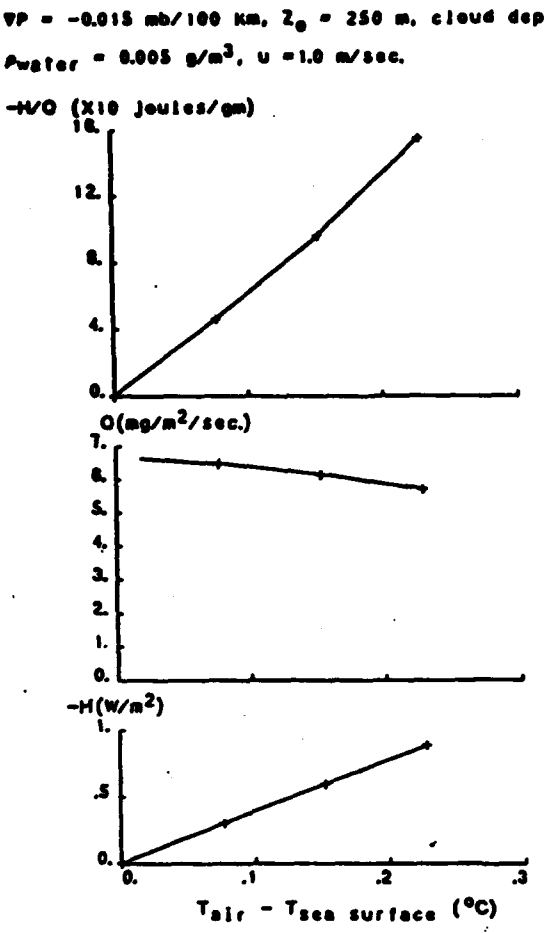


Fig. 4. The variation of heat and vapor fluxes as functions of air-sea temperture difference with the sea cooler than the air.

## 5. Entrainment with a Non-Condensing (Non-Saturated) Top Surface

The top boundary condition is easy to model when no liquid water is present since the entrainment of dry overlying air will be governed in the same way as the entrainment transfer between plumes and downdraft. The entrainment rate produces a flow of overlying air through the top boundary at a velocity equal to the Telford entrainment constant $a$ ($a \simeq 1/12$, see Telford, 1966) times the turbulence at the top of the plumes.

When liquid water drops are present in the air just under the inversion, the increase in density of entrained parcels, following the cooling from the evaporated cloud droplets, drives the downward plumes. This is an entirely different situation to eroding potentially warmer overlying air when no liquid water is present, where the descending plumes become more buoyant than the updrafts. Modeling this latter case, as was done by

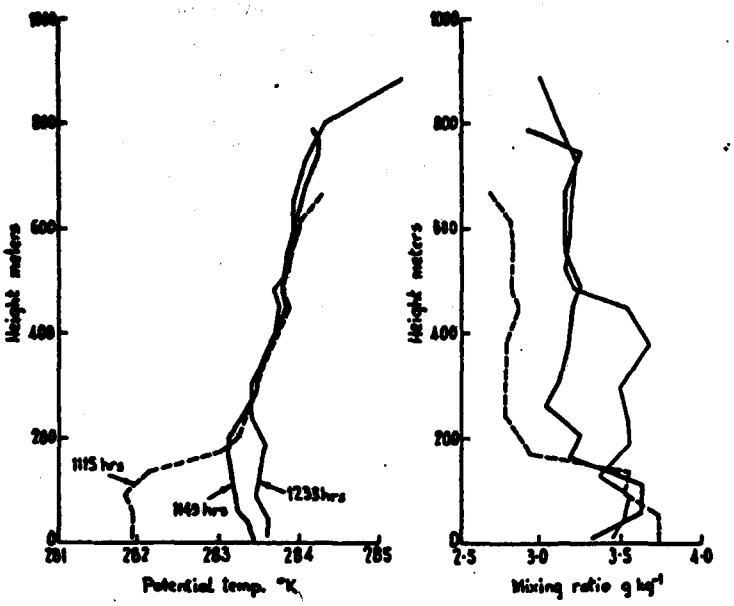


**Fig. 5.** The development of a convective layer with time, when the air is too dry to produce significant condensation (relative humidity less than 60% everywhere) (Telford and Warner, 1964). As the air heats up to the potential temperature of the overlying air, the level of the top of the convection rises, but no inversion is eroded into the overlying air. The overlying air is unstable to wet parcels so any overshooting parcels which produce condensation can carry moisture upward and so displace downward some of the drier air. At 11:49 and 12:33 the initial inversion present at 11:15 in temperature is gone, although the dryness of the air above the convective layer top is still evident. The initial inversion of 1.3 °C did not rise up to greater heights as a result of erosion, but the lower air just heated up until the inversion was gone. The inversion was probably formed during the night and dry convection is quite unable to maintain it.

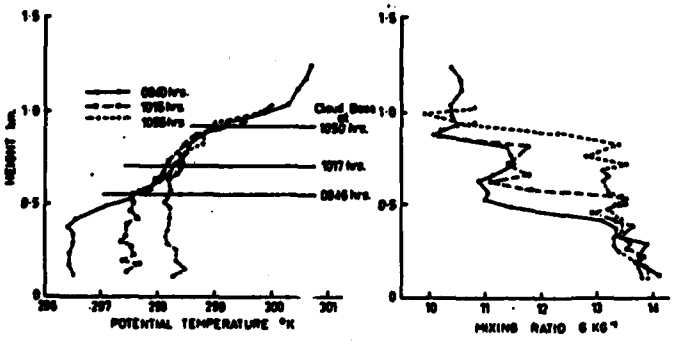


*Fig. 6.* A very similar situation to that in the previous figure, except that here the cumulus cloud was a noticeable feature above the constant potential temperature convecting layer (Warner and Telford, 1967). Here the overlying air is unstable to the wet adiabat from 500 to 1000 m so that no stratus layer could form and hence no inversion could be eroded at the top of the planetary boundary layer. The warming convective air continued to rise until it reached air of the same temperature, without ever producing an inversion. Occasional parcels overshoot and begin condensing, which moistens the air above. The cloud base is about 0.5 °C warmer in potential temperature. Only these warmest patches reach condensation level and form clouds. No inversion is formed at the top of a dry convective planetary boundary layer.

Presley (1976), shows that the plumes cannot descend when the overlying air is more than a fraction of a degree warmer. This model included the turbulence generated by the shear at the top of the convective layer. Thus it seems likely that inversions of more than a fraction of a degree cannot be formed in this way.

The lack of inversion formation in these circumstances can be seen in two time series of boundary-layer profiles shown in Figure 4 of Telford and Warner (1964), Figure 2 of Warner and Telford (1967), and in soundings in Figure 6a of Telford *et al.* (1976). These figures are reproduced here as Figures5, 6, and 7.

Figure 5 shows strong convection with very dry air where there is no suggestion of a new inversion being formed at the top of the surface layer as it heats up and deepens.

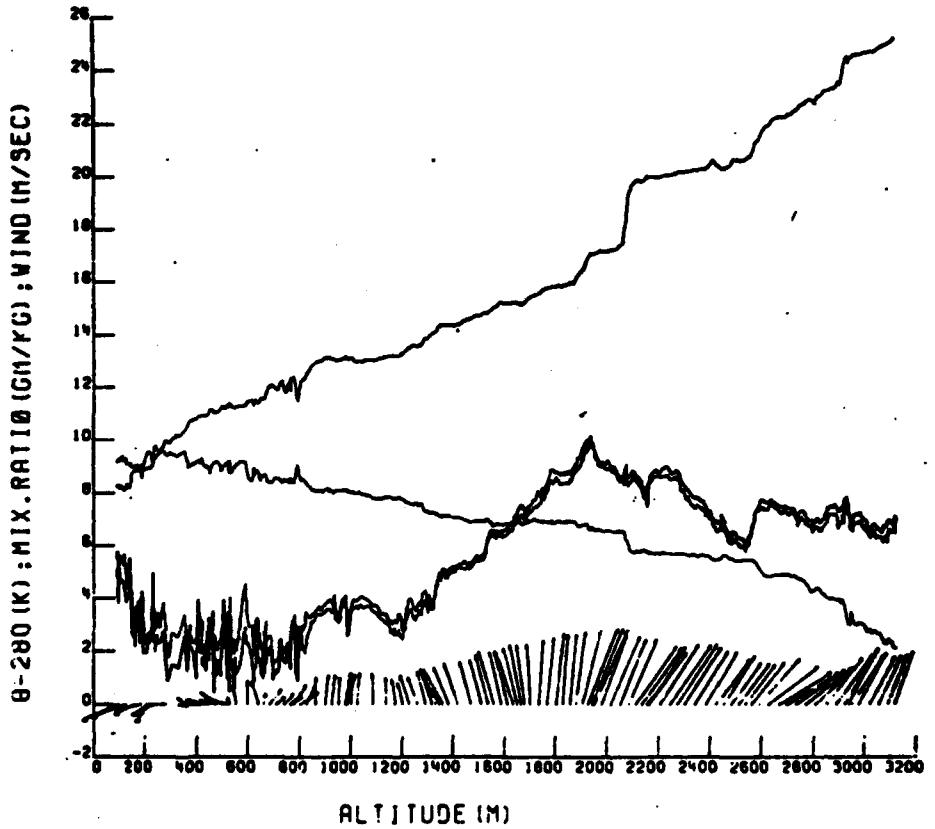


Fig. 7. A sounding over the south shore of Lake Ontario (see Telford *et al.*, 1976). The turbulence up to 800 m is probably due to the hills south of the lake disturbing the air since the increasing potential temperature with height shows that convective overturning is not the cause. From top to bottom in the figure, the traces are potential temperature, mixing ratio, wind magnitude and wind vectors. The wind magnitude shows maximum and minimum values over 2 s intervals.

There is plenty of turbulence in the planetary boundary layer, but no inversion has been formed at its top. As has been explained in the text, condensed moisture in a convecting layer, haze or cloud, is able to form an inversion.

Figure 6 looks very similar to Figure 5, except that there is now enough moisture for occasional cumulus clouds to moisten the air above the constant potential temperature layer. These clouds were observed to show a rising base level with time, some hundred meters or so above the uniformly mixed constant potential temperature region. The increasing moisture above the top of the constant potential temperature layers is probably the result of overshooting parcels reaching their condensation level and so being able to deposit moisture above the overall level reached by dry convection. No sharp inversion was formed. The overshoot levels are unstable to the wet adiabat. The last case in Figure 7 is at the top of a stable but quite turbulent layer where no temperature jump has been eroded at the top of the turbulent region.

The tops of these layers rise because the density of the air in the layer decreases with time under convective heating until it matches the next layer above, and incorporates it. The changes in moisture above the constant potential layer are probably due to a particular case of the mechanisms discussed here. It is thus concluded that turbulent entrainment is inhibited when the overlying air is appreciably warmer ($> 1$ °C warmer, say) than the air in the layer, so substantial inversions are not created in this way. Models which force this result should be viewed with caution.

Similarly, when cloudy mixtures of stratus cloud air and the overlying dry air are positively buoyant in the cloud, it appearls justifiable to assume that there is little effective entrainment of the overlying air. Thus such inversions, formed earlier when entrainment was rapid, will not diffuse to a gradual transition, but will tend to remain rather sharp. The overlying air will thus only appreciably exceed the wet-bulb temperature of the cloud when advection of warmer air is overriding the processes discussed here, because erosion is not able to form inversions in such conditions.

## 6. Critical Conditions for Entrainment at the Wet Inversion

Recent observations have been made under circumstances where there is an extensive stratus layer a few hundred meters deep, and with a base a few hundred meters above the sea surface (Telford and Wagner, 1981). Several cases show that the temperature and water vapor mixing ratio of the overlying air are such that mixtures with the cloud air have roughly the same density as the original cloud parcel before dilution. This can occur after some cloud drops from the cloudy component of the mixture have evaporated to saturate the dry-air parcel entering the mixture from the overlying air. Let us define the temperature of a cloud where mixtures with overlying air from above the inversion are neutral in buoyancy as the *critical temperature*, and the corresponding inversion temperature jump as the *critical temperature jump*. We may also refer to the critical temperature of the overlying air relative to the cloud layer. These temperatures can be calculated from the formula given above, if the parcels are lowered below cloud, are mixed, and lifted again.

These measured inversions are frequently observed to be very sharp, say 15 °C over 50 m or less. Because the negative buoyancy released by the entrainment is proportional to the volume of dry air entrained, and the turbulence driving the entrainment is closely

related to the energy released, the entrainment is likely to be a runaway process. This can be limited only by the cloud totally evaporating, or by the temperature difference (from the rising cloud top) decreasing relative to air above the rising inversion level as it erodes from below, so as to reach the critical temperature where mixtures with overlying air are no longer negatively buoyant. This can happen if the overlying air increases in wet-bulb potential temperature at some level above cloud top.

With this type of instability, there does not appear to be an external rate process to limit the overturning rate, such as when the solar heat flux to the surface determines the convection rate in the dry planetary boundary layer over land. The crucial point to note in this process is that entrainment lifts almost undiluted cloud to the inversion, because entrained overlying air is transported directly to cloud base in the form of cooler cloudy mixtures descending inside the cloud.

To a good approximation apart from the weight of the cloud drops, the limiting case of a just neutrally buoyant mixture of diluted cloud (relative to its undiluted surrounding cloud) depends only on the temperature of the cloud air relative to the temperature and mixing ratio of the overlying air. The wet bulb temperatures of the cloud and overlying air determine this stability. The proportion of dry air in the mixture makes no difference for a neutrally stable mixture if the resulting parcel is still cloudy (ignoring the weight of the drops) because if we just transfer enough drops to a mixing parcel of dry air to saturate it, it will always reach the same temperature. If this temperature is the cloud temperature, further addition of cloud does not change the temperature of the mixture, provided always that there are enough drops overall to saturate the dry parcel.

It follows that if the cloud air before mixing is warmer than this critical temperature, all mixtures still containing cloud are cooler and will be negatively buoyant, and so will promote convection until the rising inversion and the cooling cloud establishes a new critical temperature jump, or else all cloud evaporates. Similarly if the cloud is below the critical temperature, all mixtures will be positively buoyant, and this form of convection will be suppressed.

Thus, given a particular composition of the overlying air above the inversion, the top of a stratus cloud layer can never become warmer (which will decrease the temperature jump below critical) than this critical temperature where a mixture is neutrally buoyant; otherwise the runaway entrainment will erode the inversion, lift up the cloud top, and increase the temperature difference to its previous critical value, which will then stop further entrainment. Continuing surface-driven convection yields cumulus clouds if entrainment into the stratus layer does not stop in this way. Early in the growth cycle, such isolated small cumulus clouds are observed to be short-lived, frequently lasting only about 10 min, in conformity with the very unstable entrainment in these conditions.

On occasion, the unstable erosion reaches a height where the overlying air again has a wet-bulb temperature profile more stable than the wet adiabat, so that as the cloud top rises to replace inversion air which has mixed with cloud and so sunk down to cloud base, the temperature just above the rising inversion increases in wet-bulb potential temperature. This establishes a critical temperature jump again, and stops erosion, and a stable stratus cloud layer again forms. Otherwise, when the instability remains

unchecked, the whole cloud layer will evaporate and break up into cumulus clouds by the erosion of dry air evaporating all the droplets except in new updrafts.

Since the mixtures of cloud air and overlying inversion air are potentially warmer than the air below cloud base, these plumes cannot descend below the cloud base until further mixed with air convecting up from the surface. They must initially stop at the cloud base, which is slowly migrating upward as continuing entrainment of dry air at its top dries out the cloud. This will produce a stable subcloud layer as sometimes reported.

Because of convection from the sea surface, the potential temperature of dry air below cloud base cannot cool much below the ocean temperature. Thus a knowledge of sea surface temperature gives the inversion height if we know the wet-bulb potential temperature profile of the overlying air and the mixing ratio near the surface (i.e., the wet-bulb potential temperature at the surface). Because the vertical potential temperature and moisture profile of the convecting air below cloud is almost constant, this information thus determines the cloud base and, approximately, the wet-bulb potential temperature of the cloud. The cloud base will reach the surface when the inversion reaches a height where the wet-bulb potential temperature just above it equals sea surface temperature. In this condition, the air can no longer be cooled by entrainment and surface evaporation can no longer drive convection.

Since the latent heat of the water droplets at the inversion drives the process, haze droplets on soluble nuclei should also function in the same way as cloud, even if the hazy air is not saturated.

## 7. The Control Exerted by Initial Vertical Gradients

To understand the various conditions which are controlled by different vertical gradients in the overlying air, they need to be discussed separately.

### 7.1. Air warmer than the water with a stable potential temperature gradient and increasing wet-bulb potential temperature with height

This condition originates over the continents when air is dried by precipitation from tall cumulus clouds. During this process, the air subsides and entrains adjacent air, and the clouds evaporate. Thereafter, the air will cool by radiation. In this connection, the air with the lowest water vapor mixing ratio is least cooled and so remains at the highest altitudes while the moister air sinks. In addition, the potential temperature gradient in cloud will be positive at first since it will initially follow the wet adiabat before precipitation falls out, and this gradient will be somewhat further stabilized by the radiative cooling. Thus when continental air moves out over the sea, it is likely to have a strong positive potential temperature ($\theta$) gradient with height, and a smaller positive wet-bulb potential temperature ($\theta_w$) gradient.

If the surface air temperature is much colder than the sea surface temperature, then strong convective overturning will occur with stratus clouds forming, and later breaking up into cumulus clouds, as is described by Telford and Keck (1984) from observations

over the East China Sea. The exact behavior depends on the air temperatures $\theta$ and $\theta_w$ as a function of height, and these temperatures relative to the sea surface temperature.

The most interesting case from the point of fog formation, is when this initially dry air subsides over the sea, and the sea is cooler than the air. Continual cooling by radiation will slowly lower the surface air temperature until the following sequence begins.

When the surface wet-bulb temperature of the air falls below the water surface temperature, the convection can start, even though the actual temperature of the air is perhaps ten degrees or more warmer than the water. It is important to note that small parcels of air will not be buoyant when they leave the surface with the temperature and the saturated mixing ratio of the water. However, as simple mechanical stirring modifies a depth of a meter or so of air to water temperature, liquid water drops on haze will form in this saturated layer.

Once liquid water on haze drops is formed, these drops can mix with the dry air just above and cool it to below the surface temperature, since its wet-bulb potential temperature is lower than the surface temperature. Thus convection has started with cooled, subsaturated parcels descending from the top of the layer to the sea surface and displacing upward buoyant air with a higher mixing ratio, which can form more haze at the layer top to repeat the process. Let us ignore for simplicity in discussing the temperature profile the differences between temperature and virtual temperature. Quantitative precision is left for the computer model we described above.

Once this layer becomes deeper than 10 m or so, the adiabatic cooling up from the surface in the rising parcels will appreciably increase the liquid water available at its top, and the erosion rate will increase.

Referring to Figure 8, we have height as ordinate and potential temperature as abscissa. The original potential temperature of the sounding $\theta_0$ is drawn, with the potential temperature $\theta_e$ of the saturated air at the same wet-bulb temperature (this is not the wet-bulb potential temperature, which is obtained by returning to surface pressure along the wet adiabat rather than the dry adiabat as has been done for potential temperature in this illustration). This latter line gives the critical potential temperature $\theta_e$ for a stratus cloud layer top which is neutrally stable for each level.

If $\theta_e$ at the surface is less than the surface potential temperature $\theta_s$, vapor-driven convection will occur up to an inversion which is eroded by the condensed liquid water at the top of the surface layer. The inversion will erode upward with nearly constant potential temperature approaching the profile of $\theta_e$ since this critical temperature controls the stability of mixtures; when the saturated air is warmer than $\theta_e$, the mixtures will always sink. There will be a sudden increase in potential temperature at the rising inversion where the temperature changes abruptly from $\theta_s$ to $\theta_0$.

When the air following this profile of constant $\theta_s$ in the well mixed subcloud cloud air erodes at sufficient height to reach the sloping $\theta_e$ line, a layer of stratus cloud will begin to form. Continued addition of water vapor to the air will deepen the cloud layer both by lowering its base and raising its top as the inversion erodes upward. The lifting condensation level will determine cloud base which will still be at the surface value of

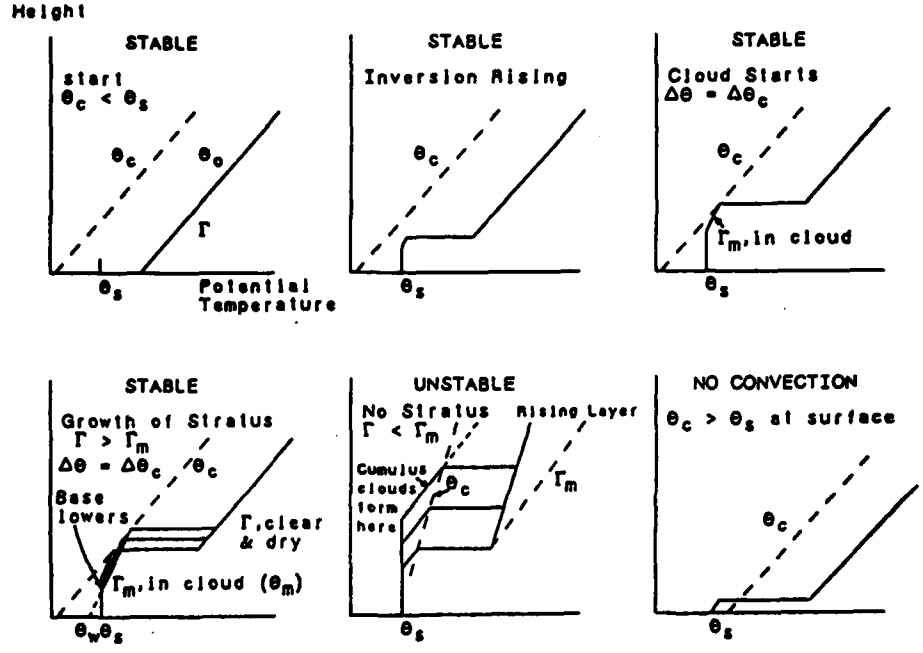


**Fig. 8.** An illustration of the constraints on the erosion of a warm air mass by a cool sea surface. Each graph represents different stages in the convection, or different conditions, and plots potential temperature (referred to surface pressure) against height. The sea surface temperature is $\theta_s$ and the critical potential temperature $\theta_c$ corresponds to the wet-bulb temperature of the dry air at each level of the original sounding. The potential temperature lapse rate of the original layer above the inversion is given by $\Gamma$, where $\Gamma_m$ is the potential temperature lapse rate of the moist adiabat. The inversions are shown as sharp, but this is only true of eroding, rising inversions. The regions below the inversion with the wet adiabatic lapse rate are filled with stratus cloud in the stable case given in the first four sketches. Linear lapse rates have been used to simplify the picture. The unstable stratus case will overturn as illustrated in Figure 9. A lowering cloud base with stratus cloud will lead to fog.

Stability is determined by the wet-bulb potential temperature above the inversion, rather than by the potential temperature. The diagram has been simplified by using a mixing ratio varying with height to keep $(\theta_0 - \theta_c)$ constant.

$\theta_s$. In the cloud, the potential temperature $\theta_m$ will follow the wet adiabat. Cloud top will be where the $\theta_m$ line intersects the $\theta_c$ line, at which height there will be an abrupt increase in potential temperature to the $\theta_0$ sounding line.

The wet-bulb potential temperature $\theta_w$ of the air in the convecting layer is where the extrapolated $\theta_m$ line intersects the surface. As moisture is added to the air, the cloud base lowers and the inversion at cloud top rises, maintaining $\theta_m = \theta_c$ at the cloud top, until cloud base reaches the surface where $\theta_m = \theta_s$. The air is then saturated at the surface, so that new buoyancy cannot be created by evaporation.

This latter situation represents fog. Clearly a deeper layer will take longer to saturate. Near the surface a critical potential temperature $\theta_c$ less than the surface potential temperature $\theta_s$ is necessary for convection to start to moisten the air. In addition, a

wet-bulb potential temperature in the sounding equal to the surface potential temperature $\theta_s$ needs to be reached at a low altitude, say less than 500 m, if the air is to be saturated to form fog in the time available.

### 7.2. A GRADIENT OF THE CRITICAL POTENTIAL TEMPERATURE LESS THAN THE POTENTIAL TEMPERATURE GRADIENT OF THE WET ADIABAT

As in the previous case, the convective layer will erode upward, utilizing the latent heat of water on haze or cloud droplets to erode an inversion to greater and greater heights. When the constant potential temperature $\theta_s$ line in the convectively overturning layer reaches the critical potential temperature $\theta_c$ line, cloud would start to form in the previous case. In the present situation, however, this is not possible because the slope of the critical potential temperature $\theta_c$ line is less stable than the wet adiabat; thus a parcel at the top of the convective layer containing condensed water drops will become increasingly warmer than the critical potential temperature $\theta_c$, the higher it is displaced by overturning.

If such a parcel overshoots into the air above, it is not buoyant because it is potentially cooler than the original sounding $\theta_0$. However, entrainment from the dry overlying air into such a parcel of condensed air at the stratus top will produce mixtures less buoyant than the undiluted cloud, which will sink back to come to rest at some point just above cloud base as clear air mixtures. In sinking back, they carry above-inversion air down to cloud base and, consequently, the cloud is displaced upward as the inversion also rises. In this case, the entrainment at the new inversion becomes more unstable so that only cumulus clouds, rather than a cloud layer, can form.

The mixtures subsiding to cloud base have a higher potential temperature than the air below, and do not immediately descend. This case is illustrated by the observational data shown in Figure 6, where cumulus clouds form in the stable air above the top of the constant potential temperature layer. However, when these data were obtained, the land surface was warming and hence the process is somewhat different.

Thus when a sharp inversion is found above the level where $\theta_c = \theta_s$, it will be modified as it erodes upward. The air with the original potential temperature $\theta_0$ is being cooled by the evaporating small cumulus clouds, toward the critical potential temperature $\theta_c$ line, so that successive overshooting small cumulus clouds become less negatively buoyant in this mixed region. The continuous upward flux of small clouds into the dry air where they are evaporated will lower the temperature of the overlying air.

As the constant $\theta_s$ region is depleted to supply the cloud forming in the air just above, it will be restored by continuing surface convection. In this case, the feedback is stable. If the lifting condensation level is too high, the cloud formed at the inversion is too cool to entrain and erosion stops until the condensation level lowers a little, and the cloud top temperature increases and entrainment starts again. If the lifting condensation level is too low, the cloud at the inversion is warmer, entrainment increases, and the influx of dry air raises the lifting condensation level.

The lifting condensation level for the small cumulus clouds will rise as the convecting layer becomes drier due to entrained air. Another way of explaining this process is that

the almost saturated ambient clear air possesses a lower wet-bulb temperature than that of the original environmental air at that level since the up and down circulation has displaced downward the mixtures formed earlier. This means that the critical potential temperature of the air displaced downwards has been modified by evaporation toward a lower temperature when the wet-bulb potential temperature decreases with height in the original sounding, as it does in this case. Here the increase in the critical potential temperature with height is less than that of the increasing potential temperature of the moist adiabat. Therefore, the constant $\theta_e$ region which extends up to the lifting condensation level will rise until it reaches a level where the new critical potential temperature is again equal to $\theta_e$. This will be the new lifting condensation level of the convecting air. Small cumulus clouds can be formed above this level.

The cloudy levels will thus tend to remain very slighly unstable to wet growth, so that the small clouds will tend to rise to a greater height and become successively larger, as they rise an increasing distance through the almost saturated clear air surroundings to reach the inversion. Greater rise above the lifting condensation level gives greater adiabatic release of liquid water, and hence longer life to the cloud at the inversion, and accumulation of larger cloudy volumes to give larger cumuli.

At the inversion, this process will greatly moisten the overlying air producing smoothing of a previously existing sharp inversion. The dry air will also tend to become modified to an almost saturated mixing ratio with a wet adiabatic lapse rate, which represents a constant wet bulb potential temperature. This is because as this condition is approached, the small cumulus clouds will rise through the now almost saturated layer, and so will evaporate less and less below the inversion.

A good example of this stage of the process is given by Telford and Keck (1984) using AMTEX data.

### 7.3. Initial stability creating a stratus layer which erodes upward until it meets unstable conditions above

After a stratus layer of appreciable thickness has formed, say a few hundred meters, and the overlying wet-bulb lapse rate is such that the air becomes cooler and denser at a rate greater than the wet adiabatic lapse rate, continued additions of moisture in the air can further raise the cloud top height and its wet-bulb potential temperature. However, total overturning now occurs, since, as diluted negative buoyant parcels form from entrainment at cloud top and sink down through the cloud and below, the returning upward flow within the cloud lifts the cloud air surrounding the descending thermals in the compensating upward flow along the wet adiabat. Thus the cloud top becomes even warmer relative to the critical temperature due to the next overlying level. This is because the upward return flow within the cloud lifts air along the wet adiabatic potential temperature lapse rate, whereas in this case wet-bulb potential temperature of the overlying dry air does not increase with height as rapidly. The cloud layer will develop downdraft regions with intervening rising regions of relatively undiluted cloud. The clouds will cool the entrained, originally overlying, dry air by evaporation until the last

piece of cloud evaporates, above the now cooled and moistened mixed regions which have displaced it upward.

Since the equilibrium level of the mixed cooled downdrafts, after they have evaporated to become clear air and have come to rest, is established by the wet adiabatic lapse rate of the bottom of the stratus layer as it is displaced upward, the cloud will be replaced by mixed dry air at the wet adiabatic lapse rate with almost saturated mixing ratio. This air now has a constant wet bulb potential temperature.

New saturated parcels from further convection starting at the surface can then rise through this layer to form cumulus clouds at the new higher altitude, but at a new inversion with a greatly reduced temperature step, as shown in Figure 9.

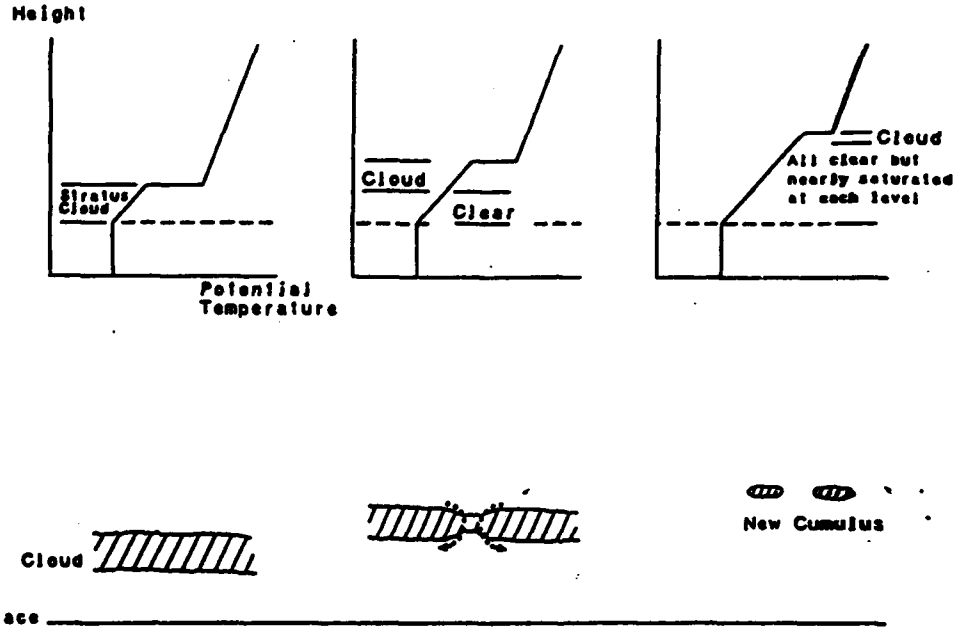


Fig. 9. Three stages in the overturning of stratus cloud, after the erosion of the overlying inversion has reached a level where the potential temperature is less stable with height than the moist adiabat. This instability is actually induced by reaching an overlying region with decreasing wet-bulb potential temperature. Parcels of cloud mixed with above-cloud air are now denser than the surrounding cloud, and sink to beneath the cloud where they evaporate just above cloud base, because they are drier. The remaining cloud is displaced upward until all cloud has evaporated.

The dry air is now almost saturated; with the same density the cloud had before the cloud moved upward. New condensation at the bottom of the displaced layer will thus remain buoyant up to the new inversion, to form cumulus clouds there.

To reiterate, because the overlying lapse rate is less stable than the wet adiabat, the overturning of a stratus cloud layer, will result in a much smaller inversion temperature jump at the much greater height of the new cloud tops, and approximately wet adiabatic stability in the clear air down to near the base of the previous stratus. The new clouds

will be small cumuli because they are now well above the critical temperature at the inversion and so cannot survive to form a continuous layer. Continued moistening from the surface, which gives more condensation into this layer, will then be slightly unstable right up to the new inversion, and so maintain the continuing formation of new cumuli, as discussed in the previous case, (b).

In order for this to happen, there must be a region above a stratus layer of less stability in wet-bulb temperature than the wet adiabatic lapse rate, i.e., a decreasing wet-bulb potential temperature with height. This is the mechanism which removes inversions and allows cumulus clouds to grow. Experimental support is given by the AMTEX 1975 data discussed by Telford and Keck (1984), but in that case the instability occurred because the high sea surface temperature heated the lower air and in this way made it unstable relative to the air at greater heights. When this criterion is encountered above a stratus layer, the sun will break through the clouds, as is commonly observed.

## 8. Discussion of Conditions Relative to some Observations of Stratus Clouds

As can be seen for the data given in Figures 1 and 2 of Chai and Telford (1983), which are taken from the stratus cloud case discussed in Telford and Wagner (1981), the layer in Figure 1 is composed of air with a potential temperature decreasing slightly with height up to cloud base, above which it follows approximately the wet adiabat to the inversion. In Figure 1 of Chai and Telford (1983), the cloud is entraining dry air into its top. There is a large wind shear within the convective layer from 200 m to the cloud base at 320 m, suggesting that there was no vertical mixing across this region from 200 to 320 m, at the time this sounding was obtained, consistent with a quite recent burst of entrainment of dry air into cloud top giving a stable layer at cloud base. This temperature profile in the regions below the inversion is very similar to profiles obtained in strong thermally driven convection over land on clear days (Warner and Telford, 1967). Figure 2 of Chai and Telford (1983), taken in a region where there was apparently no entrainment in progress at cloud tops, is very similar except that the wind magnitude is much more constant with height from the surface up through the cloud, suggesting overturning through the whole depth from the surface up to the inversion. The potential temperature also seems to increase slightly with height up to about 200 m (as usually occurs in strong dry convection), but this may be more of a measure of small horizontal changes rather than of vertical structure.

It is now possible to explain this structure as a quasi-equilibrium state, determined only by the inversion height, the sea surface temperature and the wet-bulb potential temperature in the air above the inversion, but with the inversion rising as convection continues to add moisture from the sea surface. In this case, calculations (Twomey, 1983) show that the cloud top is not being significantly cooled by radiation, and may actually be heating. This occurs in sunlight since the inversion is so large (15 °C) that the infrared optical depth in the overlying air with a mixing ratio of about 3 mg $kg^{-1}$ is small enough that average radiation comes from within a layer where the average temperature is not sufficiently colder than the cloud. This supports the idea that

radiation cooling is not an essential element to maintain the convection in at least this one particular example of a stratus layer. The explanation for fog or cloud formation given here does not need radiation to provide cooling of the air to form or sustain cloud.

The cloud can originally form because the sea provides water vapor buoyancy-driven convection which moistens the air until condensation starts at the top of the convecting layer. This liquid moisture provides a mechanism for eroding an inversion into the overlying air. Convection continues because mixtures containing a fraction of the drier warmer air entering at top are much cooled by evaporation, and descend through the cloud until they totally evaporate just above cloud base, where they will then be slightly warmer than the dry air below. An episode of overturning will heat the air at cloud base just enough to stop the rise of surface air temporarily through this level and so allow internal shear to develop. The moister cooler air coming up from the surface then condenses at the former cloud base, adding further liquid water to cool parcels enough to allow their continued descent. After the plumes of drier, and perhaps slightly warmer, air reach the surface, they are directly cooled and moistened to repeat the cycle.

This structure also means that surface air does not rise beyond the overlying inversion, so that shear can readily develop. Thus a northerly surface flow with a southerly flow above the inversion as was observed in this case, tends to provide a cooler surface flow capped by a warming flow aloft, and this flow may well tend to increase the inversion temperature jump.

The cloud can persist once the inversion increases sufficiently to give a critical temperature higher than the cloud top temperature. The continued moisture-driven convection then lowers cloud base and increases cloud top potential temperature, since the subcloud air remains near the sea surface potential temperature and the air in the cloud increases in temperature with height along the wet adiabat. When cloud top temperature again exceeds the critical temperature, further erosion from the dry air above takes place. If there is a gradient that is stable relative to the wet adiabat (i.e., increasingly warmer than the wet adiabat in wet-bulb temperature) in the air just above the inversion, as there often is, then the temperature jump at the inversion temporarily increases as the inversion lifts. A new lower cloud base level is then established and the temperature jump decreases again to its critical value following the increase in liquid water mixing ratio at cloud top.

If the air above the inversion continues to increase in temperature with height relative to the wet adiabatic lapse rate as the inversion rises, or warmer air is advected aloft, then the cloud base can ultimately descend toward the surface, because continued addition of moisture with a lowering of cloud base is possible at each step until a new higher critical temperature is reached at cloud top.

If the lapse rate in the air above the inversion is less than the wet adiabat, and if the inversion temperature step has decreased enough under continued upward growth of the cloud top, convective instability will overturn the whole cloudy layer and eventually allow, as the temperature step at the new inversion becomes small enough, substantial continued upward growth of cumulus cloud from the well mixed moist surface layer. When most of this layer has moved up to form clouds and the overlying dry air has

moved down to near the previous stratus base, further cumulus clouds will continue to form as moisture continues to be added from the sea surface.

## 9. Summary

The usual form of latent heat driven instability that can occur with a rising cloud parcel in a stable dry air layer (with less stability than the wet adiabatic lapse rate) depends on latent heat released on growing drops which make the parcel warmer and less dense than the dry surrounding air.

The quite different form of instability discussed here (see also Chai and Telford, 1983) can occur inside a layer cloud because mixing in dry air at cloud top cools in-cloud parcels and makes them dense enough to sink through the layer and displace the remaining cloud upward. In simple terms it is roughly equivalent to pumping up sea water and spraying it into the dry air above the inversion until it saturates the air, and has a liquid water content and temperature matching the cloud top.

In both cases, that of latent heat giving buoyancy to a rising cloud in dry surroundings, and diluted negatively buoyant blobs descending inside a cloud, the latent heat of evaporation of water controls the relative density. In the latter case, the lapse rate of wet-bulb temperature of the dry air above cloud must be more stable than the wet adiabatic lapse rate to prevent complete overturning and evaporation. When the inversion forms at the top of a cloudy stratus layer, overshooting cloudy parcels are strongly negatively buoyant.

For the first case, the virtual potential temperature of the air around the cloud controls the density difference, and in the second case the wet-bulb potential temperature of the overlying air determines the density difference for incloud parcels formed by mixing at the top surface.

Thick haze is often seen at inversions, and the latent heat of water in particles will produce cooling through evaporation. If the wet-bulb temperature of the overlying air is less than the hazy top temperature, then mixtures will be cooled enough to become dense enough to sink. After condensation starts, continued convection from the surface will create an increasing inversion step in potential temperature as the just saturated top of the noncloudy layer erodes upward. The saturated top of the layer can create a large enough inversion temperature step to give equal wet-bulb temperatures across the inversion transition. When this stage is reached, erosion will stop. With continued addition of moisture from the sea surface, the wet-bulb potential temperature of the layer will again increase with further erosion, but now the condensation will persist to give a cloud layer.

Over the sea, convection can occur in air warmer than the water because of this process, assisted by buoyancy from water vapor. Convection can continue in air over a constant temperature water surface, since evaporation of droplets cools the entrained air down to the surface temperature, and the vapor-driven convection continues up from the surface even if there is a downward heat flux to a slightly cooler surface.

The overturning of stratus layers will leave dry, almost saturated, air with a wet

adiabatic lapse rate. This is probably the reason that the average atmospheric lapse rate is fairly close to the wet adiabat, except where modified by dry convection from the surface.

Because the lapse rate in the dry air above the inversion varies, a stratus layer may well form in stable conditions, and then erode later at a greater height when it reaches an unstable region which overturns and evaporates it. This process leaves the air almost saturated and with a constant wet-bulb potential temperature with height.

Fogs tend to be found more frequently over colder water in mid-ocean since a cooler surface reduces the height where the wet-bulb potential temperature of the air equals sea surface temperature. In order to form fog (cloud at the surface), the wet-bulb potential temperature of the air must exceed that of the ocean at an altitude close enough to the surface for the convection process to saturate this layer of air in a reasonable time.

Air heated over hot desert also acquires an elevated wet-bulb potential temperature. Thus when such an air mass moves over water, fog can also form, as happens over the Pacific ocean near San Diego.

Radiative cooling with the resulting downward convection contributes to the whole process but it appears from this discussion that it does not play an essential role in the fog-formation process. Radiative cooling is, of course, essential in conditioning the atmosphere as a whole. Similarly, convective stirring over patches of ocean with a sea surface temperature warmer than average may play some role.

For the model presented, the times for convective transfer to lower the cloud base towards the surface are reasonable, but it is noted that this estimation requires an assumption about the roughness height of the sea surface.

## Acknowledgments

This paper, including the particular model calculations used here, was prepared under Navy Contract N00014–75–C0598 in relation to studies of fog formation over the ocean. The data used were obtained under field studies and data analysis supported by the National Science Foundation Grant ATM–8012929.

## References

Ball, F. K.: 1960, 'Control of Inversion Height by Surface Heating', *Quart. J. Roy. Meteorol. Soc.* 86, 483–494.

Chai, S. K.: 1978, 'Lowering Stratus Cloud in Surface Driven Convection over the Sea', Ph.D. Dissertation, Univ., of Nevada, Reno, 146 pp.

Chai, S. K. and Telford, J. W.: 1983, 'Convection Model for Stratus Cloud over a Warm Water Surface', *Boundary-Layer Meteorol.* 26, 25–49.

Deardorff, J. W.: 1980, 'Cloud Top Entrainment Instability', *J. Atmos. Sci.* 37, 131–147.

Deardorff, J. W.: 1983, 'A Multi-Limit Mixed-Layer Entrainment Formulation', *Jour. Phys. Ocean.* 13, 988–1002.

Guldberg, C. M. and Mohn, H.: 1876, 'Etudes sur les mouvements de l'atmosphère', Pt. 1 Christiania. 39 pp.

Lilly, D. K.: 1968, 'Models of Cloud-Topped Mixed Layers Under a Strong Inversion', *Quart. J. R. Meteorol. Soc.* 94, 292–309.

Manton, M. J.: 1980, 'On the Modelling of Mixed Layers and Entrainment in Cumulus Clouds', *Boundary-Layer Meteorol.* 19, 337–358.

Presley, J. D.: 1976, 'Free Convective Plumes in the Atmosphere', Ph.D. Dissertation, Univ. of Nevada-Reno, 162 pp.
Randall, D. A.: 1980a, 'Entrainment into a Stratocumulus Layer with Distributed Radiative Cooling', *J. Atmos. Sci.* 37, 148–159.
Randall, D. A.: 1980b, 'Conditional Instability of the First Kind Upside-Down', *J. Atmos. Sci.* 37, 125–130.
Saunders, P. M.: 1964, 'Sea Smoke and Steam Fog', *Quart. J. Roy. Meteorol. Soc.* 90, 156–165.
Smithsonian Meteorological Tables: 1966, Sixth Revised Edition, Smithsonian Miscellaneous Collections, Vol. 114, The Smithsonian Institution, 527 pp.
Squires, P.: 1958, 'Penetrative Downdraughts in Cumuli', *Tellus* 10, 381–389.
Telford, J. W.: 1966, 'The Convective Mechanism in Clear Air', *J. Atmos. Sci.* 23, 652–666.
Telford, J. W.: 1970, 'Convective Plumes in a Convective Field', *J. Atmos. Sci.* 27, 347–358.
Telford, J. W.: 1972, 'A Plume Theory for the Convective Field in Clear Air', *J. Atmos. Sci.* 29, 128–134.
Telford, J. W.: 1975, 'The Effects of Compressibility and Dissipation Heating on Boundary Layer Plumes', *J. Atmos. Sci.* 32, 108–115.
Telford, J. W.: 1981, 'The Surface Roughness and Planetary Boundary Layer', *Pure Appl. Geophys.* 119, 278–293.
Telford, J. W.: 1982, 'A Theoretical Value for von Karman's Constant', *Pure Appl. Geophys.* 120, 648–661.
Telford, J. W. and Warner, J.: 1962, 'On the Measurement from an Aircraft of Buoyancy and Vertical Air Velocity in Cloud', *J. Atmos. Sci.* 19, 415–423.
Telford, J. W. and Warner, J.: 1964, 'Fluxes of Heat and Vapor in the Lower Atmosphere Derived from Aircraft Observations', *J. Atmos. Sci.* 21, 539–548.
Telford, J. W. and Presley, J. D.: 1978, 'The Surface Boundary Layer as a Part of the Overlying Convective Layer', *Pure Appl. Geophys.* 117, 664–689.
Telford, J. W. and Wagner, P. B.: 1981, 'Observations of Condensation Growth Determined by Entity Type Mixing', *Pure Appl. Geophys.* 119, 934–965.
Telford, J. W. and Chai, S. K.: 1982, 'Fog, Stratus and Cumulus Formation in Warm Air over Cooler Water', *Preprints of the Conference on Cloud Physics*, November 15–18, 1982, Chicago, Illinois, 7–8.
Telford, J. W. and Keck, T. S.: 1984, 'Inversions, Entrainment into Clouds, and Invariance of the Wet Bulb Potential Temperature with Height', submitted for publication.
Telford, J. W., Vaziri, A., and Wagner, P. B.: 1976, 'Aircraft Observations in the Planetary Boundary Layer under Stable Conditions', *Boundary-Layer Meteorol.* 10, 353–377.
Twomey, S.: 1983, 'Radiative Effects in California Stratus', *Contrib. Atmos. Phys.* 56, 429–439.
Warner, J. and Telford, J. W.: 1963, 'Some Patterns of Convection in the Lower Atmosphere', *J. Atmos. Sci.* 20, 313–318.
Warner, J. and Telford, J. W.: 1967, 'Convection Below Cloud Base', *J. Atmos. Sci.* 24, 374–382.
Woodcock, A. H.: 1982, 'Fog, and Tidal Current Connection at Cape Cod Canal – Early Recognition and Recent Measurements', *Bull. Am. Meteorol. Soc.* 63, 161–166.

# END

# FILMED

11-84

# DTIC